UNIVERSIDADE DE LISBOA

INSTITUTO SUPERIOR TÉCNICO

Engineering Characterisation of Bioreactors for Human Pluripotent Stem Cell Expansion and Cardiac Differentiation

Diogo do Espírito Santo Nogueira

Supervisors: **Doctor** Joaquim Manuel Sampaio Cabral

Doctor Carlos André Vitorino Rodrigues

Thesis approved in public session to obtain the PhD Degree in

Bioengineering

Jury final classification: Pass with Distinction

2021

TÉCNICO LISBOA

UNIVERSIDADE DE LISBOA

INSTITUTO SUPERIOR TÉCNICO

Engineering Characterisation of Bioreactors for Human Pluripotent Stem Cell Expansion and Cardiac Differentiation

Diogo do Espírito Santo Nogueira

Supervisors: **Doctor** Joaquim Manuel Sampaio Cabral

Doctor Carlos André Vitorino Rodrigues

Thesis approved in public session to obtain the PhD Degree in

Bioengineering

Jury final classification: Pass with Distinction

Jury

Chairperson: **Doctor** Duarte Miguel de França Teixeira dos Prazeres, Instituto Superior Técnico, Universidade de Lisboa

Members of the Committee:

Doctor Vítor Manuel Geraldes Fernandes, Instituto Superior Técnico, Universidade de Lisboa

Doctor Robert Zweigerdt, Hannover Medical School, Germany

Doctor Maria Margarida de Carvalho Negrão Serra, IBET – Instituto de Biologia Experimental e Tecnológica

Doctor Frederico Castelo Alves Ferreira, Instituto Superior Técnico, Universidade de Lisboa

Doctor Carlos André Vitorino Rodrigues, Instituto Superior Técnico, Universidade de Lisboa

Funding Institutions

Fundação para a Ciência e Tecnologia

2021

ACKNOWLEDGEMENTS

The human being is a social animal. We constantly being changed by those who cross our paths every day. As such, I would like to thank all of those who left a bit of themselves in me, and contributed for me to become the person I am now. But it would be unfair to all of those who contributed with even more to just leave it at this, so, I will now especially thank those who carried me through this doctoral thesis. This work is as mine as it is yours.

Firstly, I thank my supervisors, who went above and beyond anything I could have ever asked. I would like to thank Professor Joaquim Cabral, for introducing me to Biological Engineering back in the first year of the course, as that helped kickstart the long path I have treaded since then. I thank him for accepting me at SCERG for my Master's thesis, for giving me the honour of being supervised by him, for bringing me to the world of bioreactors, and for all the opportunities he has given me throughout these years. I also thank his availability, for answering my e-mails so quickly and at any time and for all the good-humoured scientific discussions (including those about the bureaucracies and involving environment). Undoubtedly, without his help, I could never have got so much from this PhD. I would also like to thank Carlos Rodrigues, who introduced me to the Vertical-Wheel bioreactors and who agreed to supervise me on this adventure. I know I am not that easy to work with, so thank you for your patience, for answering my questions at any time, for correcting everything on very short notice (including this whole thesis in record time). Thank you for being honest when I needed it, but also for picking me up in hard times. Thank you for all the good-humoured talks about popular culture and entertainment and for all the chess games. I also thank you for teaching me so much, not only about stem cells, but also so many other things (fixing computers, driving in Lisbon, etc.). Even though you cheer for SCP, it is a pleasure to call you not only a supervisor, but a close friend.

I thank Professor Margarida Diogo and Professor Tiago Fernandes, who helped me start my adventure at SCERG and who taught me and still teach me so much. Thank you for easing me into stem cells when I knew next to nothing about them. It is thanks to you that I had the courage and motivation to pursue this PhD.

I also want to thank all of my lab 2 colleagues (present and former), Cláudia, Mariana, Ana Rita, Teresa, João Cotovio, Carina, João Carreira, André, Margarida, Fábio, Laura, Paola, Leonor, Adriana, Maria, William, Inês, you are incredible all-around. Cláudia, thank you for aiding me in the lab, not only at the beginning of my PhD but throughout. Mariana, thank you for being exceedingly kind and helpful, and for being always willing to share your experience and knowledge about all things cardio. Ana Rita, Teresa and Carina, thank you for all the help in my brief neural incursions and for bringing joy to the lab (together with João Cotovio). Fábio, thank you for all the support, for always reaching out to check if I am alive, and for all the scientific and gaming discussions. João Carreira, thank you for everything you have taught me and for being the "lab surgeon". Laura and Silvia, grazie mille for all the Italian lessons (which I am planning to retake after the thesis!) Paola, thank you for all the support and for bringing a "breath of fresh air" in how we do things. William and Inês, thank you for giving me the opportunity to help you around in the lab for being incredible and extremely supportive; I am sorry for being always in

a rush, but I hope to make up for it after the thesis. Margarida, thank you for all the good times, for all the support and company in the lab and for all the car rides.

I also want to acknowledge all other members of SCERG. Miguel, thank you for the support, for all the laughs and for having been a great colleague who I look up to and who has motivated me to be better for the last 10 years. Carina, thank you for being one of my funniest and most unique friends (and I thank you, Fábio and Carlos, the Fellowship of the Ring, for finally convincing me to watch the *Lord of the Rings* films!) Cátia, thank you for all your work with the SCERG website and for teaching me all the web design 101s. Professor Frederico, Ana, André, Cristiana and Marília thank you for all the advice, support and help. Jaqueline, thank you for taking care of so many aspects of lab management and for being a great motivator. A very special thank you to Sarini, for all the fun moments, the pranks, the jokes, the songs, and for being there when I needed. Life at SCERG is much more boring without you, so never go back to Zaragoza! Thanks to each and everyone of you (and I am really sorry if I forgot someone) and I hope we can have our amazing lunch hours again soon.

I would like to thank Professor Vítor Geraldes, from DEQ-IST, and Master student Pedro Neto for the invaluable help with Chapter IV—for the availability, the development of the model, the meetings and for answering all of my questions so promptly.

I also want to thank Professor Robert Zweigerdt and Margarida Serra for agreeing to argue my thesis, for the great scientific discussion and for all the tips to improve this thesis and my future work.

A word of acknowledgement to PBS Biotech for the scientific work discussion and for all the equipment support. Thank you to FCT as well for the financial support throughout the PhD (PD/BD/128376/2017).

I also want to thank my Biological Engineering colleagues, who made life much easier during the course and I am very grateful for having them be a part of my life. A special thanks to Bárbara and Manel who have supported me a lot during these last times.

A huge shout out to my church community, in particular to “Pastoral Juvenil de Linda-a-Velha” who are my second family and are always looking after me. Thank you, PDF and Ausenda for helping me organise my life in so many aspects. Carolina and Nanci, thank you especially for the last two years, for all the talks, the good times and all the “go write your thesis” messages. A special thank you also to our group “Roma 2000” who still keep up with us even though we get crazier by the day. Thank you also to our “boss”, Felipa, for kickstarting this adventure, and for being always so ready to listen to my problems. Mariana, thank you for your unfiltered honesty that makes me want to comment everything with you; Daniel, thank you for all the motivation; and thank you both for the conversations and for KFC. Gustavo and Joana, thank you for reaching out so much, for all the good times and for our recent gaming adventures (with Filipa, Diogo and Manel). Thank you, and Marta, Margarida, Ana Isabel, Cecília, João, Teresa and Manu for all the adventures. Família Tiles, thank you for all the time together, and I hope we can go to Tiles again soon! António, Ana, Filipa, Gonçalo, Karol, Leonor, Maria and Rita, thank you for worrying about me and for trying to cheer me up, especially in the days before the thesis delivery. Alex, thank you for trusting in me and for helping me be a better person (even though you probably do not realise yet). Sandra, thank you for caring so much about me even from so far away, thank you for the good moments, for being a great listener, and for the long WhatsApp audios which sometimes keep

me company. And there are so many other people I would love to thank that would fill pages and pages. But before finishing, I have to thank two very special people. Dani, thank you for being a great friend and brother, for all the shared moments, for making me strive to be better, and for always trying to get me to do stuff instead of locking myself in my personal bubble. I am sorry for the lack of time in the past months, but I will try to make up for it. Rodrigo, it is hard to put into words how much I owe you. Thank you for letting me share everything with you and for always listening to my insecurities and answering them in the best possible way, even at 3 AM. Thank you also for teaching me so much every day. Thank you for all the music, stickers, Tweets, TikToks, Brazilian memes, workout videos and everything else. You are the brilliant one, and I hope one day I can be as great a friend and a person as you. Finally, thank you all for having been present in my thesis defence and for the 400 live comments!

A huge thank you to all my other friends who shaped my life in one way or another.

Finally, I would like to thank my family, for all the help and for all the support. Thank you to my mother and uncle, and I am sorry for being so absent in the past times. I hope I can make up to you. Thank you to my father and grandmother, who left all too early but who helped me and still help shape who I am.

ABSTRACT

Cardiovascular diseases (CVDs) impair the quality of life of patients and are responsible for millions of deaths every year. While treatments can already mitigate some symptoms and protect the heart following myocardial infarction, the death of cardiomyocytes is so far irreparable due to their limited proliferation. Human induced pluripotent stem cells (hiPSCs) can self-renew and differentiate into all cell types of the human body, and they can be reprogrammed from the patients' cells. As such, hiPSCs can potentially be applied for the development of novel treatments for a myriad of CVDs. For that purpose, methods for their scalable and robust expansion and cardiac differentiation must be developed. The single-use Vertical-Wheel bioreactors (VWBRs) apply a novel and gentle agitation mechanism and are available at laboratory and production scales. As such, they have the potential to be applied for clinical-scale biomanufacturing of hiPSC-derived cardiomyocytes.

This thesis aimed at developing a protocol for integrated expansion and cardiac differentiation of hiPSCs as aggregates in 100 mL VWBRs, as well as characterising these bioreactors in terms of oxygen mass transfer. Initially, the expansion under various different conditions was tested, namely in terms of different feeding strategies—repeated batch and fed-batch—and dextran sulfate (DS) supplementation. In optimal conditions (repeated batch and DS supplementation), a maximum cell density of $(2.3 \pm 0.2) \times 10^6$ cells·mL^{-1} was achieved in 5 days, representing a 9.3 ± 0.6–fold increase relatively to the inoculum. Following the optimisation of the expansion stage, and based on previous reports, the conditions were adjusted to maximise the cardiac differentiation. By applying continuous control of WNT signalling, a maximum 73.3% cardiomyocytes could be obtained following 15 days of differentiation. In order to predict the effect of larger scales on the culture, namely in terms of agitation and oxygen mass transfer, a computational fluid dynamics model was developed and validated with experimental data. This model predicted the mixing profile inside the 100 mL VWBR, as well as the volumetric mass transfer coefficient (k_La) of the system at different agitation velocities.

The results obtained show that the VWBR can sustain aggregate expansion and cardiac differentiation of hiPSCs. Although more extensive studies and optimisation are required, this system shows promise for the biomanufacturing of hiPSC-derived cardiomyocytes under Good Manufacturing Practices for the development of hiPSC-based cardiac therapies, or for pharmacological applications.

Keywords

human induced pluripotent stem cells; cardiomyocytes; cardiac differentiation; Vertical-Wheel bioreactors; computational fluid dynamics

RESUMO

As doenças cardiovasculares (CVDs) limitam a qualidade de vida dos pacientes e são responsáveis por milhões de mortes todos os anos. Embora os tratamentos possam mitigar alguns sintomas e proteger o coração após enfarte do miocárdio, a morte de cardiomiócitos é, até ao momento, irreparável devido à sua limitada capacidade de proliferação. As células estaminais pluripotentes induzidas humanas (hiPSCs) têm a capacidade de se auto-renovarem e de se diferenciarem em todos os tipos de células do corpo humano, e podem ser reprogramadas a partir das células dos próprios pacientes. Portanto, as hiPSCs poderão potencialmente ser aplicadas no desenvolvimento de tratamentos inovadores para uma miríade de CVDs. Com este intuito, metodologias para a sua expansão e diferenciação cardíaca de forma escalonável e robusta terão que ser desenvolvidas. Os biorreatores Vertical-Wheel (VWBRs), descartáveis, têm um inovador e gentil sistema de agitação, e encontram-se disponíveis às escalas de laboratório e de produção. Assim sendo, têm potencial para serem aplicados na biomanufatura à escala clínica de cardiomiócitos derivados de hiPSCs.

O âmbito desta tese foi o desenvolvimento de um protocolo integrado para expansão e diferenciação cardíaca de hiPSCs enquanto agregados em VWBRs de 100 mL, bem como a caracterização destes reatores em termos de transferência de massa de oxigénio. Inicialmente, foi testada a expansão sob várias condições, nomeadamente em termos de estratégias de alimentação – descontínua repetida (*repeated batch*) e semi-contínua – e suplementação com sulfato de dextrano (DS). Nas condições ótimas (alimentação descontínua repetida e suplementação com DS), foi atingida uma densidade celular máxima de $(2,3 \pm 0,2) \times 10^6$ células·mL^{-1} em 5 dias, representando um aumento de 9,3 ± 0,6 vezes face ao inóculo. Após a otimização da etapa de expansão, e com base em estudos prévios, as condições foram ajustadas com o intuito de maximizar a diferenciação cardíaca. A utilização de uma estratégia de controlo contínuo da via de sinalização WNT levou à obtenção de um máximo de 73,3% de cardiomiócitos após 15 dias de diferenciação. De forma a prever o efeito do aumento de escala na cultura, nomeadamente no que respeita à agitação e à transferência de massa de oxigénio, um modelo de dinâmica de fluidos computacional foi desenvolvido e validado com dados experimentais. Este modelo pôde prever o perfil de agitação no interior do VWBR de 100 mL, assim como o coeficiente volumétrico de transferência de massa (k_La) do sistema a diferentes velocidades de agitação.

Os resultados obtidos demonstram que o VWBR pode sustentar a expansão e diferenciação cardíaca de hiPSCs enquanto agregados. Embora seja necessário realizar estudos e otimizações mais extensos, este sistema revelou-se promissor para a biomanufatura de cardiomiócitos derivados de hiPSCs sob Boas Práticas de Fabrico para o desenvolvimento de terapias cardíacas baseadas em hiPSCs, assim como para aplicações farmacológicas.

Palavras-chave

células estaminais pluripotentes induzidas humanas; cardiomiócitos; diferenciação cardíaca; biorreatores Vertical-Wheel; dinâmica de fluidos computacional

LIST OF CONTENTS

LIST OF TABLES

LIST OF FIGURES

LIST OF ABBREVIATIONS

A

AT – adipose tissue

B

BdtBPP – *bis*(2,4-di-*tert*-butylphenyl)phosphate
bFGF – basic fibroblast growth factor
BFP – blue fluorescent protein
BM – bone marrow
BMP – bone morphogenic protein

C

CDM3 – chemically-defined medium, 3 components
cDNA – complementary DNA
CFD – computational fluid dynamics
CHIR – CHIR99021
CHO – Chinese Hamster Ovary
CIP – cleaning in place
CPC – cardiac progenitor cell
cTNI – cardiac troponin I
cTNT – cardiac troponin T
CVD – cardiovascular disease

D

DAPI – 4′,6-diamidino-2-phenylindole
DKK – Dickkopf-related protein
DMEM – Dulbecco's Modified Eagle's Medium
DoE – Design of Experiments
DPBS – Dulbecco's phosphate-buffered saline
DS – dextran sulfate

E

E8 – Essential 8
EB – embryoid body
EC – extracapillary
EC_{50} – half-maximal effective concentration
ECM – extracellular matrix
EDTA – ethylenediaminetetraacetic acid
eGFP – enhanced green fluorescent protein
EMA – European Medicines Agency
ESC – embryonic stem cell
EV – extracellular vesicle

F

FACS – fluorescence-activated cell sorting
FBS – foetal bovine serum
FDA – Food and Drug Administration
FGF – fibroblast growth factor
FHF – first heart field

G

GAPDH – glyceraldehyde-3-phosphate dehydrogenase
GATA – GATA-binding protein
GCV – ganciclovir
GFR – glial cell line-derived neurotrophic factor receptor
GiWi – GSK3 inhibition/WNT inhibition
$GiWi_{cont}$ – continuous GSK3 inhibition/WNT inhibition
GMP – Good Manufacturing Practices
GREM – GREMLIN
GSK – glycogen synthase kinase

H

HCN – hyperpolarisation-activated cyclic nucleotide-gated channel
hESC – human embryonic stem cell
hHSPC – human haematopoietic stem/progenitor cell
hiPSC – human induced pluripotent stem cell
HLA – human leukocyte antigen
hMSC – human mesenchymal stromal cell
hNSC – human neural stem cell
hPL – human platelet lysate
hPSC – human pluripotent stem cell

HSVtk – herpes simplex virus thymidine kinase
HUCAC – human umbilical cord artery cell

I
IC – intracapillary
ICM – inner cell mass
iPSC – induced pluripotent stem cell
ITG – integrin
IWP – inhibitor of WNT production
IWR – inhibitor of WNT response

J
JNK – c-Jun N-terminal kinase

K
KAI – kangai
KDR – kinase insert domain receptor
KLF – Krüppel-like factor
KO – KnockOut

L
LES – large eddy simulation

M
MACS – magnetic-activated cell sorting
MEF – myocyte-specific enhancer factor
MEM – Minimum Essential Medium
mESC – mouse embryonic stem cell
MESP – mesoderm posterior
MHC – myosin heavy chain (protein)
miPSC – mouse induced pluripotent stem cell
miRNA – micro RNA
miRNA switch – miRNA-responsive, synthetic modified mRNA switch
MLC – myosin light chain (protein)
MLC2a – myosin light chain 2, atrial isoform
MLC2v – myosin light chain 2, ventricular isoform
mRFP – monomeric red fluorescent protein
mRNA – messenger RNA
***MYH* –** myosin heavy chain (gene)
***MYL* –** myosin light chain (gene)

N
NRG – neuroregulin

O
OCT – octamer-binding transcription factor
OUR – oxygen uptake rate
OTR – oxygen transfer rate
OXPHOS – oxidative phosphorylation

P
PAX – paired box protein
PDGFR – platelet-derived growth factor receptor
PECAM – platelet endothelial cell adhesion molecule
PEG – polyethylene glycol
PLGA – poly(lactic-co-glycolic acid)
PNIPAAm – poly(N-isopropylacrylamide)
PVA – polyvinyl alcohol

Q
QbD – Quality by Design
QES – Quantum Cell Expansion System
qRT-PCR – quantitative real-time polymerase chain reaction

R
RBC – red blood cell
RCCS – rotary cell culture system
ROCK – Rho-associated, coiled-coil containing protein kinase
RPMI – Roswell Park Memorial Institute

S
SEM – standard error of the mean
SHF – second heart field
SIP – steaming in place
SIRP – signal regulatory protein
sMHC – soluble myosin heavy chain

SOX – (sex-determining region Y)-box transcription factor

SSEA – stage-specific embryonic antigen

STBR – stirred tank bioreactor

T

TBPP – *tris*(2,4-di-*tert*-butylphenyl)phosphate

TBX – T-box transcription factor

TGF – transforming growth factor

THY – thymus cell antigen

TMRM – tetramethylrhodamine methyl ester percholate

TRA – tumour rejection antigen

TNNT – troponin T

TUJ1 – neuron-specific class III β-tubulin

U

UCB – umbilical cord blood

UCM – umbilical cord matrix

V

VCAM – vascular cell adhesion molecule

VEGF – vascular endothelial growth factor

VWBR – Vertical-Wheel bioreactor

W

WALE – wall-adapting local eddy-viscosity

WHO – World Health Organization

WNT – wingless-related integration site

AIM OF STUDIES AND THESIS OUTLINE

Cardiovascular diseases are the leading cause of death in the world and, in the surviving cases, are responsible for a significant decrease in the quality of life of the surviving patients. Although a number of preventive drugs, as well as therapies aiming to protect the heart and/or restore blood flow post–myocardial infarction already exist, regenerating the adult heart is still very difficult. In fact, adult cardiomyocytes are post-mitotic, and their death *en masse* following an infarction event leads to their replacement by fibrotic tissues.

In 2006, the ground-breaking development of methods of reprogramming somatic cells to an embryonic-like state revolutionised medicine. Human induced pluripotent stem cells (hiPSCs) are able to self-renew and to differentiate into all cell types of the body. As such, it is now possible to obtain *quasi*-embryonic cells from adult tissues, which is not only advantageous due to their differentiation potential, this also allows for the generation of patient-specific cells envisioning diverse applications, including drug screening and disease modelling, as well as Regenerative Medicine.

Naturally, the number of cells required for either of these applications will have to be developed in large-scale systems which allow for their bioproduction under Good Manufacturing Practices. Bioreactors present many desirable characteristics, being 3D, scalable systems which allow for monitoring and control of the culture and permit the application of different medium feeding strategies. In particular, the Vertical-Wheel bioreactors (VWBRs), by PBS Biotech, apply a large vertical impeller, combining radial and axial agitation, which, along with the U-shaped bottom of the vessel, allow for efficient agitation of the culture with minimal power input. Furthermore, the vessels are single-use, limiting contamination, and are available at many scales, from 100 mL to 80 L, allowing their use from lab scale studies to large scale process development. As such, VWBRs have the potential to be used for the production of hiPSC-derived cardiomyocytes aiming at studying cardiovascular diseases or, prospectively, for *in vivo* cardiac regeneration.

The objective of this thesis was to develop a protocol for integrated expansion and differentiation of hiPSCs in Vertical-Wheel bioreactors, as well as to characterise this system in terms of oxygen mass transfer, envisaging the scale-up of the protocol towards more clinically compatible scales. Specifically, this thesis aimed to answer the following research questions:

1. Can the VWBR sustain **integrated hiPSC expansion and cardiac differentiation**? What are the **optimal conditions** for this bioprocess?
2. Which **engineering characteristics** distinguish the **VWBR** from other bioreactor systems? Specifically, are the **hydrodynamics** and **oxygen mass transfer** of the bioreactor suitable for hiPSC culture?

With the intent of answering these questions, this thesis was structured as follows:

Chapter I initially introduces some concepts regarding stem cells, in particular human pluripotent stem cells (hPSCs). Then, general concepts for their culture in bioreactors, along with the state-of-the-art in single-use bioreactor for stem cells are discussed. A description of human heart

development is presented, along with its translation to *in vitro* protocols for cardiac differentiation of hPSCs. Finally, strategies for purification and maturation of hPSC-derived cardiomyocytes are reviewed.

Chapter II details the development of a protocol for expansion of hiPSCs in VWBRs, applying different feeding strategies (repeated batch and fed-batch), and testing the effect of anti-aggregation and anti-apoptosis molecule dextran sulfate (DS). The repeated batch approach led to the highest fold expansion, particularly when combined with DS supplementation.

Following the establishment of the expansion conditions, **Chapter III** describes initial attempts of inducing cardiac differentiation of hiPSCs in VWBRs. It was possible to generate hiPSC-derived cardiomyocytes, however, considerable cell death was observed. As such, this protocol still requires optimisation, nevertheless, it was a first step towards achieving a robust protocol for cardiac differentiation of hiPSCs in VWBRs.

Chapter IV details some initial results in the characterisation of the PBS MINI 0.1 VWBR, in terms of velocity profiles and volumetric oxygen mass transfer coefficient (k_La), along with experimental validation of the results. Implementation of this model at higher scales will allow for the development of scale-up strategies for the hiPSC culture being optimised at a 60 mL working volume.

Finally, **Chapter V** provides general conclusions about the overall work, some future work which has to be developed, as well as possible future trends for the field.

CHAPTER I.

INTRODUCTION

The contents of this chapter were partially based on the following publications:

Nogueira, D. E. S., C. A. V. Rodrigues and J. M. S. Cabral (2021). Emerging strategies for scalable human induced pluripotent stem cell expansion and differentiation. *Methods in iPSC Technology*. A. Birbrair, Elsevier**:** 163-185. Reproduced with permission. Copyright 2021, Elsevier.

Nogueira, D. E. S., J. M. S. Cabral and C. A. V. Rodrigues (2021). Single-Use Bioreactors for Human Pluripotent and Adult Stem Cells: Towards Regenerative Medicine Applications. *Bioengineering (Basel)* **8**(5): 68. Reproduced under the terms of the Creative Commons CC-BY license. Copyright 2021, The Authors.

I.1. Stem cells

The expression “Regenerative Medicine” dates back to at least 1992 (Kaiser 1992), but its concept, the regeneration of tissues and cells damaged by ageing, injury or disease, can be found as far back as Greek mythology (Schneider 2004, Power and Rasko 2008). Enraged by Prometheus’s betrayal, Zeus chained him to a rock and had his liver being eaten by an eagle every day, while it would fully regenerate every night. While Regenerative Medicine is not yet this efficient, landmark discoveries in stem cell biology and bioengineering in the past few years are leading to exciting advances that may revolutionise the field in the next decades.

Stem cells do not have a specialised function but, at the same time, are of crucial importance for human development and homeostasis. In fact, an individual loses about 0.5% of their human cells per day (Bianconi et al. 2013, Sender et al. 2016, Liu et al. 2018b), as such, the long lifespans characteristics of humans can only be achieved by stem cell–based cellular mechanisms which replenish these cells at the same rate as they die. This is possible through the two main and unique characteristics of stem cells—the ability to self-renew and to differentiate.

The self-renewal of stem cells is their capacity to generate, among the daughter cells formed during division, one which is identical to the parental cell. *In vivo*, independently of the stem cell division being symmetrical (forming two daughter stem cells), or asymmetrical (generating one stem cell and one differentiated cell) the stem cell pool is always maintained, thus sustaining the homeostasis of the body (He et al. 2009, Fuchs and Chen 2013).

As for the differentiation, it consists of the transformation of the stem cell into a specialised, functional cell, such as a cardiac, neural or blood cell. Intermediate, progenitor cells are also generally formed throughout this differentiation process. The types of progeny a stem cell can generate depend on its differentiation potential (Zakrzewski et al. 2019) (Figure I.1).

Totipotent cells generate all cell types of an organism, along with extraembryonic tissues which support it, including the placenta and the umbilical cord. As such, by itself, a totipotent cell can generate a whole organism. The zygote, and its subsequent divisions, are totipotent.

Pluripotent stem cells can also generate all cell types of an organism, but are unable to form the extraembryonic tissues. Embryonic stem cells (ESCs) are pluripotent and are obtained from *in vitro* culture of cells from the inner cell mass (ICM) of the blastocyst. Somatic cells can also be reprogrammed to a *quasi*-pluripotent state (induced pluripotent stem cells (iPSCs)), which will be discussed further on section I.1.1.

Multipotent stem cells have the potential to differentiate into at least two different cell types. Many adult stem cells, such as haematopoietic stem/progenitor cells or mesenchymal stromal cells, are multipotent.

Unipotent stem cells have the most limited differentiation potential, and can generate a single type of terminally differentiated cell. Spermatogonial stem cells, for instance, only differentiate into sperm.

The first major description of stem cells dates from 1961, when Till and McCulloch investigated the proliferative ability of adult mouse bone marrow (BM) cells when injected in isologous hosts (Till and McCulloch 1961). Since then, almost six decades of stem cell research have allowed for countless

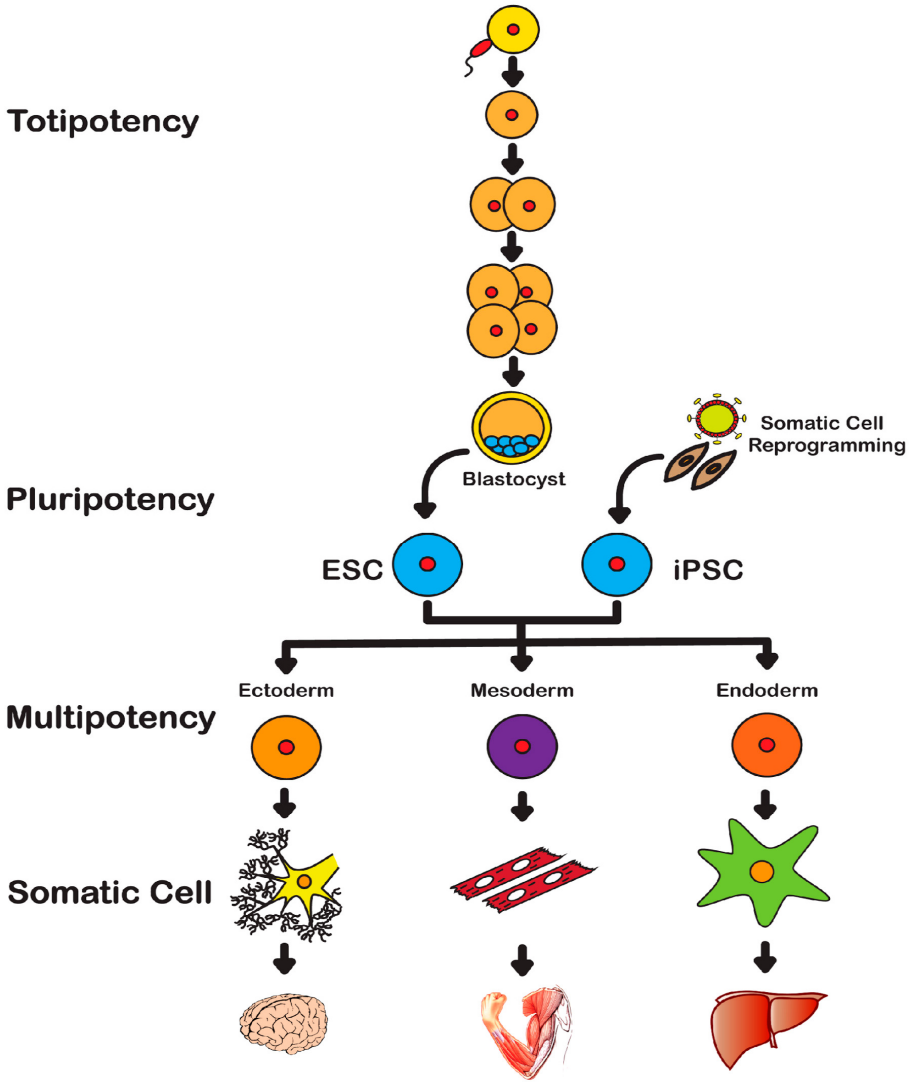

Figure I.1 – Overview of the differentiation potential of stem cells. The zygote is totipotent, as it is able to generate a full individual. ESCs are isolated from the ICM of the blastocyst, and they are pluripotent as they can generate any cell type from the three germ layers (ectoderm, mesoderm and endoderm), albeit not the extra-embryonic tissues. iPSCs, obtained from reprogramming of somatic cells, are similar to ESCs. Adult stem cells are either multipotent, generated a limited number of different cell types, or unipotent if they can only generate one cell type. These cells terminally differentiate into the somatic cells which compose the tissues. From Menon et al. (2016). Reproduced under the terms of the Creative Commons CC-BY license. Copyright 2016, The Authors.

advances in the field, including the ability to use these cells for the benefit of human health. Human pluripotent stem cells (hPSCs), which will be discussed in the following sections, are of particular interest, due to their extensive differentiation potential.

I.1.1. Pluripotent stem cells

Following fecundation, the zygote successively divides and develops (Figure I.2). As it develops, it eventually forms the blastocyst, a structure composed of an outer layer of cells, the trophoblast, and an ICM. The trophoblast generates the extraembryonic structures, such as the placenta, which will support the embryo and allow it to develop *in utero*. Meanwhile, the ICM will form the gastrula, which is composed of three layers, the endoderm, mesoderm and ectoderm. Each of these layers will eventually

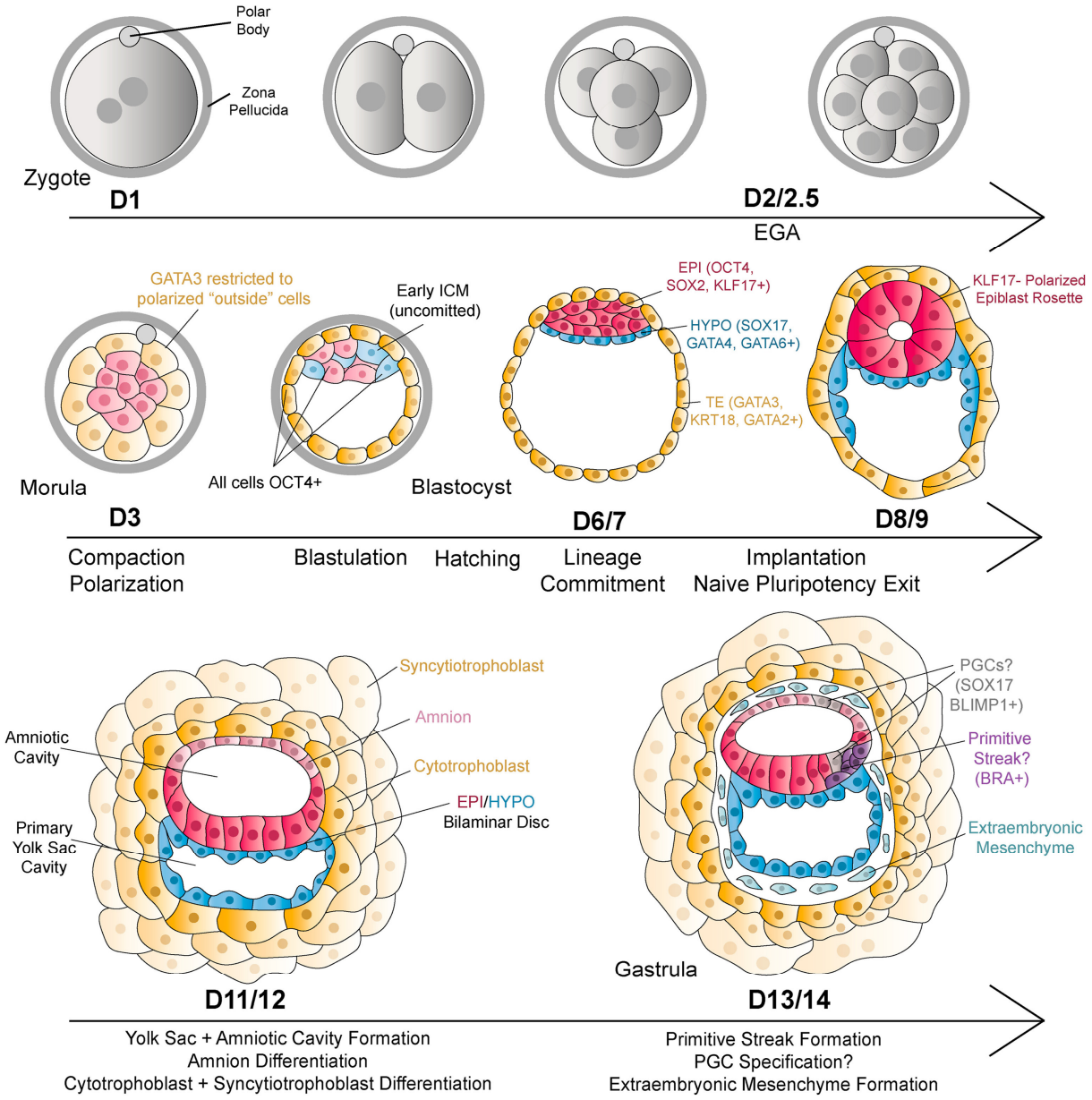

Figure I.2 – Initial stages of human embryonic development. Initially, the zygote divides successively, until forming the 16-cell morula. The interior cells of the morula will form the ICM of the blastocyst, while the exterior cells will generate the trophoectoderm. From the ICM, the epiblast and the hypoblast will form, and will eventually generate the ectoderm and endoderm, respectively. By day 14 post-coitum, some BRACHYURY^{+} cells will be observed at the posterior epiblast, marking the formation of the primitive streak. From Weatherbee et al. (2021). Reproduced with permission. Copyright 2021, Elsevier.

differentiate into distinct types of somatic cells, which will develop in various biological systems and, eventually, a complete, mature individual (Gerri et al. 2020, Ghimire et al. 2021). As such, by culturing cells from the ICM *in vitro*, it is possible to obtain human embryonic stem cells (hESCs), which can differentiate into all cell types of the body.

Mouse embryonic stem cells (mESCs) were first derived in 1981 and were shown to be able to differentiate both *in vitro*, and *in vivo* via tumour formation (Evans and Kaufman 1981, Martin 1981). Later, in 1998, Dr James Thomson and co-workers successfully reported the first isolation of hESCs, and their maintenance in culture for 5 months (Thomson et al. 1998). This symbolised a major

breakthrough for medicine, as these cells not only provided new insights in embryonic development (reviewed in Heemskerk and Warmflash (2016)), they also represented a new source of cells for organ models on a dish (Clevers 2016, McCauley and Wells 2017) as well as potential for Regenerative Medicine (Ilic and Ogilvie 2017).

However, despite its importance, the pluripotency of hESCs is also problematic for *in vivo* applications, due to the possibility of forming benign tumours (teratomas) when transplanted to a host (Blum et al. 2009). As such, transplanted derivatives of these cells must be completely depleted of undifferentiated hESCs prior to use. Moreover, hESC isolation requires the destruction of human embryos, which is ethically problematic and restricts the use of these cells in various countries (Matthews and Morali 2020).

In 2006, Takahashi and Yamanaka first reported the derivation of mouse iPSCs (miPSCs) (Takahashi and Yamanaka 2006) (earning Dr Shinya Yamanaka the Nobel Prize in Physiology or Medicine in 2012), which was followed by the generation of human iPSCs (hiPSCs) in 2007 by the labs of both Dr Shinya Yamanaka (Takahashi et al. 2007) and Dr James Thomson (Yu et al. 2007). These cells are derived from somatic cells, by reprogramming them to a pluripotent state via administration of a combination of factors expressed by hESCs, such as OSKM (octamer-binding transcription factor (OCT) 4, (sex-determining region Y)-box transcription factor (SOX) 2, Krüppel-like factor (KLF) 4, C-MYC), NANOG, LIN28, etc.

The reprogramming of somatic cells to hiPSCs has already been achieved with several different approaches (Figure I.3). The factor delivery may be performed through retroviral (Takahashi et al. 2007, Yu et al. 2007) or lentiviral (Warlich et al. 2011) transduction—infecting only dividing cells or all cells, respectively—, or by a transposase/transposon system (piggyBac) (Woltjen et al. 2009). In all of these cases, the transgene is integrated in the genome of the host cells. Naturally, this poses an important security concern, in particular concerning the administration of oncogenic factors such as C-MYC, as such, a myriad of non-integrating methods have since been developed. Transduction using adenoviruses (Zhou and Freed 2009) and Sendai viruses (Nishimura et al. 2011) allows for persistent gene expression for cellular reprogramming, but with the possibility of removing the viral genome. Factor delivery may also be performed via transfection with plasmids (Si-Tayeb et al. 2010) or minicircles (Jia et al. 2010) (the latter lacking bacterial DNA), avoiding the use of viruses. Other viable non-integrating options are reliant on RNA (messenger RNA (mRNA) (Warren et al. 2010) or micro RNA (miRNA) (Anokye-Danso et al. 2011)), proteins (Kim et al. 2009) or small molecules (Li and Rana 2012). The choice of the reprogramming method to use will naturally be dependent on the application (with non-integrating methods preferrable for *in vivo* applications), on their efficiency, time and cost, and on specificities of the cells to be reprogrammed.

The use of hiPSCs allows for the harnessing of pluripotency while overcoming the ethical issues involved with embryo manipulation. As such, there are substantially less restrictions associated with these cells. Moreover, since they are derived from somatic cells, hiPSCs allow to overcome issues related with recipient/donor variability, such as rejection or graft-versus-host disease. In fact, the advent of hiPSCs was an important achievement for “precision medicine”, a new paradigm in medicine

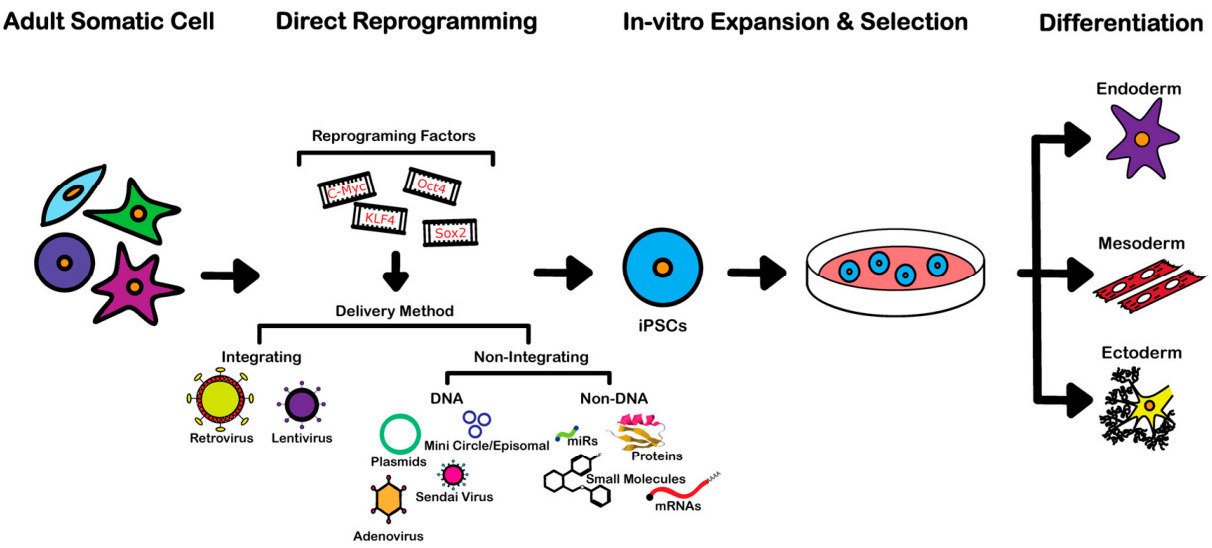

Figure I.3 – Methods of somatic cell reprogramming to iPSCs. Delivery of reprogramming factors can be performed via integrating or non-integrating delivery, the latter consisting of DNA– and non-DNA–based methods. Following their expansion and selection *in vitro*, these iPSCs can be differentiated into cells from the three germ layers. From Menon et al. (2016). Reproduced under the terms of the Creative Commons CC-BY license. Copyright 2016, The Authors.

consisting in the development of diagnostic mechanisms and therapies tailor-made to the needs of each specific individual (Mirnezami et al. 2012, Collins and Varmus 2015).

Conversely, hiPSCs can maintain some epigenetic memory of their differentiated state, such as methylation profiles, which can restrict or lead their differentiation potential to a specific lineage. These "primed" hiPSCs can, however, be converted to a "naïve" state (Yagi et al. 2017), with an increased growth and differentiation potential (described in more detail in section I.1.2.6).

I.1.2. Large-scale culture of human pluripotent stem cells

Pharmacological applications of hiPSCs are evolving towards high-throughput systems, such as labs-on-a-chip (Neuzi et al. 2012, Chan et al. 2013), allowing for parallel testing of various conditions, which may require high numbers of cells. The use of hiPSCs and derivatives in Regenerative Medicine will also require mechanisms of reproducible and controlled large-scale production of these cells under Good Manufacturing Practices (GMP) (Figure I.4). Specifically, about 10^9–10^{10} cells are expected to be required for regeneration of organs such as the heart or the liver (Zweigerdt 2009).

Traditional hiPSC culture relied on 2D culture platforms, such as tissue culture plates or T-flasks, where the cells grow as a monolayer to confluency before being passaged. This scale-out strategy is feasible if small numbers of cells are required. However, since the number of plates or flasks increases with each successive passage, it rapidly becomes labour-intensive and impractical at a production scale. Furthermore, culturing cells on non-physiological 2D systems (e.g., culture plates) affects factors such as cell structure or sensitivity to signalling and apoptosis, ultimately having a decisive effect on cell fate (Krtolica et al. 2007, Baker and Chen 2012). These limitations have promoted the research of alternative culture platforms for hiPSC expansion, such as bioreactors.

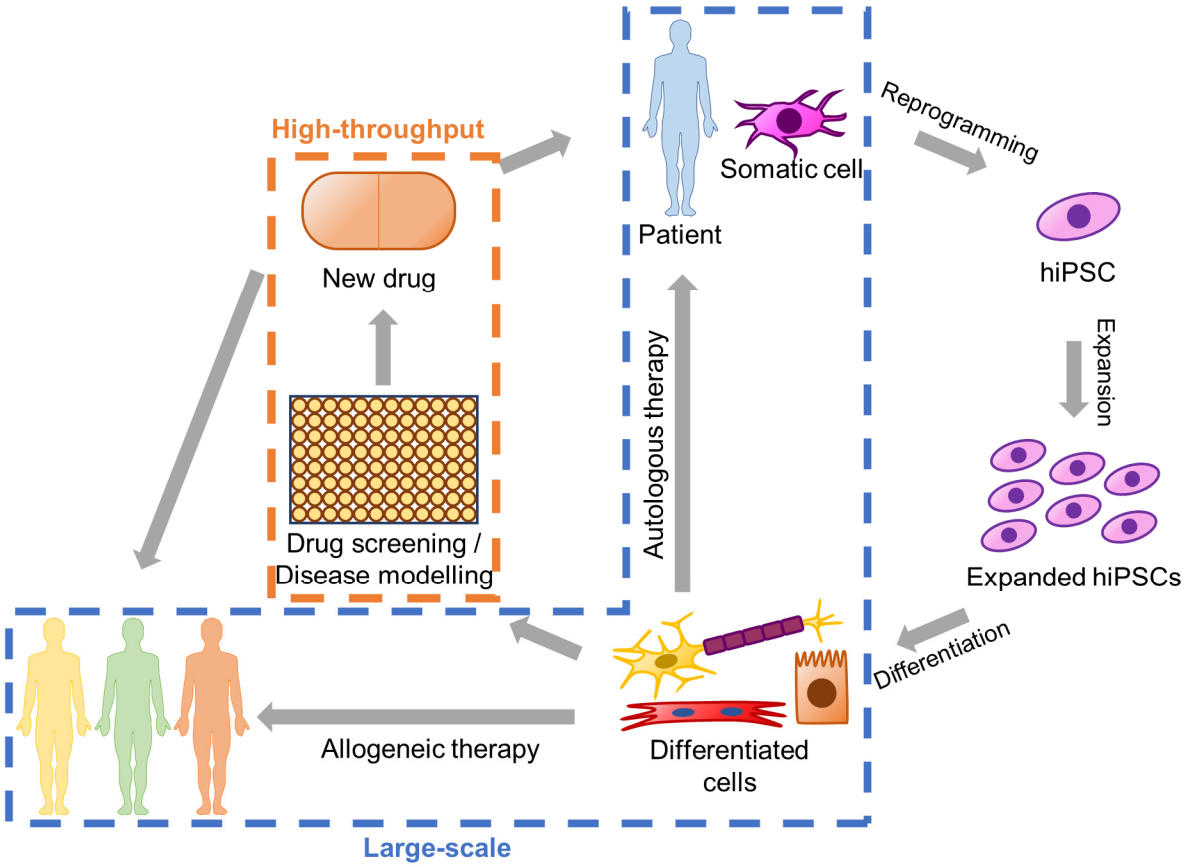

Figure I.4 – Patient-derived hiPSCs can be used for a variety of applications. Differentiated hiPSCs can be used for drug screening and disease modelling, as well as for therapeutic approaches. From Nogueira et al. (2021b). Reproduced with permission. Copyright 2021, Elsevier.

Bioreactors provide many culture possibilities which are advantageous for quality manufacturing of hiPSCs. These culture platforms are equipped with agitation mechanisms in order to ensure the homogeneity of the system and an even distribution of nutrients and oxygen. Many bioreactors are available from bench to industrial scales, allowing for scalability of the culture without increasing the number of vessels. Moreover, bioreactors normally contain several probes to monitor essential culture parameters (e.g., temperature, pH, dissolved oxygen, concentration of specific nutrients and metabolites), and control systems which act automatically to maintain these parameters within a desired range. Finally, bioreactor cultures are compatible with a variety of medium feeding strategies, from repeated batch (commonly used in 2D static cultures), to fed-batch (Schwedhelm et al. 2019) and perfusion (Serra et al. 2010, Kropp et al. 2016), which may provide additional process improvements and cellular outcomes. Nevertheless, traditional stirred-tank bioreactors (STBRs) were optimised for applications where the cells are not the final product. Therefore, the need for new bioreactors arises; these should be optimised for the specific needs of hiPSCs, allowing for their undifferentiated expansion, and/or exploring specific cues which may induce the cells into differentiation.

Unlike hiPSCs, differentiated cells are not naturally proliferative (Ruijtenberg and van den Heuvel 2016, Liu et al. 2019), leading to the importance of optimising the undifferentiated expansion phase. Besides bioreactor geometry, other parameters such as the culture medium, the oxygen concentration and the pH, also have an effect on the overall performance of the culture and may

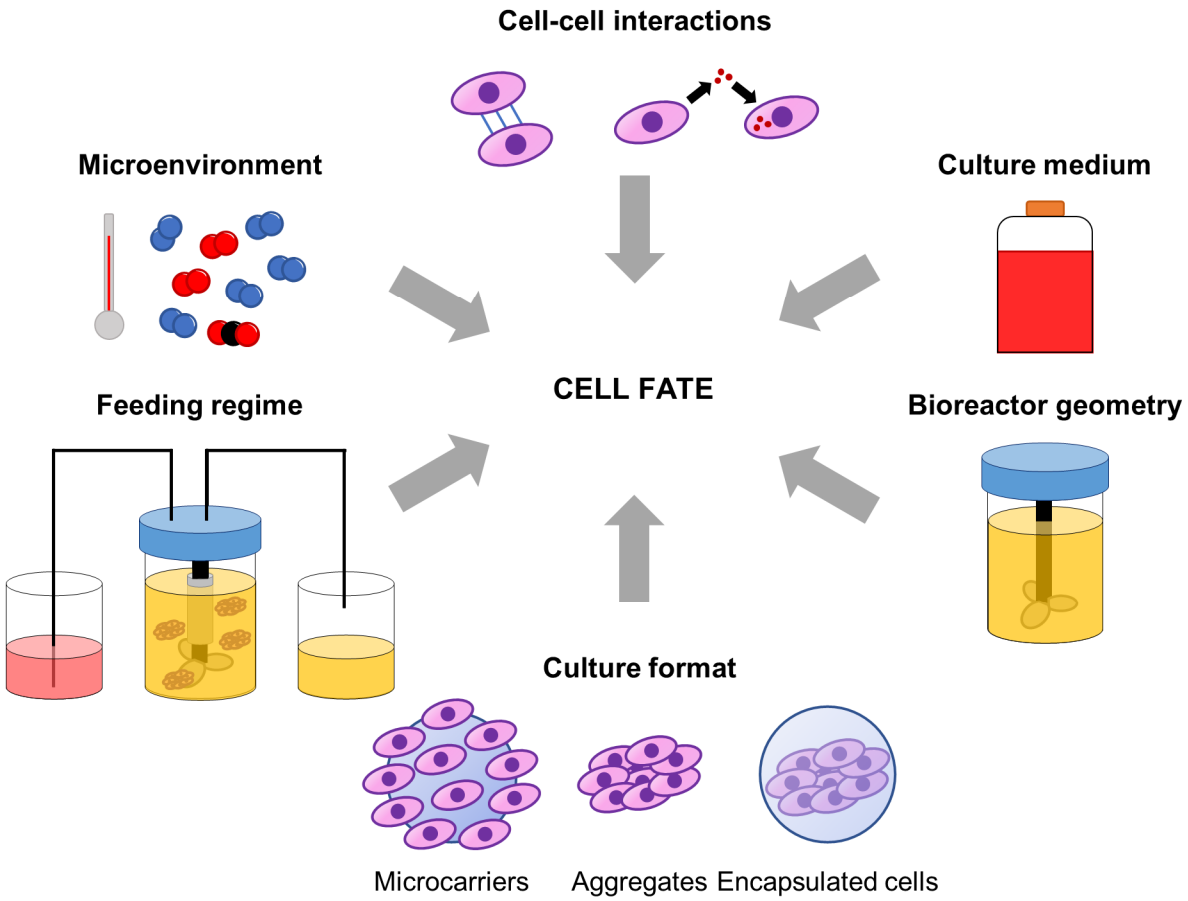

Figure I.5 – Cell fate is influenced by a variety of factors, ranging from cell communication to the conditions which are used for cell culture. Appropriate control of these factors is required to ensure robust expansion and differentiation of hiPSCs. From Nogueira et al. (2021b). Reproduced with permission. Copyright 2021, Elsevier.

influence both hiPSC expansion and differentiation (Figure I.5). This section will detail some of the factors which affect the growth of hiPSCs and should be taken into consideration to design a bioreactor culture.

I.1.2.1. Microenvironment

The microenvironment in which the cells are expanded, particularly factors such as temperature, pH, osmolarity or atmosphere, is vital to guarantee not only cell viability, but also the success of specific differentiation strategies.

Cell culture is routinely performed at 37 °C, the normal temperature of the human body. The medium pH and osmolarity should be maintained at adequate values to promote undifferentiated cell growth, with the pH being typically kept at the physiological value of 7.4, and the osmolarity at about 290–350 mOsm L^{-1} (Ludwig et al. 2006b, Chen et al. 2011b, Rajala et al. 2011). Notably, some studies suggest hiPSC expansion to be optimal at other pH values, as low as 7.1 (Ludwig et al. 2006b, Kuo et al. 2020). The rapid growth of proliferative cells, such as hiPSCs, is supported by glycolysis even in the presence of oxygen, in a phenomenon known as the Warburg effect (Vander Heiden et al. 2009, Varum et al. 2011) (Figure I.6). One of the by-products of glycolysis is lactate, and its accumulation with hiPSC proliferation leads to a gradual decrease in pH over time. If the culture pH decreases substantially

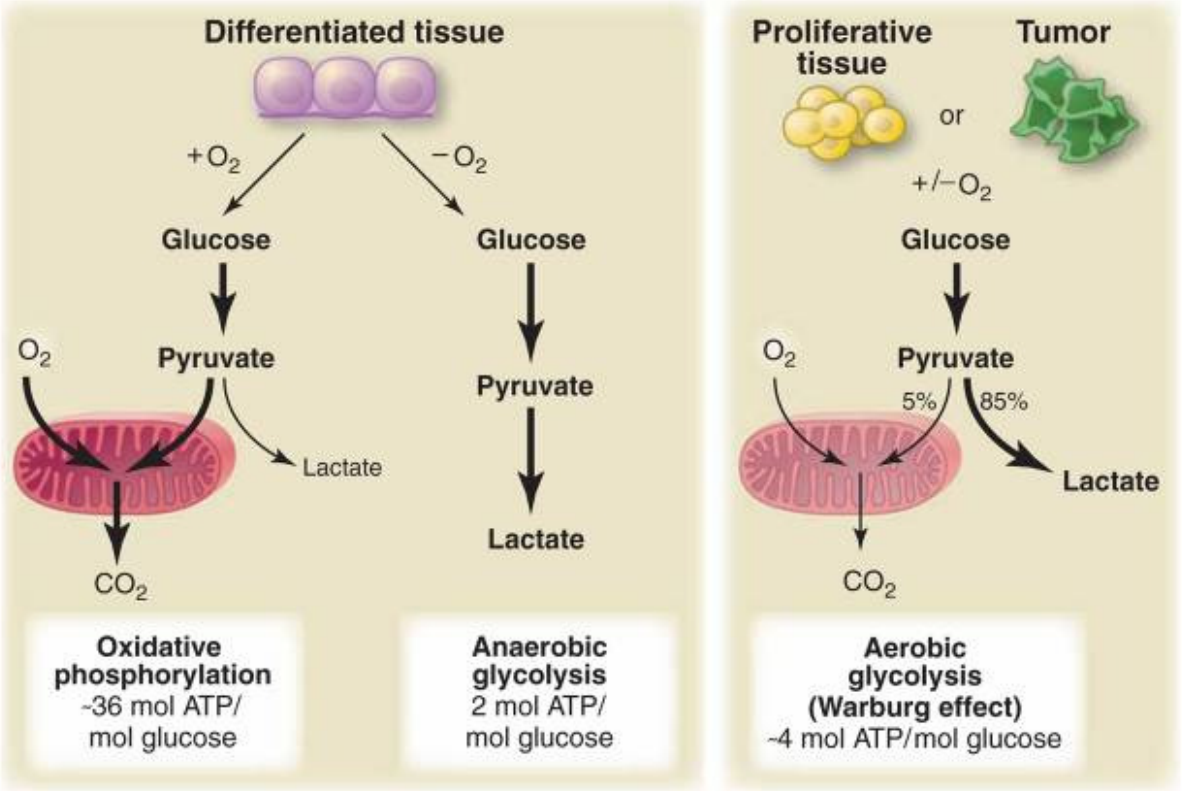

Figure I.6 – Representation of the metabolism of differentiated tissues and proliferative tissues. Cells in differentiated tissues rely on oxidative phosphorylation for their energy demand when in the presence of oxygen. In its absence, the cells switch to a glycolytic metabolism, with a notorious smaller yield in ATP. Conversely, proliferative tissues predominantly rely on glycolysis, even in the presence of oxygen (Warburg effect). From Vander Heiden et al. (2009). Reprinted with permission from AAAS. Copyright 2009, American Association for the Advancement of Science.

beyond physiological values, hiPSC growth is impaired (Liu et al. 2018a). For this reason, cells are cultured in a 5–10% CO_2 atmosphere which, in combination with the high concentrations of sodium bicarbonate present in most hiPSC culture media, mitigates the pH decrease effect of lactate. Bioreactor systems can provide more advanced pH control by addition of base when the bicarbonate/CO_2 buffering effect is not sufficient.

Although many studies describe cell culture in an air/CO_2 atmosphere, with an oxygen concentration of about 20%, *in vivo*, the embryo is subjected to an hypoxic environment (about 3% oxygen (Burton and Jaunaiux 2001)), likely as a protection against oxidative stress. Therefore, culture of hPSCs under hypoxia (2–6% O_2) has been shown to lead to a more robust maintenance of pluripotency (Ezashi et al. 2005, Fynes et al. 2014) and increased genomic stability (Forsyth et al. 2006), as well as improved expansion in suspension culture (Serra et al. 2010). Moreover, oxygen control has also been demonstrated to improve specific differentiation outcomes; for instance, hypoxia (4% O_2) has been described to enhance cardiac differentiation in bioreactors (Niebruegge et al. 2009), whereas hyperoxia (60% O_2) was shown to lead to increased pancreatic differentiation (Hakim et al. 2014). Despite these results, the effect of oxygen in hPSC cultures is still shrouded in some controversy and requires further study. For instance, and contrast with other studies, Chen and co-workers observed hypoxia to impair the growth rate of hiPSCs with no significant impact in the maintenance of pluripotency

(Chen et al. 2009). In aggregate culture systems, this analysis is even more complex as due to diffusional limitations, there is a gradient of oxygen concentrations towards the centre of the aggregates even in controlled cultures at atmospheric oxygen (Van Winkle et al. 2012, Wu et al. 2014). As such, there is no clear consensus on how oxygen control may impact the bioprocessing of hiPSCs, but new advances in the field, such as more detailed metabolomic and transcriptomic analysis, as well as characterising the oxygen distribution profiles under various atmosphere compositions, will undoubtedly provide more insights on the ideal conditions for expansion and differentiation of these cells.

I.1.2.2. Culture media

One of the most important aspects in hiPSC culture is the culture medium. Besides maintaining a suitable pH and osmolarity, the culture medium provides the necessary nutrients for cell expansion (e.g., sugars, amino acids, lipids) and growth factors which maintain the cells in an undifferentiated state. Many formulations for hiPSC maintenance are commercially available, including mTeSR1, mTeSR Plus, TeSR2, mTeSR3D, TeSR-E8, TeSR-E8 3D (all from STEMCELL Technologies), Essential 8 (E8), E8 Flex, StemPro, StemFlex (all from Thermo Fisher Scientific), NutriStem (Biological Industries) and PluriSTEM (Millipore).

Dulbecco's Modified Eagle's medium (DMEM)/F12 is the most common basal medium for hiPSC culture, as it was shown to perform better for expansion of these cells in comparison to other basal media (Chen et al. 2011b). This medium is comprised of DMEM, a formulation for mammalian cells with high concentrations of nutrients, and Ham's F12, an optimised formulation for serum-free culture of Chinese Hamster Ovary (CHO) cells. Although DMEM/F12 supplies many of the nutrients the cells require for their growth, including glucose, vitamins and amino acids, this medium cannot sustain hiPSC growth by itself. For that reason, hiPSC culture media contain additional supplements which improve cell survival, growth and maintenance of pluripotency. mTeSR1, one of the most widespread media for hiPSC expansion, supplements the basal DMEM/F12 with 18 additional components, including bovine serum albumin, vitamins, antioxidants, minerals, lipids and growth factors (Ludwig et al. 2006a, Ludwig et al. 2006b, Ludwig and Thomson 2007). Although this formulation uses animal-derived components, which are a source of contamination and are susceptible to lot-to-lot variations, it was a deliberate choice for the medium to be more affordable for routine use; a xeno(geneic)-free commercial version, TeSR2, is also available. Another commonly described medium for hiPSC expansion is E8, which is completely xeno-free and chemically-defined (Chen et al. 2011b). This medium is comprised of only eight components, including the basal medium DMEM/F12, sodium bicarbonate, insulin (essential in cell proliferation and glucose metabolism), transferrin (for iron transport and cellular oxygen uptake), ascorbic acid (for enhanced proliferation), selenite (for protection against oxidative stress), and growth factors basic fibroblast growth factor (bFGF) and transforming growth factor (TGF) β1 (which act together in the maintenance of pluripotency) (Nakashima and Omasa 2016, Kuo et al. 2020).

The culture medium is one of the driving costs in hiPSC culture. Commercial media, such as mTeSR1 and E8, are priced at over €450 per litre. Additionally, bFGF, one of the growth factors which is present in these media due to its requirement for maintenance of pluripotency, rapidly degrades at 37 °C, enforcing daily medium changes even for low density cultures. As hiPSC expansion processes

approach industrial scales, reducing the cost of media and ensuring new formulations compatible with less frequent feeding are challenges that still need to be overcome. Some recent formulations, such as mTeSR Plus or E8 Flex, allow for less frequent medium exchanges by stabilising bFGF, reducing its degradation at 37 °C. Other formulations, such as mTeSR3D and TeSR-E8 3D, were designed envisaging culture of hiPSC as three-dimensional aggregates, reducing the overall cost of the process by using a fed-batch regime. Also, the composition of mTeSR1 and E8 media are completely disclosed and can be manufactured in-house, ensuring a lower cost, especially if the growth factors, which are the most expensive components of these media, are also produced in the laboratory. More recently, Kuo and co-workers described B8 (Kuo et al. 2020), a novel medium formulation based on E8, with re-optimised concentrations of each component, and with the addition of neuroregulin (NRG) 1 for enhanced cell growth. Moreover, this formulation utilises a more potent and thermostable bFGF variant, bFGF-G3, which eliminates the requirement of medium replacement between cell passages. This medium, which was tested for 100 passages without affecting pluripotency, can be manufactured with basic laboratory skills, with production costs of about €15 per litre, thus representing an important achievement for the large-scale bioreactor culture of hiPSCs.

Complementing the commercially available medium formulations, some studies describe additional improvements which may enhance hiPSC culture. Most notably, inhibitors of the Rho-associated, coiled-coil containing protein kinase (ROCK) have widespread use for the initial survival of single cell and/or low density hPSC cultures (Watanabe et al. 2007, Li et al. 2009). More recently, Lipsitz and co-workers described the use of dextran sulfate (DS) (Lipsitz et al. 2018a). Polysulfated compounds such as DS have been traditionally applied in the biopharmaceutical industry (e.g., for insect (Dee et al. 1997) and CHO cells (Hyoung Park et al. 2016)) for their anti-aggregation effect, via surface charge modulation, as well for their anti-apoptotic activity (Dee et al. 1997, Zanghi et al. 2000).

I.1.2.3. Medium feeding regimes

One additional factor which has a major influence on the performance of a bioreactor culture is the medium feeding regime. Most commonly, the culture medium must be replaced at fixed time intervals, in a repeated batch approach, reminiscent of 2D cultures. A repeated batch feeding scheme is simple to implement, however, it leads to large variations in culture parameters, such as pH and nutrient/metabolite concentrations, at each medium change, which may be detrimental for cell growth. For this reason, alternative feeding strategies have been employed to mitigate these sudden changes in the culture environment (Figure I.7).

With the advent of media optimised for fed-batch culture, this feeding regime has started to be explored as an alternative for traditional repeated batch cultures (Schwedhelm et al. 2019). In this case, the medium is not replaced and, instead, a concentrated supplement with nutrients/growth factors is added to the culture, greatly reducing the stress of frequent modification of the culture environment. Furthermore, this strategy also allows for the accumulation of paracrine factors which may be beneficial for cell growth. However, the low refresh rate of nutrients, along with the accumulation of toxic metabolites, such as lactate, over various days of culture, require cell passaging every 3/4 days in order not to compromise cell growth and metabolism.

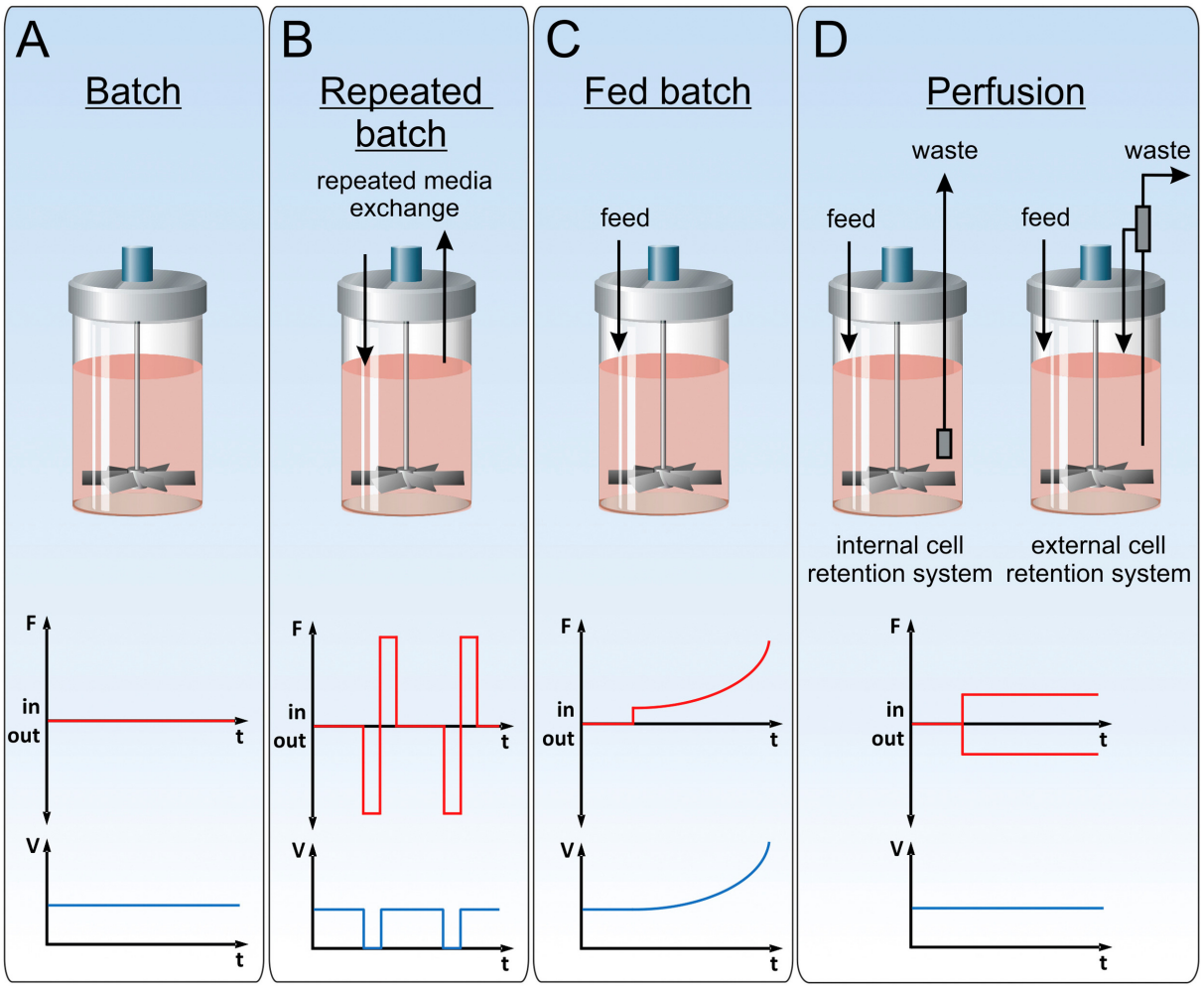

Figure I.7 – Medium feeding regimes in bioreactors. **A** In batch mode, the culture medium is added to the bioreactor at the beginning of the culture, with no supplementary feeding throughout. **B** A repeated batch strategy consists on repeated medium exchanges (typically every 24 h), where the spent medium is replaced by fresh medium. **C** In fed-batch, the culture medium is supplemented throughout the culture, either continuously or at repeated intervals. **D** Perfusion feeding strategies consist of continuous withdrawal of spent medium and replenishment with fresh medium, maintaining the volume of the culture. The cells are maintained in culture through a cell retention system, which may be internal or external to the bioreactor. From Kropp et al. (2017). Reproduced under the terms of the Creative Commons CC-BY-NC-ND license. Copyright 2017, The Authors.

Another feeding regime which has already been described for hiPSC growth is cyclic perfusion (Kempf et al. 2014), a variation of the repeated batch approach where only a small portion of the medium is replaced at fixed and frequent time intervals. This ensures a regular flux of nutrients and removal of metabolites, while reducing the magnitude of the variations in the culture. In a perfusion strategy, this medium flux is continuous, with a constant removal of spent medium and feeding of fresh medium, all while ensuring retention of the cells in the culture vessel, using devices such as spin filters (Serra et al. 2010, Kropp et al. 2016). Bioreactor operation under perfusion avoids drastic changes in the culture, as the evolution of parameters such as pH or concentrations are constant and gradual. This system, which more closely resembles a physiological environment, was shown to lead to a 47% higher final cell density in comparison to repeated batch approaches, for a maximum of $(2.85 \pm 0.34) \times 10^6$ cells·mL^{-1} in 7 days (Kropp et al. 2016). Implementing perfusion may be technically more demanding than other

feeding strategies, however, this feeding regime is compatible with automation, which may bring added value to the development of process-scale hiPSC-derived products.

I.1.2.4. 3D cell culture formats

The transition from 2D cultures to 3D is not straightforward, and, thus, different approaches for hiPSC culture in suspension have arisen, either 1) using microcarriers for cell adhesion, 2) allowing the cells to self-organise as aggregates, or 3) encapsulating the cells in a biomaterial. All of these systems have their advantages and drawbacks, as such, the selection of the system to employ will depend on factors such as the desired cell type, the bioreactor configuration or the final application of the cells.

I.1.2.4.1. Microcarriers

2D cell cultures are based on the adhesion of cells to a material, often mediated by a substrate, such as complex extra-cellular matrix protein mixtures (e.g., Matrigel or Geltrex, both derived from Engelbreth-Holm-Swarm mouse tumours), or recombinant human proteins (e.g., laminin or vitronectin). Consequently, the simplest approach to translate these cultures to 3D would be to promote the adherence of cells to matrix-coated particles.

Microcarriers are small particles (e.g., ~ 100–255 μm diameter for spherical microcarriers) with low density (~ 1.02–1.32 g/L), allowing them to remain in suspension in an agitated culture setting. Microcarriers can be classified according to their porosity; while in solid/microporous microcarriers the cells adhere and grow in their surface, macroporous microcarriers allow for cell growth inside the pores, thus increasing the available surface area for cell growth. The great majority of published studies of microcarrier-based expansion of hPSCs employ solid or microporous microcarriers, although expansion of hESCs in macroporous microcarriers has already been described (Storm et al. 2010). A variety of microcarriers of different materials are commercially available, including polystyrene, dextran, cellulose, gelatine or glass (extensively reviewed elsewhere (Chen et al. 2011a, Chen et al. 2013)). These microcarriers can be coated with matrices used for 2D culture to promote cell adhesion (e.g., Matrigel (Nie et al. 2009, Leung et al. 2011, Bardy et al. 2013, Fan et al. 2014, Ting et al. 2014), laminin (Heng et al. 2012, Lam et al. 2015), vitronectin (Heng et al. 2012, Fan et al. 2014, Badenes et al. 2016, Rodrigues et al. 2018)). In addition to expansion, differentiation of hPSCs in microcarriers has also been described, into cell types such as cardiomyocytes (Ting et al. 2014), neural progenitors (Bardy et al. 2013) and endodermal cells (Lock and Tzanakakis 2009).

Microcarriers provide a large surface-to-volume ratio for cell growth. Moreover, since the cells grow on the surface of the microcarriers, in direct contact with the culture medium, diffusional limitations are reduced. Conversely, the cells are highly susceptible to shear stress due to agitation-derived phenomena, such as bead collisions and small turbulent eddies (Croughan et al. 1987, Cherry and Papoutsakis 1988).

At the end of the culture, the cells need to be detached from the microcarriers, generally via enzymatic dissociation, and separated via size-based methods, such as filtration. This harvest procedure may be damaging to the cells and impact their viability. As such, new microcarrier types have been developed, whose composition allows for a gentle separation of the cells from the microcarriers.

Rodrigues and co-workers describe the use of dissolvable microcarriers coated with Synthemax II, a peptide containing the RGD sequence of vitronectin (Rodrigues et al. 2019). When the cells are to be harvested, these microcarriers can be degraded with ethylenediaminetetraacetic acid (EDTA) and pectinase, overcoming the need of a filtration step. The usage of these microcarriers for hiPSC expansion in spinner flasks allowed the recovery of 92 ± 4% of the cells at the end of culture, a two-fold increase over conventional polystyrene microcarriers. Another possible approach consists in using microcarriers which, by their characteristics, could forgo a harvesting step altogether. Newman and McBurney detail the growth and differentiation of mouse embryonic carcinoma cells on laminin-coated poly-(D,L lactic co-glycolic acid) microcarriers (Newman and McBurney 2004). Given the degradability and biocompatibility of these microcarriers, they can be transplanted into a patient, eliminating the requirement for cell-microcarrier separation even for therapeutic approaches. Furthermore, the composition of these microcarriers allowed the encapsulation and gradual release of differentiation-inducing growth factors. In particular, the encapsulation of retinoic acid promoted cell differentiation into neurons, in a higher proportion than cultures with soluble retinoic acid. The use of microcarriers as delivery vehicles of molecules that may influence stem cell fate is also an interesting strategy for microcarrier-based bioprocesses for hiPSC manufacturing.

I.1.2.4.2. Cell aggregates

Promoting cell adhesion to a matrix is a simple approach to translate the know-how in 2D cultures to 3D. However, while in suspension, hiPSC aggregate spontaneously, even without external matrices. Therefore, an alternative approach to the use of microcarriers is to inoculate bioreactors with single cells or cell clumps and allow them to form aggregates. This approach constitutes a simplification of the cell expansion process by not only reducing the amount of materials required (which may also simplify the overall GMP compliance of the process), but also by reducing the load of the downstream processing in comparison with microcarrier cultures.

Aggregates gradually increase in size as the culture progresses and cells expand. The expansion in aggregate sizes promotes the formation of gradients (e.g., nutrients, cytokines, oxygen) in their interior, due to diffusion from the surface to the centre. As the aggregates grow larger, the availability of medium components for the innermost cells diminishes, possibly leading to undesired effects such as spontaneous differentiation or necrosis as the aggregate diameter increases beyond 300–400 µm (Van Winkle et al. 2012, Wu et al. 2014). Overcoming these phenomena requires tight monitoring of aggregate sizes during culture and frequent passaging, by aggregate dissociation and inoculation to new vessels. Aggregation may be controlled by the bioreactor agitation, as higher agitation speeds will convey more shear, thus reducing the aggregate size. To complement the effect of agitation, non-physical aggregation control methods may also be applied, such as the aforementioned DS (Lipsitz et al. 2018a). In addition to avoiding diffusion limitations, aggregate size control is also of importance for hiPSC differentiation, as specification of some lineages has been shown to be more efficient on a tight range of aggregate sizes (Bauwens et al. 2008, Olmer et al. 2018, Branco et al. 2019).

Initial studies on hPSC aggregate culture were geared towards the optimisation of the culture conditions, including the use of either rapamycin (Krawetz et al. 2010) or heat shock treatment (Singh

et al. 2010) in addition to ROCK inhibitor to improve cell survival and/or expansion. Later studies described the expansion of these cells for various serial passages (Chen et al. 2012), including in xeno-free conditions (Abbasalizadeh et al. 2012, Wang et al. 2013). Hunt and co-workers proved the importance of both the inoculation density and the agitation rate in the expansion of hESCs as aggregates using a factorial design approach (Hunt et al. 2014). More recently, hPSC culture as aggregates has been combined with other strategies in order to further improve the process, namely through perfusion (Kropp et al. 2016) and oxygen control (Abecasis et al. 2017), and by culture in novel bioreactor systems (Schwedhelm et al. 2019, Borys et al. 2020). Differentiation of hPSC aggregates into cardiac (Halloin et al. 2019), neural (Serra et al. 2009) and hepatic (Freyer et al. 2016) lineages, in bioreactors, has already been achieved. Moreover, cell differentiation as aggregates constitutes a reliable platform for the generation of organoids, which are self-assembled cellular structures with characteristics resembling the structure and organisation of a specific organ (Fatehullah et al. 2016). For instance, the generation of brain (Qian et al. 2016, Silva et al. 2020b), cardiac (Drakhlis et al. 2021, Hoang et al. 2021), kidney (Przepiorski et al. 2018) and retina (Ovando-Roche et al. 2018) organoids derived from hiPSC aggregates has already been described.

I.1.2.4.3. Encapsulation

Most protocols of hPSC expansion in bioreactors use a microcarrier or aggregate approach. However, in both cases, the shear stress conveyed by the agitation remains a problem which may negatively impact the cells. Microencapsulation of cells in a biomaterial, such as a hydrogel, is a promising strategy to not only protect the cells from shear stress, but also to provide cues which may promote cell self-renewal or differentiation into a specific lineage (Dixon et al. 2014, Lenzini et al. 2019). The method for cell harvesting at the end of culture depends on the biomaterial used for encapsulation, but may consist on temperature or pH shift (Li et al. 2016, Rodrigues et al. 2017), or on enzymatic degradation of the biomaterial (Lou et al. 2014). Alternatively, if the cells are to be used for Regenerative Medicine applications, some cell-biomaterial composites can potentially be transplanted directly to a patient (Du et al. 2014, Huang and Jiang 2018). A number of different materials have already been shown to successfully accommodate hPSC expansion and/or differentiation, including alginate (Jing et al. 2010, Serra et al. 2011, Dixon et al. 2014, Hunt et al. 2017), cellulose (Lou et al. 2014), collagen (Dixon et al. 2014), fibrin (Goetzke et al. 2019) and poly(N-isopropylacrylamide) (PNIPAAm)–polyethylene glycol (PEG) (Rodrigues et al. 2017, Lin et al. 2018).

To this date, a limited number of studies describe dynamic suspension culture of encapsulated hPSCs. Serra and co-workers describe alginate encapsulation of hESCs, as single cells, as aggregates, and attached to microcarriers, along with expansion in spinner flasks and subsequent cryopreservation (Serra et al. 2011). While culture of hESCs encapsulated as single cells was unviable, encapsulation of hESCs on microcarriers led to the best overall results. Exponential growth was observed for 19 days and cryopreservation of these cells led to increased viability after thawing. Overall, hESC encapsulation improved the performance of both dynamic suspension culture and post-thawing cell recovery. Cardiac differentiation of hESCs encapsulated in poly-L-lysine-coated alginate in spinner flasks has also been detailed (Jing et al. 2010), with over 30% of the cells expressing cardiac markers after 15 days.

I.1.2.5. Single-use bioreactors for stem cell biomanufacturing

Despite all the advances in stem cell products for human use, regulation by agencies such as the European Medicines Agency (EMA) and the US Food and Drug Administration (FDA) is a critical concern. EudraLex (available online at https://ec.europa.eu/health/documents/eudralex, accessed on the 10th of April 2021) details the legislation for pharmaceutical products in the European Union, and Volume 4, in particular, details the guidelines for GMP for medicinal products for human and veterinary use. These GMP apply to various steps of the life of a stem cell product, from the cell bank establishment and maintenance, to the manufacturing, downstream processing, fill and finish (Figure I.8). Among other things, GMP guidelines aim to avoid product contamination, thus requiring the sterilisation of the reagents and materials. Whenever possible, cleaning in place (CIP) and steaming in place (SIP) should be applied to sterilise materials between batches. The same regulation also permits and suggests the use of single-use technologies (EudraLex Volume 4, Part IV). In particular, the bioreactor parts which directly contact the cells can be disposable, which minimises the risk of contamination, and overrides the need for their sterilisation, thus reducing the time between batches and allowing a faster process pipeline and, thus, a higher productivity.

The following sections will detail some single-use bioreactor platforms which have already been successfully applied in the biomanufacturing of stem cells. Although not all of these systems have been used for hPSC culture, they are nevertheless presented due to their potential for prospective manufacturing of these cells. A summary of the results obtained in these bioreactors is presented in Table I.1.

I.1.2.5.1. Single-use stirred tank bioreactors

STBRs have been one of the most commonly used set-ups for the manufacturing of a variety of products, such as viruses or recombinant proteins, in a multitude of cell types including bacterial, insect, plant or animal cells (van Lier et al. 1990, Velez-Suberbie et al. 2013, Raven et al. 2015, Schmideder and Weuster-Botz 2017). STBRs typically employ a glass or stainless-steel vessel, along with one or multiple impellers distributed along the height of the bioreactor and ensuring efficient agitation of the medium (Figure I.9). Depending on the frailty of the cells, different impellers can be employed—Rushton turbines are suitable for more resistant cell types, such as bacteria, while animal cells, which are more shear-sensitive, require gentler mechanisms of agitation such as marine or pitched-blade impellers. In fact, shear stress is a common point of contention in the translation of stem cell culture to 3D, due to its effect in cell fate (reviewed in Stolberg and McCloskey (2009), Earls et al. (2013)). Nevertheless, there is a notorious lack of studies in this regard, with only a few reports of phenomena such as agitation-induced hPSC differentiation (Leung et al. 2011), as well as priming of human mesenchymal stromal cells (hMSCs) towards an osteogenic fate through high shear stress (Yourek et al. 2010). The decades of STBR use in the biopharmaceutical industry ensure these bioreactors are now very well characterised, in terms of agitation profiles, shear stress, power dissipation and oxygen mass transfer, with well-established empirical correlations, as well as defined criteria for scale-up (Özbek and Gayik 2001, Nienow 2009, Liu et al. 2016). In STBRs, however, the existence of “hot-spots” of high shear forces has been described as well as “dead zones" where mixing is inferior or

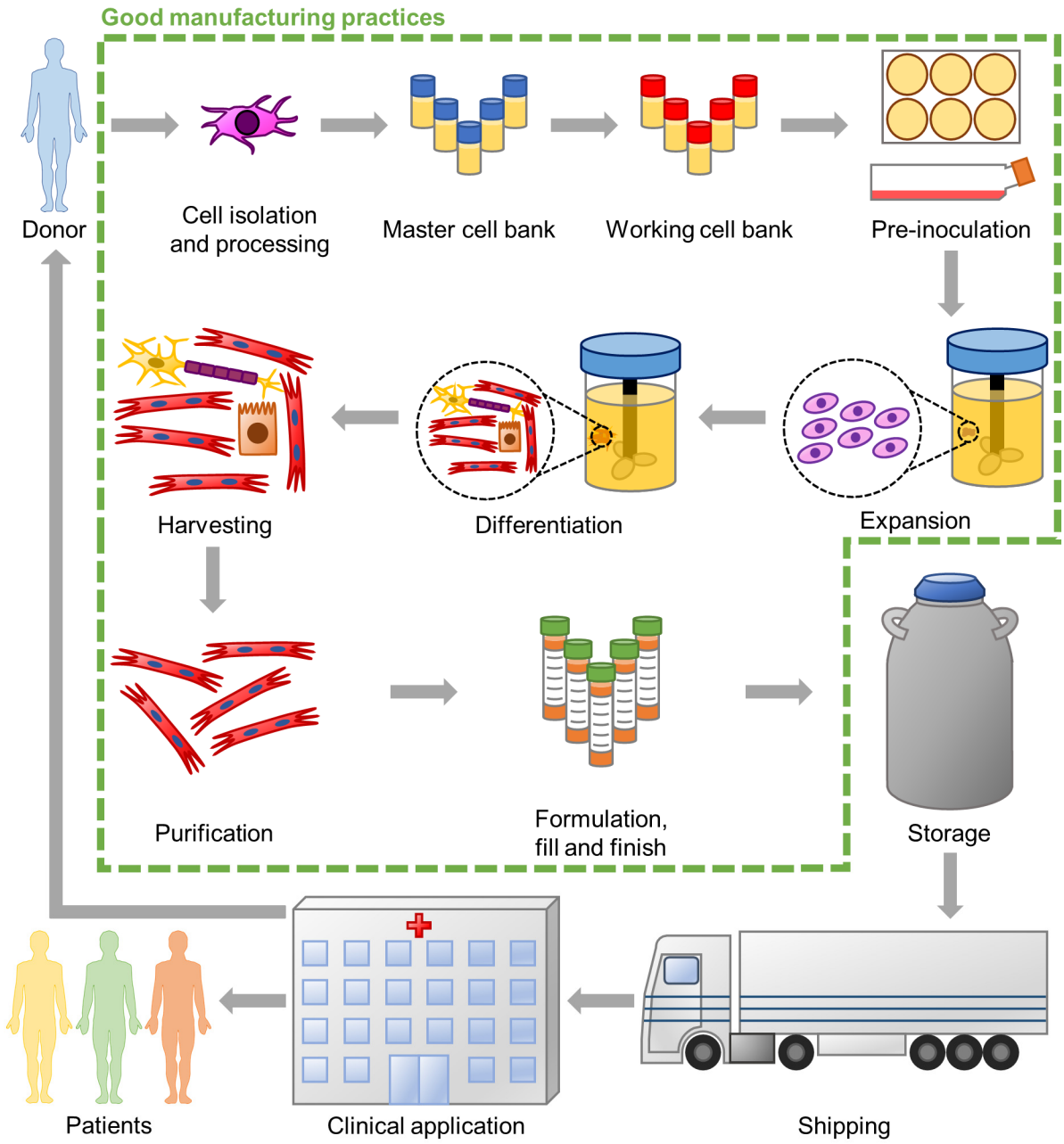

Figure I.8 – Process pipeline for the production and clinical application of a stem cell product (either autologous or allogeneic). European Medicines Agency legislation established good manufacturing practices to be applied from the initial cell isolation and processing to the product fill and finish, while also requiring a clear definition on the storage and shipping conditions of the finished cell product. We note that the figure depicts a general stem cell product pipeline and, although most processes already at clinical scale do not perform yet differentiation in the bioreactors. However, we believe the field will move towards that direction as using planar platforms will be hardly feasible at a clinical scale. From Nogueira et al. (2021a). Reproduced under the terms of the Creative Commons CC-BY license. Copyright 2021, The Authors.

almost inexistant. This heterogeneous mixing profile may give cues for undue cell differentiation and/or apoptosis due to the high shear itself or cell settling and formation of very large cell aggregates.

Table I.1 – Comparison of single-use bioreactor systems for stem cell culture. Working volume ranges indicate a change in volume during the culture. Final cell densities presented are the maximum average obtained among different conditions and/or donors. hHSPC – human haematopoietic stem/progenitor cell; hNSC – human neural stem cell; RBC – red blood cell. From Nogueira et al. (2021a). Reproduced under the terms of the Creative Commons CC-BY license. Copyright 2021, The Authors.

Bioreactor type	Cell type	Working volume/area	Culture time (days)	Maximum final cell density	Reference
Stirred tank	hiPSCs	125 mL	7	$(2.9 \pm 0.3) \times 10^6$ cells·mL^{-1}	Kropp et al. (2016)
		1.0–1.5 L	7	$(1.99 \pm 0.09) \times 10^6$ cells·mL^{-1}	Kwok et al. (2018)
	hMSCs	15 mL	8	8.1×10^5 cells·mL^{-1}	Rafiq et al. (2017)
		100–200 mL	10	1.8×10^5 cells·mL^{-1}	Rotondi et al. (2021)
		1.0–2.0 L	7	4.1×10^5 cells·mL^{-1}	Cunha et al. (2017)
		2.0 L	7	$(2.7 \pm 0.2) \times 10^5$ cells·mL^{-1}	Schirmaier et al. (2014)
		1.0–2.4 L	14	~ 1×10^5 cells·mL^{-1}	Grein et al. (2016)
		35 L	7	3.1×10^5 cells·mL^{-1}	Schirmaier et al. (2014)
		50 L	11	2.6×10^5 cells·mL^{-1}	Lawson et al. (2017)
	hHSPCs	10 mL	10	1.4×10^7 cells·mL^{-1}	Ratcliffe et al. (2012)
Fixed bed	hMSCs	3 mL	20.8	N/A[(1)]	Weber et al. (2007)
		14.2 mL	5.6	$(2.9 \pm 0.1) \times 10^6$ cells·mL^{-1}	Weber et al. (2010)
		60 mL	7.0	1.75×10^6 cells·mL^{-1}	Weber et al. (2010)
		300 mL	6.9	2.05×10^6 cells·mL^{-1}	Weber et al. (2010)
		500 mL	7	$(8.3 \pm 1.6) \times 10^5$ cells·mL^{-1}	Mizukami et al. (2013)
Hollow fibre	hESCs	2.1 m^2	5	3.4×10^4 cells·cm^{-2}	Roberts et al. (2012)
	hiPSCs	2.1 m^2	6–7	$(3.3 \pm 0.4) \times 10^4$ cells·cm^{-2}	Paccola Mesquita et al. (2019)
	hNSCs	2.1 m^2	7–11	1.5×10^5 cells·cm^{-2}	Tirughana et al. (2018)
	hMSCs	2.1 m^2	7–9	N/A[(2)]	Russell et al. (2018)
		2.1 m^2	17 ± 6	$(4.7 \pm 0.6) \times 10^3$ cells·cm^{-2}	Haack-Sørensen et al. (2016)
		2.1 m^2	8 ± 2	$(8.0 \pm 2.5) \times 10^3$ cells·cm^{-2}	Mennan et al. (2019)
		2.1 m^2	5	$(9.8 \pm 1.0) \times 10^3$ cells·cm^{-2}	Mizukami et al. (2018a)
		2.1 m^2	5	$(1.1 \pm 0.2) \times 10^4$ cells·cm^{-2}	Mizukami et al. (2018b)
		2.1 m^2	7.9–9.9	$(1.8 \pm 0.2) \times 10^4$ cells·cm^{-2}	Lambrechts et al. (2016)
		2.1 m^2	6	$(1.9 \pm 0.3) \times 10^4$ cells·cm^{-2}	Vymetalova et al. (2020)
		2.1 m^2	6	2.9×10^4 cells·cm^{-2}	Haack-Sørensen et al. (2018)
		2.1 m^2	6–13	4.7×10^4 cells·cm^{-2}	Nold et al. (2013)

Bioreactor type	Cell type	Working volume/area	Culture time (days)	Maximum final cell density	Reference
Rotating bed	hNSCs	4 mL	3	~ 5×10^5 cells·mL^{-1}	Chiang et al. (2012)
	hMSCs	10 mL	14	N/A[1]	Sakai et al. (2009)
	hMSCs	2000 cm^2	5	$(1.2 \pm 0.1) \times 10^4$ cells·cm^{-2}	Neumann et al. (2014)
		6000 cm^2	9	$(5.8 \pm 0.9) \times 10^4$ cells·cm^{-2}	Reichardt et al. (2013)
Rocking motion	hESCs	150 mL[3]	4	2.8×10^6 cells·mL^{-1}	Davis et al. (2018)
		400 mL[3]	4	1.4×10^6 cells·mL^{-1}	Davis et al. (2018)
		1.0 L[3]	4	1.3×10^6 cells·mL^{-1}	Davis et al. (2018)
	hMSCs	50–200 mL	100	$(1.32 \pm 0.09) \times 10^6$ cells·mL^{-1}	Nguyen et al. (2019)
		50–600 mL	10	4.4×10^4 cells·mL^{-1}	da Silva et al. (2019)
		50–600 mL	11	2.2×10^5 cells·mL^{-1}	da Silva et al. (2020)
	hHSPC-RBCs	200 mL – 1 L	33	4.5×10^{12} cells·mL^{-1}	Timmins et al. (2011)
Vertical-Wheel	hiPSCs	60 mL	80	N/A[1]	Silva et al. (2021)
		80 mL	9	$(1.21 \pm 0.02) \times 10^6$ cells·mL^{-1}	Rodrigues et al. (2018)
		300 mL	8	$(8.6 \pm 1.5) \times 10^5$ cells·mL^{-1}	Rodrigues et al. (2018)
		100 mL	6	$(6.3 \pm 0.4) \times 10^5$ cells·mL^{-1}	Borys et al. (2020)
		100 mL	6	$(6.5 \pm 0.6) \times 10^5$ cells·mL^{-1}	Borys et al. (2021)
		500 mL	6	~ 4×10^5 cells·mL^{-1}	Borys et al. (2021)
	hMSCs	60 mL	4	1.1×10^5 cells·mL^{-1}	Yuan et al. (2018)
		60–100 mL	7	$(5.3 \pm 0.4) \times 10^5$ cells·mL^{-1}	de Sousa Pinto et al. (2019)
		60–100 mL	7–11	5.3×10^5 cells·mL^{-1}	de Almeida Fuzeta et al. (2020)
		90–92 mL	5	~ 6×10^5 cells·mL^{-1}	Lembong et al. (2020)
		2.2 L	14	~ 3×10^5 cells·mL^{-1}	Sousa et al. (2015)

[1]Non-proliferative and/or differentiating cells.

[2]The exact cell density achieved is not stated by the authors but is inferred from the text to be around 10^5 cells·cm^{-2}.

[3]Part of a consecutive passage experiment with increasing scale; overall fold increase of ~ 280 over 16 days. Individual experiments at each scale with optimised conditions led to better results, but the exact cell density is not indicated in the article.

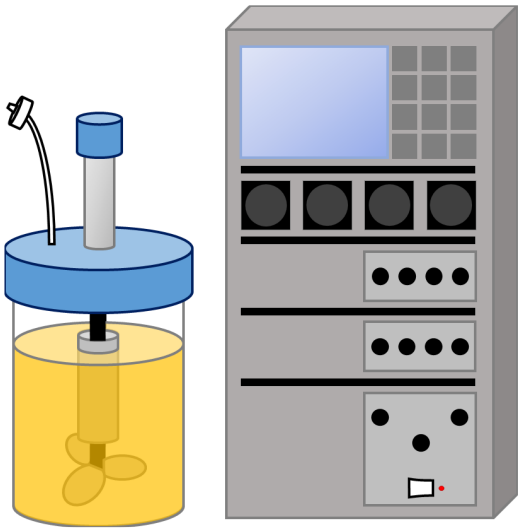

Figure I.9 – Schematics of a stirred-tank bioreactor vessel and controller unit. From Nogueira et al. (2021a). Reproduced under the terms of the Creative Commons CC-BY license. Copyright 2021, The Authors.

The STBR can be easily converted into a single-use system, by replacing parts which contact the cells with disposable equipment, such as the vessel itself, the impeller and the probes. Examples of commercially available single-use STBRs which have already been successfully applied for stem cell culture are described in Table I.2. Together, these systems cover from a 10 mL laboratory scale to a 200 L production scale.

Table I.2 – Examples of single-use stirred tank bioreactor systems with successful use for stem cell culture. From Nogueira et al. (2021a). Reproduced under the terms of the Creative Commons CC-BY license. Copyright 2021, The Authors.

Bioreactor	Company	Impeller	Working volume range
BioBLU®	Eppendorf	Eight-blade or pitched-blade	100 mL – 40 L
Mobius® CellReady	EMD Millipore	Marine (scoping)	1.0–2.4 L
Ambr®	Sartorius Stedim Biotech	Pitched-blade or Rushton	10–250 mL
BIOSTAT® CultiBag STR Plus	Sartorius Stedim Biotech	Three- or six-blade	12.5–200 L
UniVessel® SU	Sartorius Stedim Biotech	Three-blade	600 mL – 2.0 L

Kropp and co-workers have described the expansion of hiPSCs as aggregates in BioBLU bioreactors (125 mL working volume), using different feeding strategies. By applying a perfusion strategy, where constant withdrawal of wasted medium and replenishment of fresh medium are performed (retaining the cells inside the vessel), the cell yield was improved by 47% in comparison to a repeated batch approach, with a discrete medium exchange every 24 h. The authors obtained a final density of $(2.85 \pm 0.34) \times 10^6$ cells·mL^{-1}, although with a shift to a metabolism more reliant on oxidative phosphorylation (Kropp et al. 2016). Kwok and colleagues expanded hiPSCs as aggregates in Mobius CellReady bioreactors at a 1.5 L scale, generating a total of 2 billion cells (Kwok et al. 2018). hPSC differentiation in STBRs is also possible—Halloin and co-workers have adapted a standard cardiac differentiation protocol and report the generation of about 1×10^6 cardiomyocytes·mL^{-1} at both 100 mL and 350–500 mL scales, with purity above 90%. The bioreactors used in this study are available with

both single-use and reusable vessels, which should allow for easy transition of protocols developed on one of those formats to the other (Halloin et al. 2019).

Microcarrier-adherent hMSC expansion has also been described, in Mobius CellReady, Univessel SU and CultiBag STR bioreactors. Schirmaier et al. optimised adipose tissue (AT)–derived hMSC culture at a 2 L scale, followed by a scale-up experiment to 35 L, and were able to maintain a similar cell density at both scales—$(0.27 \pm 0.02) \times 10^6$ cells·mL^{-1} and 0.31×10^6 cells·mL^{-1}, respectively (Schirmaier et al. 2014). Lawson and co-workers attempted BM-hMSC culture at a 50 L scale, obtaining 1.28×10^{10} cells in 11 days of culture (Lawson et al. 2017).

While obtaining high cell numbers is vital for production of cells to be used in a clinical setting, bioprocess optimisation is preferably performed in a high-throughput platform. Ratcliffe and colleagues performed human haematopoietic stem/progenitor cell (hHSPC) expansion in the Ambr 15 bioreactor system, a fully-automated and controlled platform entailing 24 vessels with 15 mL maximum volume, allowing for the simultaneous testing of many different conditions. By optimising culture parameters, including inoculation density, oxygen tension and medium feeding, the authors could obtain a maximum density of 1.37×10^7 cells·mL^{-1} in 11 days (Ratcliffe et al. 2012). This platform was also used for optimisation of BM-hMSC expansion with microcarriers in serum-free medium, resulting in over 8.1×10^5 cells·mL^{-1} and a 10-fold increase in reproducibility in comparison to serum-containing, manual culture (Rafiq et al. 2017).

I.1.2.5.2. Fixed bed bioreactors

Fixed bed bioreactors are a common staple of the food and wastewater industry due to their set-up—a vessel filled with a macroporous material or large beads to which cells and/or enzymes may be attached, and through which the liquid phase is passed through continuously (Figure I.10). In fact, many studies have already described the use of fixed bed bioreactors for applications such as production of biodiesel (Watanabe et al. 2001, Salum et al. 2010) and biohydrogen (Chang et al. 2002), and various aspects of wastewater treatment (Kim and Logan 2000, Chen et al. 2005). Beyond the possibility for these applications, fixed bed bioreactors also have some characteristics which have led to their use for culture of anchorage-dependant mammalian cells. The geometry and set-up of these bioreactors confer a large surface-to-volume ratio, allowing for a smaller footprint compared to stirred-tank bioreactors and enabling a much higher volumetric productivity. Depending on their mechanism, fixed bed bioreactors may also be naturally compatible with a perfusion feeding regime, and, due to the lack of agitation, the shear stress conveyed to the cells is low. The lack of an impeller is, simultaneously, a disadvantage, due to allowing for the formation of concentration gradients (of nutrients, metabolites, growth factors, oxygen, etc.) inside the bioreactor. Moreover, cell harvesting until the end of the culture is impossible, rendering cell growth monitoring notably difficult. Nevertheless, fixed bed bioreactors have seen use for applications such as viral production in mammalian cells (Rajendran et al. 2014, Powers et al. 2016, Valkama et al. 2018), and even hHSPC expansion (Meissner et al. 1999).

Single-use fixed bed bioreactors require both a single-use vessel and cell adhesion matrix. Weber and co-workers have developed a small-scale disposable fixed bed bioreactor system using a 3 mL plastic syringe, connected to two 250 mL flasks for medium feeding and for waste, and equipped

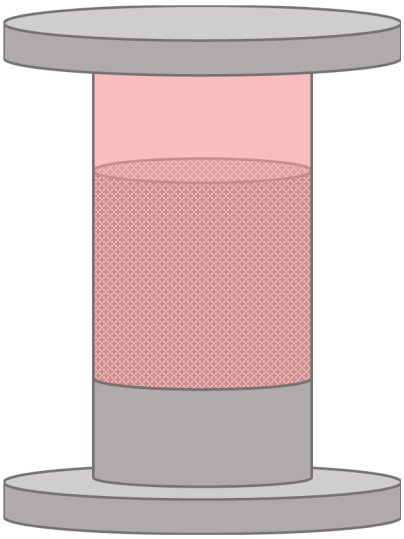

Figure I.10 – Schematics of a fixed bed bioreactor. From Nogueira et al. (2021a). Reproduced under the terms of the Creative Commons CC-BY license. Copyright 2021, The Authors.

with a small oxygen sensor in the outflow. This bioreactor system was used for the culture of alginate-encapsulated hMSC-TERTs. These cells are hMSCs transfected with telomerase, which compensates the telomere shortening which occurs during mitosis, thus enabling for more population doublings in comparison to unaltered hMSCs (Simonsen et al. 2002). The encapsulated hMSC-TERTs were not proliferative, but could be maintained in culture for at least 500 hours with increasing viability (Weber et al. 2007). The same group also described larger-scale fixed bed bioreactor systems—using 60 mL glass syringes, and glass tubes between two stainless-steel plates (serving as lid and bottom) for a volume of 300 mL. These bioreactors were filled with 2 mm diameter non-porous borosilicate glass spheres which served as surface for cell adhesion and made use of non-invasive oxygen sensors both at the inlet and the outflow. At the 300 mL scale, the authors were able to produce 6.2×10^8 hMSC-TERTs after 167.3 hours of culture, however, only 50% to 60% of the inoculated cells attached to the borosilicate spheres (Weber et al. 2010). Mizukami and colleagues have used a commercial fixed bed bioreactor system—FibraStage® bottles (discontinued) loaded with Fibra-Cel® disks, both from Eppendorf (previously from New Brunswick Scientific) for the expansion of human cord blood-derived hMSCs. The bellows at the base of the bottle control the medium level by compression and expansion. With one 500 mL FibraStage bottle, the authors could produce $(4.15 \pm 0.81) \times 10^8$ cells in 7 days of culture (Mizukami et al. 2013).

I.1.2.5.3. Hollow fibre bioreactors

Hollow fibre bioreactors are composed of numerous capillary tubes inside an outer shell, which, similarly to fixed bed bioreactors, confer them a high surface area with a low footprint (Figure I.11). In hollow fibre bioreactors, the cells adhere to the surface of the capillaries, either on the intracapillary (IC) or the extracapillary (EC) loop. Medium and reagents may be pumped through the loop in which the cells are adhered to, contacting them directly. The capillary membrane is semipermeable, thus also enabling diffusion of dissolved gases and small molecules (e.g., glucose, lactate) through it, and allowing for mass exchange between the cells and the fluids perfused through the other loop (Barckhausen et al. 2016). Once more, the lack of an impeller reduces the shear stress conveyed to cells, especially due to

the two-loop system and the possibility of indirect mass transfer. However, the growth of cells inside the hollow fibre bioreactors is hard to monitor due to the impossibility of cell harvesting until the end of culture. Having a membrane-based system also renders these bioreactors particularly susceptive to fouling—as the capillary membrane pores clog, either due to the cells or other solids, mass transfer through the capillaries becomes increasingly difficult (MacDonald et al. 2001). The high cell densities which can be obtained in a hollow fibre reactor, along with the resulting high product titres, have led this configuration to be attractive for the production of recombinant proteins, monoclonal antibodies and viruses (Yazaki et al. 2001, Jardin et al. 2008, Tapia et al. 2014), while also seeing use for wastewater treatment (Pankhania et al. 1994, Gimenez et al. 2011) and biocatalytic reactions (Krastanov et al. 2007, Wang et al. 2016). Furthermore, hollow fibre bioreactors have already been applied for the bioproduction of stem cells for clinical trials (Tirughana et al. 2018).

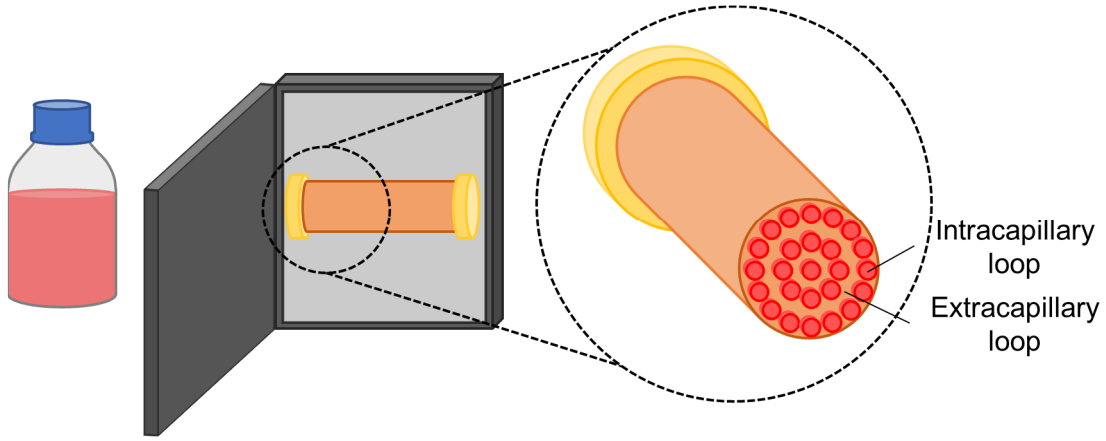

Figure I.11 – Schematics of a hollow fibre bioreactor system and close-up of the hollow fibre module. From Nogueira et al. (2021a). Reproduced under the terms of the Creative Commons CC-BY license. Copyright 2021, The Authors.

Regarding single-use hollow fibre bioreactors for stem cell expansion, many studies describe the use of the Quantum® Cell Expansion System (QES; Terumo BCT). This closed and fully automated system is composed of about 11,500 hollow fibres, providing a 2.1 m^2 surface area for cell growth (the same as 120 T-175 flasks) with a 0.3 m^2 footprint.

Roberts and co-workers have harvested up to 5.4 × 10^8 hESCs in 5 days in the QES, achieving 1.8-fold the cell density of T-25 flasks in an equivalent time, while reducing medium consumption per unit area in 68% (Roberts et al. 2012). Mesquita and colleagues demonstrated hiPSCs could be expanded in the QES, and that laminin coating of the IC area was more favourable (both in terms of the maximum cell number and the time require to achieve it) for cell growth over vitronectin, possibly due to a stronger interaction of laminin with the QES fibres. Furthermore, to overcome some of the monitoring limitations of the bioreactor system, the authors correlated the total number of cells with the produced lactate, allowing them to estimate the growth curve of the hiPSCs. After 6–7 days of culture, the authors obtained an average of (6.9 ± 0.9) × 10^8 cells with laminin coating (Paccola Mesquita et al. 2019). Tirughana et al. described the production of GMP-grade human neural stem cells (hNSCs) in the QES. These hNSCs were modified to produce the prodrug-activating enzyme cytosine deaminase. A total of 1.4–3 × 10^9 of these cells could be obtained in one QES in 7–10 days, allowing for the production of an FDA-approved clinical lot (1.5 × 10^{10} cells) in 7 parallel bioreactors in 9 days, which was then used in a phase I trial with 7 brain tumour patients. The same cell line was additionally modified by adenoviral

transduction in the QES to produce a modified carboxylesterase, and 1.5–1.8 × 10^9 cells could be recovered after 8 days. Using 5 QES in parallel, a clinical lot of 8 × 10^9 transduced hNSCs was produced for a future study regarding the treatment of metastatic neuroblastoma patients (Tirughana et al. 2018).

The QES has already been extensively described for the culture of hMSCs of various sources—AT (Haack-Sørensen et al. 2016, Haack-Sørensen et al. 2018, Mizukami et al. 2018b), BM (Nold et al. 2013, Russell et al. 2018, Mennan et al. 2019), umbilical cord matrix (UCM) (Mizukami et al. 2018a, Mennan et al. 2019, Vymetalova et al. 2020) and periosteum (Lambrechts et al. 2016). Of these studies, Haack-Sørensen and co-workers were able to obtain the highest cell number. The authors performed a comparison of two media—foetal bovine serum (FBS) or human platelet lysate (hPL)-supplemented—for the derivation of hMSCs from an inoculum of the stromal vascular fraction of human subcutaneous abdominal fat, over the course of two passages in the QES. Overall, this study revealed hPL to be more favourable for cell growth. In the first passage, hPL increased cell yield by 5-fold and in half of the expansion time when compared to FBS (9 days for hPL vs 17 days for FBS). Both supplements led to comparable growth in the second passage, but with a higher difference in the expansion time (6 days for hPL vs 21 days for FBS). FBS is an animal-derived supplement, which complicates the approval process in the case of a clinical-grade process. In contrast, hPL is of human origin, being free of xenogeneic components. Nevertheless, this supplement may also suffer from batch-to-batch variability (Bieback et al. 2019). At the end of culture, up to 5.5 × 10^8 AT-MSCs were obtained in 9 days from stromal vascular fractions and 6.1 × 10^8 AT-MSCs were recovered after the first passage, following 6 days in culture (Haack-Sørensen et al. 2018). Russell and colleagues have performed a cost breakdown, comparing automated hMSC expansion in the QES with manual culture for the production of 100 doses of 10^8 cells (for a clinical trial with 100 patients). The automated system allowed for savings of about 49% in reagents and consumables, having an estimated cost of about $108,000 for 100 doses while hands-on work could be reduced from 361.6 hours (in a 24.0 week production time, thus requiring two technologists) to 35.0 hours (for a 20.0 week production, demanding a single technologist) (Russell et al. 2018). Mizukami et al. performed a more thorough cost-of-goods analysis, comparing a multilayer vessel, a stirred tank bioreactor, a packed bed bioreactor and a QES. While the QES resulted in a higher cell proliferation rate, expansion fold and harvesting efficiency, its high consumable and equipment cost led it to be predicted as the least cost-effective option. In fact, for the QES to compete with the other systems at an economical level, it would require a 7-fold increase in harvesting density, along with an 85% consumable and equipment cost reduction and a 28% in medium cost savings (Mizukami et al. 2018a).

I.1.2.5.4. Rotary cell culture systems

The advancements in space travel in the past years have led to significant research in the effects of microgravity in humans, and more specifically, in some cell types. While cell culture has already taken off to space (Wnorowski et al. 2019), microgravity can also be simulated on Earth. The rotary cell culture system (RCCS) is a bioreactor developed by NASA which can be used to culture cells in a microgravity environment (Figure I.12). In this bioreactor system, the cells are inoculated in a high aspect ratio cylindrical vessel, which is completely filled with medium. The vessel rotates horizontally and will cause

the medium inside to rotate as well. If operating at a certain range of speeds, after some time, the medium will rotate at the same velocity as the vessel itself, unlike in other bioreactor systems where the fluid is moving in reference to the vessel walls (e.g., agitated liquid and still vessel walls). This minimises the effect of the Earth's gravity on the particles inside the vessel, resulting in an effective gravitational force of $10^{-2} \times g$ (Lelkes et al. 1998). Moreover, the particles inside the vessel have an almost null terminal velocity, and, as such, move with the medium upon the rotational axis, with limited movement alongside other axes – a cell will return to approximately the same location upon each complete vessel rotation. As such, the cells can be cultured in suspension in a laminar regime, thus, with minimal shear stress ($< 5 \times 10^{-2}$ Pa), further reduced by the lack of a headspace, and, consequently, no formation of air bubbles (Tsao et al. 1992, Lelkes et al. 1998, Hammond and Hammond 2001). Ensuring both these effects will require the rotation of the RCCS in a limited velocity range – a low rotation speed will not overcome the Earth's gravitational force, causing the cells to settle, while high rotation will result in a predominant centrifugal force which will drive the cells towards the outer wall (Figure I.12B-D). Furthermore, while the low shear stress conveyed by the RCCS limits the extent of shear-mediated cell damage, it also limits mass transfer by convection. In fact, in the RCCS, diffusive mass transfer prevails, which may lead to the formation of microenvironments of low nutrient concentration and high waste accumulation in the vicinity of the cells (Cowger et al. 1999, Hammond and Hammond 2001).

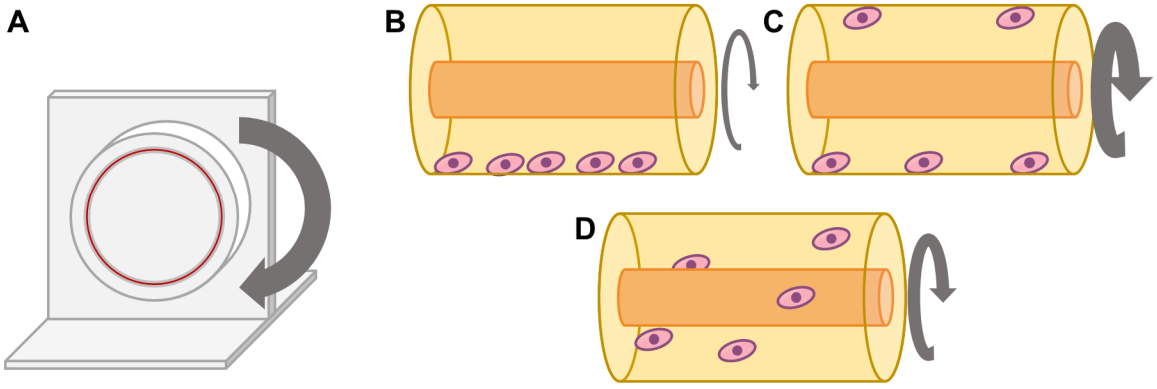

Figure I.12 – Schematics of a rotary cell culture system. **A** Rotator base with one vessel. **B** At low rotation speeds, the cells will settle along the bottom of the vessel. **C** At very high rotational speeds, the cells will be subjected to a predominant centrifugal force, driving them towards the outer wall of the vessel. **D** At a certain velocity range, the cells will be in suspension, in a simulated microgravity environment. From Nogueira et al. (2021a). Reproduced under the terms of the Creative Commons CC-BY license. Copyright 2021, The Authors.

Single-use RCCS operate using disposable vessels, or cassettes, as these are the only part of the bioreactor which directly contacts the cells. Single-use RCCS systems are available commercially from Synthecon, but only at a 10 mL and 50 mL scale, limiting their scalability.

Chiang and co-workers have employed the RCCS for hESC-derived hNSC culture and observed the effect of simulated microgravity in the development of these cells. RCCS culture led to increased β-adrenoreceptor expression and subsequent mitochondrial function of hNSCs, with increased mitochondrial mass and ATP production. Moreover, the proliferation of the hNSCs was increased, leading to a final density of ~ 5×10^5 cells·mL^{-1} after 3 days, a 2-fold increase over the static control (Chiang et al. 2012). The culture of adult BM-hMSCs in these bioreactors has also been described. Cells were harvested from BM and seeded in the RCCS in chondrogenic medium. The results were compared

with a standard protocol of cartilage production in conical tubes. After 2 weeks, RCCS culture led to about 3-fold larger (diameter-wise) and 10-fold heavier cellular constructs in relation to conical tubes, with a 1.5-fold higher glycosaminoglycan/DNA ratio and with histological and immunohistological characteristics of hyaline cartilage (Sakai et al. 2009).

I.1.2.5.5. Rotating bed bioreactors

Rotating bed bioreactors apply rotation to the previously-described fixed bed system – the cells adhere to plates, which rotate inside the vessel (Figure I.13). These bioreactors can be operated at full volume, or similarly to roller bottles, by not filling the vessel totally, and allowing for the cells to intermittently contact the medium and the headspace. Rotating bed bioreactors share most advantages and disadvantages of fixed bed bioreactors—both provide a large surface-to-volume ratio, are compatible with perfusion and convey low shear stress to the cells, while cell harvesting and monitoring cannot be performed during the culture. Rotating bed bioreactors, however, can provide some more homogeneity to the contents of the vessel by means of rotation employed. Applications of these systems also include biocatalysis (Lan et al. 2013, Abdella et al. 2016) and wastewater treatment (Jafari et al. 2015, Pourakbar et al. 2018), and it has already seen use in mammalian cell culture (Suck et al. 2007).

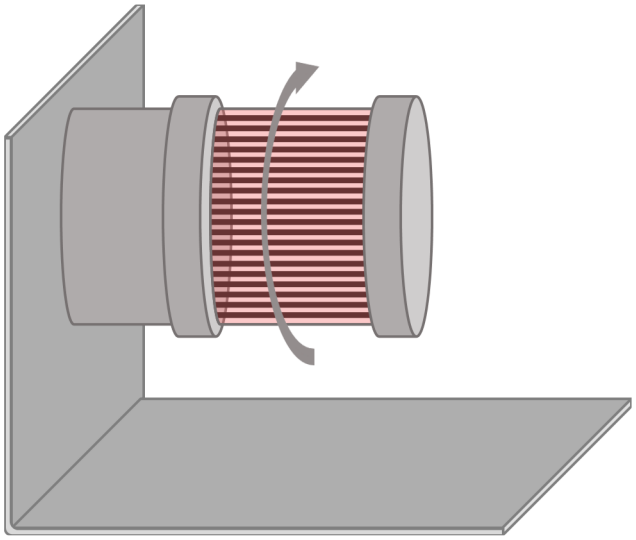

Figure I.13 – Schematics of a rotating bed bioreactor. From Nogueira et al. (2021a). Reproduced under the terms of the Creative Commons CC-BY license. Copyright 2021, The Authors.

Zellwerk GmbH has developed the disposable rotating bed Z®RP 2000 H and Z®RP 8000 H bioreactor systems, providing 2000 cm^2 and 8000 cm^2 of cell attachment area, respectively. These bioreactors consist of a cylindrical vessel containing a bed of polycarbonate plates which rotate through the action of a magnetic drive. Their set-up allows for operation under a perfusion feeding regime. Moreover, they are equipped with a sampling device for supernatant analysis as well as pH and oxygen sensors connected to a control unit. The single-use parts comprise the vessel, tubing system and measuring devices (Reichardt et al. 2013, Neumann et al. 2014).

Neumann and colleagues characterised the Z®RP 2000 H bioreactor and applied it for UCM-hMSC expansion. The authors verified homogenisation of the culture under normal operating conditions for both a half-full (70 mL) and full (120 mL) vessel, and the Bodenstein number was characteristic of a

stirred-tank reactor-type mixing even for the lowest mixing speed and full volume. After 5 days of culture, a total of (2.46 ± 0.24) × 10^7 hMSCs could be obtained at a 125 mL scale, maintaining hMSC immunophenotype and trilineage differentiation potential (Neumann et al. 2014). Reichardt et al. applied rotating bed bioreactors with a 6000 cm^2 surface area and a 340 mL working volume for human umbilical cord artery cells (HUCACs), harvesting (3.48 ± 0.55) × 10^8 cells in 9 days, albeit with full depletion of glucose at some timepoints (despite the perfusion feeding regime). The authors compared bioreactor culture to maintenance in static T-25 flasks and estimated 311 of these flasks would be required to achieve the same cell numbers, encompassing an over 3-fold increase in medium volume necessary (about 12.1 L versus 3.83 ± 0.69 L in the bioreactor) (Reichardt et al. 2013).

I.1.2.5.6. Rocking motion bioreactors

Rocking motion bioreactors were first described in 1998 (Singh 1999) and were established as an alternative to STBRs in the culture of insect and mammalian cells for processes such as production of viruses and recombinant proteins. These bioreactors rely on an impeller-free agitation mechanism where the vessel, a plastic bag, is placed on the top of a base which moves in a back-to-forth rocking motion. The agitation causes the formation of waves in the air-liquid interface, ensuring efficient mixing, with a high mass transfer and no particle settling, while also avoiding high shear stress (Figure I.14) (Kalmbach et al. 2011, Marsh et al. 2017). Cell damage is further avoided by the lack of a sparging mechanism and associated bubble formation. While the shear stress generally increases with the agitation velocity, at certain agitation speeds a resonance phenomenon is observed, causing unusual behaviour such as higher vorticity and shear stress. Zhan et al. observed that, for a half-filled 10 L rocking motion bioreactor, agitation at 15 rpm led to an approximation to the natural frequency of the bioreactor (calculated by approximating its shape to a perfect ellipse), causing higher turbulence than agitation at 22 rpm and 30 rpm (Zhan et al. 2019). As such, during process development with this bioreactor system, it is important to estimate the natural frequency and avoid choosing a rocking velocity close to this frequency.

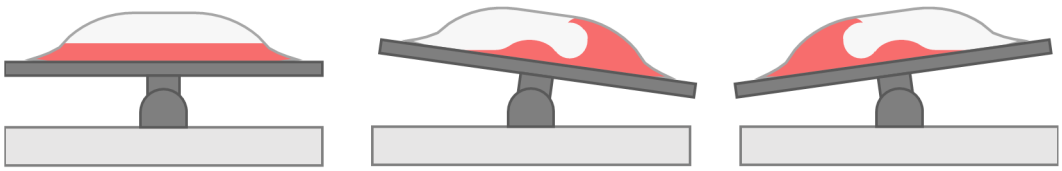

Figure I.14 – Schematics of a rocking motion bioreactor. The back-and-forth rocking motion of the base will lead to the formation of waves inside the vessel, allowing for an efficient mixing. From Nogueira et al. (2021a). Reproduced under the terms of the Creative Commons CC-BY license. Copyright 2021, The Authors.

Rocking motion bioreactors were first developed as single-use, employing a disposable culture bag. Rocking motion bioreactors commercially available include the Xuri Cell Expansion System (previously WAVE Bioreactor™) and Cellbag™ vessels from Cytiva, and the Biostat® RM and Flexisafe® RM bags (replacing CultiBag) from Sartorius, and cover working volumes from 50 mL up to 500 L.

Davis and co-workers have cultured both hESCs and hiPSCs as aggregates in the Xuri Cell Expansion System, with perfusion and non-perfusion Cellbags, at various scales—150 mL, 250 mL and 1 L—and also performed consecutive passage experiments. The authors also optimised the culture

conditions and were able to obtain up to 9.5-fold expansion in 4 days. Serial passaging from 250 mL to 1 L under optimised conditions led to a 39.2-fold expansion (~ 3.9×10^9 cells in 8 days), while passages from two sequential 150 mL bioreactors to 250 mL and to 1 L in non-optimised conditions resulted in a cumulative 280-fold increase in cell number (~ 1.7×10^{10} cells in 16 days). The authors also estimated how operating these bioreactors under automated perfusion, besides allowing a closed process and ensuring sterility, could lead to a substantial increase in cell yield per spent medium—from 4.2×10^5 cells/mL in 6-well plates to 1.5×10^6 cells/mL in 1 L perfusion bioreactors (Davis et al. 2018).

hMSC expansion in rocking motion bioreactors has also been demonstrated by different groups. Nguyen and colleagues were able to expand these cells for 100 days in bioreactors with a 200 mL working volume, maintaining hMSC viability and chondrogenic and osteogenic differentiation potential. A maximum of $(2.64 \pm 0.18) \times 10^8$ cells were counted on day 40. However, despite a decrease to $(8.7 \pm 2.1) \times 10^7$ cells by day 90, the authors did not observe dead cells through a LIVE/DEAD assay and speculated the decrease in countable cell number to be attributed not to cell death, but to hMSC migration to the inside of the microcarrier pores (Nguyen et al. 2019). Da Silva et al. observed some cell deposition in Cellbags, which resulted in stagnated cell growth, and designed an acrylic grid which would allow for the Cellbag to remain in contact with the base for temperature control, but would also raise the Cellbag wall, avoiding cell deposits. The authors also verified some deposits at the Cellbag wall due to the microcarriers sticking to it. The adhesion phase was first performed in spinner flasks, then in the modified Cellbags in dynamic conditions, and in static with reduced volume. The latter conditions led to the best overall cell expansion, with a final yield of 2.56×10^8 UCM-hMSCs in 600 mL (da Silva et al. 2019). The same group then compared the expansion of these cells in the modified Cellbags (600 mL working volume) and 500 mL spinner flasks. Neither platform impacted hMSC tri-lineage differentiation potential nor differently regulated biological systems, however, spinner flask culture was more efficient, both in terms of final cell number and in the time at which the maximum was achieved. Maximum cell yields of $(4.65 \pm 0.14) \times 10^8$ cells in 6 days and 1.32×10^8 cells in 11 days were obtained for the spinner flask and the rocking motion bioreactor, respectively (da Silva et al. 2020).

Timmins and colleagues have used rocking motion bioreactors for production of red blood cells (RBCs) from umbilical cord blood (UCB)-derived hHSPCs. By controlling the cell density at regular intervals, the authors obtained an average 2.25×10^8–fold increase in cell number in 33 days—a production averaging 4.5×10^{15} RBCs in a culture of up to 1 L of working volume, and allowing to harvest 560 units of RBCs per UCB donation (Timmins et al. 2011).

I.1.2.5.7. Vertical-Wheel bioreactors

As mentioned in section I.1.2.5.1, stirred tank bioreactors are the gold standard in traditional bioprocessing approaches, but are undesirable for stem cell culture due to the high levels of shear stress their agitation mechanism conveys. While most other bioreactor systems already mentioned avoid the issue by not employing an impeller, this impairs mass transfer and may compromise the homogeneity of the culture. The Vertical-Wheel™ bioreactors (VWBRs), introduced by PBS Biotech, were designed to provide a homogeneous culture environment while using a more gentle and efficient agitation mechanism (Figure I.15) (Croughan et al. 2016). The vessels contain a large vertical wheel, which

format results in both radial and axial agitation. Moreover, the U-shaped bottom of the vessel avoids “dead zones” underneath the impeller, thus limiting cell settling. Overall, this results in a more efficient mixing, allowing for low agitation speeds to be used and, consequently, less shear stress to be conveyed to the cells. Furthermore, the large size of the impeller allows for the dissipation of its rotational energy over a substantial area, thus resulting in narrower gradients of energy dissipation rate, with maximum values of 20–25% compared to horizontal-blade impellers (Croughan et al. 2016). These bioreactors can have two different agitation mechanisms: in AirDrive VWBRs, agitation is controlled by bubble sparging, which are captured in specific zones of the vertical wheel, allowing for its motion; in MagDrive VWBRs, agitation is driven by magnetic coupling between magnets present in the vertical impeller and in the base unit. These bioreactors were developed to be single-use and are available in various scales, from 100 mL to 80 L (MagDrive) or from 3 L to 500 L (AirDrive), and feature an imbedded automatic controller starting from the 3 L units (Figure I.15). The characterisation of VWBRs is so far limited and, as such, no empirical correlations for bioreactor scale-up are yet available, but reports of computational fluid dynamics (CFD)–based hydrodynamic modelling have already been published (Croughan et al. 2016, Borys et al. 2021).

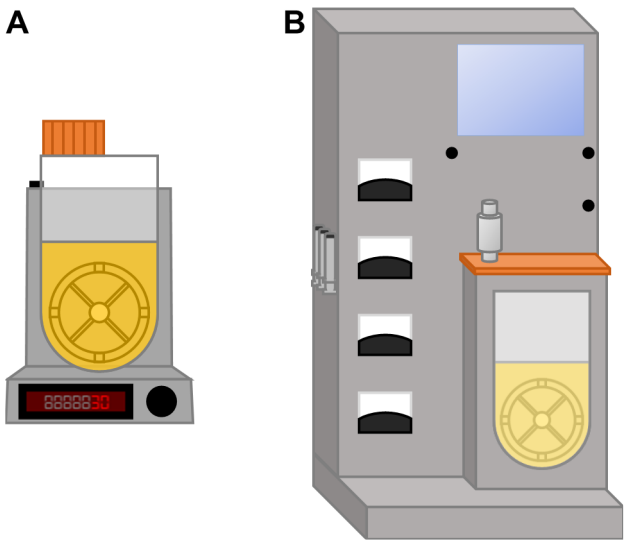

Figure I.15 – Schematics of a Vertical-Wheel bioreactor. **A** 100 mL vessel with base. **B** 3 L vessel with embedded controller. From Nogueira et al. (2021a). Reproduced under the terms of the Creative Commons CC-BY license. Copyright 2021, The Authors.

hiPSC culture in VWBRs has already been described, culturing the cells attached to vitronectin-coated microcarriers (maximum yield of (1.0 ± 0.1) × 10^8 cells in 9 days at an 80 mL scale, and (2.6 ± 0.5) × 10^8 in 8 days using a 300 mL working volume (Rodrigues et al. 2018)). Borys and colleagues tested hiPSC expansion in 100 mL VWBR and found normoxic conditions using repeated batch to lead to a higher cell growth than experiments with hypoxia (3%) and/or batch conditions. By performing a low-density inoculation with pre-formed aggregates, they obtained up to (6.3 ± 0.4) × 10^8 cells in 6 days, and about 2.1 × 10^{12} cells in 28 days, over the course of 4 consecutive passages (Borys et al. 2020). The same group then optimised the culture protocol, in terms of inoculation (pre-formed aggregates vs. single cells) and agitation speed, as well as harvesting enzyme and exposure time. With the optimised conditions, a maximum of (6.5 ± 0.6) × 10^8 cells could be obtained, which could be passaged to 500 mL

volume vessels (Borys et al. 2021). In all cases, the expression of pluripotency markers and differentiation potential of the cells were found to be maintained. In a recent study, Silva and colleagues have demonstrated cerebellar differentiation of hiPSCs in VWBRs. The dynamic culture system was shown not only to maintain cell viability for at least 80 days of differentiation, but also both to enhance extracellular matrix formation and to activate angiogenesis-related pathways in comparison to the static control (Silva et al. 2021). This spontaneous onset of angiogenesis, in particular, is a very promising development, as *in vitro* organoids are generally limited in this regard and necessitate alternative strategies for blood vessel formation (Kim et al. 2016).

Various studies also describe hMSC expansion in VWBRs. Yuan and colleagues developed a method for scalable BM-hMSC aggregation (Yuan et al. 2018). The authors designed thermal responsive PNIPAAm microcarriers to which cells could attach at 37 °C, and be detached from at the end of expansion by incubation at 23 °C. Following thermal detachment and microcarrier removal from the vessel, the cells would be left to spontaneously aggregate. The authors performed cell expansion, harvesting and aggregation in both spinner flasks and VWBRs. In the spinner flask, the harvesting resulted in mainly single cells which did not aggregate even after 24 h. Expansion in the VWBRs at a 60 mL scale led to a production of 6.8×10^6 cells in 4 days, which could be harvested in 10 min at 23 °C and could form aggregates, with comparable diameter and cell viability to an microwell plate–based protocol, as well as with a similar immunomodulation and cytokine secretion. Lembong and co-workers also describe BM-hMSC expansion in VWBRs, using a xeno-free, fed-batch approach. Following optimisation of the cell and microcarrier concentration, as well as the agitation, the fed-batch and microcarrier addition strategies, and harvesting process (speed, quench hold time and solution temperature) the authors could obtain $1.8\text{-}5.5 \times 10^7$ cells across hMSCs of five different donors after 5 days in a 92 mL working volume (Lembong et al. 2020). Another report of xeno-free UCM- and AT-hMSCs expansion in VWBRs led to the production of $(5.3 \pm 0.4) \times 10^7$ and $(3.6 \pm 0.7) \times 10^7$ cells, respectively, in 7 days and with a 100 mL working volume. Furthermore, the VWBR was established as an economical alternative to T-175 flasks, as a cost analysis estimated a reduction of the process cost per dose, from $17,000 to $11,100 for UCM-hMSCs and from $21,500 to $11,100 for AT-hMSCs (de Sousa Pinto et al. 2019). Similar conditions were used for production of extracellular vesicles (EVs) from BM-, AT- and UCM-hMSCs expanded in 100 mL working volume VWBRs. EVs comprise a prospective therapy for a variety of diseases, either by their own characteristics or as drug delivery vehicles. Up to $(5.3 \pm 5.5) \times 10^7$ hMSCs were obtained after the culture (which ranged from 7 to 11 days depending on the cell donor and source). All three cell sources led to EV production in higher amounts when compared to static cultures (averaging 5.7 ± 0.9–fold higher production), with a maximum average of $(6.9 \pm 1.7) \times 10^9$ particles/mL for UCM-hMSCs. The purity of these EVs was also improved and more consistent between runs in comparison to static culture (de Almeida Fuzeta et al. 2020). Finally, BM-hMSCs have also been expanded at a 2.2 L scale, in AirDrive VWBRs. About 6.6×10^8 cells could be obtained after 14 days of culture, with a similar cell concentration to 250 mL STBRs, although with a significantly lower percentage of apoptotic cells, as well as less human leukocyte antigen (HLA)–DR expression (3% in VWBRs vs 30% in STBRs). This lower HLA-DR expression, in particular, is promising for the development of allogenic cell therapies (Sousa et al. 2015).

I.1.2.5.8. Challenges of single-use bioreactor-based processes

The various examples of single-use bioreactors presented have shown that these platforms can provide an answer to the limitations of reusable bioreactor systems for biomanufacturing of stem cells for Regenerative Medicine applications. In fact, disposable hollow fibre bioreactors have already been used in this context (Tirughana et al. 2018), and promising results on stem cell expansion and/or differentiation in other platforms, such as STBRs, rocking motion bioreactors and VWBRs may lead into clinical trials with stem cells and derivatives produced in these bioreactors in the near future. The choice of bioreactor will depend on various factors, as each bioreactor has a subset of advantages and limitations (summarised in Table I.3), however, the overall development of processes with single-use bioreactors also provides some challenges, independently of the platform of choice.

Reusable bioreactors necessitate resistant materials for their components, such as glass and/or stainless steel, in order to prolong their lifetime even under many successive/long cultures and various autoclaving or steaming cycles. The disposable parts of single-use bioreactors can employ less-resistant materials, such as polymeric compounds, as they need only to be used for one culture process. However, their sterilisation with γ-radiation and their use under culture conditions can lead to the degradation of these polymers, which then leach to the culture medium. Marghitoiu and colleagues identified 53 different extractables from four different single-use vessels (Marghitoiu et al. 2015). One of these, *bis*(2,4-di-*tert*-butylphenyl)phosphate (BdtBPP), is of special concern. BdtBPP results from the degradation of *tris*(2,4-di-*tert*-butylphenyl)phosphate (TBPP), an agent which is commonly added to polyolefins to protect them from oxidation by high temperatures or ionising radiation. BdtBPP was found to be a very potent inhibitor of cell growth (Hammond et al. 2013, Hammond et al. 2014, Liu et al. 2014), with a half-maximal effective concentration (EC_{50}) for viable cell density between 0.12 mg/L and 0.73 mg/L across 9 different CHO cell lines, while up to 2 mg/L could be extracted from single-use vessels (Hammond et al. 2013). Notably, as the ageing of single-use vessels leads to a reduction in the leachable compounds, some vessels where cell growth was impaired by the presence of BdtBPP could sustain normal cell growth after some time (Jurkiewicz et al. 2014). Nevertheless, due the possibility of leaching-mediated impaired cell growth, extensive tests on the vessel extractables and care in the use of compounds such as TBPP are of crucial importance. The lesser resistance of the single-use bioreactors in comparison to reusable systems may also limit the scale at which cultures can be performed – at very high scales, the vessels may not be able to withstand the liquid volume and rupture. While this is not a problem for autologous therapies, especially if high-density cultures can be performed, the establishment of off-the shelf products may be more difficult.

Single-use bioreactors also present an important sustainability issue. In fact, the disposal of possibly hundreds or thousands of single-use vessels over the lifetime of a process will contribute to a higher footprint, as these vessels, due to having harboured expanding cells, are treated as biological waste and cannot be recycled, being incinerated or sent to landfills. The manufacturing, packaging, sterilisation and shipping of these bioreactors also pose sustainability constraints, as these steps have to be constantly repeated throughout the process. However, a set of life cycle analyses of monoclonal antibody and adenoviral vaccine production in reusable and single-use systems actually concluded the single-use process to be more environmentally sustainable. In fact, the major environmental impact of

Table I.3 – Advantages and limitations of single-use bioreactors as a whole and specific single-use platforms. From Nogueira et al. (2021a). Reproduced under the terms of the Creative Commons CC-BY license. Copyright 2021, The Authors.

Platform	Advantages	Drawbacks/limitations
Single-use bioreactors	• Compatible with GMP guidelines • Pre-sterilised—no CIP and SIP necessary • Closed systems—minor contamination risk • Reduced downtime and higher productivity • Lower overall environmental impact than reusable systems • Lower initial investment	• Risk of leachables—possible cell growth impairment • Maximum scale limited by material resistance • Environmental impact of vessel manufacturing, packaging, shipping and disposal throughout the whole process • High running costs
Stirred tank	• Vast know-how and characterisation • Available at many different scales • Availability of empirical correlations and criteria for variable estimation and scale-up • Variety of agitation mechanisms • Some are naturally compatible with perfusion	• High overall shear stress • Heterogeneity of shear stress distribution—existence of hot-spots and stagnated zones
Fixed bed	• Low shear stress • High surface-to-volume ratio and small footprint • Naturally compatible with perfusion	• Formation of concentration gradients • Cell harvesting only possible at the end of the culture • Difficult cell monitoring
Hollow fibre	• Low shear stress • High surface-to-volume ratio and small footprint • Semipermeable membrane system, allowing for indirect mass exchange • Naturally compatible with perfusion	• Formation of concentration gradients • Cell harvesting only possible at the end of the culture • Difficult cell monitoring • Susceptibility to fouling • Expensive operation • Available only at a single scale (2.1 m^2)
Rotary cell culture system	• Low shear stress • Simulated microgravity environment • No air bubbles • Some are naturally compatible with perfusion	• Formation of concentration gradients • Available only at small scales (up to 50 mL)
Rotating bed	• Low shear stress • High surface-to-volume ratio and small footprint • Intermittent contact with medium and headspace • Naturally compatible with perfusion	• Cell harvesting only possible at the end of the culture • Difficult cell monitoring
Rocking motion	• Efficient mixing with low shear stress • No air bubbles • Some are naturally compatible with perfusion • Available at many different scales	• Resonance phenomenon—spike of shear stress at certain rocking velocities • Some cell deposition and microcarrier sticking to vessel walls
Vertical-Wheel	• Efficient mixing with low shear stress • Vessel format avoids cell settling at the beneath the impeller • Narrow gradients of energy dissipation rate • Available at many different scales • Naturally compatible with perfusion starting from the 3 L scale	• Still not well-characterised • Small-scale (100 mL and 500 mL) bioreactors not controlled and incompatible with perfusion

traditional systems lies on the sterilisation, specifically, on the water for injection and clean steam requirements. Conversely, the end of life of disposable systems was found not to be significant in comparison to the impact of both their production and of the bioprocess operation. As such, overall, single-use bioreactors were considered by the authors a “greener” approach, but their environmental impact can be reduced even further by, for instance, ensuring the bioproduction facility is as close as possible to the site of vessel manufacturing, and by promoting the recycling of any non-contaminated parts, namely, the packages and wrapping (Pietrzykowski et al. 2013). Furthermore, this study focused on traditional biological processes, as such, it still remains unanswered if the same conclusions can be extrapolated to the bioproduction of stem cells with its associated specificities.

The transition to disposable systems is also of economic concern (Levine et al. 2013, Rogge et al. 2015). While disposable vessels are less expensive than their reusable counterparts, resulting in a smaller initial investment, the need for new vessels for each bioreactor run may lead to higher running costs through the process lifetime. The differences in single-use bioreactor process cost will depend not only on the lower initial investment and higher consumable cost, but also on other factors such as the time saved in sterilisation cycles and the potential lower risk of contaminated batches. Furthermore, processes with single-use bioreactors may face smaller regulatory hurdles, reducing the time-to-market, and, consequently, the pay-back and pay-out times. The evaluation of the most financially attractive process will require a thorough economic analysis. Even with this analysis, the choice will depend on what the final goals are—for instance, to obtain a higher profit in the lifetime of the process or to break even with the initial costs at the earliest opportunity.

I.1.2.6. Emerging trends in human induced pluripotent stem cell culture

Since the first derivation of hiPSCs in 2007, these cells have held much promise in the impact they could have on medical practices, especially concerning precision medicine approaches. While the ability to mass-expand hiPSCs in bioreactors, using strategies such as those here described, was certainly an important achievement in this regard, there is still a long path to be treaded before the use of these cells is commonplace.

One important point lies in the cells themselves. hiPSCs have been described to retain some epigenetic memory of their pre-reprogramming state, such as methylation profiles, which can impact their differentiation potential and skew it towards the cell type of origin (Nishino et al. 2011, Tesarova et al. 2016). This enforces the usage of specific primed hiPSC lines to obtain a desired cell type with a high yield. Alternatively, following reprogramming, hiPSCs can be led towards a more naïve state of pluripotency, featuring ICM-like gene expression and hypomethylation (reviewed in Yagi et al. (2017)). Lipsitz and co-workers describe a four-inhibitor formulation which leads primed hPSCs towards a naïve state (Lipsitz et al. 2018b). Naïve cells were shown to expand 5.7 ± 0.2-fold higher than primed cells in bioreactors, without loss of pluripotency or karyotypic abnormalities. Similar conclusions were obtained by Rohani and colleagues following a culture medium–induced transition to a naïve state—higher growth rates (~ 1.5-fold) and enhanced aggregation. The authors also observed a robust expression of naïve pluripotency markers and hallmarks of X chromosome reactivation (Rohani et al. 2020). Thereupon, the

usage of naïve hiPSCs may not only facilitate differentiation methodologies, but also improve the cell numbers which are harvested at the end of culture.

One additional strategy, which was described to improve stemness of mESCs, is the subjection of the cells to a microgravity environment. The phenomena which lead to increased stemness are still not well known but may include microgravity-induced activation of specific signalling pathways, such as wingless-related integration site (Wnt) 1, improved nutrient consumption and lower shear stress. The effect of microgravity on differentiation, however, is still controversial. Indeed, while it has been described to inhibit cell terminal differentiation in both directed and spontaneous differentiation of mESCs (Blaber et al. 2015, Lei et al. 2018b), other studies detail improved differentiation into pancreatic lineages (Wang et al. 2012b) and retina organoids (DiStefano et al. 2018) on microgravity bioreactors, as well accelerated neural differentiation of hESCs (Come et al. 2008). Moreover, temporary exposure of hPSC-derived cardiac progenitor cells (CPCs) to microgravity has been shown to increase final cardiomyocyte purity and yield, the latter up to 4-fold in comparison to normal gravity culture (Jha et al. 2016). Therefore, while more detailed studies of microgravity in pluripotency and differentiation are still required, particularly on human cells, the usage of microgravity bioreactors for hiPSC culture may not only eventually improve the quality of cells to some extent, but also provide important insights on the behaviour of living organisms in space.

Regardless of the overall strategy, the transition of any of these methodologies from the laboratory to an industrial, manufacturing scale will require the design of robust bioprocesses with a tight quality control. This has led regulatory agencies to promote the implementation of Quality by Design (QbD) processes (Lipsitz et al. 2016). This approach combines scientific knowledge with risk analysis in order to determine a design space where the process can operate without affecting the final product quality. As the knowledge about the process increases, it can be modified iteratively. Therefore, while traditional processes require extensive quality control at a product level, the QbD framework employs quality control throughout the production, reducing the risk of unsuitable products and ultimately resulting in a less expensive and more robust bioprocess. Advancements in machine learning may also contribute to the development of robust bioprocessing technologies, by exploring interactions between the cells and their environment which are not immediately evident, and how those are directly translated in stem cell behaviour (Joutsijoki et al. 2016, Orita et al. 2019, Williams et al. 2020). Finally, the implementation of fully automated processes is also of importance in the establishment of robust bioprocesses as a means of minimising operator variability and errors (Kulik et al. 2016).

I.2. Heart development and cardiac differentiation

The heart is one of the most important organs in the human body. It functions as a mechanical pump—after being filled with blood, the heart contracts and the blood is readily delivered through arteries to the rest of the body.

The human heart has a four-chambered structure, being composed of two atria, at the top and two ventricles, at the bottom (Weinhaus and Roberts 2005). The left and right chambers are separated by a septum, avoiding mixture of the blood in both sides, and a one-way valve borders the atrium and the ventricle and prevents blood backflow. The heart wall is divided in three layers—the endocardium,

the myocardium and the epicardium (from the innermost to the outermost layer). Surrounding the heart is a liquid-filled sac termed pericardium. The contractions of the heart are mostly a function of the cardiac muscle cells, or cardiomyocytes, which are the main type of cell which comprises the myocardium. Amongst these cells, some neuron-like cells, the pacemaker cells, ensure a synchronous and stable contraction along the whole heart.

The main function of the heart is to ensure proper oxygenation and nutrient supply to the various cells of the body (Weinhaus and Roberts 2005) (Figure I.16). Oxygenated, or atrial, blood is supplied from the lungs through the pulmonary vein and enters the left atrium of the heart. As the atria contract (atrial systole), the arterial blood moves towards the left ventricle, passing through a one-way valve which impedes backflow to the atrium. Following the atrial systole, a ventricular systole displaces the blood from the heart to the rest of the body through a complex arterial system. This will allow the cells to receive oxygen and nutrients, and to dispose of carbon dioxide and toxic metabolites. Following both contractions, the heart will relax (diastole), After oxygen and nutrient exchange, the now-venous blood will return to the heart through the veins and enter the right atrium. Following atrial systole, the blood will pass the valve to the right ventricle, and after ventricular systole, the venous blood will be transported to the lungs through the pulmonary arteries. Gas exchange occurs through the alveoli, ensuring the blood is depleted of carbon dioxide and enriched in oxygen. This arterial blood will travel back to the left atrium via pulmonary veins and the cycle begins anew.

A healthy heart generally contracts at a rate of 60–100 bpm (Clarke et al. 1976, Abba and Garba 2020). This rate can, however, be influenced by activity, as strenuous physical effort will increase the beating (and respiratory) rate, ensuring a higher oxygen supply to the muscles, and, consequently, a higher ATP production (Cheng et al. 2008), whereas resting periods are characterised by a slower beating and respiratory rate, as only a basal activity of the body needs to be maintained (Cajochen et al. 1994). Blood pumping will, evidently, result in a higher strain in the walls of the blood vessels, due to the higher mechanical pressure applied. Regular control of the arterial pressure and of the beating rate (normally measured on the left arm, wrist, or leg) is important to ensure the health of the circulatory system and diagnose and act upon problems.

While the heart has a crucial function for maintenance of the body, it is as fragile as it is important. In fact, cardiomyocytes have an extremely limited proliferation ability (Bergmann et al. 2009, Mollova et al. 2013, Hesse et al. 2018), as such, when the heart is damaged, the dead muscle cells are replaced by fibrous tissue, forming a non-muscular scar which limits the blood-pumping ability of the heart (Richardson et al. 2015). As such, cardiovascular diseases (CVDs) represent a serious threat and severely limit the quality of life of afflicted patients. Moreover, they have remained for many years the leading cause of death in the world (https://www.who.int/news-room/fact-sheets/detail/the-top-10-causes-of-death, accessed on the 25th of May 2021). Their prevalence is not expected to decrease in the following years due to an increasing incidence of risk factors, such as obesity, high cholesterol intake, sedentarism, alcohol consumption and smoking (Virani et al. 2021). In fact, some of these factors have been exacerbated due to the lockdown and limitations imposed by the ongoing COVID-19 pandemic.

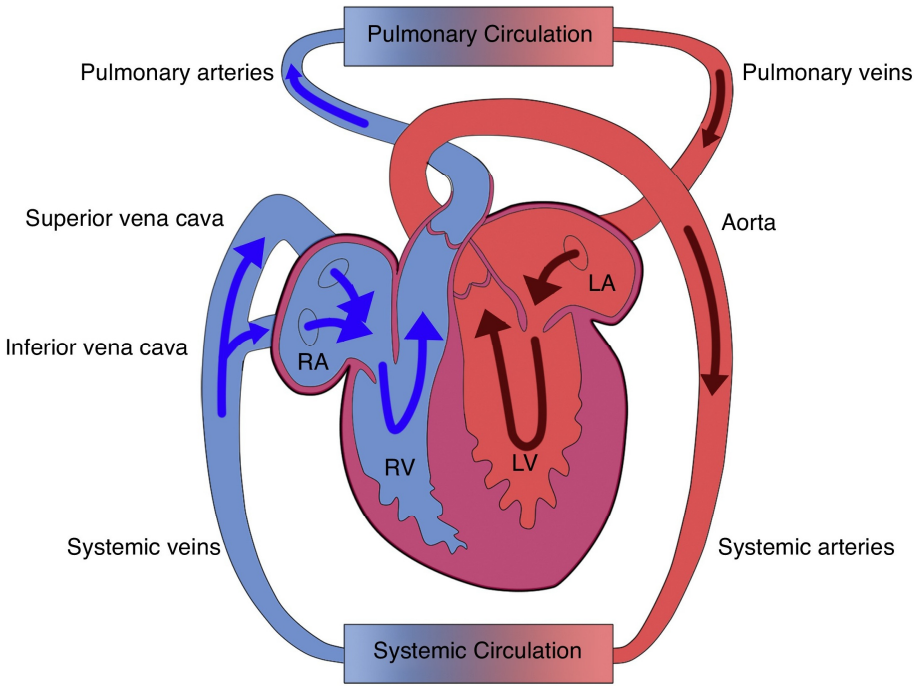

Figure I.16 – Physiology of the heart and bodily circulation. Oxygenated blood (red) enters the left atrium (LA) from the pulmonary veins and is pumped towards the left ventricle (LV). Following ventricular contraction, the blood is pumped to aorta and distributed to the tissues through the systemic arteries. Deoxygenated blood (blue) is returned to the heart through the systemic veins and the venae cavae. Blood enters through the right atrium (RA), the right ventricle (RV), and is pumped to the lungs through the pulmonary arteries. Gas exchange occurs at the alveoli, replenishing the blood in oxygen and allowing for its recirculation to the body. From Sun and Kontaridis (2018). Reproduced with permission. Copyright 2018, Elsevier.

While a cure for damaged hearts is still not available, several treatments can be used to attempt to restore some of its function and/or to overcome debilities in blood pumping. Drugs such as β-blockers (role in slowing heart rate, reduction of infarct size and prevention of arrythmias (Becker and Gore 1991, Kim et al. 2020)), anticoagulants (Homma et al. 2012, Onwordi et al. 2018) or aspirin (avoids platelet aggregation (Vane 1971, Hennekens et al. 1997)) have shown a positive effect on heart protection following myocardial infarction. In some situations, surgical intervention may be necessary, for instance, to reduce blood vessel obstruction via stenting or coronary angioplasty (Weaver et al. 1997, Zhu et al. 2001, Scheller et al. 2003), to perform a coronary bypass, allowing for an alternative pathway over compromised vessels for blood flow (Jones et al. 2009), or to implant a cardiac pacemaker to overcome defects in the cardiac conduction system (Gordon et al. 1998, Merin et al. 2009). The most severe cases may require a full cardiac transplantation, thus replacing the damaged heart with a functional one, stemming from recent corpses. However, cadaveric hearts are not readily available and may lead to complications related with donor-host incompatibility, including rejection. Moreover, transplantation is not an option for a variety of patients as a result of other underlying pathologies (Deng 2002). As such, scientists have long searched for alternatives to transplantation, and that answer may have been found in hPSCs. Achieving cardiac differentiation of hPSCs requires an understanding of the *in vivo* mechanisms involved in the heart formation, as such, the following section will detail how this occurs in the embryo, followed by some strategies to recapitulate these phenomena *in vitro*.

I.2.1. Human cardiogenesis

This section will describe some of the steps involved in cardiac formation in the embryo (Figure I.17), with greater detail on the steps leading to the heart tube formation, as these are of particular importance in understanding how to recapture cardiac differentiation *in vitro*. A comprehensive description of the whole process of human cardiac development is available by Buijtendijk et al. (2020).

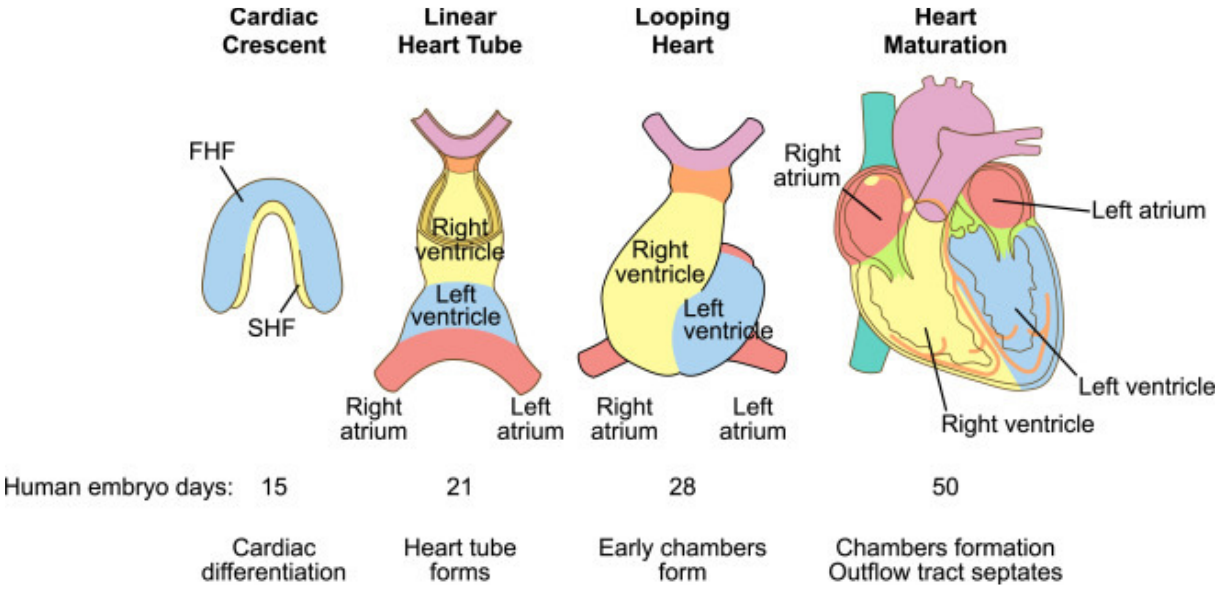

Figure I.17 – Heart development. The cardiac crescent is formed by cells migrated from the mesoderm. As the embryo folds, the cardiac crescent will form the heart tube. Following looping of the heart tube and septation, the heart acquires its mature form. From Chemello et al. (2020). Reproduced with permission. Copyright 2020, Elsevier.

After fecundation and formation of the zygote, this cell undergoes successive divisions until forming the morula, a cell sphere comprising about 16 cells. At this point, the cells will start to organise and differentiate, forming an outer cell layer, the trophoblast, and an ICM. The ICM then forms an embryonic disc composed of two layers, the epiblast and the hypoblast (primitive ectoderm and endoderm, respectively).

Cardiac development can be considered to start with the gastrulation, at the third week of embryogenesis. In this stage, the primitive streak, a midline structure in the epiblast, is formed. This leads the epiblast cells along the primitive streak to detach and migrate, forming a new layer, the mesoderm, between the previous two. This three-layered structure is termed gastrula, and from its three layers, the ectoderm, mesoderm and endoderm, different types of somatic cells will be formed. In the mesoderm, WNT signalling maintains these cells undifferentiated. Some of the mesodermal cells migrate to the anterior embryo, where WNT signalling is inhibited, allowing for their cardiac differentiation via bone morphogenic protein (BMP) signalling. These cells are termed first heart field (FHF) cells and can be differentiated to cardiomyocytes and smooth muscle cells. The FHF cells form the cardiac crescent, which expresses transcription factors insulin gene enhancer protein (ISL) 1 and NK2 homeobox 5 (NKX2.5), and which is bordered by BMP inhibitors and fibroblast growth factors (FGFs) secreted by the neural tube and the endoderm, respectively. Primitive cardiomyocytes then being to contract and to electrically couple, initiating myocardial formation. At the same time, some of the cells which have migrated to the anterior embryo have undergone epithelial-to-mesenchymal transition and

begin endocardial formation between the precardiac mesoderm and the endoderm. At the end of the third week of cardiac development, the embryo starts to fold, and the cardiac crescent originates a heart tube, comprised of two to three layers of cardiomyocytes and an inner layer of endocardial cells, separated by extracellular matrix (ECM; cardiac jelly).

At the fourth week of embryonic development, the heart tube begins to bend. Some of the cells which have remained in the mesoderm, rapidly proliferating through canonical WNT signalling, will at this stage migrate and differentiate into cardiomyocytes, integrating and expanding the folding heart tube. These cells are termed second heart field (SHF) cells, and, besides cardiomyocytes and smooth muscle cells, can also generate endothelial cells. The successive bending of the heart tube then leads to ventricular and then atrial formation, and the left and right chambers are then divided by septation, to avoid the mixture of arterial and venous blood. The septation process also starts the formation of the heart valves, which impede blood backflow. The cardiac conduction system develops concomitantly with the chambers, allowing the electrical impulse to be propagated to the individual cardiomyocytes through Purkinje fibres, and the heart to start to function properly.

Following all of these processes, the heart is already functional. However, its development is not restricted to the *in-utero* phase. In fact, the heart continues to mature over childhood, adolescence and early adulthood. This process is further detailed in section I.2.4.

I.2.2. *In vitro* protocols for cardiac differentiation of human pluripotent stem cells

A variety of protocols for hPSC differentiation have already been described, by applying some of the lessons gathered from human cardiogenesis. The efficiency of these protocols is generally measured in terms of expression of cardiac-specific genes, including cardiac troponins T (cTNT) and I (cTNI), myosin heavy chain (MHC) or myosin light chain (MLC) 2, in both its atrial (MLC2a) and ventral (MLC2v) isoforms.

I.2.2.1. Embryoid bodies

Embryoid bodies (EBs) are aggregates resulting from spontaneous differentiation of hPSCs and are formed by self-aggregation of these cells in low-attachment platforms and culture in medium with FBS for 2 weeks or more. hPSC differentiation as EBs results in cells from the three germ layers of embryonic development, which allows it to potentially generate cardiomyocytes.

The first report of EB formation using hESCs dates from 2000, from Itskovitz-Eldor and co-workers. The authors detected a minority of spontaneously contracting EBs and performed α-actinin staining, confirming the cardiac identity of their cells (Itskovitz-Eldor et al. 2000). The same group later performed a more thorough characterisation of the EB-generated cardiomyocytes. A maximum of 8.1% of the EBs exhibited contractile zones (29.4% of these areas staining positively for cTNI), with increasingly sarcomeric organisation throughout the differentiation time and with electrophysiological characteristics of cardiomyocyte tissue (Kehat et al. 2001).

Since these first reports, other authors introduced some improvements in the standard EB protocol in an attempt to increase its cardiogenic potential. Laflamme and co-workers performed

implantation of hESC-derived cardiomyocytes in uninjured rat hearts. The authors employed a Percoll gradient centrifugation step at day 21 of differentiation to increase purity to ~ 15% cardiomyocytes, as well as a heat shock treatment (30 min at 43 °C) 24 h prior to graft implantation to improve cell survival. This heat shock treatment additionally increased graft size three-fold (Laflamme et al. 2005). Mohr et al. used microwells to control EB size and obtained the highest percentage of contracting EBs (~ 18–20%), as well as higher cardiac gene expression (2- to 4-fold higher than the control) when specifying EB diameter at 300–400 µm, despite similar expression of MLC2a with 100 µm and 300 µm EBs (Mohr et al. 2010). The cardiomyogenic potential of hPSC differentiation as EBs could be further improved by combining this protocol with other strategies, such as addition of growth factors and/or small molecules (Xu et al. 2002, Kattman et al. 2011, Kempf et al. 2011, Ren et al. 2011, Wei et al. 2012, Kamakura et al. 2013, Mehta et al. 2014, Qiu et al. 2017), or the culture on/encapsulation in hydrogels (Hazeltine et al. 2014, Puig-Sanvicens et al. 2015). In fact, Burridge and colleagues attained up to 89% $cTNI^+$ cardiomyocytes combining hypoxia in the first 4 days of differentiation, mesoderm induction with BMP4 and bFGF in medium with polyvinyl alcohol (PVA) between days 0 and 2, FBS supplementation at day 2–4, and EB adhesion and insulin supplementation from day 4-9 (Burridge et al. 2011). One particularly innovative protocol focused on the mitochondrial alterations throughout differentiation – while hPSC mitochondria are generally spherical with few cristae, the mitochondria of somatic cells are filamentous and contain many cristae. In fact, the metabolism of these two cell types is very distinct; whereas hPSCs support proliferation through glycolysis, somatic cells rely on oxidative phosphorylation for their energy needs, and thus require a more robust mitochondrial network. As such, treatment of hiPSC EBs with M1, a small molecule which promotes mitochondrial fusion, was shown to promote spontaneous cell differentiation, in particular to the cardiac lineage (2- to 3-fold increase in percentage of beating EBs), without changes in endoderm and ectoderm markers (Lees et al. 2019).

I.2.2.2. Inductive co-culture

The ectoderm and endoderm play important roles in human cardiogenesis, mainly through the secretion of growth factors which localise and border the CPCs and control their differentiation. As it follows, harnessing the potential of these germ layers for *in vitro* culture could allow for cardiac differentiation with limited to no additional stimuli.

Mummery and co-workers performed co-culture of hESCs with either visceral endoderm cells or liver parenchymal–like cells. These two cell types present similar protein secretion profiles and promoted cardiac differentiation of hESCs, resulting in 35 ± 10% of wells with beating areas, with a majority of the formed cardiomyocytes having a ventricular-like action potential (Mummery et al. 2003). It was later shown that the feeder layer on which hPSCs were expanded prior to co-culture had an impact on cardiac differentiation—mouse embryonic fibroblasts supported both undifferentiated hPSC expansion and cardiac induction to greater effect than human feeders (Pekkanen-Mattila et al. 2012). Cyclosporin-A, an immunosuppressant, was also detailed to improve upon differentiation of hiPSCs via co-culture, allowing for a 4.3-fold increase in the percentage of beating areas when applied at day 8. These beating colonies could then be maintained for over 10 months following replating (Fujiwara et al. 2011).

Co-culture of hiPSCs with already–cardiac differentiated cells was also proven to promote cardiac differentiation of the former. Chu and colleagues found that covering monolayer hiPSCs with a layer of hiPSC-derived cardiomyocytes would generate about 3% $cTNT^+$ cells with two different cell lines, which had a very distinct cardiac differentiation efficiency using the WNT signalling protocol (described in section I.2.2.4). Curiously, simultaneous culture of both cell types did not result in cardiac induction (Chu et al. 2020).

I.2.2.3. TGFβ and FGF signalling

The TGFβ signalling pathway (Figure I.18) is highly conserved between multicellular organisms and involved in a variety of cellular processes, including proliferation, migration, differentiation and apoptosis, although it is overexpressed in a variety of diseases (e.g., cancer). The TGFβ superfamily includes notorious cytokines such as activins, Nodals and BMPs (Akhurst and Hata 2012, Kubiczkova et al. 2012). FGF signalling (Figure I.19) is also highly conserved between species, and has a role on both progenitor cell behaviour, as well as the homeostasis of the adult tissues (Turner and Grose 2010, Ornitz and Itoh 2015). Both these signalling pathways can act at a transcriptional level, or via miRNA processing.

The TGFβ and FGF signalling pathways play crucial roles in the development of the human heart. In fact, BMP signalling is responsible for initial differentiation of FHF fields, and secretion of BMP inhibitors and FGF by the layers adjacent to the cardiac crescent spatially restrict this structure. *In vitro* activation of these signalling pathways using growth factors in a temporally localised manner has been shown in various reports to be able to directly conduct hPSCs towards a cardiac fate.

Initial cardiac mesoderm specification using growth factors is generally performed by medium supplementation of two members of the TGFβ superfamily—activin A and BMP4—concomitantly with or followed by bFGF. Starting from day 4/5 of differentiation, cardiac differentiation may be further enhanced via WNT inhibition (with growth factors or small molecules) and supplementation with vascular endothelial growth factor (VEGF). Re-supplementation with bFGF after about one week of differentiation was described to enhance the proliferation of the resulting cardiac cells (Mima et al. 1995, Yang et al. 2008). Some studies also describe this protocol under a hypoxic environment, which can mimic the oxygen tension to which the embryo is subjected (Yang et al. 2008, Kamakura et al. 2013, Thavandiran et al. 2013, Pesl et al. 2014, Weinberger et al. 2016, Ohashi et al. 2019, Souidi et al. 2021), although very low oxygen tensions may negatively affect cardiac differentiation and cause DNA damage and cellular senescence (Gaber et al. 2013). Directed cardiac differentiation with growth factors in 2D is moderately efficient, having been reported to generate over 30% $cTNT^+$ cells (Laflamme et al. 2007, Carpenter et al. 2012). 3D differentiation protocols have been shown to generate populations with much higher cardiomyocyte content, with about 80% $cTNT^+$ cells being generated in 250 mL bioreactors (Matsuura et al. 2012), and forced aggregation in microwell plates resulting in up to 95% $cTNT^+$ cells following differentiation (Pesl et al. 2014).

Other reports established some additional improvements on the growth factor-based cardiac differentiation protocol. Applying a similar methodology to their previous spontaneous differentiation report, Laflamme and colleagues subjected hESC-derived cardiomyocytes to a heat shock treatment,

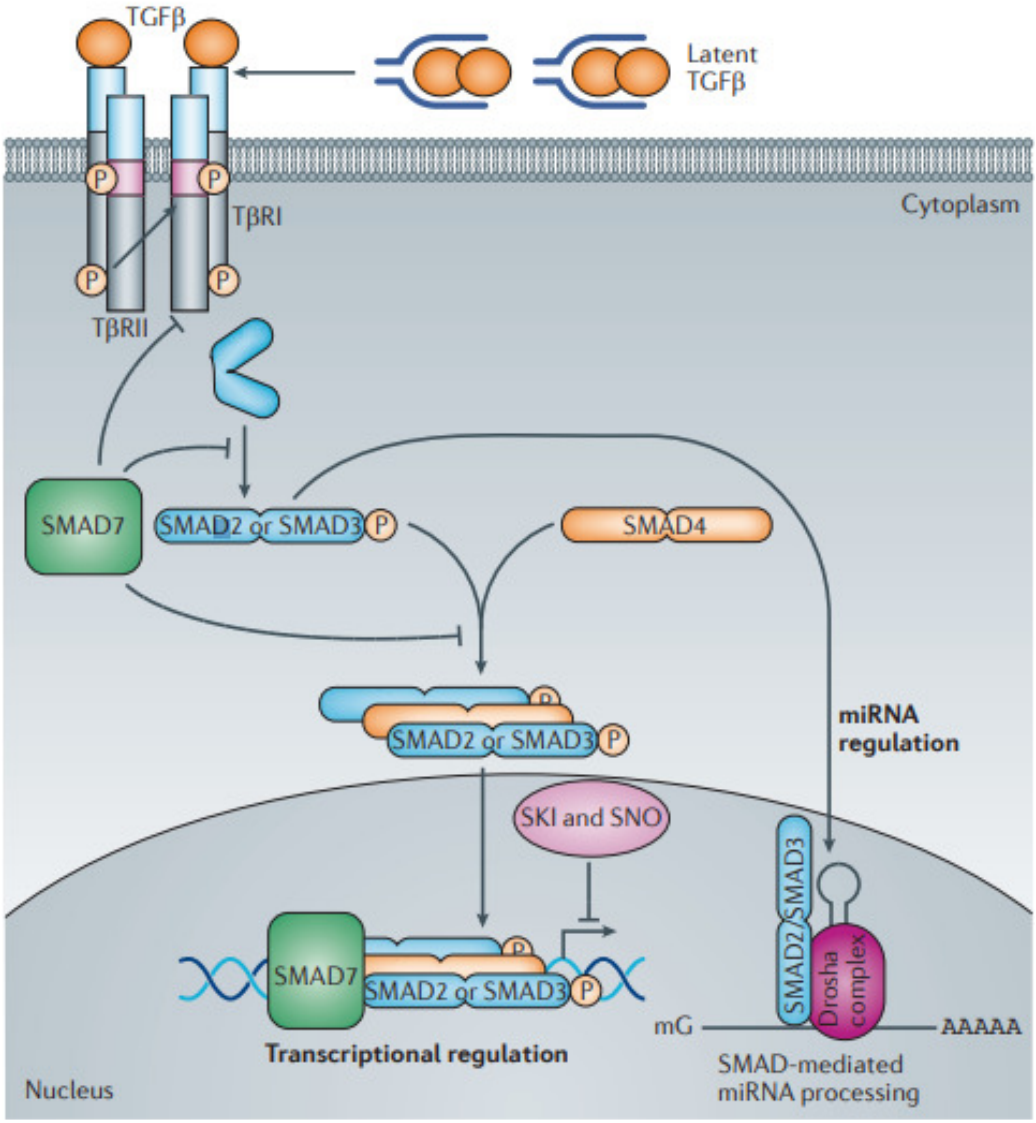

Figure I.18 – Overview of the canonical TGFβ signalling pathway. Following activation, the TGFβ receptors (TβRs) phosphorylate SMADs, which will act on transcriptional regulation of specific genes and/or on processing of miRNA for gene regulation. From Akhurst and Hata (2012). Reprinted by permission from Springer Nature: Nature Publishing Group, Nature Reviews Drug Discovery, Copyright 2012.

which, along with the use of Matrigel and a pro-survival cocktail, allowed the cardiomyocytes to engraft infarcted rat hearts and attenuate the disease progression (Laflamme et al. 2007). BMP inhibition by NOGGIN and subsequent retinoic acid inhibition at the mid-differentiation stage improved 2D cardiac differentiation with a cardiomyocyte yield of 64.7 ± 0.9%. Intriguingly, retinoic acid signalling could be modulated to promote the generation of different subtypes of cardiomyocytes – atrial for its activation and ventricular with its inhibition (Zhang et al. 2011). Molecules which were also shown to improve cardiac differentiation include G-protein coupled receptor apelin (involved in mesodermal cell migration) (Wang et al. 2012a) and trichostatin A (inhibits histone deacetylases, which would otherwise repress cardiac transcription factors GATA-binding protein (GATA) 4, myocyte-specific enhancer factor (MEF) 2C and NKX2.5) (Lim et al. 2013).

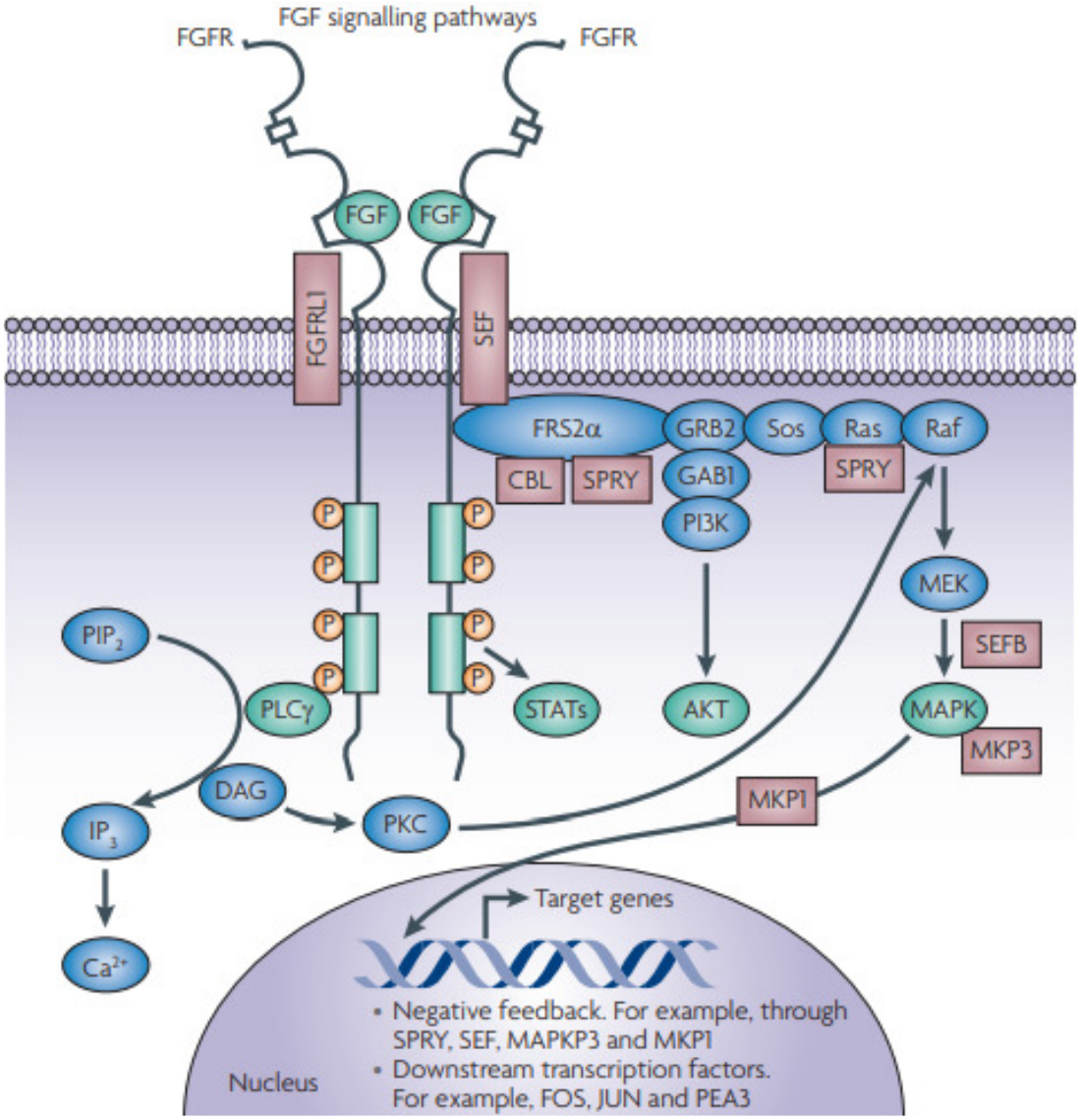

Figure I.19 – Overview of the FGF signalling pathway. Following ligand binding, the phosphorylation of kinase domains and docking of adaptor proteins will activate the RAS-RAF-MAPK, PI3K-AKT, signal transducer and activator of transcription (STAT) and phospholipase Cy (PLCγ) pathways. Regulation of target genes may be performed at a transcriptional level or via miRNAs. From Turner and Grose (2010). Reprinted by permission from Springer Nature: Nature Publishing Group, Nature Reviews Cancer, Copyright 1969.

I.2.2.4. WNT signalling

WNT signalling (Figure I.20) is a highly conserved pathway, responsible for embryonic development and adult tissue homeostasis. Canonical WNT signalling relies on β-catenin. When this pathway is not activated, β-catenin is phosphorylated by glycogen synthase kinase (GSK) 3 and subsequently degraded. Upon WNT activation, the mechanisms of β-catenin phosphorylation are stopped, allowing for translocation of β-catenin to the nucleus and activation of target genes (Clevers 2006, Komiya and Habas 2008, Patel et al. 2019).

Similarly to the signalling pathways mentioned in the previous section, WNT signalling is inextricably involved in human cardiogenesis. Its role was found to be biphasic—while canonical WNT

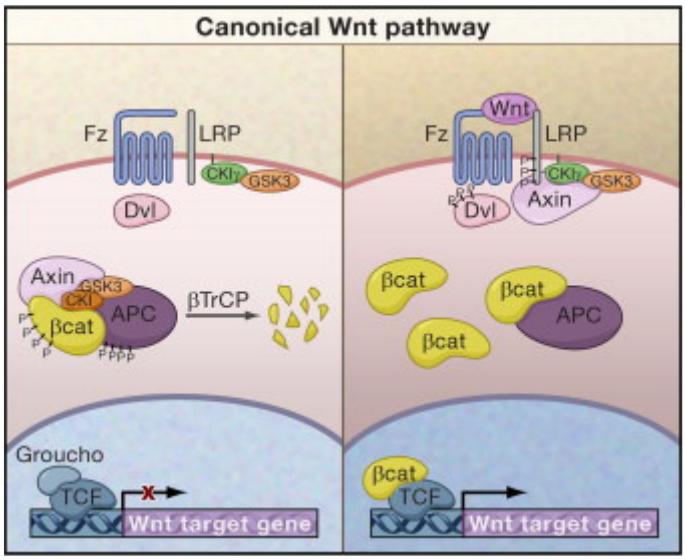

Figure I.20 – Overview of the canonical WNT signalling pathway. When the pathway is inactive, β-catenin (βcat) is phosphorylated by casein kinase (CK) 1 and glycogen synthase kinase (GSK) 3. After phosphorylation, β-catenin is recognised for ubiquitination and degraded. Groucho binds to T-cell factor (TCF), inhibiting the transcription of target genes. Activation of the WNT signalling pathway will lead to Axin docking away from the destruction complex, and thus impede β-catenin degradation. As such, β-catenin will translocate to the nucleus, displacing Groucho and allow for transcription of the WNT target genes. From Clevers (2006). Reproduced with permission. Copyright 2006, Elsevier.

signalling is involved in mesoderm formation and in the rapid proliferation of mesodermal cells, it also prevents their differentiation; cardiac commitment requires the migration of some of these cells to the anterior embryo, where WNT signalling is inhibited. *In vitro*, the same effects are observed, as WNT activation is necessary for mesoderm specification (as the lack of factors which mimic the primitive streak leads to ectoderm differentiation (Paige et al. 2010)), but the following differentiation into cardiac mesoderm lineages requires the inhibition of canonical WNT signalling.

Paige and co-workers developed some studies regarding the role of WNT signalling on hESC differentiation. They report that endogenous canonical WNT signalling is necessary for activin A– and BMP4-mediated cardiac differentiation, as the cardiogenic potential of hESCs was well-correlated with the upregulation of canonical WNT genes *WNT1*, *WNT3a* and *WNT8a*. Initial addition of WNT inhibitor Dickkopf-related protein (DKK) 1 would impair this differentiation, while exogenous WNT3a could improve it, and rescue it in the cell lines with less cardiogenic potential. Following mesoderm formation, DKK1 supplementation could improve cardiac differentiation by 70% (Paige et al. 2010). Lian and colleagues applied this stage-specific WNT modulation to develop a more robust hPSC cardiac differentiation protocol. This protocol relies only on medium supplementation with small molecules—GSK3 inhibitor CHIR99021 (CHIR) for the first day of differentiation and an inhibitor of WNT production/response (IWP/IWR) between days 3 and 5. The initial WNT activation was also shown to regulate activin/NODAL and BMP signalling, further evidencing the role of the crosstalk of all these signalling pathways in cardiac differentiation. Overall, the GSK3 inhibition/WNT inhibition (GiWi) protocol could generate up to 98% cTNT^{+} cells in 15 days in 2D culture, with a yield of 15 cardiomyocytes/hPSC, without the necessity of expensive growth factors (Lian et al. 2012, Lian et al. 2013a). The same group also described the importance of insulin throughout the cardiac differentiation protocol. While both hPSC

self-renewal and cardiomyocyte proliferation rely on insulin, this protein was also shown to impair cardiac mesoderm specification via canonical WNT signalling, with this effect varying depending on the type of protocol—the GiWi protocol was only negatively affected, by 40%, when insulin was added on day 1 (Lian et al. 2013b).

The GiWi protocol has also already been described for 3D cardiac differentiation of hPSCs. Correia and co-workers performed cardiac differentiation of hiPSCs during 6-8 days in 2D, followed by a forced aggregation strategy in microwell plates and culture in orbital suspension. This protocol was compared to a fully 2D differentiation. The 3D strategy improved the cardiomyocyte purity of the resulting population—as the aggregation of cells with analogous surface proteins is facilitated, thus allowing for the formation of cardiomyocyte-enriched spheroids—with over 70% expression in cardiomyocyte markers identified for various independent hESC and hiPSC lines. Furthermore, this approach also resulted in an enhanced maturation. In fact, cardiomyocytes generated in 3D conditions showed differences in amino acid metabolism, a shift in transcriptome and fluxome from glycolysis to oxidative phosphorylation (OXPHOS), and improved electrophysiology (Correia et al. 2018). Branco and colleagues used microwell plates to form hiPSC aggregates with a controlled size, observing the differentiation to be ideal with 3 days of culture prior to differentiation, along with a starting aggregate diameter of 289 ± 12 μm, generating over 90% $cTNT^+$ cells. The authors also performed a transcriptomic analysis which gave insight on how 2D and 3D cardiac differentiation differ. Namely, 3D differentiation leads to a hypoxic environment inside the aggregates which, in turn, acts in important cardiac pathways (e.g., TGFβ/NODAL) and favours glycolysis, striking a balance between pluripotency maintenance and mesendoderm priming. Furthermore, a more thorough structural and functional maturation of the cardiomyocytes was observed (Branco et al. 2019).

Kempf and co-workers expanded and differentiated hPSCs as aggregates in 100 mL bioreactors, using a cyclic perfusion feeding regime for expansion. While batch cultures led to the upregulation of genes correlated with negative regulation of growth, cyclic perfusion resulted in the upregulation of *BMP2*, a gene of the TGFβ superfamily. While cyclic perfusion resulted in less cells in 2 days (60 million vs 79 million with batch) and in a slower upregulation of mesodermal genes T-box transcription factor (*TBX*) *2* and mesoderm posterior (*MESP*) *1*, it also resulted in upregulation of cardiac genes *ISL1* and *NKX2.5* and, consequently, in cardiac differentiation, which was not observed in aggregates from batch cultures. Following differentiation, an average of 4.0×10^7 cardiomyocytes could be recovered (62.9 ± 7.3% $cTNT^+$ cells), a majority with a ventricular-like action potential (Kempf et al. 2014). Laco et al. performed differentiation of hiPSCs attached to microcarriers in 300 mL bioreactors, with oxygen tension controlled at 30%. By the end of cell expansion, after 5 days, the authors could obtain $6.0 \pm 1.2 \times 10^8$ cells, while differentiation resulted in $2.2 \pm 0.4 \times 10^9$ cardiomyocytes with over 80% of the total cells expressing cTNT. Following a 4-day lactate selection step and 4 days in recovery medium, the purity in cTNT was increased to over 96%, with a final cardiomyocyte yield of 1.9×10^9 (Laco et al. 2020).

In a variation from the traditional GiWi protocol, Tsao and colleagues employed a “self-differentiating” material, allowing for minimal operator handling throughout the process. The use of uncoated and poly(lactic-co-glycolic acid) (PLGA)-coated silica particles, allowing for burst release of

CHIR and gradual release of IWP-2, respectively, allowed for mimicry of the traditional GiWi protocol, and requiring only exchange of medium without molecules. This protocol led to the generation of 30.3 ± 1.9% cTNT$^+$ cells in 15 days, a slight reduction over the differentiation with dissolved molecules, but allowing for this method to be a viable alternative (Tsao et al. 2018).

The GiWi protocol is typically performed using the chemically defined Roswell Park Memorial Institute (RPMI) 1640 medium, supplemented with B-27 (minus insulin for up to the first week of differentiation), an undefined and xenogeneic supplement with 21 components. Naturally, the transition to a simpler, defined and xeno-free medium formulation would greatly improve the protocol in terms of cost, reproducibility and prospective transition to the clinic. This motivation led Burridge and colleagues to subtract the components of B-27, one at a time, and observe how each removal affected cardiac differentiation. Interestingly, stripping B-27 of all its components except for ascorbic acid 2-phosphate (which absence led to complete cell death) could still sustain cardiac differentiation, although with reduced cell yield. The optimal medium developed by the authors (chemically-defined medium, 3 components; CDM3), contains only RPMI 1640, ascorbic acid and recombinant human albumin (instead of its bovine variant found in B-27), and could generate about 85% cTNT$^+$ cells. Furthermore, this xeno-free medium can be combined with defined matrices for a fully chemically defined process. While laminin allows for long-term cellular adhesion, due to its prohibitive cost, vitronectin is a more attractive matrix, in spite of requiring frequent passaging and replating (Burridge et al. 2014). CDM3 was also shown to support cardiac differentiation of hPSCs as aggregates in suspension culture. Prior to differentiation, the aggregates were expanded in E8 for 2 days, as this expansion time was found to improve subsequent cardiac commitment. By applying continuous WNT control (i.e., inhibiting WNT signalling directly after its activation, between days 1 and 3 of differentiation), Halloin et al. could produce over 90% cardiomyocytes in 500 mL bioreactor systems, with a density of about 1×10^6 cardiomyocytes·mL^{-1} (Halloin et al. 2019).

I.2.2.5. Direct control of gene expression

Cell differentiation is a very complex process, governed by a multitude of systems, but is associated with, and a consequence of, changed gene expression (by the action of internal or external stimuli). While the differentiation protocols described in the previous sections serve as stimuli to induce endogenous changes in gene expression (through cell-cell interactions or by modulating cell signalling), it is also possible to deliver genes to a cell (for instance through viral transduction), allowing for a tighter control of its fate and forgoing other stimuli. In fact, reprogramming of somatic cells to hiPSCs relies on this principle—delivery of a mixture of pluripotency genes such *OCT4*, *SOX2*, *KLF4* and *C-MYC* can lead a fully differentiated cell to an embryonic-like state (Takahashi et al. 2007). Dixon and colleagues have assayed combination of 15 genes in terms of their potential to cardiac differentiate hESCs (a reporter cell line tagged with myosin heavy chain (*MYH*) *6*–monomeric red fluorescent protein (mRFP)) without additional exogenous stimuli. The full genetic cocktail was successful in the formation of α-actinin$^+$ cells. The authors then identified four core factors—*GATA4*, *TBX5*, *NKX2.5* and *BAF60c* (*GTNB*)—which absence severely compromised cardiac differentiation, but which sole presence (i.e. without additional genes) led to the highest number of mRFP$^+$ cells of all the tested combinations.

Cardiac specification of hESCs required at least 5 days of *GTNB* expression. More thorough studies found *GTNB* to specify hESCs towards mesendoderm, with further differentiation towards muscle lineages and, more specifically, cardiomyocytes. Up to 12.1% $cTNI^+$ cells could be obtained following 28 days of differentiation (Dixon et al. 2011).

Gene expression can also be controlled by the action of miRNAs. These small, non-coding RNAs regulate genes at the post-transcription level, with each miRNA regulating several different mRNAs (Wilson et al. 2010). Different cell states have different miRNA "fingerprints", and the identification of the miRNome associated with specific lineages, along with their targets, may give important insights on how cell differentiation is controlled at the post-transcriptional level, which, in turn, may clue on the development of novel *in vitro* protocols. miR-1 has been identified in the heart, and is thought to lead to the downregulation of genes from non-cardiac mesoderm. In fact, its overexpression in spontaneous differentiation was shown to lead to up-regulation of myosin heavy chain at the end of differentiation (Wilson et al. 2010, Garate et al. 2018). Rasekhi and co-workers explored the possibility of obtaining cardiomyocytes from hiPSCs by lentiviral transduction of miR-1 and treatment with pro-cardiogenic molecule 5'-azacitidine. This combined strategy led to the higher expression of cardiac markers post-differentiation, with an about 4000-fold increase in cardiac-specific gene troponin T (*TNNT*) *2* in comparison to the untreated control (Rasekhi et al. 2017).

I.2.2.6. Matrix sandwich

Culture of adherent cells is generally mediated by an ECM, such as Matrigel, which is used to coat the tissue culture plates. The choice of ECM impacts stem cell behaviour (Guilak et al. 2009), and also, as described by Zhang et al., how it is presented to the cells. In fact, culturing the cells on top of a matrix forces them with an apical-basal polarity, but overlaying hPSCs cultured on Matrigel with an additional Matrigel layer, and combining it with a growth factor CD protocol was shown to promote EMT, as observed by the presence of cells with a migratory mesenchymal phenotype. Furthermore, this protocol reduces cell death post-activin A addition and can generate up to 98% $cTNT^+$ cells after 30 days (with a yield of 11 cardiomyocytes/hPSC), with increased maturation in comparison to traditional protocols (Zhang et al. 2012). The cardiogenic potential of this protocol can be further increased by the addition of BMP antagonist GREMLIN (GREM) 2, which controls cardiac laterality and differentiation into cardiomyocytes *in vivo*. BMP inhibition in general led to increased proliferation of CPCs, while only GREM2 (via c-Jun N-terminal kinase (JNK) signalling) promoted faster cardiac differentiation as well as the formation of more contractile areas (Bylund et al. 2017).

I.2.3. Purification of human pluripotent stem cell-derived cardiomyocytes

With the major breakthroughs in cardiac differentiation of hPSCs of the last years, it is already possible to generate cardiomyocytes with high purity (over 90%). Nevertheless, should undifferentiated hPSCs remain following the differentiation protocol (potentially, even as little as 10 cells (Cunningham et al. 2012)), these may form teratomas after transplantation to a host. Even when not considering this

risk, the presence of non-cardiac cells on a graft or in a cell model may cause an aberrant behaviour. As such, purification of the cell product is of crucial importance, regardless of its use.

I.2.3.1. Density centrifugation

The earliest report of purification of hPSC-derived cardiomyocytes relied on density centrifugation. In this methodology, the authors established a discontinuous Percoll gradient (two layers with different Percoll concentrations) to which the cells were loaded. Following centrifugation, the cells split into four fractions—above the least dense Percoll layer (fraction I), within the least dense Percoll layer (fraction II), at the interface of both layers (fraction III) and within the densest Percoll layer (fraction IV). The cardiomyocyte content (starting from 17 ± 4% soluble (s) MHC^+ cells derived from hESC EBs) increased with the density of the layer, with fractions I and II containing 3-5% of soluble MHC (sMHC), fraction III having a sMHC content of 36 ± 3%, and 70 ± 5% of the cells in fraction IV being $sMHC^+$ (Xu et al. 2002). The relative simplicity of this protocol led to some other early studies applying it for cardiomyocyte enrichment (Laflamme et al. 2005, McDevitt et al. 2005, Laflamme et al. 2007), however, its non-specificity led it to being replaced by other purification methodologies.

I.2.3.2. Drug-based purification

Different cell types respond differently to drugs—a molecule which affects one cell type (positively or negatively) may have little to no impact on another. These differences in cell response may be taken advantage of in order to ablate contaminant cell types.

Doxorubicin is a chemotherapeutic agent which can inhibit the growth and proliferation of cancer cells—since hPSCs have similar growth characteristics, this drug can also cause their death. Furthermore, low doses of doxorubicin (but which could remove ~ 90% of contaminant hESCs following differentiation) were shown not to interfere with the viability, structure, gene and protein expression or electrophysiology of hESC-derived cardiomyocytes (Chour et al. 2021).

When this difference in cellular response does not occur naturally, it can be enforced by genetic modifications. Anderson and colleagues attempted two different strategies based on genomic alterations to enrich hESC-derived cardiomyocyte populations. On the first strategy, the authors used a herpes simplex virus thymidine kinase (HSVtk)/ganciclovir (GCV) suicide gene system. The treatment of HSVtk-transfected cells with GCV leads to the phosphorylation of this antibiotic and its incorporation in *de novo*–produced DNA chains, culminating in cellular death. As such, supplementing the post-differentiation culture with GCV allows for selective cell ablation—while the non-proliferating cardiomyocytes will remain in culture, contaminant cell types which are proliferative will be killed. The authors' second approach relied on cellular expression of an antibiotic-resistance gene associated with a cardiac-specific gene—in this case, puromycin resistance from the *MYH6* promoter. In this case, cells expressing *MYH6* (i.e., cardiomyocytes) were protected from puromycin, while the remainder of the cell population could be removed by culture supplementation with this antibiotic. Starting from a cell population with 6.3 ± 3.4% α-$actinin^+$ cells, the authors could enrich it to 33.4 ± 2.1% or 91.5 ± 4.3% of cells expressing this protein with GCV or puromycin-based selection, respectively (Anderson et al.

2007). Naturally, antibiotic-based selection can be performed with other gene-antibiotic combinations, such as Zeocin™ resistance associated with the myosin light chain (*MYL*) *2* promoter (selecting ventricular cardiomyocytes only) (Chow et al. 2013).

I.2.3.3. Fluorescence- and magnetic-activated cell sorting

Two very powerful methodologies for cell purification are fluorescence-activated cell sorting (FACS) and magnetic-activated cell sorting (MACS). FACS sorts cells based on their fluorescence—the cells are excited a laser and are attributed a negative or positive charge to the cells depending on whether or not they are fluorescent, which, after passage through electromagnetic plates, allows for their deflection onto distinct collection points. By using fluorophore-conjugated antibodies which label specific proteins at the surface of the cells, it is possible to sort the cells based on the expression of these proteins. A similar type of separation can be performed with MACS. By labelling the cells with antibodies linked to magnetic particles and by loading the cells to a column under the influence of a magnetic field, it is possible to retain the cells in the column. Elution is performed by removing the column from the influence of the magnetic field. In both cases, selection can be positive—by labelling a marker expressed by the cells of interest—or negative—when contaminant cell types are labelled instead, thus depleting them from the loaded cell mixture.

During the time of the first studies on purification of cardiomyocytes, the knowledge of cardiac-specific surface proteins was very limited. As such, those studies relied on reporter cell lines, genetically modified with an enhanced green fluorescent protein (eGFP) gene in the locus of a cardiac-specific gene, allowing for fluorescent detection and sorting of cells expressing that gene, even if it encodes for an intracellular protein. This has allowed for FACS of cardiomyocytes based on the presence of MLC2v (Huber et al. 2007), α-MHC (Ritner et al. 2011) and NKX2.5 (also amenable for CPC purification) (Elliott et al. 2011). The use of the *NKX2.5*$^{eGFP/w}$ reporter cell line shed light on two prospective surface markers which could allow for cardiomyocyte separation without requiring genetic modification. In fact, over 70% of the eGFP$^+$ cells at day 14 were vascular cell adhesion molecule (VCAM) 1$^+$ and/or signal regulatory protein (SIRP) α$^+$ (Elliott et al. 2011), allowing for cardiomyocyte selection by FACS and/or MACS using these markers (Dubois et al. 2011, Uosaki et al. 2011). Surface markers which have already been tested for purification at the CPC stage include hyperpolarisation-activated cyclic nucleotide-gated channel (HCN) 4 (Spater et al. 2013), glial cell line-derived neurotrophic factor receptor (GFR) α2 (Ishida et al. 2016), kangai (KAI) 1 (Takeda et al. 2018) and platelet-derived growth factor receptor (PDGFR) α alone (Fukushima et al. 2020), or in tandem with kinase insert domain receptor (KDR) (Kattman et al. 2011). In an example of negative selection, Dubois and colleagues stripped differentiating EBs at day 20 from the majority of SIRPα$^-$ cells by sorting for expression of thymus cell antigen (THY) 1, platelet endothelial cell adhesion molecule (PECAM) 1, PDGFRβ and integrin (ITG) α1—labelling fibroblasts, endothelial cells, smooth muscle cells and other non-myocyte cells, respectively (Dubois et al. 2011).

An alternative FACS-based method for cardiomyocyte purification which does not rely on cell markers has been presented by Hattori and co-workers. hPSC-derived cardiomyocytes have a high mitochondrial content, allowing them to be distinguished from contaminant cell types using mitochondrial labelling dyes. Due to its non-toxicity and fast washout from the cells, tetramethylrhodamine methyl ester

percholate (TMRM) was elected by the authors for mitochondrial dyeing, and following FACS, over 99% of the collected cells were cardiomyocytes and comprised 60-90% of the α-actinin$^+$ cells prior to sorting (Hattori et al. 2010). Another approach used molecular beacons—hairpin structures with both a fluorophore and a quencher with specificity towards a specific mRNA sequence. Upon hybridisation with the target mRNA, the fluorophore and the quencher are distanced, allowing for fluorescence-based sorting of the cells. The authors targeted either *TNNT2* or *MYH6/7* expression, finding one of the molecular beacons for *MYH6/7* (MHC1-MB) to yield the highest signal-positive cell ratio. By applying purification by FACS with this molecular beacon, the authors could purify a starting population of ~ 40% of cTNI$^+$ cells to about 97% of these cells (Ban et al. 2013).

I.2.3.4. miRNA switches

As mentioned in section I.2.2.5, each cell type has a specific miRNA fingerprint, and the identification of cardiac-specific miRNAs has been taken advantage of to induce hPSC cardiac differentiation. Miki and co-workers have harnessed these distinct miRNA signatures for purification of hPSC-derived cardiomyocytes. The authors designed miRNA-responsive, synthetic modified mRNA switches (miRNA switches), which translation depended on their target miRNA. Transfection of cells with blue fluorescent protein (BFP)-tagged miR-1-, miR-208a- and miR-499a-5p-switches could enhance the purity of a 24.4 ± 2.1% cTNT$^+$ population (at day 20 of EB differentiation with growth factors) to over 95% via FACS, with the miR-208a-switch equally sorting day 8 hPSC-derived cardiomyocytes. When these switches were combined with apoptosis inducer Bim, they could selectively ablate non-target cells. In fact, miR-1- and miR-208a-Bim-switches successfully generated about 90% cTNT$^+$ cells in three different cell lines, without necessitating fluorescent sorting and with no alteration in the expression profile of the cells. Notably, the authors also generated miRNA switches which could purify endothelial cells, hepatocytes and insulin-producing cells, highlighting their versatility (Miki et al. 2015).

I.2.3.5. Metabolic selection

Differentiation of hPSCs to cardiomyocytes is accompanied by a metabolic shift. The rapid proliferation of hPSCs is sustained by a predominantly glycolytic metabolism, allowing to meet both energetic and biomass demands (Vander Heiden et al. 2009, Varum et al. 2011), whereas the non-proliferative cardiomyocytes opt for OXPHOS, allowing for a more thorough conversion of the substrate to energy. Possible carbon and energy sources for cardiomyocytes include glucose, lactate and fatty acids, granting these cells some metabolic flexibility for their high energy demand. In fact, foetal cardiomyocytes predominantly rely on lactate as their energy source (Piquereau and Ventura-Clapier 2018).

This unique metabolic characteristic of cardiomyocytes has led to the development of a metabolic-based purification protocol. Tohyama et al. observed how, following spontaneous differentiation of hPSCs as EBs, the cells could be cultured in medium lacking glucose but containing lactate, and how that would lead to the death of non-myocytes. Remarkably, this enriched a starting population of 8.1 ± 2.9% cardiomyocytes to 98.3 ± 0.9% (measured through α-actinin expression), with

a recovery yield of 74.4 ± 12.1%. Furthermore, moderate (4 mM) lactate concentrations did not affect the culture pH—lactate consumption was rapid owing to the high activity of the tricarboxylic acid cycle (Tohyama et al. 2013). The high efficiency, low cost, technical simplicity and the unnecessity of genetic modification of the cells have established lactate metabolic selection as a desirable method for hPSC-derived cardiomyocyte purification, regardless of the differentiation protocol, with described final cardiomyocyte content of over 80% (Burridge et al. 2014, Hemmi et al. 2014, Fuerstenau-Sharp et al. 2015, Qian et al. 2016, Pei et al. 2017, Tohyama et al. 2017, Friedman et al. 2018, Lei et al. 2018a, Nose et al. 2018, Horikoshi et al. 2019, Fang et al. 2020, Laco et al. 2020, Nemade et al. 2020). Notably, replacing lactate by fatty acids and 3,3',5-triiodo-L-thyronine resulted in a similar purification, while simultaneously inducing cardiomyocyte maturation (Horikoshi et al. 2019) (discussed in more detailed in section I.2.4.2).

I.2.4. Maturation of human pluripotent stem cell-derived cardiomyocytes

In vivo cardiac development is a lengthy process, starting with mesoderm formation at the second week of embryogenesis (Buijtendijk et al. 2020), and persisting after birth with cardiomyocyte maturation (Mollova et al. 2013). This maturation occurs at several levels (Figure I.21). Structurally, adult cardiomyocytes are rod shaped, with aligned sarcomeres and potential multinucleation (England and Loughna 2013, Gunthel et al. 2018). While atrial cardiomyocytes express both MLC2a and MLC2v, adult ventricular cardiomyocytes only express MLC2v (England and Loughna 2013). The heart also matures electrophysiologically along time. A correctly developed conduction system, which allows for a synchronous contraction of the heart chambers, relies on the maturation of the calcium handling of the cells and their electrical coupling—a deficient development of this conduction system can lead to arrythmias (Christoffels and Moorman 2009, Buijtendijk et al. 2020, Sutanto et al. 2020). Cardiomyocyte metabolism also changes through time—their proliferative ability decreases (Mollova et al. 2013), and these cells become more reliant on fatty acid oxidation for their energy requirements (in opposition to the predominantly lactate-based mechanism of foetal cardiomyocytes) (Piquereau and Ventura-Clapier 2018), with a more robust mitochondrial mechanism (Pohjoismaki and Goffart 2017). This also relates to the mechanisms through which the whole heart grows and develops along time—while the initial development of the heart occurs through hyperplasia (the continued multiplication of its cells), as the cardiomyocytes lose the ability to proliferate, heart growth instead occurs through hypertrophy (an increase in the individual cell volume) (Piquereau and Ventura-Clapier 2018). In fact, throughout the first 20 years of human life, the cardiomyocyte volume was described to increase about 8.6-fold (Mollova et al. 2013). In short, *in vivo* development and maturation of the cardiac system is a complex and prolonged process. As such, differentiating hPSCs into mature cardiomyocytes *in vitro*, with the intent of correctly replicating the adult heart for disease models or to avoid arrhythmic phenomena upon transplantation, is a difficult undertaking. A putative protocol for this effect would need to recapitulate years-long development phenomena in a considerably short (weeks or months) culture time. Nevertheless, many studies have already worked on accelerating the generation of hPSC-derived cardiomyocytes with mature characteristics. The maturation is generally evaluated on several terms, including morphology (shape, sarcomere alignment), phenotype (expression of MLC2 isoforms) action potentials, response to

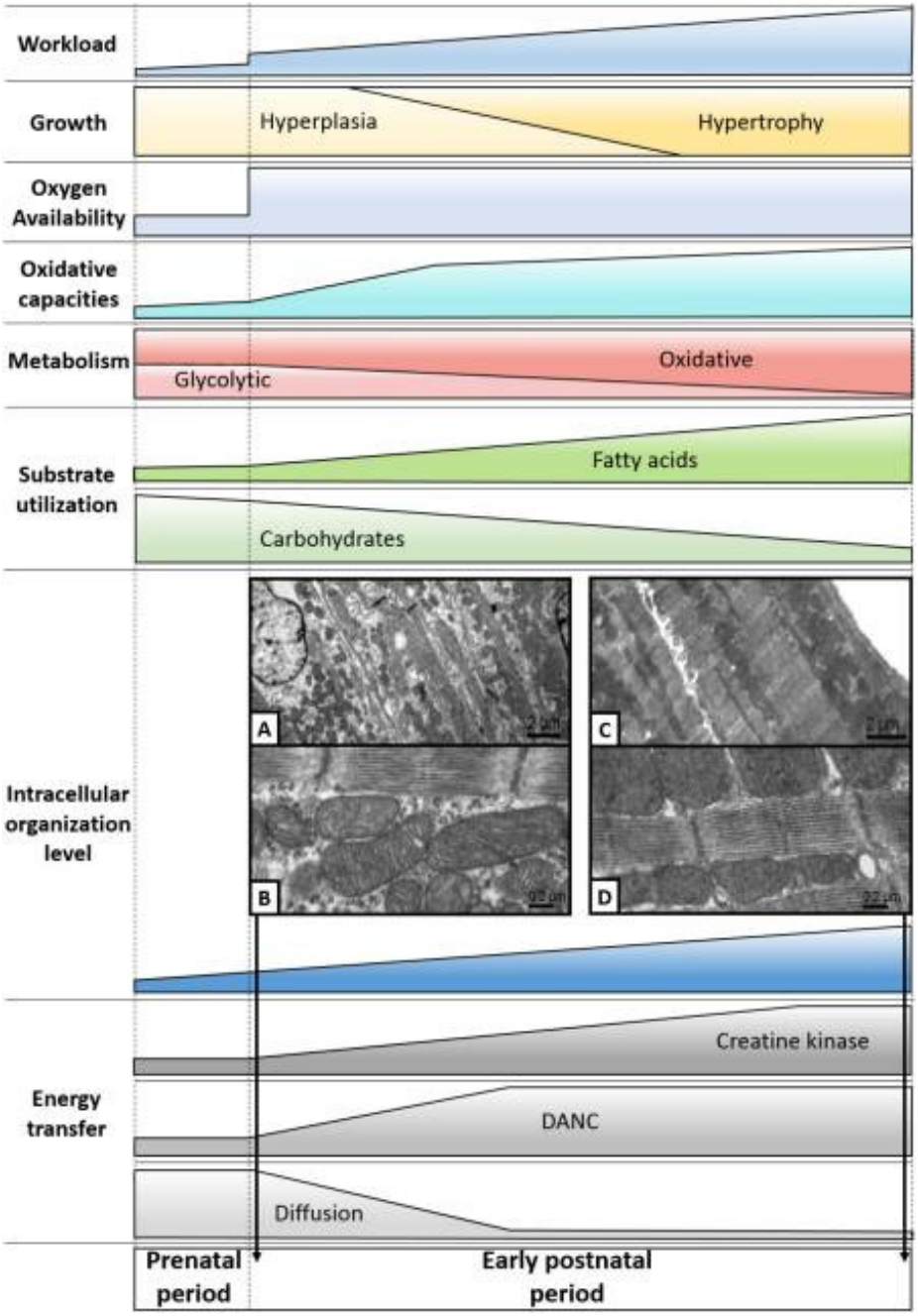

Figure I.21 – Overview of cardiomyocyte maturation. The increased workload caused by post-natal human growth and development is compensated by heart growth, initially by hyperplasia and then by hypertrophy. With the higher oxygen availability in the post-natal period, the oxidative capacities of the heart increase and the metabolism shifts from glycolysis to oxidation, with an increased preference towards fatty acid use. Cardiomyocytes also mature at a structural level, with increased intracellular organisation through time. Images shown for the intracellular organisation level show **A, B** 3-day-old and **C, D** 63-day-old cardiomyocytes from mouse papillary muscle, demonstrating an increased structural organisation with time. From Piquereau and Ventura-Clapier (2018). Reproduced under the terms of the Creative Commons CC-BY licence. Copyright 2018, Piquereau and Ventura-Clapier. Adapted from Piquereau et al. (2010). Reproduced with permission. Copyright 2010, The Authors.

drugs and proliferative ability. The following sections describe strategies which have already been applied for hPSC-derived cardiomyocyte maturation.

I.2.4.1. Prolonged culture

The most evident mechanism to achieve cardiomyocyte maturity is to prolong the culture time. Kamakura and colleagues differentiated hiPSCs into cardiomyocytes with an EB-based protocol with growth factors and maintained these cardiomyocytes in culture for one year. Throughout the year-long culture, the beating rate of the cardiomyocytes slowed down, and their area increased. The $MLC2v^+$/ $MLC2a^+$ cell ratio also gradually increased (up to 60%) and mature sarcomeric structures (M-bands) were formed, but were still in a minority. In fact, the authors report a heterogenous maturation profile even after 360 days in culture, but nevertheless improved in comparison to 30-day cardiomyocytes (Kamakura et al. 2013). Fukushima and co-workers also observed structural maturation of hiPSC-derived cardiomyocytes (from a growth factor– and small molecule–based protocol and with MACS purification at day 5) over long-term (200 days) culture, with accompanying loss of proliferative ability. Furthermore, most of these cardiomyocytes exhibited ventricular-like action potentials (96% at day 91) (Fukushima et al. 2020). While the cells could benefit from increased maturation via an even further extended culture time, from a biomanufacturing perspective, especially if the intent is to obtain mature patient-derived cells, it would be preferred to apply other maturation approaches which could decrease the required hPSC-to-mature cardiomyocyte time.

I.2.4.2. Medium supplementation

Specific medium supplementation strategies have also been shown to drive hPSC-derived cardiomyocytes to a more mature phenotype, including supplementation with foetal bovine serum (in opposition to serum replacement) (Bettiol et al. 2007), apolipoprotein A-1 (Ng et al. 2011), trichostatin A (Lim et al. 2013) and ascorbic acid (Cao et al. 2012). Ascorbic acid, in particular, was shown to have an improved effect during mid-stage cardiac differentiation (days 2-6)—more specifically through collagen synthesis–mediated cardiac progenitor cell proliferation (Cao et al. 2012)—and has been used in many reports since (Spater et al. 2013, Mehta et al. 2014, Friedman et al. 2018, Yassa et al. 2018), including as one of three components of a simple and chemically-defined medium formulation for cardiac differentiation (Burridge et al. 2014). Medium supplementation can also direct cellular metabolism—by feeding the cells with a fatty acid–rich, glucose-free medium, cardiomyocytes can be simultaneously enriched and led towards a fatty acid metabolism–based phenotype, characteristic of adult cardiomyocytes. In fact, this purification and maturation protocol led to the formation of more structurally mature cardiomyocytes, with a rod shape, sarcomeric organisation and a high number of mitochondria (Horikoshi et al. 2019). High fatty acid concentrations, however, may induce lipotoxicity. Medium supplementation with galactose may prevent this lipotoxicity and enhance the oxidative metabolism of cells. In fact, culture of hiPSC-derived cardiomyocytes in glucose-free and galactose- and fatty acid–supplemented medium showed increased OXHPOS activity and structural and electrophysiological maturation of the cells (Correia et al. 2017).

I.2.4.3. Matrix composition and presentation

The extracellular matrix plays a crucial role in stem cell lineage specification, not only by its composition, but also by its stiffness and presentation (Guilak et al. 2009). The cardiac ECM has already been documented (Rienks et al. 2014, Silva et al. 2020a), which can give cues on to how to adapt it to *in vitro* culture. Arshi et al. showed that cardiac differentiation is promoted by stiff matrices (~ 10 kPa) in both hESCs and mESCs, also with enhanced maturation. In fact, although this was only tested for murine cells, mESC-derived cardiomyocytes were able to electrically couple with neonatal cardiomyocytes (Arshi et al. 2013). Electrically-conductive matrices are also important for cardiomyocyte maturation—as hPSC-derived cardiomyocytes lack a conduction system, using a conductive matrix, such as graphene, has the potential to improve cell-cell electrical communication and enhance structural and functional maturation of the generated cardiac tissue as a whole (Wang et al. 2017). Transiently culturing the cells between two matrix layers—a matrix sandwich (described in more detail in section I.2.2.6)—can also improve the maturation of the resulting cardiomyocytes. In fact, 30-day cardiomyocytes generating with this protocol are comparable to cardiomyocytes from 60-90 days of EB differentiation (though still with an embryonic phenotype) (Zhang et al. 2012).

I.2.4.4. Culture format

As it was extensively described in section I.1.2, 3D culture is advantageous in various manners, especially when considering cellular production at a clinical scale. It was also recently shown that cardiac differentiating hiPSCs as aggregates results in a hypoxic microenvironment, which, in turn, promotes the activation of pathways important in cardiogenesis (Branco et al. 2019). Simultaneously, 2D culture impairs cardiac maturation due to deficient activation of hypertrophic signalling (responsible for the growth of adult cardiac tissue) (Friedman et al. 2018). Naturally, transitioning 3D cardiac differentiation to bioreactors would be greatly advantageous to not only induce the hypoxic-mediated maturation, but also to generate a cell number more compatible with Regenerative Medicine and pharmacological applications (Kempf et al. 2014, Halloin et al. 2019). hPSC-derived cardiomyocytes can also be cultured as cardiac tissues on pillars (engineered heart tissues), allowing for their physical stimulation. This intensity training was shown to lead to enhanced morphological characteristics, in terms of size and shape, although the functional maturation, which was nonetheless observed in terms of characteristics such as metabolism and calcium handling, was not as robust (Ronaldson-Bouchard et al. 2018).

I.2.4.5. Electrical stimulation

The rate of heart contractions is controlled by the generation of periodical electrical stimuli by specialised pacemaker cells (Baruscotti et al. 2010, Weisbrod et al. 2016). Mimicking this pacemaker cell–mediated electrical stimulation *in vitro* might drive hPSC-derived cardiomyocytes towards a more mature phenotype. Simple approaches, such as stimulation with electrodes (Hernandez et al. 2016) and on aligned fibres (Mohammadi Amirabad et al. 2017), were already shown to have a positive effect on hPSC differentiation. Nunes and colleagues developed “biowires”, by cultivation of hiPSC-derived cardiomyocytes on sutured collagen gel and subsequent electrical stimulation. This culture methodology

increased both the structural and electrophysiological properties of the cells (Nunes et al. 2013). Cardiomyocyte maturation may be further developed by combination of electrical stimulation with engineered topographies. Richards and co-workers reported that the incorporation of conductive nanowires in hiPSC-derived cardiac spheroids, which by itself was shown to allow the formation of an electrically conductive network (Tan et al. 2015), could also be combined with electrical stimulation to further cell communication and mature said electrical network even more (Richards et al. 2016). Vaithilingam and colleagues performed electrical stimulation of hPSC-derived cardiomyocytes on a 3D printed meant to mimic stacked myofibrils. This combined approach resulted in an improved structural maturation of the cardiomyocytes, with increased sarcomere length and alignment (Vaithilingam et al. 2019). Electrical stimulation may also be applied to engineered heart tissues, promoting the formation of a stronger and denser cardiomyocyte network. Incidentally, gene expression analysis revealed an upregulation of genes involved in inflammatory response, likely as a protection against the oxidative stress generated by the electrical stimulation (Hirt et al. 2014).

References

Abba, S. and A. M. Garba (2020). An IoT-Based Smart Framework for a Human Heartbeat Rate Monitoring and Control System. *Proceedings* **42**(1): 36.

Abbasalizadeh, S., M. R. Larijani, A. Samadian and H. Baharvand (2012). Bioprocess development for mass production of size-controlled human pluripotent stem cell aggregates in stirred suspension bioreactor. *Tissue Eng Part C Methods* **18**(11): 831-851.

Abdella, A., T. E.-S. Mazeed, A. F. El-Baz and S.-T. Yang (2016). Production of β-glucosidase from wheat bran and glycerol by Aspergillus niger in stirred tank and rotating fibrous bed bioreactors. *Process Biochemistry* **51**(10): 1331-1337.

Abecasis, B., T. Aguiar, E. Arnault, R. Costa, P. Gomes-Alves, A. Aspegren, M. Serra and P. M. Alves (2017). Expansion of 3D human induced pluripotent stem cell aggregates in bioreactors: Bioprocess intensification and scaling-up approaches. *J Biotechnol* **246**: 81-93.

Akhurst, R. J. and A. Hata (2012). Targeting the TGFbeta signalling pathway in disease. *Nat Rev Drug Discov* **11**(10): 790-811.

Anderson, D., T. Self, I. R. Mellor, G. Goh, S. J. Hill and C. Denning (2007). Transgenic enrichment of cardiomyocytes from human embryonic stem cells. *Mol Ther* **15**(11): 2027-2036.

Anokye-Danso, F., C. M. Trivedi, D. Juhr, M. Gupta, Z. Cui, Y. Tian, Y. Zhang, W. Yang, P. J. Gruber, J. A. Epstein and E. E. Morrisey (2011). Highly efficient miRNA-mediated reprogramming of mouse and human somatic cells to pluripotency. *Cell Stem Cell* **8**(4): 376-388.

Arshi, A., Y. Nakashima, H. Nakano, S. Eaimkhong, D. Evseenko, J. Reed, A. Z. Stieg, J. K. Gimzewski and A. Nakano (2013). Rigid microenvironments promote cardiac differentiation of mouse and human embryonic stem cells. *Sci Technol Adv Mater* **14**(2): 025003.

Badenes, S. M., T. G. Fernandes, C. S. Cordeiro, S. Boucher, D. Kuninger, M. C. Vemuri, M. M. Diogo and J. M. Cabral (2016). Defined Essential 8 Medium and Vitronectin Efficiently Support Scalable Xeno-Free Expansion of Human Induced Pluripotent Stem Cells in Stirred Microcarrier Culture Systems. *PLoS One* **11**(3): e0151264.

Baker, B. M. and C. S. Chen (2012). Deconstructing the third dimension: how 3D culture microenvironments alter cellular cues. *J Cell Sci* **125**(Pt 13): 3015-3024.

Ban, K., B. Wile, S. Kim, H. J. Park, J. Byun, K. W. Cho, T. Saafir, M. K. Song, S. P. Yu, M. Wagner, G. Bao and Y. S. Yoon (2013). Purification of cardiomyocytes from differentiating pluripotent stem cells using molecular beacons that target cardiomyocyte-specific mRNA. *Circulation* **128**(17): 1897-1909.

Barckhausen, C., B. Rice, S. Baila, L. Sensebe, H. Schrezenmeier, P. Nold, H. Hackstein and M. T. Rojewski (2016). GMP-Compliant Expansion of Clinical-Grade Human Mesenchymal Stromal/Stem Cells Using a Closed Hollow Fiber Bioreactor. *Methods Mol Biol* **1416**: 389-412.

Bardy, J., A. K. Chen, Y. M. Lim, S. Wu, S. Wei, H. Weiping, K. Chan, S. Reuveny and S. K. Oh (2013). Microcarrier suspension cultures for high-density expansion and differentiation of human pluripotent stem cells to neural progenitor cells. *Tissue Eng Part C Methods* **19**(2): 166-180.

Baruscotti, M., A. Barbuti and A. Bucchi (2010). The cardiac pacemaker current. *J Mol Cell Cardiol* **48**(1): 55-64.

Bauwens, C. L., R. Peerani, S. Niebruegge, K. A. Woodhouse, E. Kumacheva, M. Husain and P. W. Zandstra (2008). Control of human embryonic stem cell colony and aggregate size heterogeneity influences differentiation trajectories. *Stem Cells* **26**(9): 2300-2310.

Becker, R. C. and J. M. Gore (1991). Adjunctive use of beta-adrenergic blockers, calcium antagonists and other therapies in coronary thrombolysis. *The American Journal of Cardiology* **67**(3): 25-31.

Bergmann, O., R. D. Bhardwaj, S. Bernard, S. Zdunek, F. Barnabe-Heider, S. Walsh, J. Zupicich, K. Alkass, B. A. Buchholz, H. Druid, S. Jovinge and J. Frisen (2009). Evidence for cardiomyocyte renewal in humans. *Science* **324**(5923): 98-102.

Bettiol, E., L. Sartiani, L. Chicha, K. H. Krause, E. Cerbai and M. E. Jaconi (2007). Fetal bovine serum enables cardiac differentiation of human embryonic stem cells. *Differentiation* **75**(8): 669-681.

Bianconi, E., A. Piovesan, F. Facchin, A. Beraudi, R. Casadei, F. Frabetti, L. Vitale, M. C. Pelleri, S. Tassani, F. Piva, S. Perez-Amodio, P. Strippoli and S. Canaider (2013). An estimation of the number of cells in the human body. *Ann Hum Biol* **40**(6): 463-471.

Bieback, K., B. Fernandez-Munoz, S. Pati and R. Schafer (2019). Gaps in the knowledge of human platelet lysate as a cell culture supplement for cell therapy: a joint publication from the AABB and the International Society for Cell & Gene Therapy. *Transfusion* **59**(11): 3448-3460.

Blaber, E. A., H. Finkelstein, N. Dvorochkin, K. Y. Sato, R. Yousuf, B. P. Burns, R. K. Globus and E. A. Almeida (2015). Microgravity Reduces the Differentiation and Regenerative Potential of Embryonic Stem Cells. *Stem Cells Dev* **24**(22): 2605-2621.

Blum, B., O. Bar-Nur, T. Golan-Lev and N. Benvenisty (2009). The anti-apoptotic gene survivin contributes to teratoma formation by human embryonic stem cells. *Nat Biotechnol* **27**(3): 281-287.

Borys, B. S., T. Dang, T. So, L. Rohani, T. Revay, T. Walsh, M. Thompson, B. Argiropoulos, D. E. Rancourt, S. Jung, Y. Hashimura, B. Lee and M. S. Kallos (2021). Overcoming bioprocess bottlenecks in the large-scale expansion of high-quality hiPSC aggregates in vertical-wheel stirred suspension bioreactors. *Stem Cell Res Ther* **12**(1): 55.

Borys, B. S., T. So, J. Colter, T. Dang, E. L. Roberts, T. Revay, L. Larijani, R. Krawetz, I. Lewis, B. Argiropoulos, D. E. Rancourt, S. Jung, Y. Hashimura, B. Lee and M. S. Kallos (2020). Optimized serial expansion of human induced pluripotent stem cells using low-density inoculation to generate clinically relevant quantities in vertical-wheel bioreactors. *Stem Cells Transl Med* **9**(9): 1036-1052.

Branco, M. A., J. P. Cotovio, C. A. V. Rodrigues, S. H. Vaz, T. G. Fernandes, L. M. Moreira, J. M. S. Cabral and M. M. Diogo (2019). Transcriptomic analysis of 3D Cardiac Differentiation of Human Induced Pluripotent Stem Cells Reveals Faster Cardiomyocyte Maturation Compared to 2D Culture. *Sci Rep* **9**(1): 9229.

Buijtendijk, M. F. J., P. Barnett and M. J. B. van den Hoff (2020). Development of the human heart. *Am J Med Genet C Semin Med Genet* **184**(1): 7-22.

Burridge, P. W., E. Matsa, P. Shukla, Z. C. Lin, J. M. Churko, A. D. Ebert, F. Lan, S. Diecke, B. Huber, N. M. Mordwinkin, J. R. Plews, O. J. Abilez, B. Cui, J. D. Gold and J. C. Wu (2014). Chemically defined generation of human cardiomyocytes. *Nat Methods* **11**(8): 855-860.

Burridge, P. W., S. Thompson, M. A. Millrod, S. Weinberg, X. Yuan, A. Peters, V. Mahairaki, V. E. Koliatsos, L. Tung and E. T. Zambidis (2011). A universal system for highly efficient cardiac differentiation of human induced pluripotent stem cells that eliminates interline variability. *PLoS One* **6**(4): e18293.

Burton, G. J. and E. Jaunaiux (2001). Maternal vascularisation of the human placenta: does the embryo develop in a hypoxic environment? *Gynecol Obstet Fertil* **29**(7-8): 503-508.

Bylund, J. B., L. T. Trinh, C. P. Awgulewitsch, D. T. Paik, C. Jetter, R. Jha, J. Zhang, K. Nolan, C. Xu, T. B. Thompson, T. J. Kamp and A. K. Hatzopoulos (2017). Coordinated Proliferation and Differentiation of Human-Induced Pluripotent Stem Cell-Derived Cardiac Progenitor Cells Depend on Bone Morphogenetic Protein Signaling Regulation by GREMLIN 2. *Stem Cells Dev* **26**(9): 678-693.

Cajochen, C., J. Pischke, D. Aeschbach and A. A. Borbely (1994). Heart rate dynamics during human sleep. *Physiol Behav* **55**(4): 769-774.

Cao, N., Z. Liu, Z. Chen, J. Wang, T. Chen, X. Zhao, Y. Ma, L. Qin, J. Kang, B. Wei, L. Wang, Y. Jin and H. T. Yang (2012). Ascorbic acid enhances the cardiac differentiation of induced pluripotent stem cells through promoting the proliferation of cardiac progenitor cells. *Cell Res* **22**(1): 219-236.

Carpenter, L., C. Carr, C. T. Yang, D. J. Stuckey, K. Clarke and S. M. Watt (2012). Efficient differentiation of human induced pluripotent stem cells generates cardiac cells that provide protection following myocardial infarction in the rat. *Stem Cells Dev* **21**(6): 977-986.

Chan, C. Y., P. H. Huang, F. Guo, X. Ding, V. Kapur, J. D. Mai, P. K. Yuen and T. J. Huang (2013). Accelerating drug discovery via organs-on-chips. *Lab Chip* **13**(24): 4697-4710.

Chang, J.-S., K.-S. Lee and P.-J. Lin (2002). Biohydrogen production with fixed-bed bioreactors. *International Journal of Hydrogen Energy* **27**(11-12): 1167-1174.

Chemello, F., E. N. Olson and R. Bassel-Duby (2020). Biochemistry of Development: Striated Muscle. *Reference Module in Life Sciences*, Elsevier.

Chen, A. K., X. Chen, A. B. Choo, S. Reuveny and S. K. Oh (2011a). Critical microcarrier properties affecting the expansion of undifferentiated human embryonic stem cells. *Stem Cell Res* **7**(2): 97-111.

Chen, A. K., S. Reuveny and S. K. Oh (2013). Application of human mesenchymal and pluripotent stem cell microcarrier cultures in cellular therapy: achievements and future direction. *Biotechnol Adv* **31**(7): 1032-1046.

Chen, B.-Y., S.-Y. Chen and J.-S. Chang (2005). Immobilized cell fixed-bed bioreactor for wastewater decolorization. *Process Biochemistry* **40**(11): 3434-3440.

Chen, G., D. R. Gulbranson, Z. Hou, J. M. Bolin, V. Ruotti, M. D. Probasco, K. Smuga-Otto, S. E. Howden, N. R. Diol, N. E. Propson, R. Wagner, G. O. Lee, J. Antosiewicz-Bourget, J. M. Teng and J. A. Thomson (2011b). Chemically defined conditions for human iPSC derivation and culture. *Nat Methods* **8**(5): 424-429.

Chen, H. F., H. C. Kuo, W. Chen, F. C. Wu, Y. S. Yang and H. N. Ho (2009). A reduced oxygen tension (5%) is not beneficial for maintaining human embryonic stem cells in the undifferentiated state with short splitting intervals. *Hum Reprod* **24**(1): 71-80.

Chen, V. C., S. M. Couture, J. Ye, Z. Lin, G. Hua, H. I. Huang, J. Wu, D. Hsu, M. K. Carpenter and L. A. Couture (2012). Scalable GMP compliant suspension culture system for human ES cells. *Stem Cell Res* **8**(3): 388-402.

Cheng, T. M., A. V. Savkin, B. G. Celler, S. W. Su and L. Wang (2008). Nonlinear modeling and control of human heart rate response during exercise with various work load intensities. *IEEE Trans Biomed Eng* **55**(11): 2499-2508.

Cherry, R. S. and E. T. Papoutsakis (1988). Physical mechanisms of cell damage in microcarrier cell culture bioreactors. *Biotechnol Bioeng* **32**(8): 1001-1014.

Chiang, M. C., H. Lin, Y. C. Cheng, C. H. Yen, R. N. Huang and K. H. Lin (2012). Beta-adrenoceptor pathway enhances mitochondrial function in human neural stem cells via rotary cell culture system. *J Neurosci Methods* **207**(2): 130-136.

Chour, T., L. Tian, E. Lau, D. Thomas, I. Itzhaki, O. Malak, J. Z. Zhang, X. Qin, M. Wardak, Y. Liu, M. Chandy, K. E. Black, M. P. Lam, E. Neofytou and J. C. Wu (2021). Method for selective ablation of undifferentiated human pluripotent stem cell populations for cell-based therapies. *JCI Insight* **6**(7): e142000.

Chow, M. Z., L. Geng, C. W. Kong, W. Keung, J. C. Fung, K. R. Boheler and R. A. Li (2013). Epigenetic regulation of the electrophysiological phenotype of human embryonic stem cell-derived ventricular cardiomyocytes: insights for driven maturation and hypertrophic growth. *Stem Cells Dev* **22**(19): 2678-2690.

Christoffels, V. M. and A. F. Moorman (2009). Development of the cardiac conduction system: why are some regions of the heart more arrhythmogenic than others? *Circ Arrhythm Electrophysiol* **2**(2): 195-207.

Chu, A. J., E. J. Zhao, M. Chiao and C. J. Lim (2020). Co-culture of induced pluripotent stem cells with cardiomyocytes is sufficient to promote their differentiation into cardiomyocytes. *PLoS One* **15**(4): e0230966.

Clarke, J. M., J. Hamer, J. R. Shelton, S. Taylor and G. R. Venning (1976). The rhythm of the normal human heart. *Lancet* **1**(7984): 508-512.

Clevers, H. (2006). Wnt/beta-catenin signaling in development and disease. *Cell* **127**(3): 469-480.

Clevers, H. (2016). Modeling Development and Disease with Organoids. *Cell* **165**(7): 1586-1597.

Collins, F. S. and H. Varmus (2015). A new initiative on precision medicine. *N Engl J Med* **372**(9): 793-795.

Come, J., X. Nissan, L. Aubry, J. Tournois, M. Girard, A. L. Perrier, M. Peschanski and M. Cailleret (2008). Improvement of culture conditions of human embryoid bodies using a controlled perfused and dialyzed bioreactor system. *Tissue Eng Part C Methods* **14**(4): 289-298.

Correia, C., A. Koshkin, P. Duarte, D. Hu, M. Carido, M. J. Sebastiao, P. Gomes-Alves, D. A. Elliott, I. J. Domian, A. P. Teixeira, P. M. Alves and M. Serra (2018). 3D aggregate culture improves metabolic maturation of human pluripotent stem cell derived cardiomyocytes. *Biotechnol Bioeng* **115**(3): 630-644.

Correia, C., A. Koshkin, P. Duarte, D. Hu, A. Teixeira, I. Domian, M. Serra and P. M. Alves (2017). Distinct carbon sources affect structural and functional maturation of cardiomyocytes derived from human pluripotent stem cells. *Sci Rep* **7**(1): 8590.

Cowger, N. L., K. C. O'Connor, T. G. Hammond, D. J. Lacks and G. L. Navar (1999). Characterization of bimodal cell death of insect cells in a rotating-wall vessel and shaker flask. *Biotechnol Bioeng* **64**(1): 14-26.

Croughan, M. S., D. Giroux, D. Fang and B. Lee (2016). Novel Single-Use Bioreactors for Scale-Up of Anchorage-Dependent Cell Manufacturing for Cell Therapies *Stem Cell Manufacturing*. C. L. da Silva, L. G. Chase and M. M. Diogo. Cambridge, Elsevier**:** 105-139.

Croughan, M. S., J. F. Hamel and D. I. Wang (1987). Hydrodynamic effects on animal cells grown in microcarrier cultures. *Biotechnol Bioeng* **29**(1): 130-141.

Cunha, B., T. Aguiar, S. B. Carvalho, M. M. Silva, R. A. Gomes, M. J. T. Carrondo, P. Gomes-Alves, C. Peixoto, M. Serra and P. M. Alves (2017). Bioprocess integration for human mesenchymal stem cells: From up to downstream processing scale-up to cell proteome characterization. *J Biotechnol* **248**: 87-98.

Cunningham, J. J., T. M. Ulbright, M. F. Pera and L. H. Looijenga (2012). Lessons from human teratomas to guide development of safe stem cell therapies. *Nat Biotechnol* **30**(9): 849-857.

da Silva, J. d. S., A. Mizukami, L. V. G. Gil, J. V. de Campos, O. B. Assis, D. T. Covas, K. Swiech and C. A. T. Suazo (2019). Improving wave-induced motion bioreactor performance for human mesenchymal stromal cell expansion. *Process Biochemistry* **84**: 143-152.

da Silva, J. d. S., P. Severino, T. I. Wodewotzky, D. T. Covas, K. Swiech, L. C. Marti and C. A. T. Suazo (2020). Mesenchymal stromal cells maintain the major quality attributes when expanded in different bioreactor systems. *Biochemical Engineering Journal* **161**: 107693.

Davis, B. M., E. R. Loghin, K. R. Conway and X. Zhang (2018). Automated Closed-System Expansion of Pluripotent Stem Cell Aggregates in a Rocking-Motion Bioreactor. *SLAS Technol* **23**(4): 364-373.

de Almeida Fuzeta, M., N. Bernardes, F. D. Oliveira, A. C. Costa, A. Fernandes-Platzgummer, J. P. Farinha, C. A. V. Rodrigues, S. Jung, R. J. Tseng, W. Milligan, B. Lee, M. Castanho, D. Gaspar, J. M. S. Cabral and C. L. da Silva (2020). Scalable Production of Human Mesenchymal Stromal Cell-Derived Extracellular Vesicles Under Serum-/Xeno-Free Conditions in a Microcarrier-Based Bioreactor Culture System. *Front Cell Dev Biol* **8**: 553444.

de Sousa Pinto, D., C. Bandeiras, M. de Almeida Fuzeta, C. A. V. Rodrigues, S. Jung, Y. Hashimura, R. J. Tseng, W. Milligan, B. Lee, F. C. Ferreira, C. Lobato da Silva and J. M. S. Cabral (2019). Scalable Manufacturing of Human Mesenchymal Stromal Cells in the Vertical-Wheel Bioreactor System: An Experimental and Economic Approach. *Biotechnol J* **14**(8): e1800716.

Dee, K. U., M. L. Shuler and H. A. Wood (1997). Inducing single-cell suspension of BTI-TN5B1-4 insect cells: I. The use of sulfated polyanions to prevent cell aggregation and enhance recombinant protein production. *Biotechnol Bioeng* **54**(3): 191-205.

Deng, M. C. (2002). Cardiac transplantation. *Heart* **87**(2): 177-184.

DiStefano, T., H. Y. Chen, C. Panebianco, K. D. Kaya, M. J. Brooks, L. Gieser, N. Y. Morgan, T. Pohida and A. Swaroop (2018). Accelerated and Improved Differentiation of Retinal Organoids from Pluripotent Stem Cells in Rotating-Wall Vessel Bioreactors. *Stem Cell Reports* **10**(1): 300-313.

Dixon, J. E., E. Dick, D. Rajamohan, K. M. Shakesheff and C. Denning (2011). Directed differentiation of human embryonic stem cells to interrogate the cardiac gene regulatory network. *Mol Ther* **19**(9): 1695-1703.

Dixon, J. E., D. A. Shah, C. Rogers, S. Hall, N. Weston, C. D. Parmenter, D. McNally, C. Denning and K. M. Shakesheff (2014). Combined hydrogels that switch human pluripotent stem cells from self-renewal to differentiation. *Proc Natl Acad Sci U S A* **111**(15): 5580-5585.

Drakhlis, L., S. Biswanath, C. M. Farr, V. Lupanow, J. Teske, K. Ritzenhoff, A. Franke, F. Manstein, E. Bolesani, H. Kempf, S. Liebscher, K. Schenke-Layland, J. Hegermann, L. Nolte, H. Meyer, J. de la Roche, S. Thiemann, C. Wahl-Schott, U. Martin and R. Zweigerdt (2021). Human heart-forming organoids recapitulate early heart and foregut development. *Nat Biotechnol* **39**(6): 737-746.

Du, C., K. Narayanan, M. F. Leong and A. C. Wan (2014). Induced pluripotent stem cell-derived hepatocytes and endothelial cells in multi-component hydrogel fibers for liver tissue engineering. *Biomaterials* **35**(23): 6006-6014.

Dubois, N. C., A. M. Craft, P. Sharma, D. A. Elliott, E. G. Stanley, A. G. Elefanty, A. Gramolini and G. Keller (2011). SIRPA is a specific cell-surface marker for isolating cardiomyocytes derived from human pluripotent stem cells. *Nat Biotechnol* **29**(11): 1011-1018.

Earls, J. K., S. Jin and K. Ye (2013). Mechanobiology of human pluripotent stem cells. *Tissue Eng Part B Rev* **19**(5): 420-430.

Elliott, D. A., S. R. Braam, K. Koutsis, E. S. Ng, R. Jenny, E. L. Lagerqvist, C. Biben, T. Hatzistavrou, C. E. Hirst, Q. C. Yu, R. J. Skelton, D. Ward-van Oostwaard, S. M. Lim, O. Khammy, X. Li, S. M. Hawes, R. P. Davis, A. L. Goulburn, R. Passier, O. W. Prall, J. M. Haynes, C. W. Pouton, D. M. Kaye, C. L. Mummery, A. G. Elefanty and E. G. Stanley (2011). NKX2-5(eGFP/w) hESCs for isolation of human cardiac progenitors and cardiomyocytes. *Nat Methods* **8**(12): 1037-1040.

England, J. and S. Loughna (2013). Heavy and light roles: myosin in the morphogenesis of the heart. *Cell Mol Life Sci* **70**(7): 1221-1239.

Evans, M. J. and M. H. Kaufman (1981). Establishment in culture of pluripotential cells from mouse embryos. *Nature* **292**(5819): 154-156.

Ezashi, T., P. Das and R. M. Roberts (2005). Low O2 tensions and the prevention of differentiation of hES cells. *Proc Natl Acad Sci U S A* **102**(13): 4783-4788.

Fan, Y., M. Hsiung, C. Cheng and E. S. Tzanakakis (2014). Facile engineering of xeno-free microcarriers for the scalable cultivation of human pluripotent stem cells in stirred suspension. *Tissue Eng Part A* **20**(3-4): 588-599.

Fang, Y. H., S. P. H. Wang, Z. H. Gao, S. N. Wu, H. Y. Chang, P. J. Yang, P. Y. Liu and Y. W. Liu (2020). Efficient Cardiac Differentiation of Human Amniotic Fluid-Derived Stem Cells into Induced Pluripotent Stem Cells and Their Potential Immune Privilege. *Int J Mol Sci* **21**(7): 2359.

Fatehullah, A., S. H. Tan and N. Barker (2016). Organoids as an in vitro model of human development and disease. *Nat Cell Biol* **18**(3): 246-254.

Forsyth, N. R., A. Musio, P. Vezzoni, A. H. Simpson, B. S. Noble and J. McWhir (2006). Physiologic oxygen enhances human embryonic stem cell clonal recovery and reduces chromosomal abnormalities. *Cloning Stem Cells* **8**(1): 16-23.

Freyer, N., F. Knospel, N. Strahl, L. Amini, P. Schrade, S. Bachmann, G. Damm, D. Seehofer, F. Jacobs, M. Monshouwer and K. Zeilinger (2016). Hepatic Differentiation of Human Induced Pluripotent Stem Cells in a Perfused Three-Dimensional Multicompartment Bioreactor. *Biores Open Access* **5**(1): 235-248.

Friedman, C. E., Q. Nguyen, S. W. Lukowski, A. Helfer, H. S. Chiu, J. Miklas, S. Levy, S. Suo, J. J. Han, P. Osteil, G. Peng, N. Jing, G. J. Baillie, A. Senabouth, A. N. Christ, T. J. Bruxner, C. E. Murry, E. S. Wong, J. Ding, Y. Wang, J. Hudson, H. Ruohola-Baker, Z. Bar-Joseph, P. P. L. Tam, J. E. Powell and N. J. Palpant (2018). Single-Cell Transcriptomic Analysis of Cardiac Differentiation from Human PSCs Reveals HOPX-Dependent Cardiomyocyte Maturation. *Cell Stem Cell* **23**(4): 586-598 e588.

Fuchs, E. and T. Chen (2013). A matter of life and death: self-renewal in stem cells. *EMBO Rep* **14**(1): 39-48.

Fuerstenau-Sharp, M., M. E. Zimmermann, K. Stark, N. Jentsch, M. Klingenstein, M. Drzymalski, S. Wagner, L. S. Maier, U. Hehr, A. Baessler, M. Fischer and C. Hengstenberg (2015). Generation of highly purified human cardiomyocytes from peripheral blood mononuclear cell-derived induced pluripotent stem cells. *PLoS One* **10**(5): e0126596.

Fujiwara, M., P. Yan, T. G. Otsuji, G. Narazaki, H. Uosaki, H. Fukushima, K. Kuwahara, M. Harada, H. Matsuda, S. Matsuoka, K. Okita, K. Takahashi, M. Nakagawa, T. Ikeda, R. Sakata, C. L. Mummery, N. Nakatsuji, S. Yamanaka, K. Nakao and J. K. Yamashita (2011). Induction and enhancement of cardiac cell differentiation from mouse and human induced pluripotent stem cells with cyclosporin-A. *PLoS One* **6**(2): e16734.

Fukushima, H., M. Yoshioka, M. Kawatou, V. Lopez-Davila, M. Takeda, Y. Kanda, Y. Sekino, Y. Yoshida and J. K. Yamashita (2020). Specific induction and long-term maintenance of high purity ventricular cardiomyocytes from human induced pluripotent stem cells. *PLoS One* **15**(11): e0241287.

Fynes, K., R. Tostoes, L. Ruban, B. Weil, C. Mason and F. S. Veraitch (2014). The differential effects of 2% oxygen preconditioning on the subsequent differentiation of mouse and human pluripotent stem cells. *Stem Cells Dev* **23**(16): 1910-1922.

Gaber, N., M. Gagliardi, P. Patel, C. Kinnear, C. Zhang, D. Chitayat, P. Shannon, E. Jaeggi, U. Tabori, G. Keller and S. Mital (2013). Fetal reprogramming and senescence in hypoplastic left heart syndrome and in human pluripotent stem cells during cardiac differentiation. *Am J Pathol* **183**(3): 720-734.

Garate, X., A. La Greca, G. Neiman, C. Bluguermann, N. L. Santin Velazque, L. N. Moro, C. Luzzani, M. E. Scassa, G. E. Sevlever, L. Romorini and S. G. Miriuka (2018). Identification of the miRNAome of early mesoderm progenitor cells and cardiomyocytes derived from human pluripotent stem cells. *Sci Rep* **8**(1): 8072.

Gerri, C., S. Menchero, S. K. Mahadevaiah, J. M. A. Turner and K. K. Niakan (2020). Human Embryogenesis: A Comparative Perspective. *Annu Rev Cell Dev Biol* **36**: 411-440.

Ghimire, S., V. Mantziou, N. Moris and A. Martinez Arias (2021). Human gastrulation: The embryo and its models. *Dev Biol* **474**: 100-108.

Gimenez, J. B., A. Robles, L. Carretero, F. Duran, M. V. Ruano, M. N. Gatti, J. Ribes, J. Ferrer and A. Seco (2011). Experimental study of the anaerobic urban wastewater treatment in a submerged hollow-fibre membrane bioreactor at pilot scale. *Bioresour Technol* **102**(19): 8799-8806.

Goetzke, R., H. Keijdener, J. Franzen, A. Ostrowska, S. Nuchtern, P. Mela and W. Wagner (2019). Differentiation of Induced Pluripotent Stem Cells towards Mesenchymal Stromal Cells is Hampered by Culture in 3D Hydrogels. *Sci Rep* **9**(1): 15578.

Gordon, R. S., J. Ivanov, G. Cohen and A. L. Ralph-Edwards (1998). Permanent cardiac pacing after a cardiac operation: predicting the use of permanent pacemakers. *Ann Thorac Surg* **66**(5): 1698-1704.

Grein, T. A., J. Leber, M. Blumenstock, F. Petry, T. Weidner, D. Salzig and P. Czermak (2016). Multiphase mixing characteristics in a microcarrier-based stirred tank bioreactor suitable for human mesenchymal stem cell expansion. *Process Biochemistry* **51**(9): 1109-1119.

Guilak, F., D. M. Cohen, B. T. Estes, J. M. Gimble, W. Liedtke and C. S. Chen (2009). Control of stem cell fate by physical interactions with the extracellular matrix. *Cell Stem Cell* **5**(1): 17-26.

Gunthel, M., P. Barnett and V. M. Christoffels (2018). Development, Proliferation, and Growth of the Mammalian Heart. *Mol Ther* **26**(7): 1599-1609.

Haack-Sørensen, M., B. Follin, M. Juhl, S. K. Brorsen, R. H. Søndergaard, J. Kastrup and A. Ekblond (2016). Culture expansion of adipose derived stromal cells. A closed automated Quantum Cell Expansion System compared with manual flask-based culture. *J Transl Med* **14**(1): 319.

Haack-Sørensen, M., M. Juhl, B. Follin, R. Harary Søndergaard, M. Kirchhoff, J. Kastrup and A. Ekblond (2018). Development of large-scale manufacturing of adipose-derived stromal cells for clinical applications using bioreactors and human platelet lysate. *Scand J Clin Lab Invest* **78**(4): 293-300.

Hakim, F., T. Kaitsuka, J. M. Raeed, F. Y. Wei, N. Shiraki, T. Akagi, T. Yokota, S. Kume and K. Tomizawa (2014). High oxygen condition facilitates the differentiation of mouse and human pluripotent stem cells into pancreatic progenitors and insulin-producing cells. *J Biol Chem* **289**(14): 9623-9638.

Halloin, C., K. Schwanke, W. Lobel, A. Franke, M. Szepes, S. Biswanath, S. Wunderlich, S. Merkert, N. Weber, F. Osten, J. de la Roche, F. Polten, K. Christoph Wollert, T. Kraft, M. Fischer, U. Martin, I. Gruh, H. Kempf and R. Zweigerdt (2019). Continuous WNT Control Enables Advanced hPSC Cardiac Processing and Prognostic Surface Marker Identification in Chemically Defined Suspension Culture. *Stem Cell Reports* **13**(2): 366-379.

Hammond, M., L. Marghitoiu, H. Lee, L. Perez, G. Rogers, Y. Nashed-Samuel, H. Nunn and S. Kline (2014). A cytotoxic leachable compound from single-use bioprocess equipment that causes poor cell growth performance. *Biotechnol Prog* **30**(2): 332-337.

Hammond, M., H. Nunn, G. Rogers, H. Lee, A. L. Marghitoiu, L. Perez, Y. Nashed-Samuel, C. Anderson, M. Vandiver and S. Kline (2013). Identification of a leachable compound detrimental to cell growth in single-use bioprocess containers. *PDA J Pharm Sci Technol* **67**(2): 123-134.

Hammond, T. G. and J. M. Hammond (2001). Optimized suspension culture: the rotating-wall vessel. *Am J Physiol Renal Physiol* **281**(1): F12-25.

Hattori, F., H. Chen, H. Yamashita, S. Tohyama, Y. S. Satoh, S. Yuasa, W. Li, H. Yamakawa, T. Tanaka, T. Onitsuka, K. Shimoji, Y. Ohno, T. Egashira, R. Kaneda, M. Murata, K. Hidaka, T. Morisaki, E. Sasaki, T. Suzuki, M. Sano, S. Makino, S. Oikawa and K. Fukuda (2010). Nongenetic method for purifying stem cell-derived cardiomyocytes. *Nat Methods* **7**(1): 61-66.

Hazeltine, L. B., M. G. Badur, X. Lian, A. Das, W. Han and S. P. Palecek (2014). Temporal impact of substrate mechanics on differentiation of human embryonic stem cells to cardiomyocytes. *Acta Biomater* **10**(2): 604-612.

He, S., D. Nakada and S. J. Morrison (2009). Mechanisms of stem cell self-renewal. *Annu Rev Cell Dev Biol* **25**: 377-406.

Heemskerk, I. and A. Warmflash (2016). Pluripotent stem cells as a model for embryonic patterning: From signaling dynamics to spatial organization in a dish. *Dev Dyn* **245**(10): 976-990.

Hemmi, N., S. Tohyama, K. Nakajima, H. Kanazawa, T. Suzuki, F. Hattori, T. Seki, Y. Kishino, A. Hirano, M. Okada, R. Tabei, R. Ohno, C. Fujita, T. Haruna, S. Yuasa, M. Sano, J. Fujita and K. Fukuda (2014). A massive suspension culture system with metabolic purification for human pluripotent stem cell-derived cardiomyocytes. *Stem Cells Transl Med* **3**(12): 1473-1483.

Heng, B. C., J. Li, A. K. Chen, S. Reuveny, S. M. Cool, W. R. Birch and S. K. Oh (2012). Translating human embryonic stem cells from 2-dimensional to 3-dimensional cultures in a defined medium on laminin- and vitronectin-coated surfaces. *Stem Cells Dev* **21**(10): 1701-1715.

Hennekens, C. H., M. L. Dyken and V. Fuster (1997). Aspirin as a therapeutic agent in cardiovascular disease: a statement for healthcare professionals from the American Heart Association. *Circulation* **96**(8): 2751-2753.

Hernandez, D., R. Millard, P. Sivakumaran, R. C. Wong, D. E. Crombie, A. W. Hewitt, H. Liang, S. S. Hung, A. Pebay, R. K. Shepherd, G. J. Dusting and S. Y. Lim (2016). Electrical Stimulation Promotes Cardiac Differentiation of Human Induced Pluripotent Stem Cells. *Stem Cells Int* **2016**: 1718041.

Hesse, M., A. Welz and B. K. Fleischmann (2018). Heart regeneration and the cardiomyocyte cell cycle. *Pflugers Arch* **470**(2): 241-248.

Hirt, M. N., J. Boeddinghaus, A. Mitchell, S. Schaaf, C. Bornchen, C. Muller, H. Schulz, N. Hubner, J. Stenzig, A. Stoehr, C. Neuber, A. Eder, P. K. Luther, A. Hansen and T. Eschenhagen (2014). Functional improvement and maturation of rat and human engineered heart tissue by chronic electrical stimulation. *J Mol Cell Cardiol* **74**: 151-161.

Hoang, P., A. Kowalczewski, S. Sun, T. S. Winston, A. M. Archilla, S. M. Lemus, A. G. Ercan-Sencicek, A. R. Gupta, W. Liu, M. I. Kontaridis, J. D. Amack and Z. Ma (2021). Engineering spatial-organized cardiac organoids for developmental toxicity testing. *Stem Cell Reports* **16**(5): 1228-1244.

Homma, S., J. L. Thompson, P. M. Pullicino, B. Levin, R. S. Freudenberger, J. R. Teerlink, S. E. Ammon, S. Graham, R. L. Sacco, D. L. Mann, J. P. Mohr, B. M. Massie, A. J. Labovitz, S. D. Anker, D. J. Lok, P. Ponikowski, C. J. Estol, G. Y. Lip, M. R. Di Tullio, A. R. Sanford, V. Mejia, A. P. Gabriel, M. L. del Valle, R. Buchsbaum and W. Investigators (2012). Warfarin and aspirin in patients with heart failure and sinus rhythm. *N Engl J Med* **366**(20): 1859-1869.

Horikoshi, Y., Y. Yan, M. Terashvili, C. Wells, H. Horikoshi, S. Fujita, Z. J. Bosnjak and X. Bai (2019). Fatty Acid-Treated Induced Pluripotent Stem Cell-Derived Human Cardiomyocytes Exhibit Adult Cardiomyocyte-Like Energy Metabolism Phenotypes. *Cells* **8**(9): 1095.

Huang, J. and X. Jiang (2018). Injectable and Degradable pH-Responsive Hydrogels via Spontaneous Amino-Yne Click Reaction. *ACS Appl Mater Interfaces* **10**(1): 361-370.

Huber, I., I. Itzhaki, O. Caspi, G. Arbel, M. Tzukerman, A. Gepstein, M. Habib, L. Yankelson, I. Kehat and L. Gepstein (2007). Identification and selection of cardiomyocytes during human embryonic stem cell differentiation. *FASEB J* **21**(10): 2551-2563.

Hunt, M. M., G. Meng, D. E. Rancourt, I. D. Gates and M. S. Kallos (2014). Factorial experimental design for the culture of human embryonic stem cells as aggregates in stirred suspension bioreactors reveals the potential for interaction effects between bioprocess parameters. *Tissue Eng Part C Methods* **20**(1): 76-89.

Hunt, N. C., D. Hallam, A. Karimi, C. B. Mellough, J. Chen, D. H. W. Steel and M. Lako (2017). 3D culture of human pluripotent stem cells in RGD-alginate hydrogel improves retinal tissue development. *Acta Biomater* **49**: 329-343.

Hyoung Park, J., M. Sin Lim, J. Rang Woo, J. Won Kim and G. Min Lee (2016). The molecular weight and concentration of dextran sulfate affect cell growth and antibody production in CHO cell cultures. *Biotechnol Prog* **32**(5): 1113-1122.

Ilic, D. and C. Ogilvie (2017). Concise Review: Human Embryonic Stem Cells-What Have We Done? What Are We Doing? Where Are We Going? *Stem Cells* **35**(1): 17-25.

Ishida, H., R. Saba, I. Kokkinopoulos, M. Hashimoto, O. Yamaguchi, S. Nowotschin, M. Shiraishi, P. Ruchaya, D. Miller, S. Harmer, A. Poliandri, S. Kogaki, Y. Sakata, L. Dunkel, A. Tinker, A. K. Hadjantonakis, Y. Sawa, H. Sasaki, K. Ozono, K. Suzuki and K. Yashiro (2016). GFRA2 Identifies Cardiac Progenitors and Mediates Cardiomyocyte Differentiation in a RET-Independent Signaling Pathway. *Cell Rep* **16**(4): 1026-1038.

Itskovitz-Eldor, J., M. Schuldiner, D. Karsenti, A. Eden, O. Yanuka, M. Amit, H. Soreq and N. Benvenisty (2000). Differentiation of human embryonic stem cells into embryoid bodies compromising the three embryonic germ layers. *Mol Med* **6**(2): 88-95.

Jafari, S. J., G. Moussavi and K. Yaghmaeian (2015). High-rate biological denitrification in the cyclic rotating-bed biological reactor: Effect of COD/NO3(-), nitrate concentration and salinity and the phylogenetic analysis of denitrifiers. *Bioresour Technol* **197**: 482-488.

Jardin, B. A., Y. Zhao, M. Selvaraj, J. Montes, R. Tran, S. Prakash and C. B. Elias (2008). Expression of SEAP (secreted alkaline phosphatase) by baculovirus mediated transduction of HEK 293 cells in a hollow fiber bioreactor system. *J Biotechnol* **135**(3): 272-280.

Jha, R., Q. Wu, M. Singh, M. K. Preininger, P. Han, G. Ding, H. C. Cho, H. Jo, K. O. Maher, M. B. Wagner and C. Xu (2016). Simulated Microgravity and 3D Culture Enhance Induction, Viability, Proliferation and Differentiation of Cardiac Progenitors from Human Pluripotent Stem Cells. *Sci Rep* **6**: 30956.

Jia, F., K. D. Wilson, N. Sun, D. M. Gupta, M. Huang, Z. Li, N. J. Panetta, Z. Y. Chen, R. C. Robbins, M. A. Kay, M. T. Longaker and J. C. Wu (2010). A nonviral minicircle vector for deriving human iPS cells. *Nat Methods* **7**(3): 197-199.

Jing, D., A. Parikh and E. S. Tzanakakis (2010). Cardiac cell generation from encapsulated embryonic stem cells in static and scalable culture systems. *Cell Transplant* **19**(11): 1397-1412.

Jones, R. H., E. J. Velazquez, R. E. Michler, G. Sopko, J. K. Oh, C. M. O'Connor, J. A. Hill, L. Menicanti, Z. Sadowski, P. Desvigne-Nickens, J. L. Rouleau, K. L. Lee and S. H. Investigators (2009). Coronary bypass surgery with or without surgical ventricular reconstruction. *N Engl J Med* **360**(17): 1705-1717.

Joutsijoki, H., M. Haponen, J. Rasku, K. Aalto-Setala and M. Juhola (2016). Machine Learning Approach to Automated Quality Identification of Human Induced Pluripotent Stem Cell Colony Images. *Comput Math Methods Med* **2016**: 3091039.

Jurkiewicz, E., U. Husemann, G. Greller, M. Barbaroux and C. Fenge (2014). Verification of a new biocompatible single-use film formulation with optimized additive content for multiple bioprocess applications. *Biotechnol Prog* **30**(5): 1171-1176.

Kaiser, L. R. (1992). The future of multihospital systems. *Top Health Care Financ* **18**(4): 32-45.

Kalmbach, A., R. Bordas, A. A. Oncul, D. Thevenin, Y. Genzel and U. Reichl (2011). Experimental characterization of flow conditions in 2- and 20-L bioreactors with wave-induced motion. *Biotechnol Prog* **27**(2): 402-409.

Kamakura, T., T. Makiyama, K. Sasaki, Y. Yoshida, Y. Wuriyanghai, J. Chen, T. Hattori, S. Ohno, T. Kita, M. Horie, S. Yamanaka and T. Kimura (2013). Ultrastructural maturation of human-induced pluripotent stem cell-derived cardiomyocytes in a long-term culture. *Circ J* **77**(5): 1307-1314.

Kattman, S. J., A. D. Witty, M. Gagliardi, N. C. Dubois, M. Niapour, A. Hotta, J. Ellis and G. Keller (2011). Stage-specific optimization of activin/nodal and BMP signaling promotes cardiac differentiation of mouse and human pluripotent stem cell lines. *Cell Stem Cell* **8**(2): 228-240.

Kehat, I., D. Kenyagin-Karsenti, M. Snir, H. Segev, M. Amit, A. Gepstein, E. Livne, O. Binah, J. Itskovitz-Eldor and L. Gepstein (2001). Human embryonic stem cells can differentiate into myocytes with structural and functional properties of cardiomyocytes. *J Clin Invest* **108**(3): 407-414.

Kempf, H., M. Lecina, S. Ting, R. Zweigerdt and S. Oh (2011). Distinct regulation of mitogen-activated protein kinase activities is coupled with enhanced cardiac differentiation of human embryonic stem cells. *Stem Cell Res* **7**(3): 198-209.

Kempf, H., R. Olmer, C. Kropp, M. Ruckert, M. Jara-Avaca, D. Robles-Diaz, A. Franke, D. A. Elliott, D. Wojciechowski, M. Fischer, A. Roa Lara, G. Kensah, I. Gruh, A. Haverich, U. Martin and R. Zweigerdt (2014). Controlling expansion and cardiomyogenic differentiation of human pluripotent stem cells in scalable suspension culture. *Stem Cell Reports* **3**(6): 1132-1146.

Kim, D., C. H. Kim, J. I. Moon, Y. G. Chung, M. Y. Chang, B. S. Han, S. Ko, E. Yang, K. Y. Cha, R. Lanza and K. S. Kim (2009). Generation of human induced pluripotent stem cells by direct delivery of reprogramming proteins. *Cell Stem Cell* **4**(6): 472-476.

Kim, J., D. Kang, H. Park, M. Kang, T. K. Park, J. M. Lee, J. H. Yang, Y. B. Song, J. H. Choi, S. H. Choi, H. C. Gwon, E. Guallar, J. Cho and J. Y. Hahn (2020). Long-term beta-blocker therapy and clinical outcomes after acute myocardial infarction in patients without heart failure: nationwide cohort study. *Eur Heart J* **41**(37): 3521-3529.

Kim, J. J., L. Hou and N. F. Huang (2016). Vascularization of three-dimensional engineered tissues for regenerative medicine applications. *Acta Biomater* **41**: 17-26.

Kim, K. and B. E. Logan (2000). Fixed-bed bioreactor treating perchlorate-contaminated waters. *Environmental engineering science* **17**(5): 257-265.

Komiya, Y. and R. Habas (2008). Wnt signal transduction pathways. *Organogenesis* **4**(2): 68-75.

Krastanov, A., D. Blazheva and V. Stanchev (2007). Sucrose conversion into palatinose with immobilized Serratia plymuthica cells in a hollow-fibre bioreactor. *Process Biochemistry* **42**(12): 1655-1659.

Krawetz, R., J. T. Taiani, S. Liu, G. Meng, X. Li, M. S. Kallos and D. E. Rancourt (2010). Large-scale expansion of pluripotent human embryonic stem cells in stirred-suspension bioreactors. *Tissue Eng Part C Methods* **16**(4): 573-582.

Kropp, C., H. Kempf, C. Halloin, D. Robles-Diaz, A. Franke, T. Scheper, K. Kinast, T. Knorpp, T. O. Joos, A. Haverich, U. Martin, R. Zweigerdt and R. Olmer (2016). Impact of Feeding Strategies on the Scalable Expansion of Human Pluripotent Stem Cells in Single-Use Stirred Tank Bioreactors. *Stem Cells Transl Med* **5**(10): 1289-1301.

Kropp, C., D. Massai and R. Zweigerdt (2017). Progress and challenges in large-scale expansion of human pluripotent stem cells. *Process Biochemistry* **59**: 244-254.

Krtolica, A., O. Genbacev, C. Escobedo, T. Zdravkovic, A. Nordstrom, D. Vabuena, A. Nath, C. Simon, K. Mostov and S. J. Fisher (2007). Disruption of apical-basal polarity of human embryonic stem cells enhances hematoendothelial differentiation. *Stem Cells* **25**(9): 2215-2223.

Kubiczkova, L., L. Sedlarikova, R. Hajek and S. Sevcikova (2012). TGF-beta - an excellent servant but a bad master. *J Transl Med* **10**: 183.

Kulik, M., J. Ochs, N. König and R. Schmitt (2016). Automation in the context of stem cell production–where are we heading with Industry 4.0? *Cell Gene Therapy Insights* **2**(4): 499-506.

Kuo, H. H., X. Gao, J. M. DeKeyser, K. A. Fetterman, E. A. Pinheiro, C. J. Weddle, H. Fonoudi, M. V. Orman, M. Romero-Tejeda, M. Jouni, M. Blancard, T. Magdy, C. L. Epting, A. L. George, Jr. and P. W. Burridge (2020). Negligible-Cost and Weekend-Free Chemically Defined Human iPSC Culture. *Stem Cell Reports* **14**(2): 256-270.

Kwok, C. K., Y. Ueda, A. Kadari, K. Gunther, S. Ergun, A. Heron, A. C. Schnitzler, M. Rook and F. Edenhofer (2018). Scalable stirred suspension culture for the generation of billions of human induced pluripotent stem cells using single-use bioreactors. *J Tissue Eng Regen Med* **12**(2): e1076-e1087.

Laco, F., A. T. Lam, T. L. Woo, G. Tong, V. Ho, P. L. Soong, E. Grishina, K. H. Lin, S. Reuveny and S. K. Oh (2020). Selection of human induced pluripotent stem cells lines optimization of cardiomyocytes differentiation in an integrated suspension microcarrier bioreactor. *Stem Cell Res Ther* **11**(1): 118.

Laflamme, M. A., K. Y. Chen, A. V. Naumova, V. Muskheli, J. A. Fugate, S. K. Dupras, H. Reinecke, C. Xu, M. Hassanipour, S. Police, C. O'Sullivan, L. Collins, Y. Chen, E. Minami, E. A. Gill, S. Ueno, C. Yuan, J. Gold and C. E. Murry (2007). Cardiomyocytes derived from human embryonic stem cells in pro-survival factors enhance function of infarcted rat hearts. *Nat Biotechnol* **25**(9): 1015-1024.

Laflamme, M. A., J. Gold, C. Xu, M. Hassanipour, E. Rosler, S. Police, V. Muskheli and C. E. Murry (2005). Formation of human myocardium in the rat heart from human embryonic stem cells. *Am J Pathol* **167**(3): 663-671.

Lam, A. T., J. Li, A. K. Chen, W. R. Birch, S. Reuveny and S. K. Oh (2015). Improved Human Pluripotent Stem Cell Attachment and Spreading on Xeno-Free Laminin-521-Coated Microcarriers Results in Efficient Growth in Agitated Cultures. *Biores Open Access* **4**(1): 242-257.

Lambrechts, T., I. Papantoniou, B. Rice, J. Schrooten, F. P. Luyten and J. M. Aerts (2016). Large-scale progenitor cell expansion for multiple donors in a monitored hollow fibre bioreactor. *Cytotherapy* **18**(9): 1219-1233.

Lan, T. Q., D. Wei, S. T. Yang and X. Liu (2013). Enhanced cellulase production by Trichoderma viride in a rotating fibrous bed bioreactor. *Bioresour Technol* **133**: 175-182.

Lawson, T., D. E. Kehoe, A. C. Schnitzler, P. J. Rapiejko, K. A. Der, K. Philbrick, S. Punreddy, S. Rigby, R. Smith and Q. Feng (2017). Process development for expansion of human mesenchymal stromal cells in a 50 L single-use stirred tank bioreactor. *Biochemical engineering journal* **120**: 49-62.

Lees, J. G., A. M. Kong, Y. C. Chen, P. Sivakumaran, D. Hernandez, A. Pebay, A. J. Harvey, D. K. Gardner and S. Y. Lim (2019). Mitochondrial Fusion by M1 Promotes Embryoid Body Cardiac Differentiation of Human Pluripotent Stem Cells. *Stem Cells Int* **2019**: 6380135.

Lei, W., T. Feng, X. Fang, Y. Yu, J. Yang, Z. A. Zhao, J. Liu, Z. Shen, W. Deng and S. Hu (2018a). Signature of circular RNAs in human induced pluripotent stem cells and derived cardiomyocytes. *Stem Cell Res Ther* **9**(1): 56.

Lei, X., Y. Cao, Y. Zhang, J. Qian, Q. Zhao, F. Liu, T. Zhang, J. Zhou, Y. Gu, G. Xia and E. Duan (2018b). Effect of microgravity on proliferation and differentiation of embryonic stem cells in an automated culturing system during the TZ-1 space mission. *Cell Prolif* **51**(5): e12466.

Lelkes, P. I., D. L. Galvan, G. T. Hayman, T. J. Goodwin, D. Y. Chatman, S. Cherian, R. M. Garcia and B. R. Unsworth (1998). Simulated microgravity conditions enhance differentiation of cultured PC12 cells towards the neuroendocrine phenotype. *In Vitro Cell Dev Biol Anim* **34**(4): 316-325.

Lembong, J., R. Kirian, J. D. Takacs, T. R. Olsen, L. T. Lock, J. A. Rowley and T. Ahsan (2020). Bioreactor Parameters for Microcarrier-Based Human MSC Expansion under Xeno-Free Conditions in a Vertical-Wheel System. *Bioengineering (Basel)* **7**(3): 73.

Lenzini, S., D. Devine and J. W. Shin (2019). Leveraging Biomaterial Mechanics to Improve Pluripotent Stem Cell Applications for Tissue Engineering. *Front Bioeng Biotechnol* **7**: 260.

Leung, H. W., A. Chen, A. B. Choo, S. Reuveny and S. K. Oh (2011). Agitation can induce differentiation of human pluripotent stem cells in microcarrier cultures. *Tissue Eng Part C Methods* **17**(2): 165-172.

Levine, H. L., R. Stock, J. Lilja, A. Gaasvik, H. Hummel, T. C. Ransohoff and S. D. Jones (2013). Single-use technology and modular construction. *BioProcess International* **11**(4): 40-45.

Li, X., R. Krawetz, S. Liu, G. Meng and D. E. Rancourt (2009). ROCK inhibitor improves survival of cryopreserved serum/feeder-free single human embryonic stem cells. *Hum Reprod* **24**(3): 580-589.

Li, Z., Z. Fan, Y. Xu, W. Lo, X. Wang, H. Niu, X. Li, X. Xie, M. Khan and J. Guan (2016). pH-Sensitive and Thermosensitive Hydrogels as Stem-Cell Carriers for Cardiac Therapy. *ACS Appl Mater Interfaces* **8**(17): 10752-10760.

Li, Z. and T. M. Rana (2012). A kinase inhibitor screen identifies small-molecule enhancers of reprogramming and iPS cell generation. *Nat Commun* **3**: 1085.

Lian, X., C. Hsiao, G. Wilson, K. Zhu, L. B. Hazeltine, S. M. Azarin, K. K. Raval, J. Zhang, T. J. Kamp and S. P. Palecek (2012). Robust cardiomyocyte differentiation from human pluripotent stem cells via temporal modulation of canonical Wnt signaling. *Proc Natl Acad Sci U S A* **109**(27): E1848-1857.

Lian, X., J. Zhang, S. M. Azarin, K. Zhu, L. B. Hazeltine, X. Bao, C. Hsiao, T. J. Kamp and S. P. Palecek (2013a). Directed cardiomyocyte differentiation from human pluripotent stem cells by modulating Wnt/beta-catenin signaling under fully defined conditions. *Nat Protoc* **8**(1): 162-175.

Lian, X., J. Zhang, K. Zhu, T. J. Kamp and S. P. Palecek (2013b). Insulin inhibits cardiac mesoderm, not mesendoderm, formation during cardiac differentiation of human pluripotent stem cells and modulation of canonical Wnt signaling can rescue this inhibition. *Stem Cells* **31**(3): 447-457.

Lim, S. Y., P. Sivakumaran, D. E. Crombie, G. J. Dusting, A. Pebay and R. J. Dilley (2013). Trichostatin A enhances differentiation of human induced pluripotent stem cells to cardiogenic cells for cardiac tissue engineering. *Stem Cells Transl Med* **2**(9): 715-725.

Lin, H., Q. Du, Q. Li, O. Wang, Z. Wang, N. Sahu, C. Elowsky, K. Liu, C. Zhang, S. Chung, B. Duan and Y. Lei (2018). A Scalable and Efficient Bioprocess for Manufacturing Human Pluripotent Stem Cell-Derived Endothelial Cells. *Stem Cell Reports* **11**(2): 454-469.

Lipsitz, Y. Y., N. E. Timmins and P. W. Zandstra (2016). Quality cell therapy manufacturing by design. *Nat Biotechnol* **34**(4): 393-400.

Lipsitz, Y. Y., P. D. Tonge and P. W. Zandstra (2018a). Chemically controlled aggregation of pluripotent stem cells. *Biotechnol Bioeng* **115**(8): 2061-2066.

Lipsitz, Y. Y., C. Woodford, T. Yin, J. H. Hanna and P. W. Zandstra (2018b). Modulating cell state to enhance suspension expansion of human pluripotent stem cells. *Proc Natl Acad Sci U S A* **115**(25): 6369-6374.

Liu, J., J. H. Kennedy, M. Ronk, L. Marghitoiu, H. Lee and Y. Nashed-Samuel (2014). Ambient analysis of leachable compounds from single-use bioreactors with desorption electrospray ionization time-of-flight mass spectrometry. *Rapid Commun Mass Spectrom* **28**(21): 2285-2291.

Liu, L., W. Michowski, A. Kolodziejczyk and P. Sicinski (2019). The cell cycle in stem cell proliferation, pluripotency and differentiation. *Nat Cell Biol* **21**(9): 1060-1067.

Liu, W., Z. Ren, K. Lu, C. Song, E. C. W. Cheung, Z. Zhou and G. Chen (2018a). The Suppression of Medium Acidosis Improves the Maintenance and Differentiation of Human Pluripotent Stem Cells at High Density in Defined Cell Culture Medium. *Int J Biol Sci* **14**(5): 485-496.

Liu, X., W. Yang, Z. Guan, W. Yu, B. Fan, N. Xu and D. J. Liao (2018b). There are only four basic modes of cell death, although there are many ad-hoc variants adapted to different situations. *Cell Biosci* **8**: 6.

Liu, Y., Z.-J. Wang, J.-y. Xia, C. Haringa, Y.-p. Liu, J. Chu, Y.-P. Zhuang and S.-L. Zhang (2016). Application of Euler-Lagrange CFD for quantitative evaluating the effect of shear force on Carthamus tinctorius L. cell in a stirred tank bioreactor. *Biochemical engineering journal* **114**: 209-217.

Lock, L. T. and E. S. Tzanakakis (2009). Expansion and differentiation of human embryonic stem cells to endoderm progeny in a microcarrier stirred-suspension culture. *Tissue Eng Part A* **15**(8): 2051-2063.

Lou, Y. R., L. Kanninen, T. Kuisma, J. Niklander, L. A. Noon, D. Burks, A. Urtti and M. Yliperttula (2014). The use of nanofibrillar cellulose hydrogel as a flexible three-dimensional model to culture human pluripotent stem cells. *Stem Cells Dev* **23**(4): 380-392.

Ludwig, T. and J. A. Thomson (2007). Defined, feeder-independent medium for human embryonic stem cell culture. *Curr Protoc Stem Cell Biol* **Chapter 1**: Unit 1C 2.

Ludwig, T. E., V. Bergendahl, M. E. Levenstein, J. Yu, M. D. Probasco and J. A. Thomson (2006a). Feeder-independent culture of human embryonic stem cells. *Nat Methods* **3**(8): 637-646.

Ludwig, T. E., M. E. Levenstein, J. M. Jones, W. T. Berggren, E. R. Mitchen, J. L. Frane, L. J. Crandall, C. A. Daigh, K. R. Conard, M. S. Piekarczyk, R. A. Llanas and J. A. Thomson (2006b). Derivation of human embryonic stem cells in defined conditions. *Nat Biotechnol* **24**(2): 185-187.

MacDonald, J. M., S. P. Wolfe, I. Roy-Chowdhury, H. Kubota and L. M. Reid (2001). Effect of flow configuration and membrane characteristics on membrane fouling in a novel multicoaxial hollow-fiber bioartificial liver. *Ann N Y Acad Sci* **944**: 334-343.

Marghitoiu, L., J. Liu, H. Lee, L. Perez, K. Fujimori, M. Ronk, M. R. Hammond, H. Nunn, A. Lower, G. Rogers and Y. Nashed-Samuel (2015). Extractables analysis of single-use flexible plastic biocontainers. *PDA J Pharm Sci Technol* **69**(1): 49-58.

Marsh, D. T. J., G. J. Lye, M. Micheletti, A. O. O. Odeleye, A. Ducci and M. D. Osborne (2017). Fluid dynamic characterization of a laboratory scale rocked bag bioreactor. *AIChE Journal* **63**(9): 4177-4187.

Martin, G. R. (1981). Isolation of a pluripotent cell line from early mouse embryos cultured in medium conditioned by teratocarcinoma stem cells. *Proc Natl Acad Sci U S A* **78**(12): 7634-7638.

Matsuura, K., M. Wada, T. Shimizu, Y. Haraguchi, F. Sato, K. Sugiyama, K. Konishi, Y. Shiba, H. Ichikawa, A. Tachibana, U. Ikeda, M. Yamato, N. Hagiwara and T. Okano (2012). Creation of human cardiac cell sheets using pluripotent stem cells. *Biochem Biophys Res Commun* **425**(2): 321-327.

Matthews, K. R. and D. Morali (2020). National human embryo and embryoid research policies: a survey of 22 top research-intensive countries. *Regen Med* **15**(7): 1905-1917.

McCauley, H. A. and J. M. Wells (2017). Pluripotent stem cell-derived organoids: using principles of developmental biology to grow human tissues in a dish. *Development* **144**(6): 958-962.

McDevitt, T. C., M. A. Laflamme and C. E. Murry (2005). Proliferation of cardiomyocytes derived from human embryonic stem cells is mediated via the IGF/PI 3-kinase/Akt signaling pathway. *J Mol Cell Cardiol* **39**(6): 865-873.

Mehta, A., V. Verma, M. Nandihalli, C. J. Ramachandra, G. L. Sequiera, Y. Sudibyo, Y. Chung, W. Sun and W. Shim (2014). A systemic evaluation of cardiac differentiation from mRNA reprogrammed human induced pluripotent stem cells. *PLoS One* **9**(7): e103485.

Meissner, P., B. Schroder, C. Herfurth and M. Biselli (1999). Development of a fixed bed bioreactor for the expansion of human hematopoietic progenitor cells. *Cytotechnology* **30**(1-3): 227-234.

Mennan, C., J. Garcia, S. Roberts, C. Hulme and K. Wright (2019). A comprehensive characterisation of large-scale expanded human bone marrow and umbilical cord mesenchymal stem cells. *Stem Cell Res Ther* **10**(1): 99.

Menon, S., S. Shailendra, A. Renda, M. Longaker and N. Quarto (2016). An Overview of Direct Somatic Reprogramming: The Ins and Outs of iPSCs. *Int J Mol Sci* **17**(1): 141.

Merin, O., M. Ilan, A. Oren, D. Fink, M. Deeb, D. Bitran and S. Silberman (2009). Permanent pacemaker implantation following cardiac surgery: indications and long-term follow-up. *Pacing Clin Electrophysiol* **32**(1): 7-12.

Miki, K., K. Endo, S. Takahashi, S. Funakoshi, I. Takei, S. Katayama, T. Toyoda, M. Kotaka, T. Takaki, M. Umeda, C. Okubo, M. Nishikawa, A. Oishi, M. Narita, I. Miyashita, K. Asano, K. Hayashi, K. Osafune, S. Yamanaka, H. Saito and Y. Yoshida (2015). Efficient Detection and Purification of Cell Populations Using Synthetic MicroRNA Switches. *Cell Stem Cell* **16**(6): 699-711.

Mima, T., H. Ueno, D. A. Fischman, L. T. Williams and T. Mikawa (1995). Fibroblast growth factor receptor is required for in vivo cardiac myocyte proliferation at early embryonic stages of heart development. *Proc Natl Acad Sci U S A* **92**(2): 467-471.

Mirnezami, R., J. Nicholson and A. Darzi (2012). Preparing for precision medicine. *N Engl J Med* **366**(6): 489-491.

Mizukami, A., T. D. P. Chilima, M. D. Orellana, M. A. Neto, D. T. Covas, S. S. Farid and K. Swiech (2018a). Technologies for large-scale umbilical cord-derived MSC expansion: Experimental performance and cost of goods analysis. *Biochemical Engineering Journal* **135**: 36-48.

Mizukami, A., M. S. de Abreu Neto, F. Moreira, A. Fernandes-Platzgummer, Y. F. Huang, W. Milligan, J. M. S. Cabral, C. L. da Silva, D. T. Covas and K. Swiech (2018b). A Fully-Closed and

Automated Hollow Fiber Bioreactor for Clinical-Grade Manufacturing of Human Mesenchymal Stem/Stromal Cells. *Stem Cell Rev Rep* **14**(1): 141-143.

Mizukami, A., M. D. Orellana, S. R. Caruso, K. de Lima Prata, D. T. Covas and K. Swiech (2013). Efficient expansion of mesenchymal stromal cells in a disposable fixed bed culture system. *Biotechnol Prog* **29**(2): 568-572.

Mohammadi Amirabad, L., M. Massumi, M. Shamsara, I. Shabani, A. Amari, M. Mossahebi Mohammadi, S. Hosseinzadeh, S. Vakilian, S. K. Steinbach, M. R. Khorramizadeh, M. Soleimani and J. Barzin (2017). Enhanced Cardiac Differentiation of Human Cardiovascular Disease Patient-Specific Induced Pluripotent Stem Cells by Applying Unidirectional Electrical Pulses Using Aligned Electroactive Nanofibrous Scaffolds. *ACS Appl Mater Interfaces* **9**(8): 6849-6864.

Mohr, J. C., J. Zhang, S. M. Azarin, A. G. Soerens, J. J. de Pablo, J. A. Thomson, G. E. Lyons, S. P. Palecek and T. J. Kamp (2010). The microwell control of embryoid body size in order to regulate cardiac differentiation of human embryonic stem cells. *Biomaterials* **31**(7): 1885-1893.

Mollova, M., K. Bersell, S. Walsh, J. Savla, L. T. Das, S. Y. Park, L. E. Silberstein, C. G. Dos Remedios, D. Graham, S. Colan and B. Kuhn (2013). Cardiomyocyte proliferation contributes to heart growth in young humans. *Proc Natl Acad Sci U S A* **110**(4): 1446-1451.

Mummery, C., D. Ward-van Oostwaard, P. Doevendans, R. Spijker, S. van den Brink, R. Hassink, M. van der Heyden, T. Opthof, M. Pera, A. B. de la Riviere, R. Passier and L. Tertoolen (2003). Differentiation of human embryonic stem cells to cardiomyocytes: role of coculture with visceral endoderm-like cells. *Circulation* **107**(21): 2733-2740.

Nakashima, Y. and T. Omasa (2016). What Kind of Signaling Maintains Pluripotency and Viability in Human-Induced Pluripotent Stem Cells Cultured on Laminin-511 with Serum-Free Medium? *Biores Open Access* **5**(1): 84-93.

Nemade, H., A. Acharya, U. Chaudhari, E. Nembo, F. Nguemo, N. Riet, H. Abken, J. Hescheler, S. Papadopoulos and A. Sachinidis (2020). Cyclooxygenases Inhibitors Efficiently Induce Cardiomyogenesis in Human Pluripotent Stem Cells. *Cells* **9**(3): 554.

Neumann, A., A. Lavrentieva, A. Heilkenbrinker, M. Loenne and C. Kasper (2014). Characterization and Application of a Disposable Rotating Bed Bioreactor for Mesenchymal Stem Cell Expansion. *Bioengineering (Basel)* **1**(4): 231-245.

Neuzi, P., S. Giselbrecht, K. Lange, T. J. Huang and A. Manz (2012). Revisiting lab-on-a-chip technology for drug discovery. *Nat Rev Drug Discov* **11**(8): 620-632.

Newman, K. D. and M. W. McBurney (2004). Poly(D,L lactic-co-glycolic acid) microspheres as biodegradable microcarriers for pluripotent stem cells. *Biomaterials* **25**(26): 5763-5771.

Ng, K. M., Y. K. Lee, W. H. Lai, Y. C. Chan, M. L. Fung, H. F. Tse and C. W. Siu (2011). Exogenous expression of human apoA-I enhances cardiac differentiation of pluripotent stem cells. *PLoS One* **6**(5): e19787.

Nguyen, L., S. Bang and I. Noh (2019). Tissue Regeneration of Human Mesenchymal Stem Cells on Porous Gelatin Micro-Carriers by Long-Term Dynamic In Vitro Culture. *Tissue Eng Regen Med* **16**(1): 19-28.

Nie, Y., V. Bergendahl, D. J. Hei, J. M. Jones and S. P. Palecek (2009). Scalable culture and cryopreservation of human embryonic stem cells on microcarriers. *Biotechnol Prog* **25**(1): 20-31.

Niebruegge, S., C. L. Bauwens, R. Peerani, N. Thavandiran, S. Masse, E. Sevaptisidis, K. Nanthakumar, K. Woodhouse, M. Husain, E. Kumacheva and P. W. Zandstra (2009). Generation of human embryonic stem cell-derived mesoderm and cardiac cells using size-specified aggregates in an oxygen-controlled bioreactor. *Biotechnol Bioeng* **102**(2): 493-507.

Nienow, A. W. (2009). Scale-up, stirred tank reactors. *Encyclopedia of Industrial Biotechnology: Bioprocess, Bioseparation, and Cell Technology*: 1-38.

Nishimura, K., M. Sano, M. Ohtaka, B. Furuta, Y. Umemura, Y. Nakajima, Y. Ikehara, T. Kobayashi, H. Segawa, S. Takayasu, H. Sato, K. Motomura, E. Uchida, T. Kanayasu-Toyoda, M. Asashima, H. Nakauchi, T. Yamaguchi and M. Nakanishi (2011). Development of defective and persistent Sendai virus vector: a unique gene delivery/expression system ideal for cell reprogramming. *J Biol Chem* **286**(6): 4760-4771.

Nishino, K., M. Toyoda, M. Yamazaki-Inoue, Y. Fukawatase, E. Chikazawa, H. Sakaguchi, H. Akutsu and A. Umezawa (2011). DNA methylation dynamics in human induced pluripotent stem cells over time. *PLoS Genet* **7**(5): e1002085.

Nogueira, D. E. S., J. M. S. Cabral and C. A. V. Rodrigues (2021a). Single-Use Bioreactors for Human Pluripotent and Adult Stem Cells: Towards Regenerative Medicine Applications. *Bioengineering (Basel)* **8**(5): 68.

Nogueira, D. E. S., C. A. V. Rodrigues and J. M. S. Cabral (2021b). Emerging strategies for scalable human induced pluripotent stem cell expansion and differentiation. *Methods in iPSC Technology*. A. Birbrair, Elsevier**:** 163-185.

Nold, P., C. Brendel, A. Neubauer, G. Bein and H. Hackstein (2013). Good manufacturing practice-compliant animal-free expansion of human bone marrow derived mesenchymal stroma cells in a closed hollow-fiber-based bioreactor. *Biochem Biophys Res Commun* **430**(1): 325-330.

Nose, N., R. A. Werner, Y. Ueda, K. Gunther, C. Lapa, M. S. Javadi, K. Fukushima, F. Edenhofer and T. Higuchi (2018). Metabolic substrate shift in human induced pluripotent stem cells during cardiac differentiation: Functional assessment using in vitro radionuclide uptake assay. *Int J Cardiol* **269**: 229-234.

Nunes, S. S., J. W. Miklas, J. Liu, R. Aschar-Sobbi, Y. Xiao, B. Zhang, J. Jiang, S. Masse, M. Gagliardi, A. Hsieh, N. Thavandiran, M. A. Laflamme, K. Nanthakumar, G. J. Gross, P. H. Backx, G. Keller and M. Radisic (2013). Biowire: a platform for maturation of human pluripotent stem cell-derived cardiomyocytes. *Nat Methods* **10**(8): 781-787.

Ohashi, F., S. Miyagawa, S. Yasuda, T. Miura, T. Kuroda, M. Itoh, H. Kawaji, E. Ito, S. Yoshida, A. Saito, T. Sameshima, J. Kawai, Y. Sawa and Y. Sato (2019). CXCL4/PF4 is a predictive biomarker of cardiac differentiation potential of human induced pluripotent stem cells. *Sci Rep* **9**(1): 4638.

Olmer, R., L. Engels, A. Usman, S. Menke, M. N. H. Malik, F. Pessler, G. Gohring, D. Bornhorst, S. Bolten, S. Abdelilah-Seyfried, T. Scheper, H. Kempf, R. Zweigerdt and U. Martin (2018). Differentiation of Human Pluripotent Stem Cells into Functional Endothelial Cells in Scalable Suspension Culture. *Stem Cell Reports* **10**(5): 1657-1672.

Onwordi, E. N., A. Gamal and A. Zaman (2018). Anticoagulant Therapy for Acute Coronary Syndromes. *Interv Cardiol* **13**(2): 87-92.

Orita, K., K. Sawada, R. Koyama and Y. Ikegaya (2019). Deep learning-based quality control of cultured human-induced pluripotent stem cell-derived cardiomyocytes. *J Pharmacol Sci* **140**(4): 313-316.

Ornitz, D. M. and N. Itoh (2015). The Fibroblast Growth Factor signaling pathway. *Wiley Interdiscip Rev Dev Biol* **4**(3): 215-266.

Ovando-Roche, P., E. L. West, M. J. Branch, R. D. Sampson, M. Fernando, P. Munro, A. Georgiadis, M. Rizzi, M. Kloc, A. Naeem, J. Ribeiro, A. J. Smith, A. Gonzalez-Cordero and R. R. Ali (2018). Use of bioreactors for culturing human retinal organoids improves photoreceptor yields. *Stem Cell Res Ther* **9**(1): 156.

Özbek, B. and S. Gayik (2001). The studies on the oxygen mass transfer coefficient in a bioreactor. *Process Biochemistry* **36**(8-9): 729-741.

Paccola Mesquita, F. C., C. Hochman-Mendez, J. Morrissey, L. C. Sampaio and D. A. Taylor (2019). Laminin as a Potent Substrate for Large-Scale Expansion of Human Induced Pluripotent Stem Cells in a Closed Cell Expansion System. *Stem Cells Int* **2019**: 9704945.

Paige, S. L., T. Osugi, O. K. Afanasiev, L. Pabon, H. Reinecke and C. E. Murry (2010). Endogenous Wnt/beta-catenin signaling is required for cardiac differentiation in human embryonic stem cells. *PLoS One* **5**(6): e11134.

Pankhania, M., T. Stephenson and M. J. Semmens (1994). Hollow fibre bioreactor for wastewater treatment using bubbleless membrane aeration. *Water research* **28**(10): 2233-2236.

Patel, S., A. Alam, R. Pant and S. Chattopadhyay (2019). Wnt Signaling and Its Significance Within the Tumor Microenvironment: Novel Therapeutic Insights. *Front Immunol* **10**: 2872.

Pei, F., J. Jiang, S. Bai, H. Cao, L. Tian, Y. Zhao, C. Yang, H. Dong and Y. Ma (2017). Chemical-defined and albumin-free generation of human atrial and ventricular myocytes from human pluripotent stem cells. *Stem Cell Res* **19**: 94-103.

Pekkanen-Mattila, M., M. Ojala, E. Kerkela, K. Rajala, H. Skottman and K. Aalto-Setala (2012). The effect of human and mouse fibroblast feeder cells on cardiac differentiation of human pluripotent stem cells. *Stem Cells Int* **2012**: 875059.

Pesl, M., I. Acimovic, J. Pribyl, R. Hezova, A. Vilotic, J. Fauconnier, J. Vrbsky, P. Kruzliak, P. Skladal, T. Kara, V. Rotrekl, A. Lacampagne, P. Dvorak and A. C. Meli (2014). Forced aggregation and defined factors allow highly uniform-sized embryoid bodies and functional cardiomyocytes from human embryonic and induced pluripotent stem cells. *Heart Vessels* **29**(6): 834-846.

Pietrzykowski, M., W. Flanagan, V. Pizzi, A. Brown, A. Sinclair and M. Monge (2013). An environmental life cycle assessment comparison of single-use and conventional process technology for the production of monoclonal antibodies. *Journal of Cleaner Production* **41**: 150-162.

Piquereau, J., M. Novotova, D. Fortin, A. Garnier, R. Ventura-Clapier, V. Veksler and F. Joubert (2010). Postnatal development of mouse heart: formation of energetic microdomains. *The Journal of Physiology* **588**(13): 2443-2454.

Piquereau, J. and R. Ventura-Clapier (2018). Maturation of Cardiac Energy Metabolism During Perinatal Development. *Front Physiol* **9**: 959.

Pohjoismaki, J. L. and S. Goffart (2017). The role of mitochondria in cardiac development and protection. *Free Radic Biol Med* **106**: 345-354.

Pourakbar, M., G. Moussavi and K. Yaghmaeian (2018). Enhanced biodegradation of phenol in a novel cyclic activated sludge integrated with a rotating bed bioreactor in anoxic and peroxidase-mediated conditions. *RSC Advances* **8**(12): 6293-6305.

Power, C. and J. E. Rasko (2008). Whither prometheus' liver? Greek myth and the science of regeneration. *Ann Intern Med* **149**(6): 421-426.

Powers, A. D., B. A. Piras, R. K. Clark, T. D. Lockey and M. M. Meagher (2016). Development and Optimization of AAV hFIX Particles by Transient Transfection in an iCELLis((R)) Fixed-Bed Bioreactor. *Hum Gene Ther Methods* **27**(3): 112-121.

Przepiorski, A., V. Sander, T. Tran, J. A. Hollywood, B. Sorrenson, J. H. Shih, E. J. Wolvetang, A. P. McMahon, T. M. Holm and A. J. Davidson (2018). A Simple Bioreactor-Based Method to Generate Kidney Organoids from Pluripotent Stem Cells. *Stem Cell Reports* **11**(2): 470-484.

Puig-Sanvicens, V. A., C. E. Semino and N. I. Zur Nieden (2015). Cardiac differentiation potential of human induced pluripotent stem cells in a 3D self-assembling peptide scaffold. *Differentiation* **90**(4-5): 101-110.

Qian, X., H. N. Nguyen, M. M. Song, C. Hadiono, S. C. Ogden, C. Hammack, B. Yao, G. R. Hamersky, F. Jacob, C. Zhong, K. J. Yoon, W. Jeang, L. Lin, Y. Li, J. Thakor, D. A. Berg, C. Zhang, E. Kang, M. Chickering, D. Nauen, C. Y. Ho, Z. Wen, K. M. Christian, P. Y. Shi, B. J. Maher, H. Wu, P. Jin, H. Tang, H. Song and G. L. Ming (2016). Brain-Region-Specific Organoids Using Mini-bioreactors for Modeling ZIKV Exposure. *Cell* **165**(5): 1238-1254.

Qiu, X. X., Y. Liu, Y. F. Zhang, Y. N. Guan, Q. Q. Jia, C. Wang, H. Liang, Y. Q. Li, H. T. Yang, Y. W. Qin, S. Huang, X. X. Zhao and Q. Jing (2017). Rapamycin and CHIR99021 Coordinate Robust Cardiomyocyte Differentiation From Human Pluripotent Stem Cells Via Reducing p53-Dependent Apoptosis. *J Am Heart Assoc* **6**(10): e005295.

Rafiq, Q. A., M. P. Hanga, T. R. J. Heathman, K. Coopman, A. W. Nienow, D. J. Williams and C. J. Hewitt (2017). Process development of human multipotent stromal cell microcarrier culture using an automated high-throughput microbioreactor. *Biotechnol Bioeng* **114**(10): 2253-2266.

Rajala, K., H. Vaajasaari, R. Suuronen, O. Hovatta and H. Skottman (2011). Effects of the physiochemical culture environment on the stemness and pluripotency of human embryonic stem cells. *Stem Cell Studies* **1**(1): e3-e3.

Rajendran, R., R. Lingala, S. K. Vuppu, B. O. Bandi, E. Manickam, S. R. Macherla, S. Dubois, N. Havelange and K. Maithal (2014). Assessment of packed bed bioreactor systems in the production of viral vaccines. *AMB Express* **4**: 25.

Rasekhi, M., M. Soleimani, B. Bakhshandeh and M. Sadeghizadeh (2017). A novel protocol to provide a suitable cardiac model from induced pluripotent stem cells. *Biologicals* **50**: 42-48.

Ratcliffe, E., K. E. Glen, V. L. Workman, A. J. Stacey and R. J. Thomas (2012). A novel automated bioreactor for scalable process optimisation of haematopoietic stem cell culture. *J Biotechnol* **161**(3): 387-390.

Raven, N., S. Rasche, C. Kuehn, T. Anderlei, W. Klockner, F. Schuster, M. Henquet, D. Bosch, J. Buchs, R. Fischer and S. Schillberg (2015). Scaled-up manufacturing of recombinant antibodies produced by plant cells in a 200-L orbitally-shaken disposable bioreactor. *Biotechnol Bioeng* **112**(2): 308-321.

Reichardt, A., B. Polchow, M. Shakibaei, W. Henrich, R. Hetzer and C. Lueders (2013). Large scale expansion of human umbilical cord cells in a rotating bed system bioreactor for cardiovascular tissue engineering applications. *Open Biomed Eng J* **7**: 50-61.

Ren, Y., M. Y. Lee, S. Schliffke, J. Paavola, P. J. Amos, X. Ge, M. Ye, S. Zhu, G. Senyei, L. Lum, B. E. Ehrlich and Y. Qyang (2011). Small molecule Wnt inhibitors enhance the efficiency of BMP-4-directed cardiac differentiation of human pluripotent stem cells. *J Mol Cell Cardiol* **51**(3): 280-287.

Richards, D. J., Y. Tan, R. Coyle, Y. Li, R. Xu, N. Yeung, A. Parker, D. R. Menick, B. Tian and Y. Mei (2016). Nanowires and Electrical Stimulation Synergistically Improve Functions of hiPSC Cardiac Spheroids. *Nano Lett* **16**(7): 4670-4678.

Richardson, W. J., S. A. Clarke, T. A. Quinn and J. W. Holmes (2015). Physiological Implications of Myocardial Scar Structure. *Compr Physiol* **5**(4): 1877-1909.

Rienks, M., A. P. Papageorgiou, N. G. Frangogiannis and S. Heymans (2014). Myocardial extracellular matrix: an ever-changing and diverse entity. *Circ Res* **114**(5): 872-888.

Ritner, C., S. S. Wong, F. W. King, S. S. Mihardja, W. Liszewski, D. J. Erle, R. J. Lee and H. S. Bernstein (2011). An engineered cardiac reporter cell line identifies human embryonic stem cell-derived myocardial precursors. *PLoS One* **6**(1): e16004.

Roberts, I., S. Baila, R. B. Rice, M. E. Janssens, K. Nguyen, N. Moens, L. Ruban, D. Hernandez, P. Coffey and C. Mason (2012). Scale-up of human embryonic stem cell culture using a hollow fibre bioreactor. *Biotechnol Lett* **34**(12): 2307-2315.

Rodrigues, A. L., C. A. V. Rodrigues, A. R. Gomes, S. F. Vieira, S. M. Badenes, M. M. Diogo and J. M. S. Cabral (2019). Dissolvable Microcarriers Allow Scalable Expansion And Harvesting Of Human Induced Pluripotent Stem Cells Under Xeno-Free Conditions. *Biotechnol J* **14**(4): e1800461.

Rodrigues, C. A. V., T. P. Silva, D. E. S. Nogueira, T. G. Fernandes, Y. Hashimura, R. Wesselschmidt, M. M. Diogo, B. Lee and J. M. S. Cabral (2018). Scalable culture of human induced pluripotent cells on microcarriers under xeno-free conditions using single-use vertical-wheel (TM) bioreactors. *Journal of Chemical Technology and Biotechnology* **93**(12): 3597-3606.

Rodrigues, G. M. C., T. Gaj, M. M. Adil, J. Wahba, A. T. Rao, F. K. Lorbeer, R. U. Kulkarni, M. M. Diogo, J. M. S. Cabral, E. W. Miller, D. Hockemeyer and D. V. Schaffer (2017). Defined and Scalable Differentiation of Human Oligodendrocyte Precursors from Pluripotent Stem Cells in a 3D Culture System. *Stem Cell Reports* **8**(6): 1770-1783.

Rogge, P., D. Müller and S. R. Schmidt (2015). The single-use or stainless steel decision process. *BioProcess International* **13**(11).

Rohani, L., B. S. Borys, G. Razian, P. Naghsh, S. Liu, A. A. Johnson, P. Machiraju, H. Holland, I. A. Lewis, R. A. Groves, D. Toms, P. M. K. Gordon, J. W. Li, T. So, T. Dang, M. S. Kallos and D. E. Rancourt (2020). Stirred suspension bioreactors maintain naive pluripotency of human pluripotent stem cells. *Commun Biol* **3**(1): 492.

Ronaldson-Bouchard, K., S. P. Ma, K. Yeager, T. Chen, L. Song, D. Sirabella, K. Morikawa, D. Teles, M. Yazawa and G. Vunjak-Novakovic (2018). Advanced maturation of human cardiac tissue grown from pluripotent stem cells. *Nature* **556**(7700): 239-243.

Rotondi, M., N. Grace, J. Betts, N. Bargh, E. Costariol, B. Zoro, C. J. Hewitt, A. W. Nienow and Q. A. Rafiq (2021). Design and development of a new ambr250(R) bioreactor vessel for improved cell and gene therapy applications. *Biotechnol Lett* **43**(5): 1103-1116.

Ruijtenberg, S. and S. van den Heuvel (2016). Coordinating cell proliferation and differentiation: Antagonism between cell cycle regulators and cell type-specific gene expression. *Cell Cycle* **15**(2): 196-212.

Russell, A. L., R. C. Lefavor and A. C. Zubair (2018). Characterization and cost-benefit analysis of automated bioreactor-expanded mesenchymal stem cells for clinical applications. *Transfusion* **58**(10): 2374-2382.

Sakai, S., H. Mishima, T. Ishii, H. Akaogi, T. Yoshioka, Y. Ohyabu, F. Chang, N. Ochiai and T. Uemura (2009). Rotating three-dimensional dynamic culture of adult human bone marrow-derived cells for tissue engineering of hyaline cartilage. *J Orthop Res* **27**(4): 517-521.

Salum, T. F. C., P. Villeneuve, B. Barea, C. I. Yamamoto, L. C. Côcco, D. A. Mitchell and N. Krieger (2010). Synthesis of biodiesel in column fixed-bed bioreactor using the fermented solid produced by Burkholderia cepacia LTEB11. *Process Biochemistry* **45**(8): 1348-1354.

Scheller, B., B. Hennen, B. Hammer, J. Walle, C. Hofer, V. Hilpert, H. Winter, G. Nickenig and M. Böhm (2003). Beneficial effects of immediate stenting after thrombolysis in acute myocardial infarction. *Journal of the American College of Cardiology* **42**(4): 634-641.

Schirmaier, C., V. Jossen, S. C. Kaiser, F. Jüngerkes, S. Brill, A. Safavi-Nab, A. Siehoff, C. van den Bos, D. Eibl and R. Eibl (2014). Scale-up of adipose tissue-derived mesenchymal stem cell production in stirred single-use bioreactors under low-serum conditions. *Engineering in Life Sciences* **14**(3): 292-303.

Schmideder, A. and D. Weuster-Botz (2017). High-performance recombinant protein production with Escherichia coli in continuously operated cascades of stirred-tank reactors. *J Ind Microbiol Biotechnol* **44**(7): 1021-1029.

Schneider, M. D. (2004). Regenerative medicine: Prometheus unbound. *Nature* **432**(7016): 451-453.

Schwedhelm, I., D. Zdzieblo, A. Appelt-Menzel, C. Berger, T. Schmitz, B. Schuldt, A. Franke, F. J. Muller, O. Pless, T. Schwarz, P. Wiedemann, H. Walles and J. Hansmann (2019). Automated real-time monitoring of human pluripotent stem cell aggregation in stirred tank reactors. *Sci Rep* **9**(1): 12297.

Sender, R., S. Fuchs and R. Milo (2016). Revised Estimates for the Number of Human and Bacteria Cells in the Body. *PLoS Biol* **14**(8): e1002533.

Serra, M., C. Brito, E. M. Costa, M. F. Sousa and P. M. Alves (2009). Integrating human stem cell expansion and neuronal differentiation in bioreactors. *BMC Biotechnol* **9**: 82.

Serra, M., C. Brito, M. F. Sousa, J. Jensen, R. Tostoes, J. Clemente, R. Strehl, J. Hyllner, M. J. Carrondo and P. M. Alves (2010). Improving expansion of pluripotent human embryonic stem cells in perfused bioreactors through oxygen control. *J Biotechnol* **148**(4): 208-215.

Serra, M., C. Correia, R. Malpique, C. Brito, J. Jensen, P. Bjorquist, M. J. Carrondo and P. M. Alves (2011). Microencapsulation technology: a powerful tool for integrating expansion and cryopreservation of human embryonic stem cells. *PLoS One* **6**(8): e23212.

Si-Tayeb, K., F. K. Noto, A. Sepac, F. Sedlic, Z. J. Bosnjak, J. W. Lough and S. A. Duncan (2010). Generation of human induced pluripotent stem cells by simple transient transfection of plasmid DNA encoding reprogramming factors. *BMC Dev Biol* **10**: 81.

Silva, A. C., C. Pereira, A. Fonseca, O. P. Pinto-do and D. S. Nascimento (2020a). Bearing My Heart: The Role of Extracellular Matrix on Cardiac Development, Homeostasis, and Injury Response. *Front Cell Dev Biol* **8**: 621644.

Silva, T. P., E. P. Bekman, T. G. Fernandes, S. H. Vaz, C. A. V. Rodrigues, M. M. Diogo, J. M. S. Cabral and M. Carmo-Fonseca (2020b). Maturation of Human Pluripotent Stem Cell-Derived Cerebellar Neurons in the Absence of Co-culture. *Front Bioeng Biotechnol* **8**: 70.

Silva, T. P., R. Sousa-Luis, T. G. Fernandes, E. P. Bekman, C. A. V. Rodrigues, S. H. Vaz, L. M. Moreira, Y. Hashimura, S. Jung, B. Lee, M. Carmo-Fonseca and J. M. S. Cabral (2021). Transcriptome profiling of human pluripotent stem cell-derived cerebellar organoids reveals faster commitment under dynamic conditions. *Biotechnol Bioeng* **118**(7): 2781-2803.

Simonsen, J. L., C. Rosada, N. Serakinci, J. Justesen, K. Stenderup, S. I. Rattan, T. G. Jensen and M. Kassem (2002). Telomerase expression extends the proliferative life-span and maintains the osteogenic potential of human bone marrow stromal cells. *Nat Biotechnol* **20**(6): 592-596.

Singh, H., P. Mok, T. Balakrishnan, S. N. Rahmat and R. Zweigerdt (2010). Up-scaling single cell-inoculated suspension culture of human embryonic stem cells. *Stem Cell Res* **4**(3): 165-179.

Singh, V. (1999). Disposable bioreactor for cell culture using wave-induced agitation. *Cytotechnology* **30**(1-3): 149-158.

Souidi, M., Y. Sleiman, I. Acimovic, J. Pribyl, A. Charrabi, V. Baecker, V. Scheuermann, M. Pesl, S. Jelinkova, P. Skladal, P. Dvorak, A. Lacampagne, V. Rotrekl and A. C. Meli (2021). Oxygen Is an Ambivalent Factor for the Differentiation of Human Pluripotent Stem Cells in Cardiac 2D Monolayer and 3D Cardiac Spheroids. *Int J Mol Sci* **22**(2): 662.

Sousa, M. F., M. M. Silva, D. Giroux, Y. Hashimura, R. Wesselschmidt, B. Lee, A. Roldao, M. J. Carrondo, P. M. Alves and M. Serra (2015). Production of oncolytic adenovirus and human mesenchymal stem cells in a single-use, Vertical-Wheel bioreactor system: Impact of bioreactor design on performance of microcarrier-based cell culture processes. *Biotechnol Prog* **31**(6): 1600-1612.

Spater, D., M. K. Abramczuk, K. Buac, L. Zangi, M. W. Stachel, J. Clarke, M. Sahara, A. Ludwig and K. R. Chien (2013). A HCN4+ cardiomyogenic progenitor derived from the first heart field and human pluripotent stem cells. *Nat Cell Biol* **15**(9): 1098-1106.

Stolberg, S. and K. E. McCloskey (2009). Can shear stress direct stem cell fate? *Biotechnol Prog* **25**(1): 10-19.

Storm, M. P., C. B. Orchard, H. K. Bone, J. B. Chaudhuri and M. J. Welham (2010). Three-dimensional culture systems for the expansion of pluripotent embryonic stem cells. *Biotechnol Bioeng* **107**(4): 683-695.

Suck, K., L. Behr, M. Fischer, H. Hoffmeister, M. van Griensven, F. Stahl, T. Scheper and C. Kasper (2007). Cultivation of MC3T3-E1 cells on a newly developed material (Sponceram) using a rotating bed system bioreactor. *J Biomed Mater Res A* **80**(2): 268-275.

Sun, C. and M. I. Kontaridis (2018). Physiology of Cardiac Development: From Genetics to Signaling to Therapeutic Strategies. *Curr Opin Physiol* **1**: 123-139.

Sutanto, H., A. Lyon, J. Lumens, U. Schotten, D. Dobrev and J. Heijman (2020). Cardiomyocyte calcium handling in health and disease: Insights from in vitro and in silico studies. *Prog Biophys Mol Biol* **157**: 54-75.

Takahashi, K., K. Tanabe, M. Ohnuki, M. Narita, T. Ichisaka, K. Tomoda and S. Yamanaka (2007). Induction of pluripotent stem cells from adult human fibroblasts by defined factors. *Cell* **131**(5): 861-872.

Takahashi, K. and S. Yamanaka (2006). Induction of pluripotent stem cells from mouse embryonic and adult fibroblast cultures by defined factors. *Cell* **126**(4): 663-676.

Takeda, M., Y. Kanki, H. Masumoto, S. Funakoshi, T. Hatani, H. Fukushima, A. Izumi-Taguchi, Y. Matsui, T. Shimamura, Y. Yoshida and J. K. Yamashita (2018). Identification of Cardiomyocyte-Fated Progenitors from Human-Induced Pluripotent Stem Cells Marked with CD82. *Cell Rep* **22**(2): 546-556.

Tan, Y., D. Richards, R. Xu, S. Stewart-Clark, S. K. Mani, T. K. Borg, D. R. Menick, B. Tian and Y. Mei (2015). Silicon nanowire-induced maturation of cardiomyocytes derived from human induced pluripotent stem cells. *Nano Lett* **15**(5): 2765-2772.

Tapia, F., T. Vogel, Y. Genzel, I. Behrendt, M. Hirschel, J. D. Gangemi and U. Reichl (2014). Production of high-titer human influenza A virus with adherent and suspension MDCK cells cultured in a single-use hollow fiber bioreactor. *Vaccine* **32**(8): 1003-1011.

Tesarova, L., P. Simara, S. Stejskal and I. Koutna (2016). The Aberrant DNA Methylation Profile of Human Induced Pluripotent Stem Cells Is Connected to the Reprogramming Process and Is Normalized During In Vitro Culture. *PLoS One* **11**(6): e0157974.

Thavandiran, N., N. Dubois, A. Mikryukov, S. Masse, B. Beca, C. A. Simmons, V. S. Deshpande, J. P. McGarry, C. S. Chen, K. Nanthakumar, G. M. Keller, M. Radisic and P. W. Zandstra (2013). Design and formulation of functional pluripotent stem cell-derived cardiac microtissues. *Proc Natl Acad Sci U S A* **110**(49): E4698-4707.

Thomson, J. A., J. Itskovitz-Eldor, S. S. Shapiro, M. A. Waknitz, J. J. Swiergiel, V. S. Marshall and J. M. Jones (1998). Embryonic stem cell lines derived from human blastocysts. *Science* **282**(5391): 1145-1147.

Till, J. E. and E. A. McCulloch (1961). A direct measurement of the radiation sensitivity of normal mouse bone marrow cells. *Radiat Res* **14**: 213-222.

Timmins, N. E., S. Athanasas, M. Gunther, P. Buntine and L. K. Nielsen (2011). Ultra-high-yield manufacture of red blood cells from hematopoietic stem cells. *Tissue Eng Part C Methods* **17**(11): 1131-1137.

Ting, S., A. Chen, S. Reuveny and S. Oh (2014). An intermittent rocking platform for integrated expansion and differentiation of human pluripotent stem cells to cardiomyocytes in suspended microcarrier cultures. *Stem Cell Res* **13**(2): 202-213.

Tirughana, R., M. Z. Metz, Z. Li, C. Hall, D. Hsu, J. Beltzer, A. J. Annala, D. Oganesyan, M. Gutova and K. S. Aboody (2018). GMP Production and Scale-Up of Adherent Neural Stem Cells with a Quantum Cell Expansion System. *Mol Ther Methods Clin Dev* **10**: 48-56.

Tohyama, S., J. Fujita, C. Fujita, M. Yamaguchi, S. Kanaami, R. Ohno, K. Sakamoto, M. Kodama, J. Kurokawa, H. Kanazawa, T. Seki, Y. Kishino, M. Okada, K. Nakajima, S. Tanosaki, S. Someya, A. Hirano, S. Kawaguchi, E. Kobayashi and K. Fukuda (2017). Efficient Large-Scale 2D Culture System for Human Induced Pluripotent Stem Cells and Differentiated Cardiomyocytes. *Stem Cell Reports* **9**(5): 1406-1414.

Tohyama, S., F. Hattori, M. Sano, T. Hishiki, Y. Nagahata, T. Matsuura, H. Hashimoto, T. Suzuki, H. Yamashita, Y. Satoh, T. Egashira, T. Seki, N. Muraoka, H. Yamakawa, Y. Ohgino, T. Tanaka, M. Yoichi, S. Yuasa, M. Murata, M. Suematsu and K. Fukuda (2013). Distinct metabolic flow enables large-scale purification of mouse and human pluripotent stem cell-derived cardiomyocytes. *Cell Stem Cell* **12**(1): 127-137.

Tsao, C. J., F. Taraballi, L. Pandolfi, A. J. Velasquez-Mao, R. Ruano, E. Tasciotti and J. G. Jacot (2018). Controlled Release of Small Molecules for Cardiac Differentiation of Pluripotent Stem Cells. *Tissue Eng Part A* **24**(23-24): 1798-1807.

Tsao, Y. D., T. J. Goodwin, D. A. Wolf and G. F. Spaulding (1992). Responses of gravity level variations on the NASA/JSC bioreactor system. *Physiologist* **35**(1 Suppl): S49-50.

Turner, N. and R. Grose (2010). Fibroblast growth factor signalling: from development to cancer. *Nat Rev Cancer* **10**(2): 116-129.

Uosaki, H., H. Fukushima, A. Takeuchi, S. Matsuoka, N. Nakatsuji, S. Yamanaka and J. K. Yamashita (2011). Efficient and scalable purification of cardiomyocytes from human embryonic and induced pluripotent stem cells by VCAM1 surface expression. *PLoS One* **6**(8): e23657.

Vaithilingam, J., P. Sanjuan-Alberte, S. Campora, G. A. Rance, L. Jiang, J. Thorpe, L. Burroughs, C. J. Tuck, C. Denning, R. D. Wildman, R. J. M. Hague, M. R. Alexander and F. J. Rawson (2019). Multifunctional Bioinstructive 3D Architectures to Modulate Cellular Behavior. *Advanced Functional Materials* **29**(38): 1902016.

Valkama, A. J., H. M. Leinonen, E. M. Lipponen, V. Turkki, J. Malinen, T. Heikura, S. Yla-Herttuala and H. P. Lesch (2018). Optimization of lentiviral vector production for scale-up in fixed-bed bioreactor. *Gene Ther* **25**(1): 39-46.

van Lier, F. L., E. J. van den End, C. D. de Gooijer, J. M. Vlak and J. Tramper (1990). Continuous production of baculovirus in a cascade of insect-cell reactors. *Appl Microbiol Biotechnol* **33**(1): 43-47.

Van Winkle, A. P., I. D. Gates and M. S. Kallos (2012). Mass transfer limitations in embryoid bodies during human embryonic stem cell differentiation. *Cells Tissues Organs* **196**(1): 34-47.

Vander Heiden, M. G., L. C. Cantley and C. B. Thompson (2009). Understanding the Warburg effect: the metabolic requirements of cell proliferation. *Science* **324**(5930): 1029-1033.

Vane, J. R. (1971). Inhibition of prostaglandin synthesis as a mechanism of action for aspirin-like drugs. *Nat New Biol* **231**(25): 232-235.

Varum, S., A. S. Rodrigues, M. B. Moura, O. Momcilovic, C. A. Easley IV, J. Ramalho-Santos, B. Van Houten and G. Schatten (2011). Energy metabolism in human pluripotent stem cells and their differentiated counterparts. *PLoS One* **6**(6): e20914.

Velez-Suberbie, M. L., R. D. Tarrant, A. S. Tait, D. I. Spencer and D. G. Bracewell (2013). Impact of aeration strategy on CHO cell performance during antibody production. *Biotechnol Prog* **29**(1): 116-126.

Virani, S. S., A. Alonso, H. J. Aparicio, E. J. Benjamin, M. S. Bittencourt, C. W. Callaway, A. P. Carson, A. M. Chamberlain, S. Cheng, F. N. Delling, M. S. V. Elkind, K. R. Evenson, J. F. Ferguson, D. K. Gupta, S. S. Khan, B. M. Kissela, K. L. Knutson, C. D. Lee, T. T. Lewis, J. Liu, M. S. Loop, P. L. Lutsey, J. Ma, J. Mackey, S. S. Martin, D. B. Matchar, M. E. Mussolino, S. D. Navaneethan, A. M. Perak, G. A. Roth, Z. Samad, G. M. Satou, E. B. Schroeder, S. H. Shah, C. M. Shay, A. Stokes, L. B. VanWagner, N. Y. Wang, C. W. Tsao, E. American Heart Association Council on, C. Prevention Statistics and S. Stroke Statistics (2021). Heart Disease and Stroke Statistics-2021 Update: A Report From the American Heart Association. *Circulation* **143**(8): e254-e743.

Vymetalova, L., T. Kucirkova, L. Knopfova, V. Pospisilova, T. Kasko, H. Lejdarova, E. Makaturova, P. Kuglik, V. Oralova, E. Matalova, P. Benes, Z. Koristek and S. Forostyak (2020). Large-Scale Automated Hollow-Fiber Bioreactor Expansion of Umbilical Cord-Derived Human Mesenchymal Stromal Cells for Neurological Disorders. *Neurochem Res* **45**(1): 204-214.

Wang, I. N., X. Wang, X. Ge, J. Anderson, M. Ho, E. Ashley, J. Liu, M. J. Butte, M. Yazawa, R. E. Dolmetsch, T. Quertermous and P. C. Yang (2012a). Apelin enhances directed cardiac differentiation of mouse and human embryonic stem cells. *PLoS One* **7**(6): e38328.

Wang, J., C. Cui, H. Nan, Y. Yu, Y. Xiao, E. Poon, G. Yang, X. Wang, C. Wang, L. Li, K. R. Boheler, X. Ma, X. Cheng, Z. Ni and M. Chen (2017). Graphene Sheet-Induced Global Maturation of Cardiomyocytes Derived from Human Induced Pluripotent Stem Cells. *ACS Appl Mater Interfaces* **9**(31): 25929-25940.

Wang, Y.-Z., Z.-P. Zhao, M.-F. Li, Y.-Z. Chen and W.-F. Liu (2016). Development of a hollow fiber membrane micro-reactor for biocatalytic production of formate from CO2. *Journal of Membrane Science* **514**: 44-52.

Wang, Y., B. K. Chou, S. Dowey, C. He, S. Gerecht and L. Cheng (2013). Scalable expansion of human induced pluripotent stem cells in the defined xeno-free E8 medium under adherent and suspension culture conditions. *Stem Cell Res* **11**(3): 1103-1116.

Wang, Y., Y. Zhang, S. Zhang, G. Peng, T. Liu, Y. Li, D. Xiang, M. J. Wassler, H. S. Shelat and Y. Geng (2012b). Rotating microgravity-bioreactor cultivation enhances the hepatic differentiation of mouse embryonic stem cells on biodegradable polymer scaffolds. *Tissue Eng Part A* **18**(21-22): 2376-2385.

Warlich, E., J. Kuehle, T. Cantz, M. H. Brugman, T. Maetzig, M. Galla, A. A. Filipczyk, S. Halle, H. Klump, H. R. Scholer, C. Baum, T. Schroeder and A. Schambach (2011). Lentiviral vector design and imaging approaches to visualize the early stages of cellular reprogramming. *Mol Ther* **19**(4): 782-789.

Warren, L., P. D. Manos, T. Ahfeldt, Y. H. Loh, H. Li, F. Lau, W. Ebina, P. K. Mandal, Z. D. Smith, A. Meissner, G. Q. Daley, A. S. Brack, J. J. Collins, C. Cowan, T. M. Schlaeger and D. J. Rossi (2010). Highly efficient reprogramming to pluripotency and directed differentiation of human cells with synthetic modified mRNA. *Cell Stem Cell* **7**(5): 618-630.

Watanabe, K., M. Ueno, D. Kamiya, A. Nishiyama, M. Matsumura, T. Wataya, J. B. Takahashi, S. Nishikawa, S. Nishikawa, K. Muguruma and Y. Sasai (2007). A ROCK inhibitor permits survival of dissociated human embryonic stem cells. *Nat Biotechnol* **25**(6): 681-686.

Watanabe, Y., Y. Shimada, A. Sugihara and Y. Tominaga (2001). Enzymatic conversion of waste edible oil to biodiesel fuel in a fixed-bed bioreactor. *Journal of the American Oil Chemists' Society* **78**(7): 703-707.

Weatherbee, B. A. T., T. Cui and M. Zernicka-Goetz (2021). Modeling human embryo development with embryonic and extra-embryonic stem cells. *Dev Biol* **474**: 91-99.

Weaver, W. D., R. J. Simes, A. Betriu, C. L. Grines, F. Zijlstra, E. Garcia, L. Grinfeld, R. J. Gibbons, E. E. Ribeiro, M. A. DeWood and F. Ribichini (1997). Comparison of Primary Coronary Angioplasty and Intravenous Thrombolytic Therapy for Acute Myocardial Infarction: A Quantitative Review. *JAMA* **278**(23): 2093-2098.

Weber, C., D. Freimark, R. Pörtner, P. Pino-Grace, S. Pohl, C. Wallrapp, P. Geigle and P. Czermak (2010). Expansion of human mesenchymal stem cells in a fixed-bed bioreactor system based on non-porous glass carrier–part A: inoculation, cultivation, and cell harvest procedures. *The International journal of artificial organs* **33**(8): 512-525.

Weber, C., S. Pohl, R. Portner, C. Wallrapp, M. Kassem, P. Geigle and P. Czermak (2007). Cultivation and Differentiation of Encapsulated hMSC-TERT in a Disposable Small-Scale Syringe-Like Fixed Bed Reactor. *Open Biomed Eng J* **1**: 64-70.

Wei, H., G. Tan, Manasi, S. Qiu, G. Kong, P. Yong, C. Koh, T. H. Ooi, S. Y. Lim, P. Wong, S. U. Gan and W. Shim (2012). One-step derivation of cardiomyocytes and mesenchymal stem cells from human pluripotent stem cells. *Stem Cell Res* **9**(2): 87-100.

Weinberger, F., K. Breckwoldt, S. Pecha, A. Kelly, B. Geertz, J. Starbatty, T. Yorgan, K. H. Cheng, K. Lessmann, T. Stolen, M. Scherrer-Crosbie, G. Smith, H. Reichenspurner, A. Hansen and T. Eschenhagen (2016). Cardiac repair in guinea pigs with human engineered heart tissue from induced pluripotent stem cells. *Sci Transl Med* **8**(363): 363ra148.

Weinhaus, A. J. and K. P. Roberts (2005). Anatomy of the Human Heart. *Handbook of Cardiac Anatomy, Physiology, and Devices*. P. A. Iaizzo. Totowa, NJ, Humana Press**:** 51-79.

Weisbrod, D., S. H. Khun, H. Bueno, A. Peretz and B. Attali (2016). Mechanisms underlying the cardiac pacemaker: the role of SK4 calcium-activated potassium channels. *Acta Pharmacol Sin* **37**(1): 82-97.

Williams, B., W. Lobel, F. Finklea, C. Halloin, K. Ritzenhoff, F. Manstein, S. Mohammadi, M. Hashemi, R. Zweigerdt, E. Lipke and S. Cremaschi (2020). Prediction of Human Induced Pluripotent

Stem Cell Cardiac Differentiation Outcome by Multifactorial Process Modeling. *Front Bioeng Biotechnol* **8**: 851.

Wilson, K. D., S. Hu, S. Venkatasubrahmanyam, J. D. Fu, N. Sun, O. J. Abilez, J. J. Baugh, F. Jia, Z. Ghosh, R. A. Li, A. J. Butte and J. C. Wu (2010). Dynamic microRNA expression programs during cardiac differentiation of human embryonic stem cells: role for miR-499. *Circ Cardiovasc Genet* **3**(5): 426-435.

Wnorowski, A., A. Sharma, H. Chen, H. Wu, N. Y. Shao, N. Sayed, C. Liu, S. Countryman, L. S. Stodieck, K. H. Rubins, S. M. Wu, P. H. U. Lee and J. C. Wu (2019). Effects of Spaceflight on Human Induced Pluripotent Stem Cell-Derived Cardiomyocyte Structure and Function. *Stem Cell Reports* **13**(6): 960-969.

Woltjen, K., I. P. Michael, P. Mohseni, R. Desai, M. Mileikovsky, R. Hamalainen, R. Cowling, W. Wang, P. Liu, M. Gertsenstein, K. Kaji, H. K. Sung and A. Nagy (2009). piggyBac transposition reprograms fibroblasts to induced pluripotent stem cells. *Nature* **458**(7239): 766-770.

Wu, J., M. R. Rostami, D. P. Cadavid Olaya and E. S. Tzanakakis (2014). Oxygen transport and stem cell aggregation in stirred-suspension bioreactor cultures. *PLoS One* **9**(7): e102486.

Xu, C., S. Police, N. Rao and M. K. Carpenter (2002). Characterization and enrichment of cardiomyocytes derived from human embryonic stem cells. *Circ Res* **91**(6): 501-508.

Yagi, M., S. Yamanaka and Y. Yamada (2017). Epigenetic foundations of pluripotent stem cells that recapitulate in vivo pluripotency. *Lab Invest* **97**(10): 1133-1141.

Yang, L., M. H. Soonpaa, E. D. Adler, T. K. Roepke, S. J. Kattman, M. Kennedy, E. Henckaerts, K. Bonham, G. W. Abbott, R. M. Linden, L. J. Field and G. M. Keller (2008). Human cardiovascular progenitor cells develop from a KDR+ embryonic-stem-cell-derived population. *Nature* **453**(7194): 524-528.

Yassa, M. E., I. A. Mansour, N. I. Sewelam, H. Hamza and T. Gaafar (2018). The impact of growth factors on human induced pluripotent stem cells differentiation into cardiomyocytes. *Life Sci* **196**: 38-47.

Yazaki, P. J., L. Shively, C. Clark, C.-W. Cheung, W. Le, B. Szpikowska, J. E. Shively, A. A. Raubitschek and A. M. Wu (2001). Mammalian expression and hollow fiber bioreactor production of recombinant anti-CEA diabody and minibody for clinical applications. *Journal of immunological methods* **253**(1-2): 195-208.

Yourek, G., S. M. McCormick, J. J. Mao and G. C. Reilly (2010). Shear stress induces osteogenic differentiation of human mesenchymal stem cells. *Regen Med* **5**(5): 713-724.

Yu, J., M. A. Vodyanik, K. Smuga-Otto, J. Antosiewicz-Bourget, J. L. Frane, S. Tian, J. Nie, G. A. Jonsdottir, V. Ruotti, R. Stewart, Slukvin, II and J. A. Thomson (2007). Induced pluripotent stem cell lines derived from human somatic cells. *Science* **318**(5858): 1917-1920.

Yuan, X., A. C. Tsai, I. Farrance, J. Rowley and T. Ma (2018). Aggregation of Culture Expanded Human Mesenchymal Stem Cells in Microcarrier-based Bioreactor. *Biochem Eng J* **131**: 39-46.

Zakrzewski, W., M. Dobrzynski, M. Szymonowicz and Z. Rybak (2019). Stem cells: past, present, and future. *Stem Cell Res Ther* **10**(1): 68.

Zanghi, J. A., W. A. Renner, J. E. Bailey and M. Fussenegger (2000). The growth factor inhibitor suramin reduces apoptosis and cell aggregation in protein-free CHO cell batch cultures. *Biotechnol Prog* **16**(3): 319-325.

Zhan, C., E. Hagrot, L. Brandt and V. Chotteau (2019). Study of hydrodynamics in wave bioreactors by computational fluid dynamics reveals a resonance phenomenon. *Chemical Engineering Science* **193**: 53-65.

Zhang, J., M. Klos, G. F. Wilson, A. M. Herman, X. Lian, K. K. Raval, M. R. Barron, L. Hou, A. G. Soerens, J. Yu, S. P. Palecek, G. E. Lyons, J. A. Thomson, T. J. Herron, J. Jalife and T. J. Kamp (2012). Extracellular matrix promotes highly efficient cardiac differentiation of human pluripotent stem cells: the matrix sandwich method. *Circ Res* **111**(9): 1125-1136.

Zhang, Q., J. Jiang, P. Han, Q. Yuan, J. Zhang, X. Zhang, Y. Xu, H. Cao, Q. Meng, L. Chen, T. Tian, X. Wang, P. Li, J. Hescheler, G. Ji and Y. Ma (2011). Direct differentiation of atrial and ventricular myocytes from human embryonic stem cells by alternating retinoid signals. *Cell Res* **21**(4): 579-587.

Zhou, W. and C. R. Freed (2009). Adenoviral gene delivery can reprogram human fibroblasts to induced pluripotent stem cells. *Stem Cells* **27**(11): 2667-2674.

Zhu, M. M., A. Feit, H. Chadow, M. Alam, T. Kwan and L. T. Clark (2001). Primary stent implantation compared with primary balloon angioplasty for acute myocardial infarction: a meta-analysis of randomized clinical trials. *Am J Cardiol* **88**(3): 297-301.

Zweigerdt, R. (2009). Large scale production of stem cells and their derivatives. *Adv Biochem Eng Biotechnol* **114**: 201-235.

CHAPTER II.

STRATEGIES FOR THE EXPANSION OF HUMAN INDUCED PLURIPOTENT STEM CELLS AS AGGREGATES IN VERTICAL-WHEEL BIOREACTORS

The contents of this chapter were based on the following publication:

Nogueira, D. E. S., C. A. V. Rodrigues, M. S. Carvalho, C. C. Miranda, Y. Hashimura, S. Jung, B. Lee and J. M. S. Cabral (2019). Strategies for the expansion of human induced pluripotent stem cells as aggregates in single-use Vertical-Wheel bioreactors. *J Biol Eng* **13**: 74.

II.1. Introduction

hPSCs, due to their ability to self-renew and to generate cells derived from the three germ layers, have a great potential for drug discovery, disease modelling and, ultimately, Regenerative Medicine applications (Shi et al. 2017, Rowe and Daley 2019). hiPSCs, first derived in 2007 from reprogramming of adult somatic cells (Takahashi et al. 2007, Yu et al. 2007), are not only less ethically prohibitive than hESCs, but also open the way for personalised medicine approaches (Itzhaki et al. 2011, Sayed et al. 2016).

One of the greatest constraints in using these cells, or their derivatives, for biomedical applications is their expansion to clinically-relevant numbers, which can reach 10^9 cells per patient for Regenerative Medicine settings (Zweigerdt 2009). Traditional planar cell culture platforms, such as tissue culture plates, are unsuited for these large-scale applications (Rodrigues et al. 2011b). Alternatively, bioreactors provide a 3D, scalable environment and are compatible with different medium feeding strategies, which can improve cell growth. In fact, planar culture platforms require a "repeated batch" strategy for medium change, where the medium is replaced at fixed time intervals, causing drastic variations in culture parameters such as pH or the concentration of nutrients, growth factors or metabolites. In contrast, bioreactors open the potential for alternative feeding strategies, such as fed-batch, where concentrated medium is added without replacing the contents of the culture vessel, or perfusion, where there is constant withdrawal of spent medium and replenishment of fresh medium (Bauwens et al. 2005, Kropp et al. 2016).

Early studies on the suspension culture of hPSCs as aggregates in bioreactors focused on the optimisation of the process (Krawetz et al. 2010, Singh et al. 2010, Chen et al. 2012, Hunt et al. 2014) including the establishment of xeno-free conditions (Wang et al. 2013). More recently, Kropp and colleagues expanded hiPSCs in single-use, instrumented bioreactors, and were able to increase cell yield in 47% when applying a perfusion feeding strategy over repeated batch culture, obtaining a cell density of $(2.85 \pm 0.34) \times 10^6$ cells·mL^{-1} (Kropp et al. 2016). These studies, however, were performed using common bioreactor systems, such as stirred tank bioreactors, which were developed and extensively used for manufacturing traditional biological products, where the quality of the cells is not the major concern. These bioreactors may not constitute the best solution for hPSC culture as they often require high agitations speeds in order to keep cell aggregates efficiently in suspension, with high shear rates conveyed to the cells by the impeller. As such, new bioreactor configurations are being developed to overcome these problems and allow for large-scale stem cell culture.

One example of a novel bioreactor system is the single-use VWBR, available on a wide range of scales, from 100 mL to 80 L. The agitation in these bioreactors is provided by a large vertical impeller, which, combined with the U-shaped bottom of the vessel, allows for a better homogenisation of the vessel contents with reduced power input. Consequently, cells are exposed to lower shear stress levels, when compared to traditional alternatives (Croughan et al. 2016).

The VWBR has already been used for some stem cell-related applications, including for the growth of hMSCs (Sousa et al. 2015, Yuan et al. 2018, de Sousa Pinto et al. 2019) and, recently, it was proven to allow for the scalable expansion of hiPSCs on microcarriers in xeno-free conditions (Rodrigues et al. 2018). While microcarriers provide a surface for the cells to adhere to, thus easing transition from

2D cultures, the cells need to be detached at the end of the culture, increasing the load of the downstream processing and affecting cell quality. Culturing the cells as aggregates may provide a simpler and potentially more cost-effective process for large-scale hiPSC production (Krawetz et al. 2010, Serra et al. 2012). Moreover, with the VWBR, agitation can be used to control aggregate size, as large aggregates (> 300 µm) are subjected to diffusion problems to their centre, causing undue cell differentiation or death (Wu et al. 2014). To minimise aggregate variability, however, there is a need for additional strategies for size control beyond physical forces. Polysulfated compounds are commonly used in the biopharmaceutical industry, not only for their ability to reduce cell aggregation by modulating charges in their surface, but also for their anti-apoptotic effect on cells (Dee et al. 1997, Zanghi et al. 2000). DS, in particular, has been employed for various cell systems, such as insect (Dee et al. 1997) or CHO cells (Hyoung Park et al. 2016). Most notably, DS was recently reported to promote these effects on hPSCs without loss of pluripotency (Lipsitz et al. 2018), thus, the use of this molecule in bioreactor systems may improve the outcomes in terms of cell expansion.

In this work, hiPSCs were expanded as aggregates in VWBRs (PBS MINI 0.1), with a working volume of 60 mL (Figure II.1). The results were validated using a second cell line, evidencing the robustness of this culture system. In order to maximise the potential of this culture set-up, the novel VWBR was also combined with a fed-batch strategy, which has been seldom described for hiPSC culture (Schwedhelm et al. 2019), as well as with DS, which allowed to greatly increase the cellular growth in the reactor. The work here performed demonstrates that hiPSCs can be cultured as aggregates in the VWBRs, opening the path for current GMP-compliant protocols for expansion, and prospectively, differentiation of hiPSCs for clinical applications.

II.2. Materials and methods

II.2.1. hiPSC culture and maintenance

This work was performed using two different hiPSC lines. The F002.1A.13 cell line, (TCLab—Tecnologias Celulares para Aplicação Médica, Portugal), referred to in the text as “TCLab”, was reprogrammed from human healthy fibroblasts (46, XX), through retroviral transduction of human genes *OCT4*, *SOX2*, *C-MYC* and *KLF4*. The Gibco® human episomal induced pluripotent stem cell line (Thermo Fisher Scientific, USA), referred to in the text as “Gibco”, was derived from $CD34^+$ cord blood through EBNA-based episomal transfection of factors SOX2, OCT4, KLF4, C-MYC, NANOG, LIN28 and SV40 T antigen. The hiPSCs were cultured on 6-well tissue culture plates coated with Matrigel (1:100; Corning, USA), in mTeSR1 culture medium (STEMCELL Technologies, Canada), and kept in a humidified incubator at 37 °C and 5% CO_2. Culture medium was refreshed daily, and the cells were routinely passaged after reaching 80% confluence at a split ratio of 1:4, using EDTA (Thermo Fisher Scientific) (Beers et al. 2012). Briefly, cells were washed twice and left to incubate for 5 min with EDTA (0.5 $mmol \cdot L^{-1}$ in Dulbecco’s phosphate-buffered saline, DPBS; Thermo Fisher Scientific). Afterwards, EDTA was removed and the cells were rinsed and collected by pipetting with culture medium before

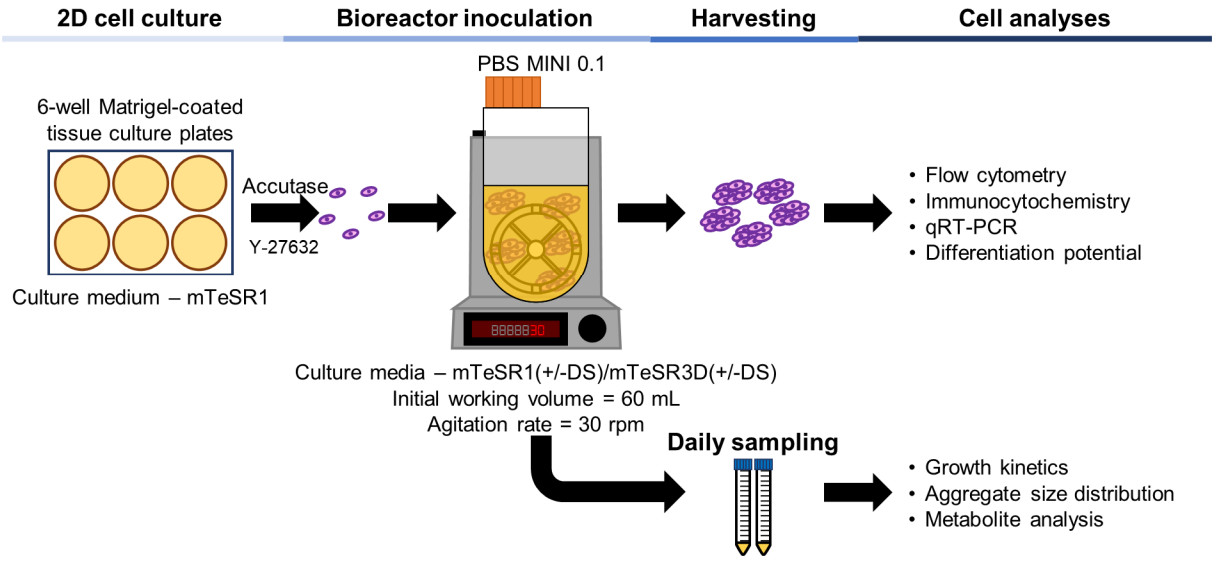

Figure II.1 – Workflow of the expansion of hiPSCs as aggregates in VWBRs. Following 2D culture in tissue culture plates, hiPSCs were dissociated into single cells with Accutase and inoculated into the PBS MINI 0.1 bioreactor, where they formed aggregates. The culture was evaluated through daily sampling and analysis of the cells after culture. From Nogueira et al. (2019). Reproduced under the terms of the Creative Commons Attribution 4.0 International License (http://creativecommons.org/licenses/by/4.0/). Copyright 2019, The Authors.

plating in new Matrigel-coated tissue culture plates. Cultures did not exceed four passages prior to bioreactor inoculation.

II.2.2. Bioreactor inoculation and operation

For this work, the PBS MINI 0.1 MAG VWBRs, which hold a maximum volume of 100 mL, were used. The working volume was selected to allow complete covering of the impeller wheel (initial working volume = 60 mL). Cells from 80% confluent 6-well tissue culture plates were incubated for 1 h in mTeSR1 supplemented with 10 µmol·L^{-1} ROCK inhibitor Y-27632 (STEMCELL Technologies) prior to harvesting with Accutase. Briefly, cells were washed once with DPBS and incubated for 7 min at 37 °C in Accutase (Sigma-Aldrich, USA). The cells were harvested and mechanically dissociated into single cells with a micropipette, and diluted with culture medium, following centrifugation at 210 × *g* for 3 min and resuspension in culture medium (mTeSR1 or mTeSR3D, STEMCELL Technologies) supplemented with Y-27632. The hiPSCs were counted with a haemocytometer, using the trypan blue dye exclusion test, and seeded in the bioreactor at a density of 2.5 × 10^5 cells·mL^{-1}. Culture medium with Y-27632 was added until reaching the working volume. For culture in mTeSR1, the medium was changed after 48 h to mTeSR1 without Y-27632, and from then on, 80% of the volume was changed daily. For culture in mTeSR3D, cells were initially cultured in seed medium, and, starting from 48 h post-inoculation, 6.7 mL of feed medium were added daily. At day 4, the medium was replaced with fresh seed medium, and from then on, 6.7 mL of feed medium were once again added daily until the end of culture. When used, DS (Sigma-Aldrich) was supplemented only on day 0 at a concentration of 100 µg·mL^{-1} (Lipsitz et al. 2018). Bioreactor cultures were maintained for 7 days and the stirring was continuously maintained at 30 rpm to keep the aggregates in suspension.

Culture sampling was performed daily. Two samples of 700 µL were collected with the reactor under agitation, and photos of the aggregates were captured with an inverted optical microscope (Leica DMI3000B/Nikon Digital Camera Dxm1200F) for later measurement. At least 50 aggregates were captured and analysed per timepoint. The area of the aggregates in each photo was determined using the FIJI software (Schindelin et al. 2012, Rueden et al. 2017), and their diameter was computed, considering the aggregates to be approximately spherical, as

$$d = \sqrt{\frac{4A}{\pi}} \tag{II.1}$$

with A as the area of the aggregate. The dispersion in aggregate size was determined as the coefficient of variation, defined as

$$C_V = \frac{SD_d}{\mu_d} \tag{II.2}$$

with SD_d as the standard deviation and μ_d as the average of the diameter for each condition. The aggregates were incubated with Accutase and mechanically dissociated into single cells as previously described. Viable cells were counted with a haemocytometer. Cell viability was over 90% at all culture days. Fold increase in cell number at a given time point was calculated as the ratio

$$FI = \frac{X}{X_0} \tag{II.3}$$

with X as the number of cells at the considered time point, and X_0 as the initial number of cells.

The viability of cells in the aggregates was assayed by incubation with 2 µmol·mL^{-1} of calcein AM during 20 min and observation of the stained aggregates under a fluorescence microscope (Leica DMI3000B/Nikon Digital Camera Dxm1200F).

At the end of culture, hiPSC aggregates were incubated for 1 h in culture medium supplemented with Y-27632 following incubation with Accutase and mechanical dissociation into single cells, as previously described, and replating on Matrigel-coated tissue culture plates at a density of 5 × 10^4 cells·cm^{-2}.

II.2.3. Glucose and lactate analysis

Culture supernatants were collected every day prior to and following medium exchange, and centrifuged at 360 × *g* for 10 min to remove dead cells and debris. The cell-free supernatants were analysed using an YSI 7100MBS Multi Channel Biochemistry Analyser (Yellow Spring Instruments, USA) for concentrations of glucose and lactate. The apparent yield of lactate from glucose was calculated for each day as

$$Y_{Lac/Glc} = \frac{\Delta Lac}{\Delta Glc} \tag{II.4}$$

with ∆Lac as the production of lactate and ∆Glc as the consumption of glucose during a given day of culture.

II.2.4. Flow cytometry

Throughout culture, cells were collected from the PBS MINI 0.1 and analysed for the expression of pluripotency and differentiation markers. The protocols for staining are described elsewhere for both intracellular (Rodrigues et al. 2011a) and surface markers (Rodrigues et al. 2018). For intracellular staining, an antibody for OCT4 (1:300; Millipore, USA) was used, and goat anti-mouse IgG-AlexaFluor 488 (1:300; Thermo Fisher Scientific) was used both as a secondary antibody and as a negative control. The gate was selected to contain only 1% of false positives (i.e. 1% of the negative control samples). For surface staining, cells were labelled with antibodies for tumour rejection antigen (TRA)-1-60 (1:10, PE-conjugated; Miltenyi Biotec, Germany) and stage-specific embryonic antigen (SSEA)-1 (1:20; FITC-conjugated, BioLegend, USA). The gate was selected to contain only 1% of false positives (i.e. 1% of the unstained samples). The cell samples were analysed with a FACSCalibur flow cytometer (Becton Dickinson, USA) and acquisition of the data was performed with the Cell Quest software (Becton Dickinson). For data analysis, Flowing Software (University of Turku, Finland) was used. A minimum of 10,000 events were analysed for each sample.

II.2.5. Immunocytochemistry

Both replated cells and aggregates were stained using previously described protocols for both intracellular (Rodrigues et al. 2011a) and surface markers (Rodrigues et al. 2018). For intracellular staining of hiPSCs, antibodies for OCT4 (1:150; Millipore) and SOX2 (1:200; R&D Systems, USA) were used, and goat anti-mouse IgG-AlexaFluor 546 (1:500; Thermo Fisher Scientific) was used as a secondary antibody. For surface staining of hiPSCs, cells were labelled with antibodies for TRA-1-60 (1:135, StemGent, USA) and SSEA-4 (1:135; StemGent) with the secondary antibody goat anti-mouse IgM-AlexaFluor 546 (1:500; Thermo Fisher Scientific) or goat anti-mouse IgG-AlexaFluor 546 (1:500), respectively. Staining of EBs was performed with antibodies for neuron-specific class III β-tubulin (TUJ1) (1:1,000; Covance, USA), α–smooth muscle actin (SMA) (1:200; Dako, Denmark), and SOX17 (1:100; R&D Systems). Staining following directed differentiation was performed with cTNT (1:200; Thermo Fisher Scientific) for cardiac differentiation, and paired box protein (PAX) 6 (1:400; Covance) and NESTIN (1:400; R&D Systems) for neural differentiation. Secondary staining was performed with goat anti-mouse IgG-AlexaFluor 546 (1:500), goat anti-rabbit IgG-AlexaFluor 546 (1:500, Thermo Fisher Scientific) or goat anti-mouse IgG-AlexaFluor 488 (1:500; Thermo Fisher Scientific). In all cases, nuclei were counterstained by incubation with 4′,6-diamidino-2-phenylindole (DAPI) (1.5 $\mu g \cdot mL^{-1}$; Sigma-Aldrich) for 5 min. Stained cells were analysed under a fluorescence microscope.

II.2.6. qRT-PCR

Total RNA from frozen cell pellets was extracted using the High Pure RNA Isolation Kit (Roche, Switzerland). Following quantification in a NanoVue™ Plus spectrophotometer (GE Healthcare, USA), 1 µg of RNA was converted to complementary DNA (cDNA) using the High-Capacity cDNA Reverse Transcriptase Kit (Life Technologies). Reactions were run in triplicate using NZYSpeedy qPCR Green Master Mix, ROX plus (NZYTech, Portugal), and primers specific for *OCT4*, *NANOG*, *SOX1*,

T/BRACHYURY and *SOX17* in a StepOne Plus Real-Time PCR System (Thermo Fisher Scientific). C_T values for each condition were normalised against the corresponding expression of the housekeeping gene glyceraldehyde-3-phosphate dehydrogenase (*GAPDH*), generating ΔC_T. RNA levels were computed as $2^{-\Delta CT}$.

II.2.7. Differentiation potential assays

II.2.7.1. Spontaneous differentiation

The differentiation potential of hiPSCs was evaluated through the EB assay. Following harvesting of cells from the PBS MINI 0.1, they were replated on 6-well ultra-low attachment tissue culture plates (Corning) in mTeSR1 supplemented with Y-27632. After 24 h, the medium was changed to EB medium, containing KnockOut (KO)-DMEM supplemented with 20% FBS, 1% (V/V) Minimum Essential Medium (MEM) non-essential amino acids, 1 mmol·L^{-1} L-glutamine and 1% (V/V) penicillin/streptomycin (all from Thermo Fisher Scientific), which was refreshed every 2 days during 4 weeks. After differentiation, the EBs were dissociated using 0.05% Trypsin-EDTA (Thermo Fisher Scientific) and plated on a 24-well tissue culture plate coated with 15 µg·mL^{-1} poly-ornithine (Sigma-Aldrich) and 20 µg·mL^{-1} laminin (Sigma-Aldrich). EB medium was changed every 2 days during 1 week, after which the cells were stained for TUJ1, α-SMA and SOX17.

II.2.7.2. Directed differentiation

Directed differentiation into both cardiomyocytes and neural progenitors was performed. Cardiac differentiation was performed through temporal modulation of the WNT signalling pathway (Lian et al. 2012, Lian et al. 2013). Briefly, hiPSCs were plated on a 12-well Matrigel-coated tissue culture plate at a density of 1.0 × 10^5 cells·cm^{-2}. After reaching 100% confluence, the medium was changed to RPMI/B27-ins (RPMI 1640 medium (Thermo Fisher Scientific), supplemented with 1× B-27 minus insulin (Thermo Fisher Scientific)), with 6 µmol·L^{-1} of CHIR (StemGent). After 24 h, the medium was changed to RPMI/B27-ins. At day 3, a half-medium change was performed with RPMI/B27-ins supplemented with IWP-4 (StemGent) to a final concentration of 5 µmol·L^{-1}, which was removed with the medium change at day 5. Starting from day 7, the medium was changed every 3 days to RPMI/B27 (RPMI 1640 medium supplemented with 1× B-27 (Thermo Fisher Scientific)) until day 15, when the cells were fixed and stained for cTNT. Neural induction was performed through the dual-SMAD inhibition protocol (Chambers et al. 2009, Fernandes et al. 2015). Briefly, hiPSCs were plated on a 24-well Matrigel-coated tissue culture plate at a density of 5.0 × 10^4 cells·cm^{-2}. After reaching 100% confluence, the medium was changed to N2B27, a 1:1 mixture of DMEM/F12 and Neurobasal medium with 1× N-2 and 1× B-27, respectively (all from Thermo Fisher Scientific), supplemented with 10 µmol·L^{-1} of SB431542 (Sigma-Aldrich) and 100 nmol·L^{-1} of LDN193189 (StemGent). Complete medium was refreshed daily for 12 days, after which the cells were fixed and stained for PAX6 and NESTIN.

II.2.8. Statistical analyses

At least three biological replicates were performed for each experiment. Data are expressed as the mean ± standard error of the mean (SEM). Statistical analyses were performed using GraphPad Prism 6 (GraphPad Software, USA). Statistical significance was determined by two-way ANOVA followed by Tukey's multiple comparisons test. Differences were considered statistically significant at $*p < 0.05$, $**p < 0.01$ and $***p < 0.001$.

II.3. Results

II.3.1. VWBRs allow the expansion of hiPSCs as aggregates

A protocol for expansion of hiPSCs as aggregates in the VWBRs was adapted from similar reports for other types of bioreactors (Kropp et al. 2016). For initial experiments, mTeSR1 was selected as the culture medium, due to being a feeder-free and serum-free medium, which has already been well-documented for the expansion of hiPSCs (Ludwig et al. 2006a, Ludwig et al. 2006b). The PBS MINI 0.1 MAG bioreactor was used with an initial working volume of 60 mL, just enough to cover the vertical wheel, to ensure the optimised hydrodynamic profile of the VWBR (Croughan et al. 2016). Preliminary tests were performed to determine the minimum stirring speed, which leads to efficient suspension of the aggregates throughout the culture time. Stirring was thus set at 30 rpm since at lower speeds aggregate sedimentation in the bottom of the vessel was observed.

For these initial experiments, two different cell lines were tested (TCLab and Gibco). In these culture conditions, the cells were able to form aggregates which grew throughout time (Figure II.2A, C) and were kept viable through 7 days of culture (Figure II.2B, D). For three independent bioreactor runs, the results were found to be reproducible, in terms of growth kinetics, aggregate size and metabolic profiles. The average growth curve obtained for this culture set-up is depicted in Figure II.2E. A maximum of $(1.2 \pm 0.1) \times 10^6$ cells·mL^{-1} and $(1.0 \pm 0.2) \times 10^6$ cells·mL^{-1} were obtained at day 7 post-inoculation with the TCLab and Gibco cell lines, respectively. The average diameter of cell aggregates was gradually increased to respective averages of 409 ± 25 µm and 338 ± 27 µm at day 7 (Figure II.2F). The dispersion of each experiment was measured through the coefficient of variation (Figure II.2G). For the TCLab cell line, the coefficient of variation was at its highest at day 1 (39 ± 5%), but generally decreased to ~ 30% in the last days of culture. For the Gibco cell line, it consistently remained below 25%. Aggregate diameter distributions at days 1, 4 and 7 are shown for a representative experiment in Figure II.2H, I. Culture medium supernatant analysis revealed that glucose levels were never depleted below 35% of fresh medium values (Figure II.2J), and lactate did not accumulate to concentrations over 16 mM (Figure II.2K). The yield of lactate from glucose remained between ~ 1.7 and ~ 2.1 throughout culture (Figure II.2L). These results overall show the implemented culture system to be robust, with similar results obtained for two different hiPSC lines.

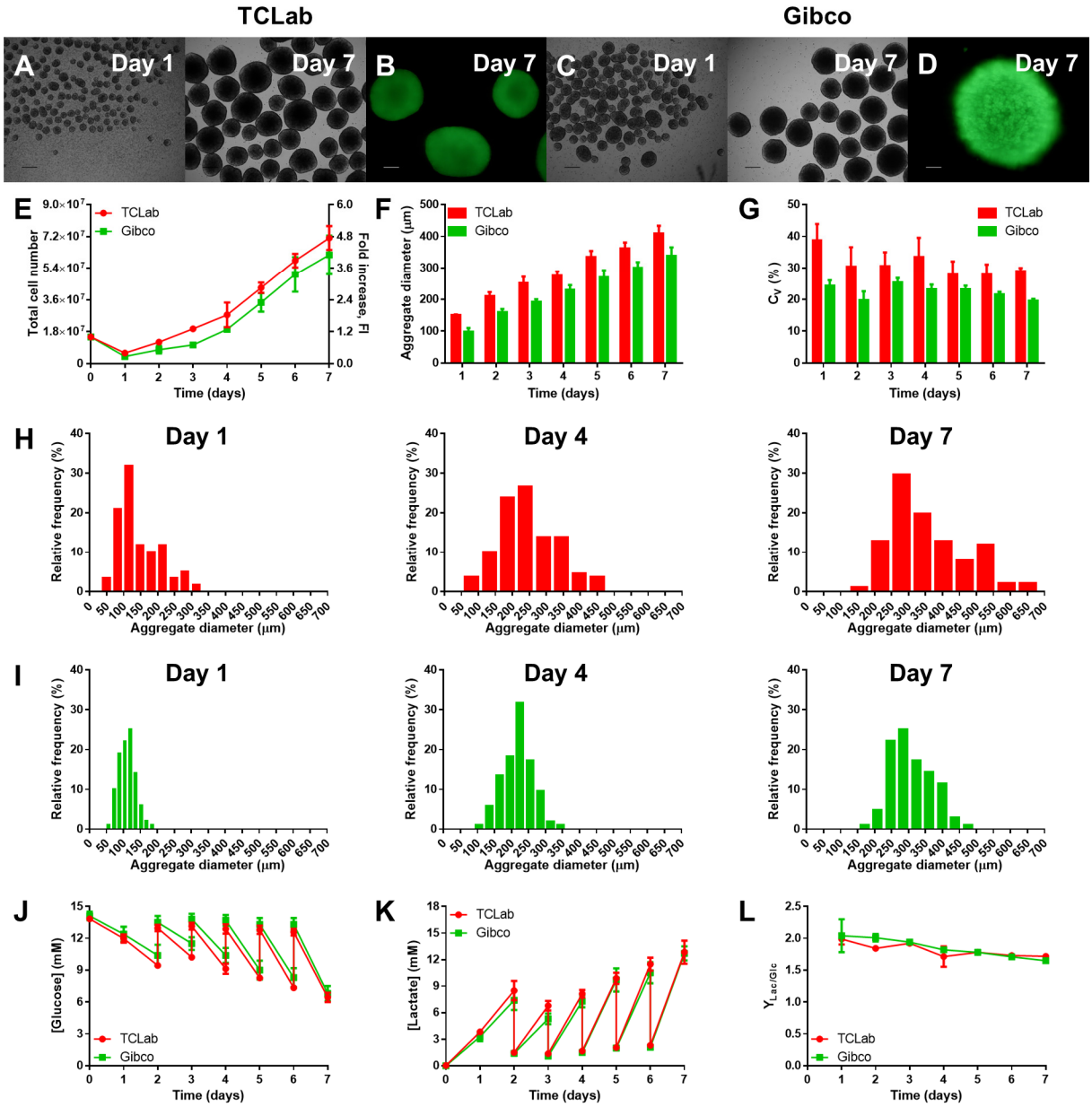

Figure II.2 – Results of the expansion of TCLab and Gibco hiPSCs with mTeSR1 in the PBS MINI 0.1 bioreactor. At day 0, the reactor was inoculated with 1.5 × 10^7 cells (2.5 × 10^5 cells·mL^{-1}) and 80% of the culture medium was changed daily starting from 48 h post-inoculation. **A-D** Representative images of cell aggregates harvested from the bioreactor, analysed through brightfield microscopy at days 1 and 7 of culture for **A** TCLab and **C** Gibco hiPSCs (scale bars = 250 µm) and through fluorescence microscopy at day 7 of culture culture for **B** TCLab and **D** Gibco hiPSCs following staining with calcein AM (scale bar = 100 µm). **E** Growth kinetics of the cells, in terms of total cell number and fold increase. **F-I** Aggregate size dynamics of the cells, in terms of **F** average aggregate diameter, **G** coefficient of variation, and aggregate size distribution profiles of a representative experiment at days 1, 4 and 7 post-inoculation for **H** TCLab and **I** Gibco hiPSCs. **J-L** Supernatant analysis of **J** glucose consumption and **K** lactate production, and **L** yield of lactate from glucose. From Nogueira et al. (2019). Reproduced under the terms of the Creative Commons Attribution 4.0 International License (http://creativecommons.org/licenses/by/4.0/). Copyright 2019, The Authors.

II.3.2. Fed-batch feeding sustains hiPSC growth but with lower cell expansion than repeated batch

Following the proof-of-concept experiments, demonstrating the use of the PBS MINI 0.1 for the expansion of two different hiPSC lines, different culture conditions were evaluated. In the previous experiments, mTeSR1 was used in repeated batch mode where, from day 2 onwards, 80% of the medium was changed daily. This approach results in significant variations in the culture parameters (e.g., glucose and lactate, as shown in Figure II.2G, H), which can have a negative effect on cell growth. However, while critical glucose and lactate concentrations were never reached with this feeding regime, daily medium changes are necessary in order to replenish components required to maintain the pluripotency of the cells, such as bFGF and TGFβ. mTeSR3D is an alternative formulation to mTeSR1, optimised for cell growth in suspension as the necessary growth factors are replenished through daily addition of a concentrated supplement. Thus, this fed-batch regime can allow for sustained maintenance of pluripotency factors, while causing less severe changes in other culture parameters.

Aggregate formation with mTeSR3D was observed (Figure II.3A), and these aggregates remained viable until the end of culture (Figure II.3B). Despite the intrinsic advantages of this feeding regime, culture in mTeSR3D presented a similar, albeit lower, cell growth profile when compared to mTeSR1 (Figure II.3C), with a maximum of (8.8 ± 1.6) × 10^5 cells·mL^{-1} at day 7. With mTeSR3D, aggregate diameter averaged 367 ± 18 μm at day 7 (Figure II.3D) with a coefficient of variation between ~ 25–40% (Figure II.3E) and following the distribution shown in Figure II.3F. These values were similar to those obtained with mTeSR1.

Expectedly, the fed-batch regime led to a more thorough consumption of glucose (Figure II.3G) without complete depletion (~ 50% prior to the medium change at day 4 and ~ 30% at day 7). Higher accumulation of lactate (Figure II.3H) was also observed, to a maximum of 19.3 mM at day 7, within the generally-considered inhibitory threshold for hPSCs of 15–20 mM (Chen et al. 2010, Horiguchi et al. 2018). The yield of lactate from glucose (Figure II.3I) was maintained between ~ 1.8 and ~ 2.0 in the first 5 days of culture, indicating an essentially glycolytic metabolism. In fact, the growth of hiPSCs is sustained by rapid consumption of glucose via conversion to lactate (glycolysis) even in the presence of oxygen, in a phenomenon known as the Warburg effect (Vander Heiden et al. 2009, Varum et al. 2011). At days 6 and 7, the yield of lactate from glucose decreased to 1.64 ± 0.03 and 1.37 ± 0.07, suggesting an increasing shift to OXPHOS. Nevertheless, this feeding regimen seems to be sufficient for the hiPSC maintenance, while minimising the variations in the culture environment to which the cells are subjected.

II.3.3. DS supplementation improves cell yield

As an attempt to improve cell growth while reducing aggregate size and size variability, both culture media used in this study, mTeSR1 and mTeSR3D, were tested with DS supplementation in the VWBRs. DS-supplemented media allowed the hiPSCs to form aggregates and their viability at day 7 was not compromised (Figure II.4A-D). Growth curves (Figure II.4E and Figure II.6 (SI)) show the hiPSCs to grow exponentially from 24 h of culture, reaching the maximum at day 5 for mTeSR1+DS or

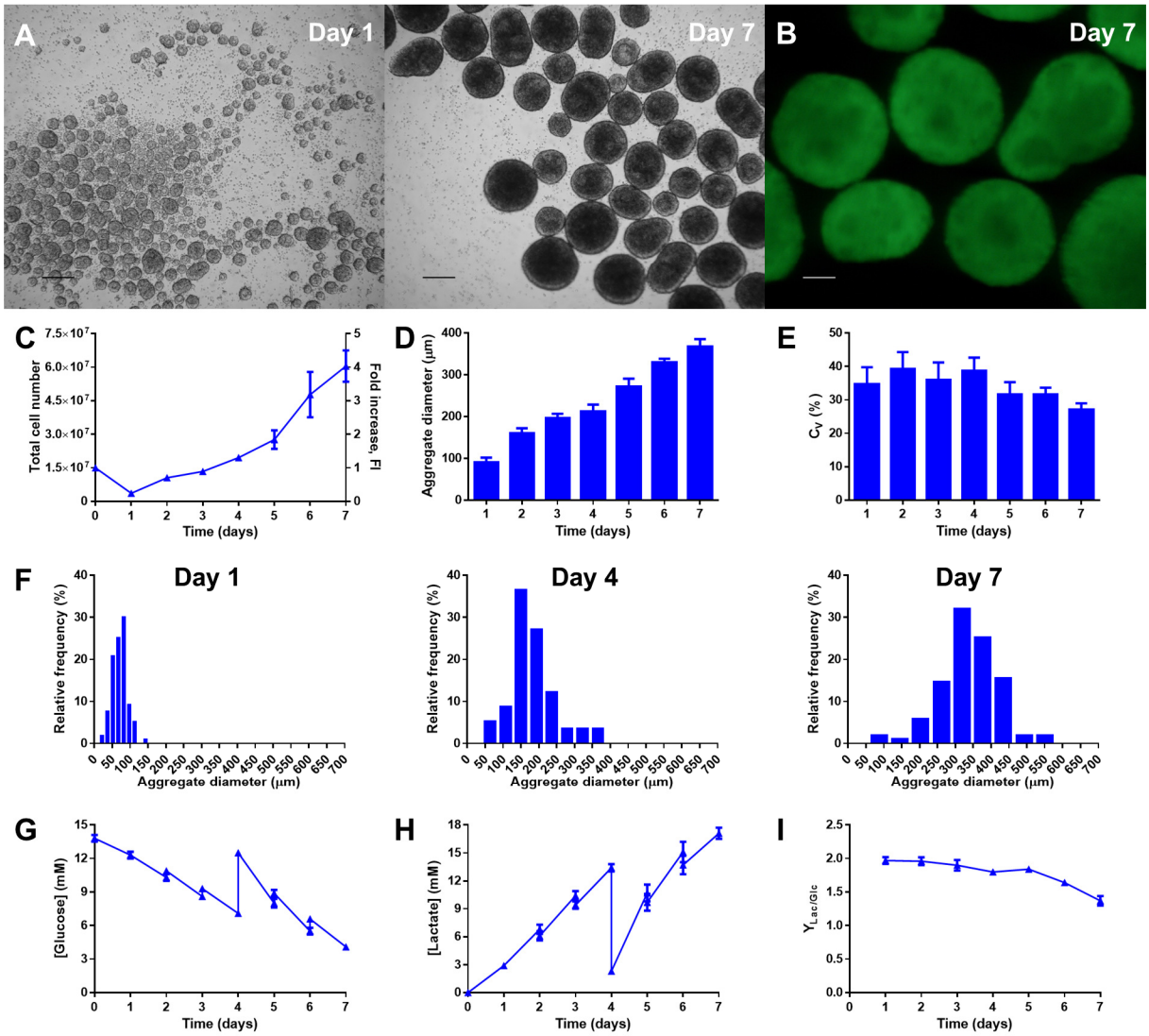

Figure II.3 – Results of the expansion of TCLab hiPSCs with mTeSR3D in the PBS MINI 0.1 bioreactor. At day 0, the reactor was inoculated with 1.5 × 10^7 cells (2.5 × 10^5 cells·mL^{-1}) and 6.7 mL of feed medium was added daily starting from 48 h post-inoculation, with a full medium change at day 4. **A-B** Representative images of cell aggregates harvested from the bioreactor, analysed through **A** brightfield microscopy at days 1 and 7 of culture (scale bars = 250 µm) and **B** fluorescence microscopy at day 7 of culture following staining with calcein AM (scale bar = 100 µm). **C** Growth kinetics of the cells, in terms of total cell number and fold increase. **D-F** Aggregate size dynamics of the cells, in terms of **D** average aggregate diameter, **E** coefficient of variation, and **F** aggregate size distribution profiles of a representative experiment at days 1, 4 and 7 post-inoculation. **G-I** Supernatant analysis of **G** glucose consumption and **H** lactate production, and **I** yield of lactate from glucose. From Nogueira et al. (2019). Reproduced under the terms of the Creative Commons Attribution 4.0 International License (http://creativecommons.org/licenses/by/4.0/). Copyright 2019, The Authors.

day 6 with mTeSR3D+DS, following which the cell density stagnated or decreased, respectively. Supplementation with DS led to a higher maximum fold expansion with both media, 9.3 ± 0.6 ((2.3 ± 0.2) × 10^6 cells·mL^{-1}) for mTeSR1+DS and 8.4 ± 0.1 ((1.79 ± 0.03) × 10^6 cells·mL^{-1}) for mTeSR3D+DS, representing a 97% and 106% increase in the number of cells versus the respective media without DS. Additionally, since the maximum in the number of cells is obtained 1 to 2 days earlier, these conditions also led to higher volumetric productivities of (4.6 ± 0.3) × 10^5 cells·mL^{-1}·d^{-1} and (2.99 ± 0.05) × 10^5

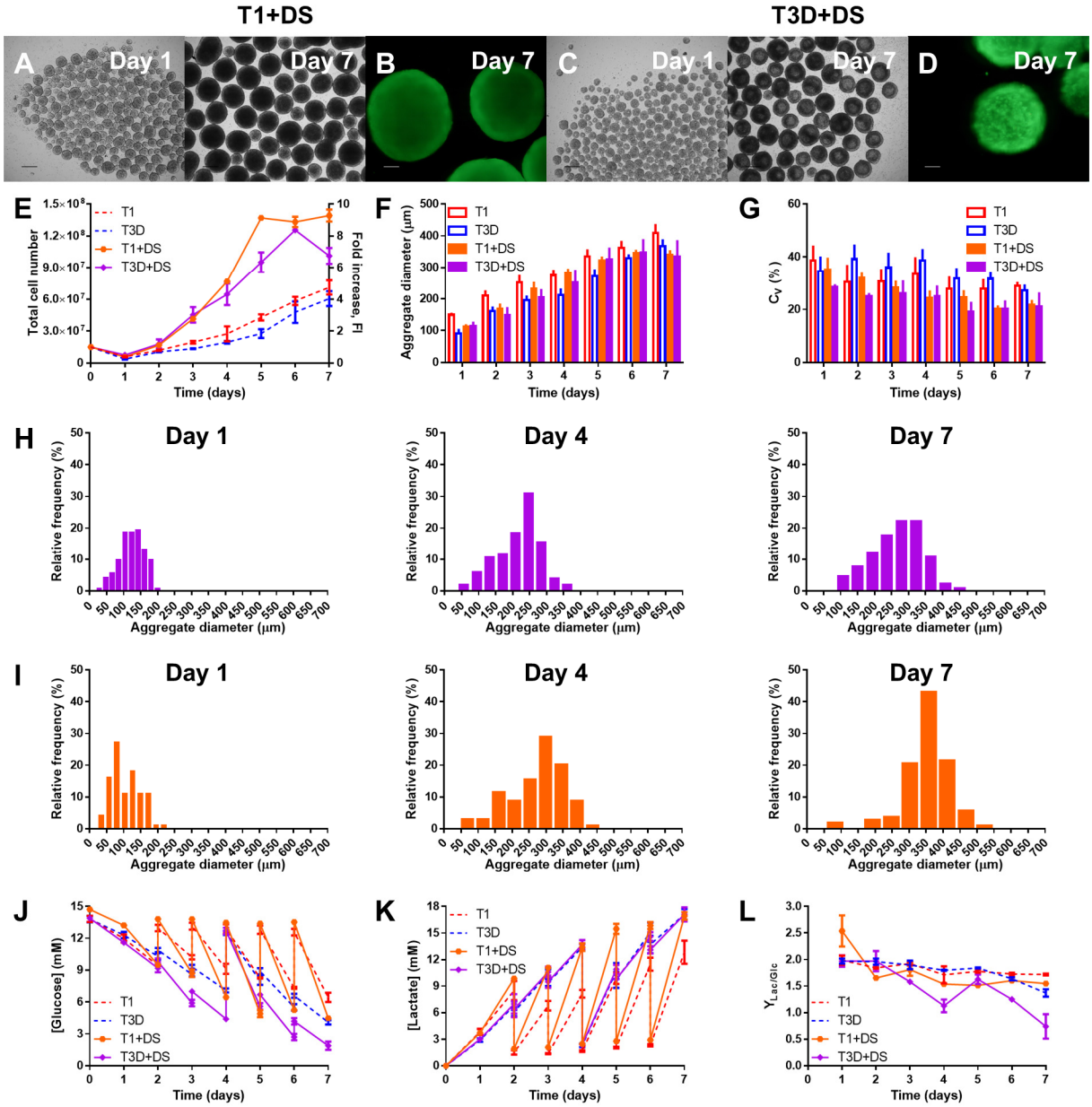

Figure II.4 – Results of the expansion of TCLab hiPSCs with mTeSR1 and mTeSR3D supplemented with dextran sulfate (T1+DS and T3D+DS, respectively) in the PBS MINI 0.1 bioreactor. At day 0, the reactors were inoculated with 1.5×10^7 cells (2.5×10^5 cells·mL^{-1}) and starting from 48 h post-inoculation, medium changes were performed according to the corresponding feeding regime. **A-D** Representative images of cell aggregates harvested from the bioreactor, analysed through brightfield microscopy at days 1 and 7 of culture in **A** T1+DS and **C** T3D+DS (scale bars = 250 µm) and through fluorescence microscopy at day 7 of culture in **B** T1+DS and **D** T3D+DS following staining with calcein AM (scale bars = 100 µm). **E** Growth kinetics of the cells, in terms of total cell number and fold increase. **F-I** Aggregate size dynamics of the cells, in terms of **F** average aggregate diameter, **G** coefficient of variation, and aggregate size distribution profiles of representative experiments at days 1, 4 and 7 post-inoculation for **H** T1+DS and **I** T3D+DS. **J-L** Supernatant analysis of **J** glucose consumption and **K** lactate production, and **L** yield of lactate from glucose. mTeSR1 (T1) and mTeSR3D (T3D) data are shown for comparison. From Nogueira et al. (2019). Reproduced under the terms of the Creative Commons Attribution 4.0 International License (http://creativecommons.org/licenses/by/4.0/). Copyright 2019, The Authors.

cells·mL^{-1}·d^{-1} for mTeSR1+DS and mTeSR3D+DS, respectively, having increased 170% and 149% from non-supplemented media.

The maximum aggregate sizes obtained at the plateau were 346 ± 11 μm and 347 ± 39 μm, respectively (Figure II.4F), with coefficients of variation of about 20% (Figure II.4G). Interestingly, the effect of DS on aggregate size was not significant during the exponential growth phase of culture. Individual aggregate diameters are also similar between both supplemented media, following comparable distributions for all culture days (Figure II.4H, I).

Considerable glucose depletion was found for both media, with as little as 28% and 8% of fresh medium values at day 7 for mTeSR1+DS and mTeSR3D+DS, respectively (Figure II.4J), and lactate was built-up until nearly 20 mM (Figure II.4K). For mTeSR1+DS, following a yield of lactate from glucose of ~ 2.5 at day 1, it stabilised between 1.5 and 1.6 towards the end of culture. For mTeSR3D+DS, this yield was maintained at ~ 2.0 for the initial days of culture, but decreased substantially starting from day 3, reaching a minimum of ~ 0.7 (Figure II.4L). This value indicates the metabolism to, most likely, have shifted to being predominantly OXPHOS, in particular with mTeSR3D+DS.

II.3.4. VWBRs do not compromise the pluripotency of the cells

Although the main purpose of expansion in a bioreactor system is to obtain large numbers of cells, it is important to guarantee that the process does not compromise cell quality, in particular hiPSC pluripotency. For that purpose, hiPSC aggregates were harvested from the PBS MINI 0.1 after culture and stained for both intracellular (OCT4 and SOX2) and surface (TRA-1-60 and SSEA-4) pluripotency markers. Figure II.5A shows representative images, demonstrating the presence of these markers after 7 days of expansion. Cell aggregates were also dissociated into single cells with Accutase and replated on Matrigel-coated 2D tissue culture plates. These cells were able to form hiPSC colonies in these conditions and representative images show expression of the aforementioned markers (Figure II.5B). Assessment of the differentiation potential of the expanded cells was performed via the EB assay (Figure II.5C), where the cells stained for markers of the three germ layers – TUJ1 (ectoderm), α-SMA (mesoderm) and SOX17 (endoderm), after 5 weeks of spontaneous differentiation. Expanded hiPSCs were also shown to be able to form both cardiomyocytes (Figure II.5D) and neural progenitors (Figure II.5E) following directed differentiation in 2D.

Quantification of pluripotency and differentiation marker expression was performed through both flow cytometry and quantitative real-time polymerase chain reaction (qRT-PCR) analyses. Flow cytometry analyses (Figure II.5F and Figure II.7 (SI)) revealed that, for all conditions, following 7 days of expansion in the VWBR, expression of pluripotency markers OCT4 and TRA-1-60 was always above 90% and expression of early differentiation surface marker SSEA-1 was maintained at less than 10%. Before and after expansion, total RNA was extracted from cell samples and the expression of pluripotency (*OCT4* and *NANOG*) and differentiation genes, namely *SOX1* (ectoderm), *T/BRACHYURY* (mesoderm) and *SOX17* (endoderm), were assayed through qRT-PCR (Figure II.5G). Expression of pluripotency genes *OCT4* and *NANOG* was high and not significantly different between days 0 and 7, while the expression of the differentiation markers was maintained low. In general, all these results point out the VWBR not to compromise the pluripotency of the cells throughout the expansion process.

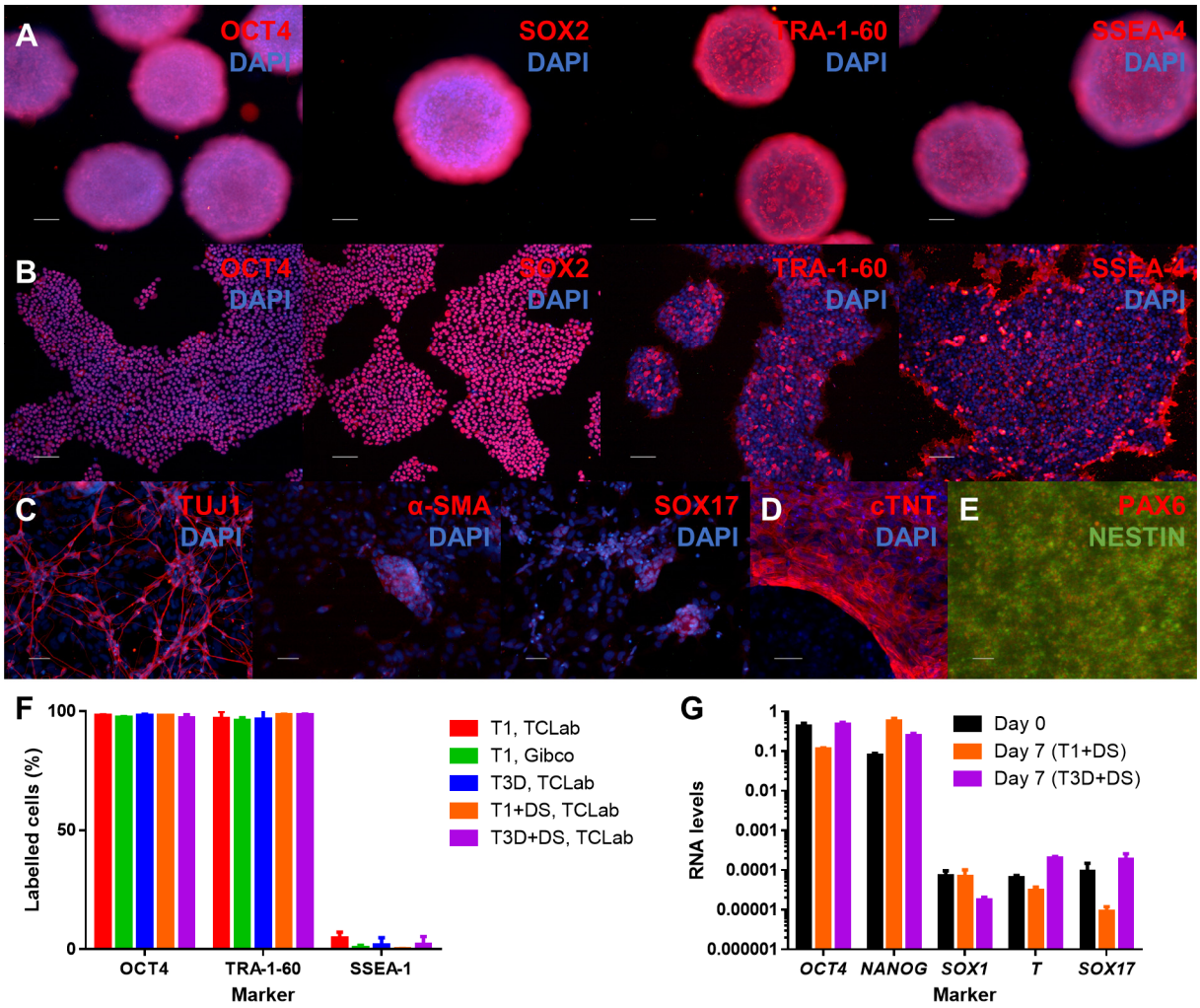

Figure II.5 – Characterisation of the hiPSCs following expansion in the PBS MINI 0.1 bioreactor. **A-B** Immunocytochemistry staining for pluripotency markers OCT4, SOX2, TRA-1-60 and SSEA-4 of **A** cell aggregates harvested from the PBS MINI 0.1 bioreactor at day 7 post-expansion (scale bars = 100 µm), and **B** of cells which were dissociated with Accutase and replated on 2D tissue culture plates (scale bars = 100 µm). **C** Immunocytochemistry staining of cells harvested from the bioreactor and left to form EBs for 5 weeks. The cells were stained for germ layer markers TUJ1 (ectoderm), α-SMA (mesoderm) and SOX17 (endoderm; scale bars = 50 µm). **D-E** Immunocytochemistry staining of cells harvested from the bioreactor and differentiated to **D** cardiomyocytes and **E** neural progenitors (scale bars = 50 µm). Cardiomyocytes were stained for cTNT, while neural progenitors were stained for PAX6 and NESTIN. **F** Flow cytometry analysis of cells harvested from the bioreactor after 7 days of expansion in the PBS MINI 0.1 bioreactor. The cells were labelled for pluripotency (OCT4 and TRA-1-60) and early differentiation (SSEA-1) markers. **G** qRT-PCR analysis of cells prior to (day 0) and following (day 7) expansion in the PBS MINI 0.1 bioreactor. The cells were tested for pluripotency (*OCT4* and *NANOG*) and germ layer (*SOX1*, *T/BRACHYURY* and *SOX17*, representing ectoderm, mesoderm and endoderm, respectively) marker expression. RNA levels are relative to expression of *GAPDH* and were computed as $2^{-\Delta CT}$. From Nogueira et al. (2019). Reproduced under the terms of the Creative Commons Attribution 4.0 International License (http://creativecommons.org/licenses/by/4.0/). Copyright 2019, The Authors.

II.4. Discussion

Therapeutic or pharmacological applications of hiPSCs require high numbers of cells. High cell densities of hPSCs have been previously attained using spinner flasks and stirred tank bioreactors, both using microcarriers as a culture support, or growing the cells as self-forming aggregates. However, some characteristics of these reactors, namely the low efficiency to keep in suspension particles such as cell-loaded microcarriers or cell aggregates, or the consequent high shear stress conveyed to the cells by the impeller at high stirring speeds, have led to research on more suitable bioreactor configurations for hPSC growth.

The work here described is intended to establish, in the PBS MINI VWBR, the culture of hiPSCs as floating aggregates. The largest barrier for the usage of this culture format is the aggregate size control (Wu et al. 2014). Since in bioreactors aggregate size is influenced by shear stress (Sen et al. 2002), the VWBR is expected to provide a significant advantage, as its novel agitation mechanism leads to a more homogeneous shear stress distribution than observed in stirred tank bioreactors (Croughan et al. 2016), contributing to a decrease in aggregate size variability and avoiding the formation of very large aggregates.

An overview of the results, already described in the previous section, is shown in Table II.1. Initial experiments with the VWBR have shown it to allow for the growth of hiPSCs with mTeSR1, with high reproducibility between different bioreactor runs and among two cell lines (Figure II.2). Cell density values and volumetric productivities were also amongst those reported in spinner flasks and traditional reactors, as well as higher than other studies reported in VWBRs (Table II.2). Culture performance can also be favourably compared with hiPSC culture on microcarriers in the VWBR (Rodrigues et al. 2018), where similar cell densities and volumetric productivities were obtained with the same cell line. Despite this, the culture set-up is barely optimised, as around 60% of the cells did not aggregate in the first 24 h of culture and therefore further optimisation should be possible to improve the present results.

Besides the promising results obtained with mTeSR1, a fed-batch feeding regime with mTeSR3D medium was tested as a means of mitigating the drastic parameter variations characteristic of a repeated batch approach, and allowing for the accumulation of growth-inducing paracrine factors (Kropp et al. 2016). The fed-batch strategy (Figure II.3) resulted in similar growth profiles and aggregate diameter distributions to repeated batch cultures but the high cell densities at the end of culture along with the slow replenishment of glucose and low dilution of lactate may have led to alterations in the metabolism of the cells. Proliferative cells, such as hiPSCs during their exponential growth, favour glycolysis for fast glucose uptake and to produce all of the molecules required for cell division (Vander Heiden et al. 2009, Varum et al. 2011). In fact, during the early days of culture, cells were metabolising glucose mainly through glycolysis, indicated by a yield of lactate from glucose close to 2. The lower yield observed at the end of culture suggests a metabolic shift to OXPHOS, which has already been reported in stirred bioreactor cultures of hiPSC (Kropp et al. 2016). Still, to our knowledge, this is only the second successful report indicating the viability of a fed-batch feeding strategy for the dynamic suspension culture of hiPSCs (Schwedhelm et al. 2019), and its optimisation could greatly increase the performance and the economic viability of this regime. A rough cost estimation based on these results led to the conclusion that mTeSR3D can provide about 10% reduction in the cost of medium spent per

Table II.1 – Main results for all different tested conditions. From Nogueira et al. (2019). Reproduced under the terms of the Creative Commons Attribution 4.0 International License (http://creativecommons.org/licenses/by/4.0/). Copyright 2019, The Authors.

Cell line	Culture medium	Fold change in cell number (day 1)	Maximum number of cells (cells/vessel)	Maximum cell density (cells·mL^{-1})	Maximum fold increase	Maximum specific growth rate (d^{-1})	Minimum doubling time (d)	Volumetric productivity (cells·mL^{-1}·d^{-1})	Maximum aggregate diameter (μm)	Minimum coefficient of variation
TCLab	mTeSR1	0.40 ± 0.03	(7.1 ± 0.7) × 10^7	(1.2 ± 0.1) × 10^6	4.8 ± 0.5	0.69 ± 0.13	1.1 ± 0.2	(1.7 ± 0.1) × 10^5	409 ± 25	28 ± 6%
Gibco	mTeSR1	0.27 ± 0.08	(6.2 ± 1.1) × 10^7	(1.0 ± 0.2) × 10^6	4.1 ± 0.7	0.66 ± 0.05	1.06 ± 0.09	(1.4 ± 0.3) × 10^5	338 ± 27	19.6 ± 0.6%
TCLab	mTeSR3D	0.24 ± 0.03	(6.1 ± 0.7) × 10^7	(8.8 ± 1.6) ×10^5	4.0 ± 0.5	1.1 ± 0.1	0.63 ± 0.06	(1.2 ± 0.1) × 10^5	367 ± 18	27 ± 2%
TCLab	mTeSR1+DS	0.38 ± 0.06	(1.4 ± 0.1) × 10^8	(2.3 ± 0.2) × 10^6	9.3 ± 0.6	1.1 ± 0.2	0.64 ± 0.11	(4.6 ± 0.3) × 10^5	346 ± 11	20 ± 1%
TCLab	mTeSR3D+DS	0.50 ± 0.07	(1.26 ± 0.02) × 10^8	(1.79 ± 0.03) × 10^6	8.4 ± 0.1	0.96 ± 0.10	0.74 ± 0.09	(2.99 ± 0.05) × 10^5	347 ± 39	19 ± 2%

Table II.2 – Comparison of aggregate-based dynamic suspension culture set-ups for the expansion of hESCs and hiPSCs. From Nogueira et al. (2019). Reproduced under the terms of the Creative Commons Attribution 4.0 International License (http://creativecommons.org/licenses/by/4.0/). Copyright 2019, The Authors.

Cell type	Culture medium	Platform type and volume	Inoculum cell density (cells·mL^{-1})	Days in culture	Maximum cell density (cells·mL^{-1})	Volumetric productivity (cells·mL^{-1}·d^{-1})	Reference
hESCs	mTeSR1	Spinner flask (100 mL)	1.8 × 10^4	6	4.5 × 10^5	7.5 × 10^4	Chen et al. (2012)
hESCs	mTeSR1	Spinner flask (50 mL)	1 × 10^6	7	2.4 × 10^6	3.4 × 10^5	Hunt et al. (2014)
hESCs	StemPro hESC SFM	Spinner flask (60 mL)	2.5 × 10^5	3–4	(1.1 ± 0.1) × 10^6	(3.7 ± 0.3) × 10^5	Krawetz et al. (2010)
hiPSCs	E8	Spinner flask (45 mL)	(4–5) × 10^5	3–4	(1.8 ± 0.3) × 10^6	(5.8 ± 0.8) × 10^5	Singh et al. (2010)
hESCs	mTeSR1	Spinner flask (100 mL)	2 × 10^4	6	(2.4 ± 0.09) × 10^5	(4.0 ± 0.2) × 10^4	Wang et al. (2013)
hiPSCs	mTeSR1/E8	Stirred tank (125 mL)	5 × 10^5	7	(2.85 ± 0.34) × 10^6	(4.07 ± 0.49) × 10^5	Kropp et al. (2016)
hiPSCs	mTeSR3D	Stirred tank (62.5–83.5 mL)	3.5 × 10^5	4 (per passage)	(7.2 ± 2.2) × 10^5	(1.8 ± 0.6) × 10^5	Schwedhelm et al. (2019)
hiPSCs	E8	Stirred tank (150 mL)	5.0 × 10^5	7	3.5 × 10^7	5.0 × 10^6	Manstein et al. (2021)
hiPSCs	mTeSR1	Vertical-Wheel (100 mL)	2.0 × 10^4	6	(6.3 ± 0.4) × 10^5	(1.05 ± 0.06) × 10^5	Borys et al. (2020)
hiPSCs	mTeSR1	Vertical-Wheel (100 mL)	2.0 × 10^4	6	(6.5 ± 0.6) × 10^5	(1.1 ± 0.1) × 10^5	Borys et al. (2021)
hiPSCs	mTeSR1	Vertical-Wheel (500 mL)	2.0 × 10^4	6	~ 4 × 10^4	~ 7 × 10^4	Borys et al. (2021)
hiPSCs	mTeSR1	Vertical-Wheel (60 mL)	2.5 × 10^5	7	(1.2 ± 0.1) × 10^6	(1.7 ± 0.1) × 10^5	This study
hiPSCs	mTeSR1+DS	Vertical-Wheel (60 mL)	2.5 × 10^5	5	(2.3 ± 0.2) × 10^6	(4.6 ± 0.3) × 10^5	This study

cell obtained. As such, the selection of the optimal medium for culture should be weighted considering the importance of both the cost and the performance.

The VWBR was shown to sustain the growth of hiPSCs with two different feeding regimes and to compare favourably with traditional bioreactor systems. However, given that the maximum cell density obtained was (1.2 ± 0.1) × 10^6 cells·mL^{-1} and that Regenerative Medicine applications can require 10^9 cells, it was considered important to develop strategies to increase the cell yield in the reactor. Additionally, the average size of the aggregates in all conditions exceeded 300 μm, which is problematic due to the diffusion limitations to the centre of the aggregate. A promising strategy that was found for both increased cell yield and aggregate size control was the supplementation of the culture media with DS. This compound was already reported to have these effects on hPSC aggregates (Lipsitz et al. 2018) due to its anti-apoptotic activity and surface charge modulation, without compromising pluripotency. In fact, DS supplementation increased cell yields in about two-fold and reduced the period of exponential growth, allowing for faster cultures (Figure II.4). At day 1, we did not observe a reduction in aggregate sizes with DS supplementation (Figure II.4F) but our results suggest that a higher absolute number of aggregates was formed in the presence of DS ((SI)). In this regard, we may hypothesise that the increase in cell number resulted from an initial formation of a higher number of aggregates that expanded to a comparable size of those cultured in the non-supplemented media.

The results obtained thus clearly favour DS supplementation of media over its absence, due to the boost in culture performance without any observed negative effect over the hiPSCs. In these conditions, the fed-batch system had a lower overall performance when compared to mTeSR1, in terms of maximum cell yield, productivity and even in the effect on the metabolic activity of the cells.

It is important to note that the pluripotency and viability of the cells cultured under the optimal condition, mTeSR1+DS, was not affected in the VWBR (Figure II.5). Indeed, after 7 days of culture, cells continued to express pluripotency markers, were able to form EBs, containing representatives of the three germ layers and to generate both cardiomyocytes and neural progenitors following directed differentiation into these lineages. At the end of the culture, cell aggregates reached over 300 μm in diameter, indicating some of the larger aggregates to be prone to diffusional limitations of nutrients and oxygen. While this could translate to necrosis in the centre of the aggregate, calcein AM/ethidium homodimer staining and confocal microscopy analysis as well as LIVE/DEAD flow cytometry ((SI)) show that dead cells are present in minority, and that there is no clear dead mass in the centre of the aggregate. Nevertheless, more prolonged culture of these cells would likely require dissociation and passaging to new culture vessels in order to maintain their viability and pluripotency over longer periods of time. Increasing the agitation at later days of culture could also reduce the diameter of the aggregates, allowing for better diffusion, while also contributing to a reduction in the variation in diameter size.

This study shows that VWBR can be considered a viable alternative for the growth of hPSCs, generating cell densities well within the range of those obtained with other types of bioreactors (Table II.2), while maintaining pluripotency. Nevertheless, there are still some challenges to tackle with this culture set-up. Namely, the process is still ill-optimised and a design of experiments (DoE) approach could be employed as a means of maximising the cellular growth and controlling cell aggregation for prospective integrated differentiation approaches inside the bioreactor. The cell yield obtained in this

study was 2.3 × 10^6 cells·mL^{-1}, after 5 days, using a repeated batch feeding strategy. Kropp and co-workers (Kropp et al. 2016) described a 47% increase in cell yield when the repeated batch feeding was replaced by perfusion, in miniaturised bioreactor systems, allowing for a maximum cell density of (2.85 ± 0.34) × 10^6 cells·mL^{-1} following 7 days in culture. Herein, the feeding modes used led to glucose depletion and lactate accumulation at later days of culture, especially in the fed-batch culture with mTeSR3D+DS, which may have hindered the achievement of higher cell densities. Operation of the PBS MINI 0.1 VWBR with perfusion is not straightforward but its implementation (either in this model or, prospectively, in higher volume models) would probably allow for higher cell densities to be obtained. Nevertheless, the cell density obtained with the present culture methodology was very close to that obtained by Kropp and co-workers with perfusion and, moreover, in comparison with that same study, our process started from half the cell density and reached the maximum cell density in less time (5 days vs 7 days). The use of *in silico* models to predict cell behaviour and adjust feeding could increase obtainable cell densities even further, as this strategy was already applied for hiPSC culture in miniaturised STBRs, leading to a final cell density of 3.5 × 10^7 cells·mL^{-1} (Manstein et al. 2021).

The PBS MINI 0.1 is a scaled-down bioreactor model, designed for process development and optimisation and not for cell production for clinical/industrial use. Assuming that 10^9 cells are required for organ regeneration (e.g., heart or liver (Zweigerdt 2009)), if the highest cell density obtained in this study, (2.3 ± 0.2) × 10^6 cells·mL^{-1}, could be maintained at higher scales, a bioreactor with a working volume of about 450 mL would be enough to meet the needs for one person. The availability of VWBR up to 80 L allow to envisage the use of higher volume models to generate cells for allogeneic settings while smaller-scale vessels (e.g., PBS 3), could be suited for an autologous cell product. Independently of the application, it is important to note that the scale-up of hPSCs is often prohibitive due to medium costs and, as such, it is crucial to carefully plan how to perform it, namely in terms of which criteria to apply (constant power input per volume, tip speed, mixing time or oxygen transfer, for instance). Previous studies already proved the PBS MINI 0.5, which can hold up to 500 mL, to be compatible with the growth of hiPSCs attached to microcarriers (Rodrigues et al. 2018) and as aggregates (Borys et al. 2021). As such, it would be important to also scale-up cell growth as aggregates, in order to generate a number of cells compatible with clinical and/or pharmacological applications.

II.5. Conclusions

One of the main bottlenecks in the usage of hPSCs in clinical or pharmacological applications is their expansion to large quantities, while maintaining their characteristics. Bioreactors provide major advantages over planar culture platforms, namely in terms of scalability, control and homogeneity, but are still not fully optimised for stem cell growth, as the shear stress caused by the impeller can greatly damage these cells. The VWBRs can mitigate this problem due to their more efficient mixing and gentler agitation set-up. The work here described is one of the first accounts of the usage of the PBS MINI VWBR for hPSC expansion as floating aggregates. This system overall has the potential to comply easily with GMP due to the single-use bioreactor system and the lack of matrices of any kind for cell adherence. The conjunction of mTeSR1 medium with DS led to a maximum increase of 9.3 ± 0.6-fold over the inoculum after only 5 days of culture, while not compromising the pluripotency of the cells.

Although there are still some challenges to face with this system, namely the usage of xeno-free media, the conversion to perfusion in order to potentially generate larger numbers of cells, and, finally, the scale-up to larger bioreactors, this study provides compelling evidence in the applicability of the VWBRs for the growth of hPSCs for diverse biomedical applications.

II.6. Supplementary information

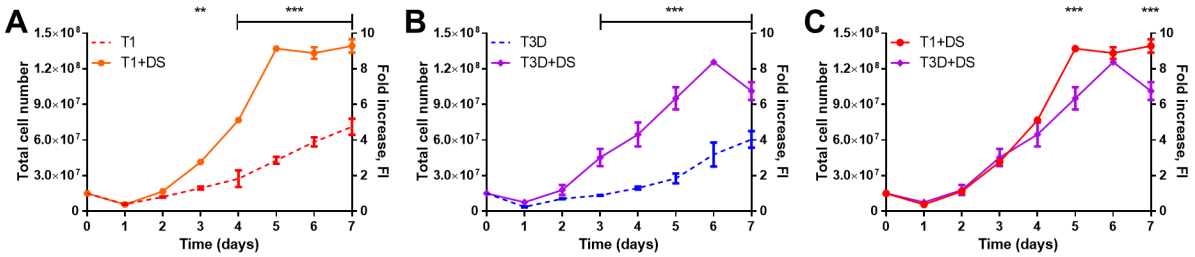

Figure II.6 (SI) – Statistical analysis of hiPSC growth curves. A set of two different culture conditions is presented in each graph: **A** mTeSR1 vs mTeSR1+DS; **B** mTeSR3D vs mTeSR3D+DS; **C** mTeSR1+DS vs mTeSR3D+DS. Differences between conditions, at a given day, were considered statistically significant at $^{**}p < 0.01$ and $^{***}p < 0.001$.

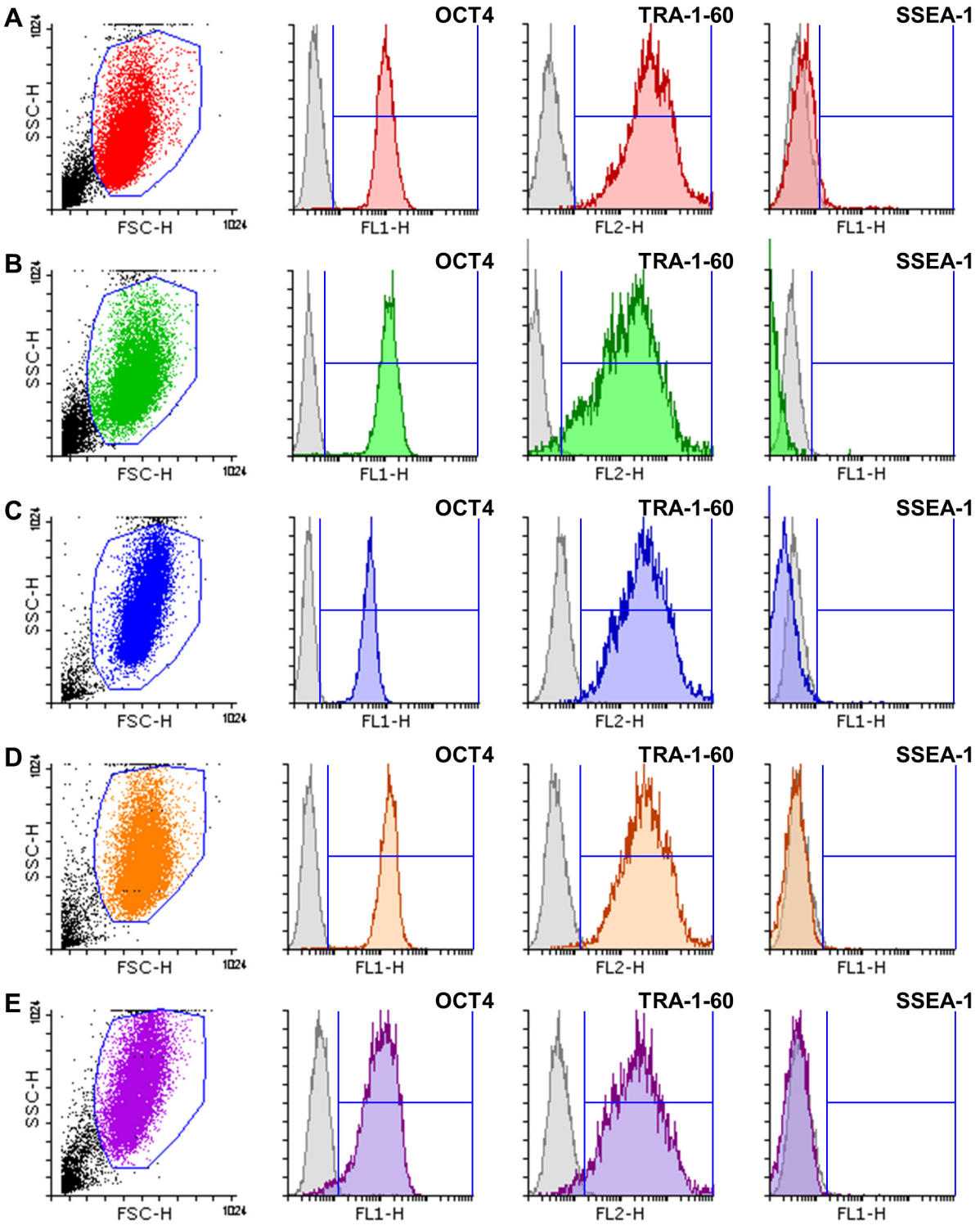

Figure II.7 (SI) – Flow cytometry analysis of hiPSCs cultured in the VWBR under the different conditions tested: **A** mTeSR1; **B** Gibco hiPSC line, mTeSR1; **C** mTeSR3D; **D** mTeSR1+DS; **E** mTeSR3D+DS. For each condition, representative images of a 2D dot plot showing population gating and histograms of OCT4, TRA-1-60 and SSEA-1 analyses, including negative controls (grey) are shown.

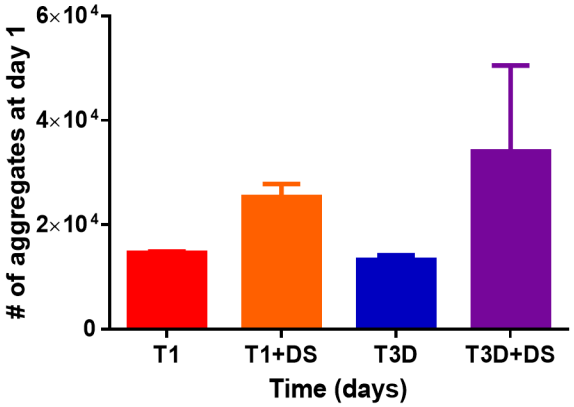

Figure II.8 (SI) – Number of hiPSC aggregates at day 1 under the different culture conditions tested. Samples (700 µL) harvested from the VWBR at day 1 were placed in a 24-well tissue culture plate and, using an optical microscope, pictures were taken, capturing all the aggregates present. Images were then analysed to count the total number of aggregates in the sample, which allowed to estimate the number of aggregates in the whole vessel. A total of two samples from two different runs were analysed for each condition.

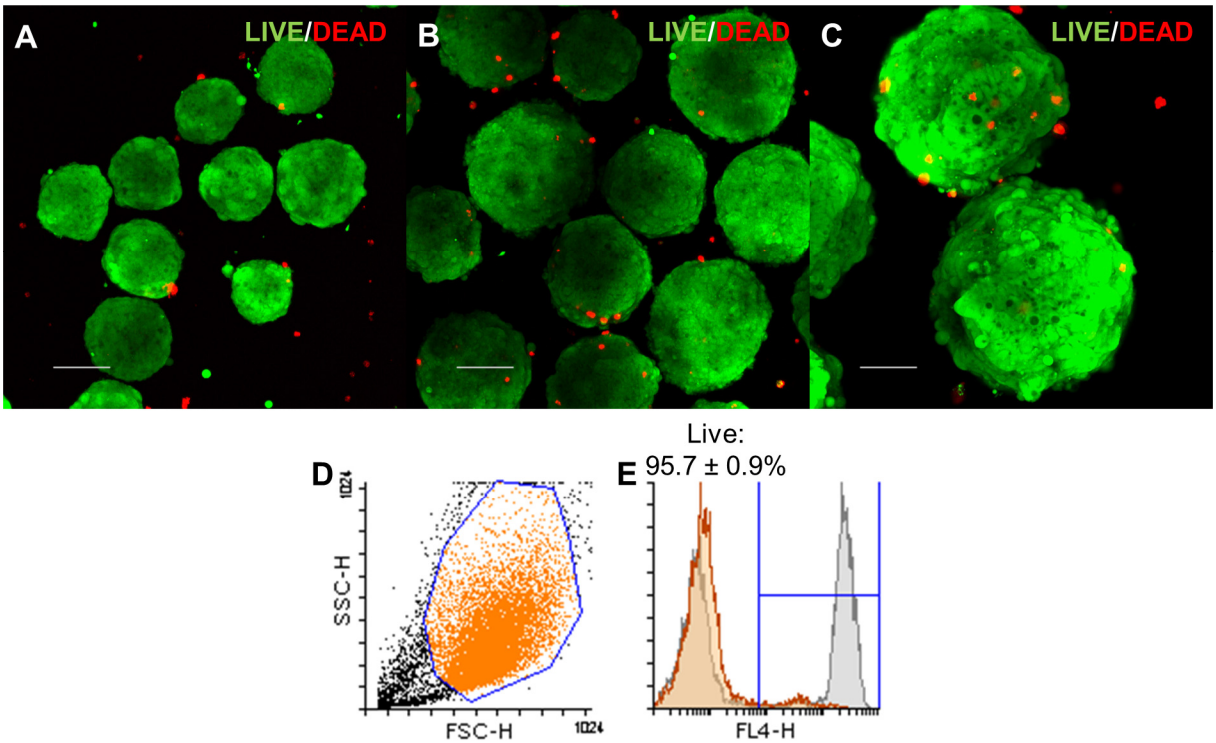

Figure II.9 (SI) – Cell viability analysis. hiPSC aggregates cultured for **A** 3 and **B, C** 7 days in the VWBR, with mTeSR1+DS, were harvested, incubated with calcein AM (2 µmol·L^{-1}) and ethidium homodimer (4 µmol·L^{-1}; Sigma-Aldrich) for 30 min and visualised using a confocal microscope. Maximum intensity projections are shown (scale bars = 100 µm). Aggregates at day 7 were also dissociated, stained with the LIVE/DEAD Fixable Far Red Dead Cell Stain Kit (Thermo Fisher), according to the manufacturer instructions and analysed by flow cytometry. Representative images of **D** a 2D dot plot showing population gating and **E** a histogram of a sample analysis (orange), including the positive control (a 50/50 mix of live cells and dead cells obtained by thermal shock) (grey). Three independent samples were analysed and percentage of live cells is shown as mean ± SEM.

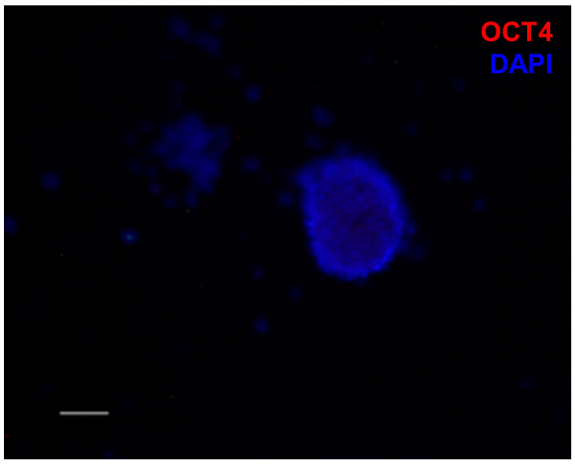

Figure II.10 (SI) – Negative control of the antibody stainings performed in Figure II.5C. Differentiated cells were stained for OCT4 (secondary antibody: goat anti-mouse IgG-AlexaFluor 546), which is not present in these cells (scale bar = 50 µm).

II.7. References

Bauwens, C., T. Yin, S. Dang, R. Peerani and P. W. Zandstra (2005). Development of a perfusion fed bioreactor for embryonic stem cell-derived cardiomyocyte generation: oxygen-mediated enhancement of cardiomyocyte output. *Biotechnol Bioeng* **90**(4): 452-461.

Beers, J., D. R. Gulbranson, N. George, L. I. Siniscalchi, J. Jones, J. A. Thomson and G. Chen (2012). Passaging and colony expansion of human pluripotent stem cells by enzyme-free dissociation in chemically defined culture conditions. *Nat Protoc* **7**(11): 2029-2040.

Borys, B. S., T. Dang, T. So, L. Rohani, T. Revay, T. Walsh, M. Thompson, B. Argiropoulos, D. E. Rancourt, S. Jung, Y. Hashimura, B. Lee and M. S. Kallos (2021). Overcoming bioprocess bottlenecks in the large-scale expansion of high-quality hiPSC aggregates in vertical-wheel stirred suspension bioreactors. *Stem Cell Res Ther* **12**(1): 55.

Borys, B. S., T. So, J. Colter, T. Dang, E. L. Roberts, T. Revay, L. Larijani, R. Krawetz, I. Lewis, B. Argiropoulos, D. E. Rancourt, S. Jung, Y. Hashimura, B. Lee and M. S. Kallos (2020). Optimized serial expansion of human induced pluripotent stem cells using low-density inoculation to generate clinically relevant quantities in vertical-wheel bioreactors. *Stem Cells Transl Med* **9**(9): 1036-1052.

Chambers, S. M., C. A. Fasano, E. P. Papapetrou, M. Tomishima, M. Sadelain and L. Studer (2009). Highly efficient neural conversion of human ES and iPS cells by dual inhibition of SMAD signaling. *Nat Biotechnol* **27**(3): 275-280.

Chen, V. C., S. M. Couture, J. Ye, Z. Lin, G. Hua, H. I. Huang, J. Wu, D. Hsu, M. K. Carpenter and L. A. Couture (2012). Scalable GMP compliant suspension culture system for human ES cells. *Stem Cell Res* **8**(3): 388-402.

Chen, X., A. Chen, T. L. Woo, A. B. Choo, S. Reuveny and S. K. Oh (2010). Investigations into the metabolism of two-dimensional colony and suspended microcarrier cultures of human embryonic stem cells in serum-free media. *Stem Cells Dev* **19**(11): 1781-1792.

Croughan, M. S., D. Giroux, D. Fang and B. Lee (2016). Novel Single-Use Bioreactors for Scale-Up of Anchorage-Dependent Cell Manufacturing for Cell Therapies *Stem Cell Manufacturing*. C. L. d. Silva, L. G. Chase and M. M. Diogo. Cambridge, Elsevier**:** 105-139.

de Sousa Pinto, D., C. Bandeiras, M. de Almeida Fuzeta, C. A. V. Rodrigues, S. Jung, Y. Hashimura, R. J. Tseng, W. Milligan, B. Lee, F. C. Ferreira, C. L. da Silva and J. M. S. Cabral (2019). [Scalable Manufacturing of Human Mesenchymal Stromal Cells in the Vertical-Wheel Bioreactor System: An Experimental and Economic Approach]. *Biotechnol J*: e1800716.

Dee, K. U., M. L. Shuler and H. A. Wood (1997). Inducing single-cell suspension of BTI-TN5B1-4 insect cells: I. The use of sulfated polyanions to prevent cell aggregation and enhance recombinant protein production. *Biotechnol Bioeng* **54**(3): 191-205.

Fernandes, T. G., S. T. Duarte, M. Ghazvini, C. Gaspar, D. C. Santos, A. R. Porteira, G. M. Rodrigues, S. Haupt, D. M. Rombo, J. Armstrong, A. M. Sebastiao, J. Gribnau, A. Garcia-Cazorla, O. Brustle, D. Henrique, J. M. Cabral and M. M. Diogo (2015). Neural commitment of human pluripotent stem cells under defined conditions recapitulates neural development and generates patient-specific neural cells. *Biotechnol J* **10**(10): 1578-1588.

Horiguchi, I., Y. Urabe, K. Kimura and Y. Sakai (2018). Effects of glucose, lactate and basic FGF as limiting factors on the expansion of human induced pluripotent stem cells. *J Biosci Bioeng* **125**(1): 111-115.

Hunt, M. M., G. Meng, D. E. Rancourt, I. D. Gates and M. S. Kallos (2014). Factorial experimental design for the culture of human embryonic stem cells as aggregates in stirred suspension bioreactors reveals the potential for interaction effects between bioprocess parameters. *Tissue Eng Part C Methods* **20**(1): 76-89.

Hyoung Park, J., M. Sin Lim, J. Rang Woo, J. Won Kim and G. Min Lee (2016). The molecular weight and concentration of dextran sulfate affect cell growth and antibody production in CHO cell cultures. *Biotechnol Prog* **32**(5): 1113-1122.

Itzhaki, I., L. Maizels, I. Huber, L. Zwi-Dantsis, O. Caspi, A. Winterstern, O. Feldman, A. Gepstein, G. Arbel, H. Hammerman, M. Boulos and L. Gepstein (2011). Modelling the long QT syndrome with induced pluripotent stem cells. *Nature* **471**(7337): 225-229.

Krawetz, R., J. T. Taiani, S. Liu, G. Meng, X. Li, M. S. Kallos and D. E. Rancourt (2010). Large-scale expansion of pluripotent human embryonic stem cells in stirred-suspension bioreactors. *Tissue Eng Part C Methods* **16**(4): 573-582.

Kropp, C., H. Kempf, C. Halloin, D. Robles-Diaz, A. Franke, T. Scheper, K. Kinast, T. Knorpp, T. O. Joos, A. Haverich, U. Martin, R. Zweigerdt and R. Olmer (2016). Impact of Feeding Strategies on the Scalable Expansion of Human Pluripotent Stem Cells in Single-Use Stirred Tank Bioreactors. *Stem Cells Transl Med* **5**(10): 1289-1301.

Lian, X., C. Hsiao, G. Wilson, K. Zhu, L. B. Hazeltine, S. M. Azarin, K. K. Raval, J. Zhang, T. J. Kamp and S. P. Palecek (2012). Robust cardiomyocyte differentiation from human pluripotent stem cells via temporal modulation of canonical Wnt signaling. *Proc Natl Acad Sci U S A* **109**(27): E1848-1857.

Lian, X., J. Zhang, S. M. Azarin, K. Zhu, L. B. Hazeltine, X. Bao, C. Hsiao, T. J. Kamp and S. P. Palecek (2013). Directed cardiomyocyte differentiation from human pluripotent stem cells by modulating Wnt/beta-catenin signaling under fully defined conditions. *Nat Protoc* **8**(1): 162-175.

Lipsitz, Y. Y., P. D. Tonge and P. W. Zandstra (2018). Chemically controlled aggregation of pluripotent stem cells. *Biotechnol Bioeng* **115**(8): 2061-2066.

Ludwig, T. E., V. Bergendahl, M. E. Levenstein, J. Yu, M. D. Probasco and J. A. Thomson (2006a). Feeder-independent culture of human embryonic stem cells. *Nat Methods* **3**(8): 637-646.

Ludwig, T. E., M. E. Levenstein, J. M. Jones, W. T. Berggren, E. R. Mitchen, J. L. Frane, L. J. Crandall, C. A. Daigh, K. R. Conard, M. S. Piekarczyk, R. A. Llanas and J. A. Thomson (2006b). Derivation of human embryonic stem cells in defined conditions. *Nat Biotechnol* **24**(2): 185-187.

Manstein, F., K. Ullmann, C. Kropp, C. Halloin, W. Triebert, A. Franke, C. M. Farr, A. Sahabian, A. Haase, Y. Breitkreuz, M. Peitz, O. Brustle, S. Kalies, U. Martin, R. Olmer and R. Zweigerdt (2021). High density bioprocessing of human pluripotent stem cells by metabolic control and in silico modeling. *Stem Cells Transl Med* **10**(7): 1063-1080.

Nogueira, D. E. S., C. A. V. Rodrigues, M. S. Carvalho, C. C. Miranda, Y. Hashimura, S. Jung, B. Lee and J. M. S. Cabral (2019). Strategies for the expansion of human induced pluripotent stem cells as aggregates in single-use Vertical-Wheel bioreactors. *J Biol Eng* **13**: 74.

Rodrigues, C. A., M. M. Diogo, C. L. da Silva and J. M. Cabral (2011a). Microcarrier expansion of mouse embryonic stem cell-derived neural stem cells in stirred bioreactors. *Biotechnol Appl Biochem* **58**(4): 231-242.

Rodrigues, C. A., T. G. Fernandes, M. M. Diogo, C. L. da Silva and J. M. Cabral (2011b). Stem cell cultivation in bioreactors. *Biotechnol Adv* **29**(6): 815-829.

Rodrigues, C. A. V., T. P. Silva, D. E. S. Nogueira, T. G. Fernandes, Y. Hashimura, R. Wesselschmidt, M. M. Diogo, B. Lee and J. M. S. Cabral (2018). Scalable culture of human induced pluripotent cells on microcarriers under xeno-free conditions using single-use vertical-wheel (TM) bioreactors. *Journal of Chemical Technology and Biotechnology* **93**(12): 3597-3606.

Rowe, R. G. and G. Q. Daley (2019). Induced pluripotent stem cells in disease modelling and drug discovery. *Nat Rev Genet*.

Rueden, C. T., J. Schindelin, M. C. Hiner, B. E. DeZonia, A. E. Walter, E. T. Arena and K. W. Eliceiri (2017). ImageJ2: ImageJ for the next generation of scientific image data. *BMC Bioinformatics* **18**(1): 529.

Sayed, N., C. Liu and J. C. Wu (2016). Translation of Human-Induced Pluripotent Stem Cells: From Clinical Trial in a Dish to Precision Medicine. *J Am Coll Cardiol* **67**(18): 2161-2176.

Schindelin, J., I. Arganda-Carreras, E. Frise, V. Kaynig, M. Longair, T. Pietzsch, S. Preibisch, C. Rueden, S. Saalfeld, B. Schmid, J. Y. Tinevez, D. J. White, V. Hartenstein, K. Eliceiri, P. Tomancak and A. Cardona (2012). Fiji: an open-source platform for biological-image analysis. *Nat Methods* **9**(7): 676-682.

Schwedhelm, I., D. Zdzieblo, A. Appelt-Menzel, C. Berger, T. Schmitz, B. Schuldt, A. Franke, F. J. Muller, O. Pless, T. Schwarz, P. Wiedemann, H. Walles and J. Hansmann (2019). Automated real-time monitoring of human pluripotent stem cell aggregation in stirred tank reactors. *Sci Rep* **9**(1): 12297.

Sen, A., M. S. Kallos and L. A. Behie (2002). Expansion of mammalian neural stem cells in bioreactors: effect of power input and medium viscosity. *Brain Res Dev Brain Res* **134**(1-2): 103-113.

Serra, M., C. Brito, C. Correia and P. M. Alves (2012). Process engineering of human pluripotent stem cells for clinical application. *Trends Biotechnol* **30**(6): 350-359.

Shi, Y., H. Inoue, J. C. Wu and S. Yamanaka (2017). Induced pluripotent stem cell technology: a decade of progress. *Nat Rev Drug Discov* **16**(2): 115-130.

Singh, H., P. Mok, T. Balakrishnan, S. N. Rahmat and R. Zweigerdt (2010). Up-scaling single cell-inoculated suspension culture of human embryonic stem cells. *Stem Cell Res* **4**(3): 165-179.

Sousa, M. F., M. M. Silva, D. Giroux, Y. Hashimura, R. Wesselschmidt, B. Lee, A. Roldao, M. J. Carrondo, P. M. Alves and M. Serra (2015). Production of oncolytic adenovirus and human mesenchymal stem cells in a single-use, Vertical-Wheel bioreactor system: Impact of bioreactor design on performance of microcarrier-based cell culture processes. *Biotechnol Prog* **31**(6): 1600-1612.

Takahashi, K., K. Tanabe, M. Ohnuki, M. Narita, T. Ichisaka, K. Tomoda and S. Yamanaka (2007). Induction of pluripotent stem cells from adult human fibroblasts by defined factors. *Cell* **131**(5): 861-872.

Vander Heiden, M. G., L. C. Cantley and C. B. Thompson (2009). Understanding the Warburg effect: the metabolic requirements of cell proliferation. *Science* **324**(5930): 1029-1033.

Varum, S., A. S. Rodrigues, M. B. Moura, O. Momcilovic, C. A. Easley IV, J. Ramalho-Santos, B. Van Houten and G. Schatten (2011). Energy metabolism in human pluripotent stem cells and their differentiated counterparts. *PLoS One* **6**(6): e20914.

Wang, Y., B. K. Chou, S. Dowey, C. He, S. Gerecht and L. Cheng (2013). Scalable expansion of human induced pluripotent stem cells in the defined xeno-free E8 medium under adherent and suspension culture conditions. *Stem Cell Res* **11**(3): 1103-1116.

Wu, J., M. R. Rostami, D. P. Cadavid Olaya and E. S. Tzanakakis (2014). Oxygen transport and stem cell aggregation in stirred-suspension bioreactor cultures. *PLoS One* **9**(7): e102486.

Yu, J., M. A. Vodyanik, K. Smuga-Otto, J. Antosiewicz-Bourget, J. L. Frane, S. Tian, J. Nie, G. A. Jonsdottir, V. Ruotti, R. Stewart, Slukvin, II and J. A. Thomson (2007). Induced pluripotent stem cell lines derived from human somatic cells. *Science* **318**(5858): 1917-1920.

Yuan, X., A. C. Tsai, I. Farrance, J. Rowley and T. Ma (2018). Aggregation of Culture Expanded Human Mesenchymal Stem Cells in Microcarrier-based Bioreactor. *Biochem Eng J* **131**: 39-46.

Zanghi, J. A., W. A. Renner, J. E. Bailey and M. Fussenegger (2000). The growth factor inhibitor suramin reduces apoptosis and cell aggregation in protein-free CHO cell batch cultures. *Biotechnol Prog* **16**(3): 319-325.

Zweigerdt, R. (2009). Large scale production of stem cells and their derivatives. *Adv Biochem Eng Biotechnol* **114**: 201-235.

CHAPTER III.

EXPANSION AND CARDIAC DIFFERENTIATION OF HUMAN INDUCED PLURIPOTENT STEM CELLS IN SINGLE-USE VERTICAL-WHEEL BIOREACTORS–AN INTEGRATED APPROACH

III.1. Introduction

CVDs, such as heart failure, have remained the leading cause of death for many years (https://www.who.int/news-room/fact-sheets/detail/the-top-10-causes-of-death, accessed on the 25th of May 2021), and their incidence can only be expected to rise due to the prevalence of risk factors such as obesity, sedentarism and smoking (Virani et al. 2021). These diseases represent a substantial socioeconomic burden and there is still not an appropriate response for them—existing therapies aim to reduce their impact by facilitating blood flow, but the loss of cardiomyocytes upon myocardial infarction is difficult to impossible to revert due to the limited regeneration capacity of these cells (Bergmann et al. 2009, Mollova et al. 2013, Hesse et al. 2018).

The discovery of hPSCs—cells which can self-renew indefinitely, and can differentiate into all cell types of the human body—has been an important advancement for the development of new strategies for heart repair. While hESCs are ethically problematic due to their isolation requiring the destruction of human embryos (Matthews and Morali 2020), hiPSCs (Takahashi et al. 2007, Yu et al. 2007) are a very promising source of cells on-demand for Regenerative Medicine, overcoming not only the ethical problems of isolation, but also, if derived from the patients' own cells, avoiding rejection upon transplantation. Furthermore, hiPSCs can also be used for drug screening and disease modelling, including in a precision medicine context, aiming for personalised therapies (Itzhaki et al. 2011, Sayed et al. 2016, Shi et al. 2017, Rowe and Daley 2019). Any of these applications, however, will necessitate a scalable and reproducible biomanufacturing protocol to generate the large numbers of cardiomyocytes required (Zweigerdt 2009).

Classical biological processes have long relied on bioreactors for the production of proteins, viruses, etc. (van Lier et al. 1990, Velez-Suberbie et al. 2013, Raven et al. 2015, Schmideder and Weuster-Botz 2017), due to providing 3D, scalable environments compatible with process monitoring and control, as well as a variety of feeding strategies. This extensive knowledge in the operation of STBRs has already seen application for hPSC biomanufacturing processes (Kropp et al. 2016, Kwok et al. 2018, Halloin et al. 2019), but it has also shown these bioreactors are not ideal due to the large shear stress "hot spots" close to the impeller and the "dead zones" with stagnant conditions. Either of these phenomena may be responsible for spontaneous cell differentiation or death (Stolberg and McCloskey 2009, Earls et al. 2013). This has led to the development of novel bioreactor systems, with agitation systems more compatible with the growth of shear-sensitive cells, including hPSCs.

The VWBRs, by PBS Biotech, are novel systems which employ a large vertical impeller, combining radial and axial agitation, along with a U-shaped bottom. These unique characteristics allow for a homogeneous shear stress distribution profile, without the evidence of "hot spots" or "dead zones", thus allowing for efficient mixing of the cells with low power input (Croughan et al. 2016). Furthermore, these bioreactors are single use, which reduces the risk of contamination. VWBRs have already been applied for hMSC expansion (Sousa et al. 2015, Yuan et al. 2018, de Sousa Pinto et al. 2019, de Almeida Fuzeta et al. 2020, Lembong et al. 2020), as well as hiPSC expansion, both with the cells attached to microcarriers (Rodrigues et al. 2018) and as aggregates (Borys et al. 2020, Borys et al. 2021). More recently, long-term cerebellar differentiation of hiPSCs has also been proven to be possible in these

bioreactor systems, with clear advantages over static conditions (Silva et al. 2021). As such, these bioreactors have the potential to be applied for cardiac differentiation of hiPSCs.

Cardiac differentiation protocols have seen many advancements in recent years, with the GiWi protocol, first reported by Lian and co-workers, being regarded as a reliable, efficient and cost-effective method for generation of hiPSC-derived cardiomyocytes (Lian et al. 2012, Lian et al. 2013). This protocol initially employs a GSK3 inhibitor in order to activate the WNT signalling pathway and direct the cells towards a mesendodermal fate. Afterwards, WNT signalling is inhibited in order to permit the generation of cardiac mesoderm and, subsequently, cardiomyocytes. This protocol has also been applied in 3D conditions (Kempf et al. 2014, Laco et al. 2020), with recent reports detailing the positive effect of 3D in terms of the maturation of the generated cardiomyocytes (Correia et al. 2018, Branco et al. 2019). A two-day gap between GSK3 inhibition and WNT inhibition is generally employed, but this may lead to the differentiation of the initial mesendodermal cell pool in non-cardiogenic primitive streak-like cells. In an attempt to increase the differentiation potential of this protocol, Halloin and colleagues have researched continuous WNT control, with WNT inhibition directly following GSK3 inhibition. This continuous GiWi ($GiWi_{cont}$) protocol was shown to more efficiently direct hiPSCs towards a cardiac fate, and to be able to generate about 1×10^6 cardiomyocytes·mL^{-1} in 500 mL bioreactors (Halloin et al. 2019).

In this work, hiPSC cardiac differentiation was performed for the first time in VWBRs. An integrated approach was used, with expansion as aggregates followed by cardiac differentiation in the same bioreactor system, the PBS MINI 0.1 with a working volume of 60 mL. Despite the need for some optimisation, it was shown that VWBRs have the potential to support hiPSC cardiac differentiation, with the possibility of generating a population of over 70% cardiomyocytes. This is an important step towards the development of hiPSC cardiac differentiation protocols under GMP, envisaging the use of these cells in pharmacological and Regenerative Medicine settings.

III.2. Materials and methods

III.2.1. hiPSC culture and maintenance

This work was performed using the Gibco® human episomal induced pluripotent stem cell line (Thermo Fisher Scientific, USA), which was derived from $CD34^+$ cord blood through EBNA-based episomal transfection of factors SOX2, OCT4, KLF4, C-MYC, NANOG, LIN28 and SV40 T antigen. The hiPSCs were cultured on 6-well tissue culture plates coated with Matrigel (1:100; Corning, USA), in mTeSR1 (STEMCELL Technologies, Canada) or E8 (Thermo Fisher Scientific) culture medium, and kept in a humidified incubator at 37 °C and 5% CO_2. Culture medium was refreshed daily, and the cells were routinely passaged after reaching 80% confluence at a split ratio of 1:4, using EDTA (Thermo Fisher Scientific) (Beers et al. 2012). Briefly, cells were washed twice and left to incubate for 5 min with EDTA (0.5 mmol·L^{-1} in DPBS; Thermo Fisher Scientific). Afterwards, EDTA was removed and the cells were rinsed and collected by pipetting with culture medium before plating in new Matrigel-coated tissue culture plates. Cultures did not exceed four passages prior to bioreactor inoculation.

III.2.2. Cardiac differentiation condition screening

For an initial screening of conditions for cardiac differentiation, cells from 80% confluent 6-well tissue culture plates were incubated for 1 h in mTeSR1 or E8 supplemented with 10 μmol·L^{-1} ROCK inhibitor Y-27632 (STEMCELL Technologies) prior to harvesting with Accutase (Sigma-Aldrich, USA). Briefly, cells were washed once with DPBS and incubated for 7 min at 37 °C in Accutase. The cells were harvested and mechanically dissociated into single cells with a micropipette, and diluted with culture medium, following centrifugation at 210 × *g* for 3 min and resuspension in mTeSR1 or E8 supplemented with Y-27632. The hiPSCs were counted with a haemocytometer, using the trypan blue dye exclusion test, and seeded in the AggreWell 800 microwell plates (STEMCELL Technologies) according to the manufacturer's instructions at 9.75 × 10^5 cells per well. After 24 h and 48 h, medium was changed to mTeSR1 or E8 without Y-27632. 72 h post-seeding, the cell aggregates were seeded onto 6-well ultra-low attachment tissue culture plates, in RPMI 1640 (Thermo Fisher Scientific), supplemented with 1× B-27 minus insulin (Thermo Fisher Scientific) (RPMI/B27-ins), with CHIR (StemGent) at varying concentrations and either with or without 0.1% Pluronic F-68 (Thermo Fisher Scientific). This timepoint was set as day 0 of differentiation. For dynamic conditions, the plates were left under the action of orbital agitation at 70 rpm. After 24 h, the medium was changed to RPMI/B27-ins and replaced every two days until day 7 of differentiation. 5 μmol·L^{-1} IWP-4 (StemGent) was added either at day 1 or day 3 and removed in the next medium change. Starting from day 7, the medium was changed every 3 days to RPMI 1640 medium supplemented with 1× B-27 (Thermo Fisher Scientific) (RPMI/B27) until day 15, when the cells were fixed and stained for cTNT.

III.2.3. Bioreactor inoculation and operation

For this work, the PBS MINI 0.1 MAG VWBRs, which hold a maximum volume of 100 mL, were used. The working volume was selected to allow complete covering of the impeller wheel (initial working volume = 60 mL). Cells from 80% confluent 6-well tissue culture plates were incubated for 1 h in mTeSR1 supplemented with 10 μmol·L^{-1} Y-27632 prior to harvesting with Accutase and resuspension in mTeSR1 supplemented with Y-27632 and 0.1% Pluronic F-68. The hiPSCs were counted with a haemocytometer, using the trypan blue dye exclusion test, and seeded in the bioreactor at a density of 5.0 × 10^5 cells·mL^{-1}. mTeSR1 with Y-27632 and Pluronic F-68 was added until reaching the working volume. After 48 h, medium was changed to mTeSR1 without Y-27632 and Pluronic F-68. 72 h post-seeding, the medium was replaced by RPMI/B27-ins, with CHIR at varying concentrations. This timepoint was set as day 0 of differentiation. After 24 h, the medium was changed to RPMI/B27-ins and replaced every two days until day 7 of differentiation. 5 μmol·L^{-1} IWP-4 (StemGent) was added either at day 1 or day 3 and removed in the next medium change. Starting from day 7, the medium was changed every 3 days to RPMI/B27, until day 15, when the cells were fixed and stained for cTNT. Stirring was continuously maintained at 30 rpm to keep the aggregates in suspension.

Culture sampling was performed daily. Two samples of 700 μL were collected with the reactor under agitation, and photos of the aggregates were captured with an inverted optical microscope (Leica DMI3000B/Nikon Digital Camera Dxm1200F) for later measurement. At least 100 aggregates were

captured and analysed per timepoint. The area of the aggregates in each photo was determined using the FIJI software (Schindelin et al. 2012, Rueden et al. 2017), and their diameter was computed, considering the aggregates to be approximately spherical, as

$$d = \sqrt{\frac{4A}{\pi}} \tag{III.1}$$

with A as the area of the aggregate. The dispersion in aggregate size was determined as the coefficient of variation, defined as

$$C_V = \frac{SD_d}{\mu_d} \tag{III.2}$$

with SD_d as the standard deviation and μ_d as the average of the diameter for each condition. The aggregates were incubated with Accutase and mechanically dissociated into single cells as previously described. Viable cells were counted with a haemocytometer. Cell viability was over 90% at all culture days. Fold increase in cell number at a given time point was calculated as the ratio

$$FI = \frac{X}{X_0} \tag{III.3}$$

with X as the number of cells at the considered time point, and X_0 as the initial number of cells.

III.2.4. Flow cytometry

Throughout culture, cells were collected from the PBS MINI 0.1 and analysed for the expression of pluripotency and differentiation markers. The protocols for staining are described elsewhere for both pluripotency markers (Rodrigues et al. 2011) and for cTNT (Branco et al. 2019). Antibodies for OCT4 (1:300; Millipore, USA), SOX2 (1:150; R&D Systems, USA) and cTNT (1:250; Thermo Fisher Scientific) were used, and goat anti-mouse IgG-AlexaFluor 488 (1:300; Thermo Fisher Scientific) served both as a secondary antibody and as a negative control. The gate was selected to contain only 1% of false positives (i.e. 1% of the negative control samples). The cell samples were analysed with a FACSCalibur flow cytometer (Becton Dickinson, USA) and acquisition of the data was performed with the Cell Quest software (Becton Dickinson). For data analysis, Flowing Software (University of Turku, Finland) was used. A minimum of 10,000 events were analysed for each sample.

III.2.5. qRT-PCR

Total RNA from frozen cell pellets was extracted using the High Pure RNA Isolation Kit (Roche, Switzerland). Following quantification in a NanoVue™ Plus spectrophotometer (GE Healthcare, USA), 1 µg of RNA was converted to cDNA using the High-Capacity cDNA Reverse Transcriptase Kit (Life Technologies). Reactions were run in triplicate using NZYSpeedy qPCR Green Master Mix, ROX plus (NZYTech, Portugal), and primers specific for *OCT4*, *NANOG*, *T/BRACHYURY*, *ISL1*, *NKX2.5*, *SOX1*, and *SOX17* in a StepOne Plus Real-Time PCR System (Thermo Fisher Scientific). C_T values for each condition were normalised against the corresponding expression of the housekeeping gene *GAPDH*,

generating ΔC_T. ΔC_T values were then normalised to day 0 values, generating $\Delta\Delta C_T$. Relative quantities were computed as $2^{-\Delta CT}$.

III.3. Results

III.3.1. Screening of cardiac differentiation conditions

The development of an integrated protocol for hiPSC expansion and cardiac differentiation in VWBRs started by testing, in static conditions, different variations of the GiWi protocol reported in the literature. Most of the previous studies using the GiWi protocol apply GSK3 inhibition during the first day of differentiation and canonical WNT inhibition between days 3 and 5 (Lian et al. 2012, Lian et al. 2013, Kempf et al. 2014, Branco et al. 2019, Laco et al. 2020). Continuous WNT control, with GSK3 inhibition directly followed by WNT inhibition, has recently been found to greatly improve cardiac differentiation (Halloin et al. 2019) and therefore this protocol was compared with the "classic" GiWi (Figure III.1). In fact, the results obtained confirmed the best performance of the $GiWi_{cont}$ protocol, leading to a 3.2-fold increase in cardiomyocyte percentage following differentiation (from 15.0% to an average of 48.4%). While the cardiac differentiation efficiency of the GiWi protocol was substantially lower than the reported by Branco and colleagues (over 90%; Branco et al. (2019)), the authors maintained the cells in microwell plates until day 7 of differentiation, while we only used microwell plates for the initial cell expansion and performed the full differentiation in ultra-low attachment tissue culture plates.

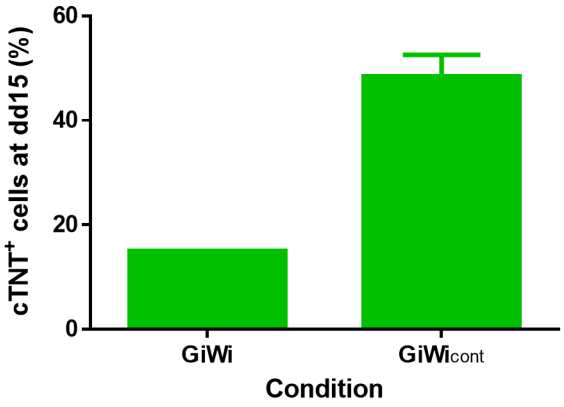

Figure III.1 – Comparison of the efficiency of cardiac differentiation of hiPSCs as aggregates in static conditions via the classic GiWi protocol and the $GiWi_{cont}$ protocol, in terms of the expression of cardiac-specific marker cTNT at differentiation day (dd) 15. One sample (n = 1) was analysed for the GiWi protocol and three independent samples (n = 3) were analysed for the $GiWi_{cont}$ protocol. Percentage of $cTNT^+$ cells is shown as mean ± SEM.

Following this analysis and before moving to the VWBR, a preliminary study in dynamic conditions was performed. For this purpose, different conditions for cardiac differentiation of hiPSCs as aggregates were assayed, using tissue culture plates on orbital shakers. Our previous work regarding the expansion of this cell line in the VWBR led to the generation of aggregates with an average diameter of 190 ± 9 µm after 3 days of expansion (Figure II.2), which is below the optimal range (Branco et al. 2019) to start the cardiac differentiation protocol. In order to improve cell survival in the short expansion phase, and to increase aggregate size towards the optimal range, supplementation of the expansion

medium with Pluronic F-68, widely used as a shear protectant (Tharmalingam et al. 2008, Manstein et al. 2021), was evaluated. However, before using this supplement in differentiation cultures, the effect of three different concentrations of Pluronic F-68 in hiPSC pluripotency was assayed in aggregates cultured under static conditions. None of the conditions tested affected the expression of pluripotency markers, with the percentage of cells expressing OCT4 and SOX2 remaining above 97% and comparing favourably to the non-supplemented control (Figure III.2). A concentration of 0.10% Pluronic F-68 was thus selected for subsequent experiments, as this concentration is also reported in other studies (Manstein et al. 2021).

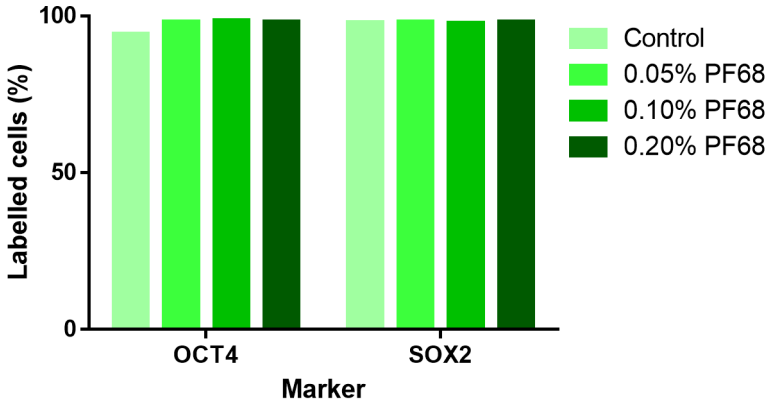

Figure III.2 – Effect of Pluronic F-68 (PF68) supplementation on the expression of pluripotency markers OCT4 and SOX2 by hiPSCs growing as aggregates in ultra-low attachment tissue culture plates under static conditions. One sample (n = 1) was analysed for all conditions.

In the next step, the effect of three variables on cardiac differentiation efficiency was tested under dynamic conditions: 1) culture medium used in the expansion phase (E8 and mTeSR1); 2) the effect of Pluronic F-68 supplementation during aggregate formation; 3) CHIR concentration at differentiation day 0 (5 μM, 8 μM and 11 μM). Static cultures, where initial aggregate formation was performed in microwell plates followed by differentiation in ultra-low attachment tissue culture plates, were used as a reference condition. Dynamic cultures were fully performed in ultra-low attachment tissue culture plates on orbital shakers. In both cases, the pre-differentiation expansion phase was set at 3 days. An overview of the results is found in Figure III.3.

In static conditions, following expansion with E8, the highest cardiac differentiation efficiency (43%) was observed for 8 μM CHIR. Dynamic cultures only generated cardiomyocytes (33%) with 5 μM CHIR and without Pluronic F-68 supplementation. All other dynamic cultures of cells expanded with E8 generated less than 3% $cTNT^+$ cells.

For mTeSR1, maximum cardiac differentiation in static conditions occurred with 8 μM and 11 μM CHIR (56%). In dynamic culture, with 5 μM of CHIR and without Pluronic F-68 supplementation, 62% $cTNT^+$ cells were obtained at the end of the protocol. The presence of Pluronic F-68 led to the same results. Supplementation with 8 μM and 11 μM of CHIR caused the differentiation to be precociously interrupted due to excessive cell aggregation.

Despite the failed differentiation for other CHIR concentrations, dynamic culture outperformed static culture in the 5 μM CHIR condition. Furthermore, expansion in mTeSR1 was found to be more favourable, either with or without Pluronic F-68 supplementation. As such, expansion with mTeSR1

(supplemented with Pluronic F-68 for 2 days) and initial differentiation with 5 μM CHIR were selected as the reference conditions for differentiation in bioreactors.

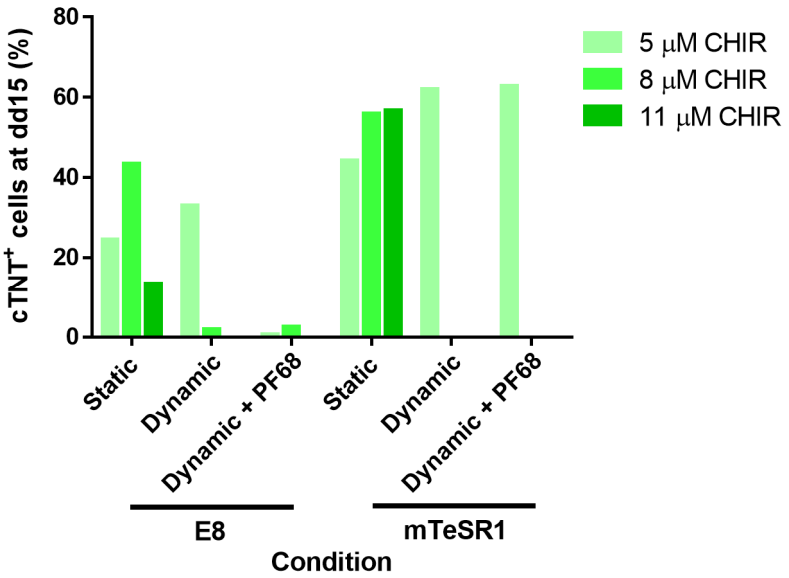

Figure III.3 – Comparison of the efficiency of cardiac differentiation of hiPSCs as aggregates in static and dynamic (with and without Pluronic F-68 (PF68) supplementation) conditions via the continuous GiWi protocol, in terms of the expression of cardiac-specific marker cTNT at differentiation day (dd) 15. One sample (n = 1) was analysed for all conditions.

III.3.2. VWBRs allow for integrated expansion and cardiac differentiation of hiPSCs

An integrated expansion and differentiation protocol was attempted in VWBRs, using the conditions found to be optimal in tissue culture plates as a starting point. Naturally, given the distinct microenvironment in the transition from plates to bioreactors (e.g., the impeller-mediated agitation), the optimal culture conditions in the VWBR might be different, as such, other protocols were tested as alternatives in parallel. The following sets of conditions were assayed (with n = 3 for condition #1 and n = 1 for the remaining):

Table III.1 – Sets of conditions tested for differentiation of hiPSCs in VWBRs.

Condition #	CHIR concentration (μM)	IWP-4 timing
1	5	d1-3
2	11	d1-3
3	5	d3-5

An overview of the results obtained for the various conditions is found in Figure III.4. The cells were able to aggregate and grow throughout the 3-day expansion phase (Figure III.4A). Following a 3-day expansion phase, an average of (7.4 ± 0.9) × 10^5 cells·mL^{-1} were obtained, representing a 1.5 ± 0.2-fold increase relatively to the inoculum (Figure III.4C). Day 3 hiPSC aggregates averaged 298 ± 25

μm of diameter (Figure III.4D), with a coefficient of variation of 19 ± 2% (Figure III.4E). Differentiation was started with the hiPSCs at this stage, under the different conditions presented in Table III.1, with each of the conditions generating aggregates with different morphologies (Figure III.4B). Spontaneously contracting aggregates were observed only following differentiation under conditions #1 and #2 ($GiWi_{cont}$ with different IWP-4 concentrations), but not with condition #3 (GiWi). Flow cytometry results (Figure III.4F) were concordant with this observation, with condition #3 failing to generate $cTNT^+$ cells, condition #2 resulting in 2.5% $cTNT^+$ cardiomyocytes and an average $cTNT^+$ population of 30 ± 22% stemming from differentiation in condition #1 (with one replicate resulting in 73.3% $cTNT^+$ cells). It should be noted, however, the need of performing replicates of both conditions #2 and #3 in order to perform a more proper comparison between the cardiomyogenic potential of the three protocols.

III.3.3. Gene expression profiles in differentiating hiPSCs

Due to the promising yet weakly reproducible results of the cardiac differentiation in VWBRs, the initial stages of the condition #1 process were characterised through qRT-PCR (Figure III.5). Expression of pluripotency genes *OCT4* and *NANOG* was stable through the expansion and the first day of differentiation but rapidly declined after WNT inhibition. Following CHIR exposure, mesendodermal marker *T/BRACHYURY* was upregulated 20-fold, and its expression remained stable until day 5 of differentiation. *SOX17* and *SOX1* were mostly downregulated throughout the process, but their expression was ~ 3-fold higher than in the inoculum by day 5 of differentiation. A 234-fold increase in the expression *ISL1*, a known SHF CPC marker (Cai et al. 2003, Bu et al. 2009), and a 4-fold increase in cardiac marker *NKX2.5*, were observed by day 5 of differentiation, indicating the cardiac commitment of at least part of the cell population.

III.4. Discussion

hiPSC-derived cardiomyocytes represent an important source of cells for diverse biomedical applications and for precision medicine approaches, but the high numbers of those cells required for these applications can only be reliably obtained using bioreactors. The unique agitation characteristics of the VWBRs render them advantageous for the culture of shear-sensitive cells such as hiPSCs and derivatives. As such, this work explored an integrated hiPSC expansion and cardiac differentiation process in those bioreactors, by adapting previously described, efficient cardiac differentiation protocols.

Prior to the establishment of a bioreactor protocol, the differentiation was optimised at a small scale in culture plates. The GiWi protocol was selected for cardiac differentiation due to its high efficiency and simplicity. This protocol employs an initial activation of the WNT signalling pathway by GSK3 inhibition, followed by canonical WNT inhibition. Between both phases, the cells are cultured without small molecules. This protocol was found to be able to produce over 90% $cTNT^+$ cells, even in a 3D environment (Correia et al. 2018, Branco et al. 2019). Nevertheless, some inconsistency in cardiac differentiation can be found between distinct runs and/or cell lines, motivating a new approach—the $GiWi_{cont}$ protocol, which applies successive activation and inhibition of WNT signalling. This novel system was described as generating over 90% cardiomyocytes in bioreactor culture

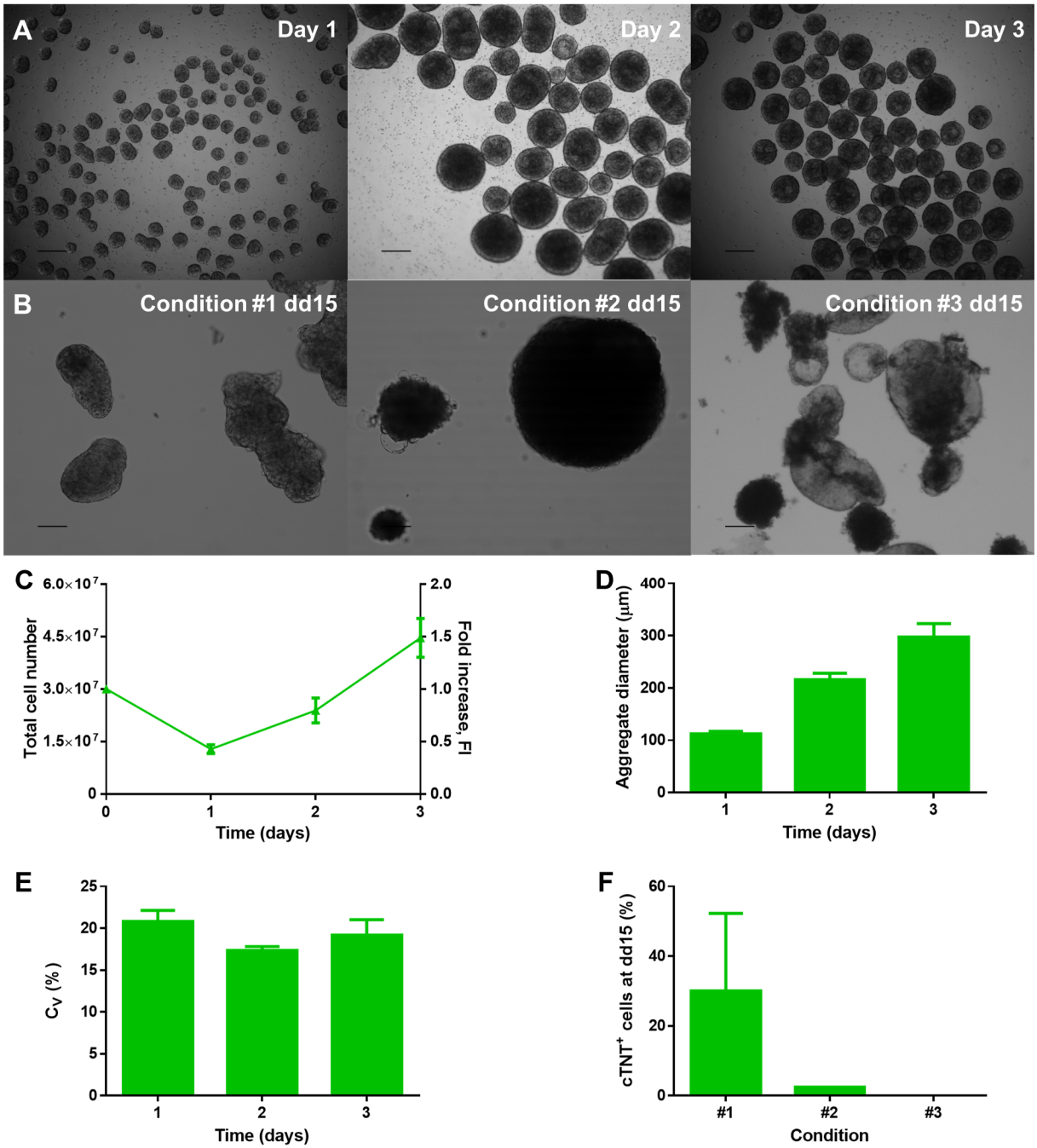

Figure III.4 – Results of the integrated expansion and differentiation of Gibco hiPSCs in the PBS MINI 0.1 bioreactor. At day 0, the reactors were inoculated with 3.0 × 10^7 cells (5.0 × 10^5 cells·mL^{-1}) and starting from 72 h post-inoculation, differentiation was performed according to the respective condition. **A-B** Representative images of cell aggregates harvested from the bioreactor, analysed through brightfield microscopy at **A** days 1, 2 and 3 of expansion (scale bars = 250 µm) and **B** differentiation day (dd) 15 for conditions #1 through #3 (scale bars = 100 µm). **C** Growth kinetics of the cells throughout expansion, in terms of total cell number and fold increase. **D-E** Aggregate size dynamics of the cells, in terms of **D** average aggregate diameter and **E** coefficient of variation. **F** Flow cytometry analysis of cells harvested from the bioreactor after 3 days of expansion and 15 days of differentiation in the PBS MINI 0.1 bioreactor. The cells were analysed for cardiac specific marker cTNT. Five different replicates (n = 5) were analysed for the growth and aggregate kinetics and three different replicates (n = 3) for flow cytometry of condition #1. In these cases, the results are shown as mean ± SEM. One sample (n = 1) was analysed for all other results.

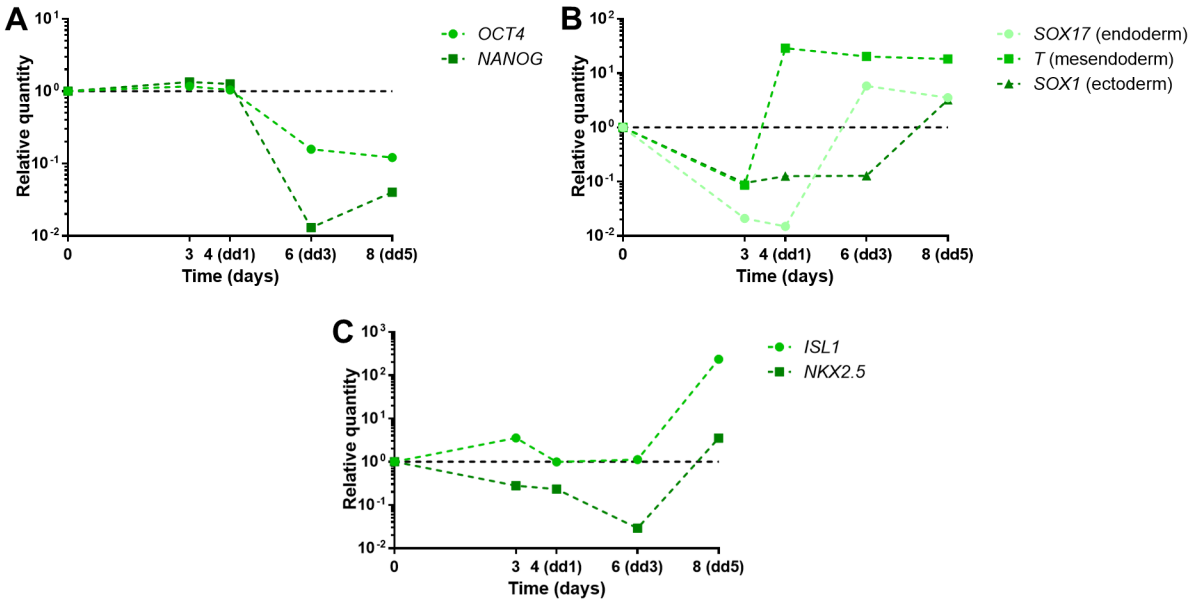

Figure III.5 – qRT-PCR analysis of cells prior to (day 0) and following (day 3) expansion, and at differentiation days (dd) 1, 3 and 5 in the PBS MINI 0.1 bioreactor. The cells were tested for **A** pluripotency (*OCT4* and *NANOG*), **B** germ layer (*SOX1*, *T/BRACHYURY* and *SOX17*, representing ectoderm, mesendoderm and endoderm, respectively) and **C** cardiac (*ISL1* and *NKX2.5*) marker expression. RNA levels are relative to expression of *GAPDH* and to day 0 and were computed as $2^{-\Delta\Delta CT}$.

(Halloin et al. 2019). We compared both protocols for differentiation of hiPSCs as aggregates in culture plates and found that the GiWi$_{cont}$ protocol could increase cardiac differentiation efficiency over 3-fold in comparison to the traditional protocol (Figure III.1). In fact, the continuous WNT control may avoid the differentiation of mesendodermal cells into a wide variety of downstream lineages, instead directing them towards cardiac mesoderm. These “cardiac-primed” cells can then generate cardiomyocytes with a notably increased efficiency in comparison to a general primitive streak-like population (Halloin et al. 2019).

A 3-day expansion phase, prior to differentiation, was established based on a previous report, and an aggregate diameter close to the described as optimal (289 ± 12 µm) was also targeted (Branco et al. 2019). However, our previous work with expansion of the used cell line in the VWBR led to the generation of aggregates with an average diameter of 190 ± 9 µm after 3 days of expansion. We opted to increase the inoculation density to 5.0 × 10^5 cells·mL^{-1}, as well as to supplement the culture medium with Pluronic F-68, a known shear-protecting agent (Tharmalingam et al. 2008, Manstein et al. 2021), in order to attempt to increase the average aggregate size to about 300 µm. hiPSCs in static culture supplemented with Pluronic F-68 maintained the expression of pluripotency markers on a range of concentration up to 0.20% (Figure III.2).

It was then necessary to assay if Pluronic F-68 could have a positive impact on cardiac differentiation (Figure III.3). Furthermore, we compared different expansion culture media (E8 or mTeSR1) and different CHIR concentrations. Finally, the effect of static vs dynamic conditions was also tested. mTeSR1 outranked E8 in almost every condition. While the use of E8 would be advantageous due to being xeno-free, the differentiation was also performed with a medium containing animal-derived components (RPMI/B27). As such, at this initial stage of optimisation of cardiac differentiation, mTeSR1

was selected as the expansion medium. Nevertheless, as a xeno-free alternative to mTeSR1, TeSR2 could have been selected. Static differentiation of mTeSR1-expanded hiPSCs was not very dependent on CHIR concentration at the tested range. Conversely, dynamic differentiation only showed promising results with 5 µM CHIR. Dynamic cultures lead to a more homogeneous cell culture microenvironment, avoiding the formation of gradients of nutrients, growth factors or other molecules. It is then expected that the cells are exposed to a higher local CHIR concentration in a dynamic environment. This higher local CHIR concentration may have caused the abnormal cell aggregation. In this condition, Pluronic F-68 did not present apparent inhibition of cardiac differentiation, so it was maintained.

Following the initial condition screening, three different protocols for integrated expansion and cardiac differentiation in VWBRs were tested (Figure III.4). The 3-day growth phase could expand the cells 1.5 ± 0.2-fold, and, as expected, a higher inoculation density combined with Pluronic F-68 supplementation could increase the average aggregate diameter, to 298 ± 25 µm. We expected these conditions to be optimal for cardiac differentiation. In fact, the base protocol—the $GiWi_{cont}$ protocol with a 5 µM CHIR concentration—could generate up to 73.3% cardiomyocytes. However, the other two bioreactor runs were less successful, with a global average of 30 ± 22% $cTNT^+$ cells at the end of differentiation. As expected, increasing the CHIR concentration to 11 µM or applying the conventional GiWi protocol seemingly resulted in impaired and non-existent cardiac differentiation, respectively. However, only one replicate was performed for either of these conditions, and more replicates would be required in order to extract meaningful conclusions. All protocols share notable cell disaggregation following IWP-4 supplementation, leading to an average 80% cell loss in comparison to the inoculum. During their *in vivo* specification, cardiac-generating cells deriving from the primitive streak undergo an epithelial-to-mesenchymal transition, acquiring a migratory profile (Buijtendijk et al. 2020). A similar change in cellular characteristics *in vitro* may be responsible for this cell disaggregation. Nevertheless, this protocol will have to be optimised in order to minimise this excessive cell loss, as this greatly impairs the potential of clinical-scale generation of cardiomyocytes. To improve cell survival, reduction of the shear stress at this stage (lower agitation speeds) or medium supplementation with molecules such as ROCK inhibitors could be explored. As this effect was observed following supplementation with IWP-4, independently of its timing (addition at day 1 or 3), its concentration could be varied or alternative WNT inhibitors (such as IWP-2 (Lian et al. 2012, Kempf et al. 2014), IWR-1 (Dahlmann et al. 2013, Pei et al. 2017, Correia et al. 2018) or WNT-C59 (Burridge et al. 2014, Han et al. 2020)) could be used. As an alternative, following the report that the medium feeding regime throughout expansion may influence the outcome of cardiac differentiation—with aggregates resulting from repeated batch culture failing to differentiate and cyclic perfusion–cultured aggregates resulting in up to 85% cardiomyocytes—a perfusion strategy could also be performed during expansion in the VWBRs in order to attempt to increase cardiac differentiation and to limit cell death (Kempf et al. 2014).

qRT-PCR analysis (Figure III.5) of the $GiWi_{cont}$ protocol with 5 µM CHIR revealed some aspects of a successful cardiac differentiation—mesendodermal induction (upregulation of *T/BRACHYURY* at differentiation day 1) as well as cardiac commitment of at least a part of the cell population (upregulation of *ISL1* and *NKX2.5* at differentiation day 5). Intriguingly, however, although expression of *T/BRACHYURY* is expected to decrease following its initial spike as the cells commit to specific

mesendodermal lineages (Lian et al. 2012, Kempf et al. 2014, Laco et al. 2020), in this case, it remained constant until day 5 of differentiation. This suggests some of the cells remain uncommitted even following WNT inhibition, which might indicate some priming towards other mesodermal lineages. Also unexpectedly, endodermal marker *SOX17* and ectodermal marker *SOX1* are mildly upregulated at day 3/5 of differentiation, respectively. The presence of non–cardiac primed cells might justify the substantial cell death under cardiomyogenic conditions. Although more biological replicates are required to strengthen any conclusions, together, these data also indicate the need for a change in the expansion and/or initial differentiation phase to more efficiently direct hiPSCs towards cardiac mesoderm. Nevertheless, these results also confirm the cardiac commitment, if partial, of the cell population, by day 5 of differentiation.

III.5. Conclusions

CVDs present a major socioeconomic burden to society, with a lack of efficient answers to them. While the solution might lie in hiPSC-derived cardiomyocytes, methods for their scalable and reproducible bioproduction are required. While bioreactors are advantageous due to providing a 3D environment compatible with bioprocess monitoring and control, the stirred tank models are optimised for traditional bioproducts where the quality of the cells is not the major concern. The novel agitation system of the VWBRs aims at mitigating shear-induced negative effects on cell growth, allowing for the culture of shear-sensitive cells such as hiPSCs. Furthermore, the disposable vessels of this bioreactor system present an advantage for clinical applications due to the minimised risk of culture contamination. Although substantial optimisation is yet required, this work is the first report of integrated expansion and cardiac differentiation of hiPSCs in VWBRs. It was found that differentiation through continuous WNT control led to more promising results than the traditional GiWi protocol. A maximum of 73.3% $cTNT^+$ cardiomyocytes could be obtained at the end of culture, despite a considerable variation between runs and substantial cell death (averaging 80% of the inoculum). Moreover, the expression of CPC markers at day 5 of differentiation was observed by qRT-PCR. We conclude that optimisation of the culture parameters is necessary envisaging the development of a robust bioprocess. In particular, different culture medium feeding regimes during the expansion phase should be evaluated as well as different small molecule (e.g., CHIR) concentrations and the use of xeno-free media throughout the protocol. This work showed the feasibility of using VWBRs for the production of hiPSC-derived cardiomyocytes, paving the way for a scalable bioprocess to enable their clinical use.

III.6. References

Beers, J., D. R. Gulbranson, N. George, L. I. Siniscalchi, J. Jones, J. A. Thomson and G. Chen (2012). Passaging and colony expansion of human pluripotent stem cells by enzyme-free dissociation in chemically defined culture conditions. *Nat Protoc* **7**(11): 2029-2040.

Borys, B. S., T. Dang, T. So, L. Rohani, T. Revay, T. Walsh, M. Thompson, B. Argiropoulos, D. E. Rancourt, S. Jung, Y. Hashimura, B. Lee and M. S. Kallos (2021). Overcoming bioprocess

bottlenecks in the large-scale expansion of high-quality hiPSC aggregates in vertical-wheel stirred suspension bioreactors. *Stem Cell Res Ther* **12**(1): 55.

Borys, B. S., T. So, J. Colter, T. Dang, E. L. Roberts, T. Revay, L. Larijani, R. Krawetz, I. Lewis, B. Argiropoulos, D. E. Rancourt, S. Jung, Y. Hashimura, B. Lee and M. S. Kallos (2020). Optimized serial expansion of human induced pluripotent stem cells using low-density inoculation to generate clinically relevant quantities in vertical-wheel bioreactors. *Stem Cells Transl Med* **9**(9): 1036-1052.

Branco, M. A., J. P. Cotovio, C. A. V. Rodrigues, S. H. Vaz, T. G. Fernandes, L. M. Moreira, J. M. S. Cabral and M. M. Diogo (2019). Transcriptomic analysis of 3D Cardiac Differentiation of Human Induced Pluripotent Stem Cells Reveals Faster Cardiomyocyte Maturation Compared to 2D Culture. *Sci Rep* **9**(1): 9229.

Bu, L., X. Jiang, S. Martin-Puig, L. Caron, S. Zhu, Y. Shao, D. J. Roberts, P. L. Huang, I. J. Domian and K. R. Chien (2009). Human ISL1 heart progenitors generate diverse multipotent cardiovascular cell lineages. *Nature* **460**(7251): 113-117.

Buijtendijk, M. F. J., P. Barnett and M. J. B. van den Hoff (2020). Development of the human heart. *Am J Med Genet C Semin Med Genet* **184**(1): 7-22.

Burridge, P. W., E. Matsa, P. Shukla, Z. C. Lin, J. M. Churko, A. D. Ebert, F. Lan, S. Diecke, B. Huber, N. M. Mordwinkin, J. R. Plews, O. J. Abilez, B. Cui, J. D. Gold and J. C. Wu (2014). Chemically defined generation of human cardiomyocytes. *Nat Methods* **11**(8): 855-860.

Cai, C.-L., X. Liang, Y. Shi, P.-H. Chu, S. L. Pfaff, J. Chen and S. Evans (2003). Isl1 identifies a cardiac progenitor population that proliferates prior to differentiation and contributes a majority of cells to the heart. *Developmental Cell* **5**(6): 877-889.

Correia, C., A. Koshkin, P. Duarte, D. Hu, M. Carido, M. J. Sebastiao, P. Gomes-Alves, D. A. Elliott, I. J. Domian, A. P. Teixeira, P. M. Alves and M. Serra (2018). 3D aggregate culture improves metabolic maturation of human pluripotent stem cell derived cardiomyocytes. *Biotechnol Bioeng* **115**(3): 630-644.

Croughan, M. S., D. Giroux, D. Fang and B. Lee (2016). Novel Single-Use Bioreactors for Scale-Up of Anchorage-Dependent Cell Manufacturing for Cell Therapies *Stem Cell Manufacturing*. C. L. d. Silva, L. G. Chase and M. M. Diogo. Cambridge, Elsevier**:** 105-139.

Dahlmann, J., G. Kensah, H. Kempf, D. Skvorc, A. Gawol, D. A. Elliott, G. Drager, R. Zweigerdt, U. Martin and I. Gruh (2013). The use of agarose microwells for scalable embryoid body formation and cardiac differentiation of human and murine pluripotent stem cells. *Biomaterials* **34**(10): 2463-2471.

de Almeida Fuzeta, M., N. Bernardes, F. D. Oliveira, A. C. Costa, A. Fernandes-Platzgummer, J. P. Farinha, C. A. V. Rodrigues, S. Jung, R. J. Tseng, W. Milligan, B. Lee, M. Castanho, D. Gaspar, J. M. S. Cabral and C. L. da Silva (2020). Scalable Production of Human Mesenchymal Stromal Cell-Derived Extracellular Vesicles Under Serum-/Xeno-Free Conditions in a Microcarrier-Based Bioreactor Culture System. *Front Cell Dev Biol* **8**: 553444.

de Sousa Pinto, D., C. Bandeiras, M. de Almeida Fuzeta, C. A. V. Rodrigues, S. Jung, Y. Hashimura, R. J. Tseng, W. Milligan, B. Lee, F. C. Ferreira, C. Lobato da Silva and J. M. S. Cabral (2019). Scalable Manufacturing of Human Mesenchymal Stromal Cells in the Vertical-Wheel Bioreactor System: An Experimental and Economic Approach. *Biotechnol J* **14**(8): e1800716.

Earls, J. K., S. Jin and K. Ye (2013). Mechanobiology of human pluripotent stem cells. *Tissue Eng Part B Rev* **19**(5): 420-430.

Halloin, C., K. Schwanke, W. Lobel, A. Franke, M. Szepes, S. Biswanath, S. Wunderlich, S. Merkert, N. Weber, F. Osten, J. de la Roche, F. Polten, K. Christoph Wollert, T. Kraft, M. Fischer, U. Martin, I. Gruh, H. Kempf and R. Zweigerdt (2019). Continuous WNT Control Enables Advanced hPSC Cardiac Processing and Prognostic Surface Marker Identification in Chemically Defined Suspension Culture. *Stem Cell Reports* **13**(2): 366-379.

Han, Z., Y. Yu, B. Cai, Z. Xu, Z. Bao, Y. Zhang, D. Bamba, W. Ma, X. Gao, Y. Yuan, L. Zhang, M. Yu, S. Liu, G. Yan, M. Jin, Q. Huang, X. Wang, B. Hua, F. Yang, Z. Pan, H. Liang and Y. Liu (2020). YAP/TEAD3 signal mediates cardiac lineage commitment of human-induced pluripotent stem cells. *J Cell Physiol* **235**(3): 2753-2760.

Itzhaki, I., L. Maizels, I. Huber, L. Zwi-Dantsis, O. Caspi, A. Winterstern, O. Feldman, A. Gepstein, G. Arbel, H. Hammerman, M. Boulos and L. Gepstein (2011). Modelling the long QT syndrome with induced pluripotent stem cells. *Nature* **471**(7337): 225-229.

Kempf, H., R. Olmer, C. Kropp, M. Ruckert, M. Jara-Avaca, D. Robles-Diaz, A. Franke, D. A. Elliott, D. Wojciechowski, M. Fischer, A. Roa Lara, G. Kensah, I. Gruh, A. Haverich, U. Martin and R. Zweigerdt (2014). Controlling expansion and cardiomyogenic differentiation of human pluripotent stem cells in scalable suspension culture. *Stem Cell Reports* **3**(6): 1132-1146.

Kropp, C., H. Kempf, C. Halloin, D. Robles-Diaz, A. Franke, T. Scheper, K. Kinast, T. Knorpp, T. O. Joos, A. Haverich, U. Martin, R. Zweigerdt and R. Olmer (2016). Impact of Feeding Strategies on the Scalable Expansion of Human Pluripotent Stem Cells in Single-Use Stirred Tank Bioreactors. *Stem Cells Transl Med* **5**(10): 1289-1301.

Kwok, C. K., Y. Ueda, A. Kadari, K. Gunther, S. Ergun, A. Heron, A. C. Schnitzler, M. Rook and F. Edenhofer (2018). Scalable stirred suspension culture for the generation of billions of human induced pluripotent stem cells using single-use bioreactors. *J Tissue Eng Regen Med* **12**(2): e1076-e1087.

Laco, F., A. T. Lam, T. L. Woo, G. Tong, V. Ho, P. L. Soong, E. Grishina, K. H. Lin, S. Reuveny and S. K. Oh (2020). Selection of human induced pluripotent stem cells lines optimization of cardiomyocytes differentiation in an integrated suspension microcarrier bioreactor. *Stem Cell Res Ther* **11**(1): 118.

Lembong, J., R. Kirian, J. D. Takacs, T. R. Olsen, L. T. Lock, J. A. Rowley and T. Ahsan (2020). Bioreactor Parameters for Microcarrier-Based Human MSC Expansion under Xeno-Free Conditions in a Vertical-Wheel System. *Bioengineering (Basel)* **7**(3): 73.

Lian, X., C. Hsiao, G. Wilson, K. Zhu, L. B. Hazeltine, S. M. Azarin, K. K. Raval, J. Zhang, T. J. Kamp and S. P. Palecek (2012). Robust cardiomyocyte differentiation from human pluripotent stem cells via temporal modulation of canonical Wnt signaling. *Proc Natl Acad Sci U S A* **109**(27): E1848-1857.

Lian, X., J. Zhang, S. M. Azarin, K. Zhu, L. B. Hazeltine, X. Bao, C. Hsiao, T. J. Kamp and S. P. Palecek (2013). Directed cardiomyocyte differentiation from human pluripotent stem cells by modulating Wnt/beta-catenin signaling under fully defined conditions. *Nat Protoc* **8**(1): 162-175.

Manstein, F., K. Ullmann, C. Kropp, C. Halloin, W. Triebert, A. Franke, C. M. Farr, A. Sahabian, A. Haase, Y. Breitkreuz, M. Peitz, O. Brustle, S. Kalies, U. Martin, R. Olmer and R. Zweigerdt (2021).

High density bioprocessing of human pluripotent stem cells by metabolic control and in silico modeling. *Stem Cells Transl Med* **10**(7): 1063-1080.

Pei, F., J. Jiang, S. Bai, H. Cao, L. Tian, Y. Zhao, C. Yang, H. Dong and Y. Ma (2017). Chemical-defined and albumin-free generation of human atrial and ventricular myocytes from human pluripotent stem cells. *Stem Cell Res* **19**: 94-103.

Raven, N., S. Rasche, C. Kuehn, T. Anderlei, W. Klockner, F. Schuster, M. Henquet, D. Bosch, J. Buchs, R. Fischer and S. Schillberg (2015). Scaled-up manufacturing of recombinant antibodies produced by plant cells in a 200-L orbitally-shaken disposable bioreactor. *Biotechnol Bioeng* **112**(2): 308-321.

Rodrigues, C. A., M. M. Diogo, C. L. da Silva and J. M. Cabral (2011). Microcarrier expansion of mouse embryonic stem cell-derived neural stem cells in stirred bioreactors. *Biotechnol Appl Biochem* **58**(4): 231-242.

Rodrigues, C. A. V., T. P. Silva, D. E. S. Nogueira, T. G. Fernandes, Y. Hashimura, R. Wesselschmidt, M. M. Diogo, B. Lee and J. M. S. Cabral (2018). Scalable culture of human induced pluripotent cells on microcarriers under xeno-free conditions using single-use vertical-wheel (TM) bioreactors. *Journal of Chemical Technology and Biotechnology* **93**(12): 3597-3606.

Rowe, R. G. and G. Q. Daley (2019). Induced pluripotent stem cells in disease modelling and drug discovery. *Nat Rev Genet*.

Rueden, C. T., J. Schindelin, M. C. Hiner, B. E. DeZonia, A. E. Walter, E. T. Arena and K. W. Eliceiri (2017). ImageJ2: ImageJ for the next generation of scientific image data. *BMC Bioinformatics* **18**(1): 529.

Sayed, N., C. Liu and J. C. Wu (2016). Translation of Human-Induced Pluripotent Stem Cells: From Clinical Trial in a Dish to Precision Medicine. *J Am Coll Cardiol* **67**(18): 2161-2176.

Schindelin, J., I. Arganda-Carreras, E. Frise, V. Kaynig, M. Longair, T. Pietzsch, S. Preibisch, C. Rueden, S. Saalfeld, B. Schmid, J. Y. Tinevez, D. J. White, V. Hartenstein, K. Eliceiri, P. Tomancak and A. Cardona (2012). Fiji: an open-source platform for biological-image analysis. *Nat Methods* **9**(7): 676-682.

Schmideder, A. and D. Weuster-Botz (2017). High-performance recombinant protein production with Escherichia coli in continuously operated cascades of stirred-tank reactors. *J Ind Microbiol Biotechnol* **44**(7): 1021-1029.

Shi, Y., H. Inoue, J. C. Wu and S. Yamanaka (2017). Induced pluripotent stem cell technology: a decade of progress. *Nat Rev Drug Discov* **16**(2): 115-130.

Silva, T. P., R. Sousa-Luis, T. G. Fernandes, E. P. Bekman, C. A. V. Rodrigues, S. H. Vaz, L. M. Moreira, Y. Hashimura, S. Jung, B. Lee, M. Carmo-Fonseca and J. M. S. Cabral (2021). Transcriptome profiling of human pluripotent stem cell-derived cerebellar organoids reveals faster commitment under dynamic conditions. *Biotechnol Bioeng* **118**(7): 2781-2803.

Sousa, M. F., M. M. Silva, D. Giroux, Y. Hashimura, R. Wesselschmidt, B. Lee, A. Roldao, M. J. Carrondo, P. M. Alves and M. Serra (2015). Production of oncolytic adenovirus and human mesenchymal stem cells in a single-use, Vertical-Wheel bioreactor system: Impact of bioreactor design on performance of microcarrier-based cell culture processes. *Biotechnol Prog* **31**(6): 1600-1612.

Stolberg, S. and K. E. McCloskey (2009). Can shear stress direct stem cell fate? *Biotechnol Prog* **25**(1): 10-19.

Takahashi, K., K. Tanabe, M. Ohnuki, M. Narita, T. Ichisaka, K. Tomoda and S. Yamanaka (2007). Induction of pluripotent stem cells from adult human fibroblasts by defined factors. *Cell* **131**(5): 861-872.

Tharmalingam, T., H. Ghebeh, T. Wuerz and M. Butler (2008). Pluronic enhances the robustness and reduces the cell attachment of mammalian cells. *Mol Biotechnol* **39**(2): 167-177.

van Lier, F. L., E. J. van den End, C. D. de Gooijer, J. M. Vlak and J. Tramper (1990). Continuous production of baculovirus in a cascade of insect-cell reactors. *Appl Microbiol Biotechnol* **33**(1): 43-47.

Velez-Suberbie, M. L., R. D. Tarrant, A. S. Tait, D. I. Spencer and D. G. Bracewell (2013). Impact of aeration strategy on CHO cell performance during antibody production. *Biotechnol Prog* **29**(1): 116-126.

Virani, S. S., A. Alonso, H. J. Aparicio, E. J. Benjamin, M. S. Bittencourt, C. W. Callaway, A. P. Carson, A. M. Chamberlain, S. Cheng, F. N. Delling, M. S. V. Elkind, K. R. Evenson, J. F. Ferguson, D. K. Gupta, S. S. Khan, B. M. Kissela, K. L. Knutson, C. D. Lee, T. T. Lewis, J. Liu, M. S. Loop, P. L. Lutsey, J. Ma, J. Mackey, S. S. Martin, D. B. Matchar, M. E. Mussolino, S. D. Navaneethan, A. M. Perak, G. A. Roth, Z. Samad, G. M. Satou, E. B. Schroeder, S. H. Shah, C. M. Shay, A. Stokes, L. B. VanWagner, N. Y. Wang, C. W. Tsao, E. American Heart Association Council on, C. Prevention Statistics and S. Stroke Statistics (2021). Heart Disease and Stroke Statistics-2021 Update: A Report From the American Heart Association. *Circulation* **143**(8): e254-e743.

Yu, J., M. A. Vodyanik, K. Smuga-Otto, J. Antosiewicz-Bourget, J. L. Frane, S. Tian, J. Nie, G. A. Jonsdottir, V. Ruotti, R. Stewart, Slukvin, II and J. A. Thomson (2007). Induced pluripotent stem cell lines derived from human somatic cells. *Science* **318**(5858): 1917-1920.

Yuan, X., A. C. Tsai, I. Farrance, J. Rowley and T. Ma (2018). Aggregation of Culture Expanded Human Mesenchymal Stem Cells in Microcarrier-based Bioreactor. *Biochem Eng J* **131**: 39-46.

Zweigerdt, R. (2009). Large scale production of stem cells and their derivatives. *Adv Biochem Eng Biotechnol* **114**: 201-235.

CHAPTER IV.

CHARACTERISATION OF THE OXYGEN MASS TRANSFER IN VERTICAL-WHEEL BIOREACTORS THROUGH COMPUTATIONAL FLUID DYNAMICS

IV.1. Introduction

The discovery and isolation of stem cells marked a major breakthrough for medicine. Their ability to self-renew and to differentiate allow for the generation of various cell types *in vitro* and on demand. hPSCs are particularly promising due to their potential to generate all types of cells of the body. While the use of hESCs is limited by ethical constraints surrounding the destruction of human embryos (Matthews and Morali 2020), hiPSCs (Takahashi et al. 2007, Yu et al. 2007) are generated from somatic cells, not only avoiding those ethical issues, but also allowing a rejection-free and/or precision medicine approach when using the patients' own cells (Sayed et al. 2016, Shi et al. 2017).

Naturally, using hiPSCs for applications such as Regenerative Medicine, drug screening or disease modelling will require high numbers of these cells, possibly 10^9 (Zweigerdt 2009). Obtaining these high numbers of cells will require scalable systems capable of supporting their expansion. Bioreactors have been regarded as promising platforms for hiPSC expansion and differentiation (Kropp et al. 2016, Kwok et al. 2018, Halloin et al. 2019) due to providing a 3D environment, compatible with monitoring and control, as well as distinct feeding medium strategies. However, STBRs were designed for traditional biological applications, where the cells are not the final product. In STBRs, the shear stress close to the impeller is considerable and may damage shear-sensitive cells, such as hiPSCs (Stolberg and McCloskey 2009, Earls et al. 2013), while stagnated zones far from the influence of the impeller may also be observed.

The shift in paradigm from cells as a factory to cells as a product has necessitated the development of novel bioreactor systems with more gentle and efficient agitation mechanisms. The VWBRs (from PBS Biotech) employ a large vertical impeller, which combination of radial and axial mixing, along with the U-shaped bottom of the vessel, allows for efficient cell suspension with reduced power input (Croughan et al. 2016). Furthermore, these bioreactors are available from bench scale (starting from 100 mL) up to production scale (with a maximum volume of 80 L). These advantages have already led to the use of the VWBR for culture of hMSCs (Sousa et al. 2015, Yuan et al. 2018, de Sousa Pinto et al. 2019, de Almeida Fuzeta et al. 2020, Lembong et al. 2020) and hiPSCs (Rodrigues et al. 2018, Borys et al. 2020, Borys et al. 2021). However, due to the relative recency of the VWBRs, they are not yet fully characterised. As such, scaling up the culture might require a trial-and-error approach, wasting time and resources with each reoptimisation at a new scale. Oxygen transfer, in particular, is a concern, as the increase in scale may be associated with a need for sparging in order to satisfy the oxygen demand of the cells.

CFD is a powerful tool, which allows to model complex bioreactor geometries under a variety of operational conditions. Furthermore, due to the discretisation (i.e., division into finite elements) of the system, the desired data (e.g., liquid velocity or oxygen concentration profiled) can be obtained locally, allowing for a more thorough understanding of the behaviour inside the bioreactor. CFD can, thus, be applied to characterise a bioreactor at various scales, facilitating the development of criteria for scaling up the culture, greatly reducing the required optimisation experiments.

This work aimed at characterising the VWBR in terms of oxygen mass transfer, in order to understand if cell culture at high densities might be limited by oxygen. A model was developed for the

100 mL VWBR and the volumetric oxygen mass transfer coefficient (k_La) was found to be in agreement with experimental data for agitation speeds between 10 and 40 rpm. The overarching goal, a characterisation of oxygen transfer at higher scales, was not yet achieved, but the implementation of the 100 mL bioreactor model herein developed at the 500 mL scale and beyond will impart critical information for the development of manufacturing scale bioprocesses for hiPSC expansion and differentiation.

IV.2. Materials and methods

IV.2.1. CFD model

In this work, the PBS MINI 0.1 MAG VWBR was characterised using CFD. The 3D model of the vessel, kindly provided by PBS Biotech, was meshed using OpenFOAM 8 (The OpenFOAM Foundation, UK). The mesh was comprised of 1.15×10^6 cells. The CFD simulations were also performed in OpenFOAM 8. No-slip boundary conditions were defined at the vessel walls, and a partial slip (20%) condition was set for the liquid surface. Impeller rotation was simulated by setting a moving reference frame. The system was considered to be isothermal (21 °C) and isobaric (1 atm), and Henry's law was considered to be applicable. The properties of the medium were set as those of pure water. The interface was set in equilibrium and saturated in oxygen, with the oxygen mass transfer limited by diffusion (two-film theory (Doran 1995)).

The flux of mass transfer of a component A is described by Fick's law as (Doran 1995)

$$J_A = \frac{N_A}{a} = - D_{AB} \frac{dC_A}{dy} \tag{IV.1}$$

with N_A as the rate of mass transfer, a as the specific area (area of mass transfer/liquid volume), D_{AB} as the diffusivity of A in B, C_A as the concentration of A and y as the distance. The rate of mass transfer at the liquid/gas interface can be written as

$$N_A = k_G a\left(C_{A,G} - C_{A,Gi}\right) = k_L a\left(C_{A,Li} - C_{A,L}\right) \tag{IV.2}$$

with k_G and k_L as the gas phase and liquid phase mass transfer coefficients, $C_{A,G}$ and $C_{A,L}$ as the concentration of A in the bulk gas and the bulk liquid and $C_{A,Gi}$ and $C_{A,Li}$ as the concentration of A in the interface for the gas and for the liquid. This rate may also be expressed considering a global mass transfer coefficient, as well as a global driving force, as

$$N_A = K_G a\left(C_{A,G} - C^*_{A,G}\right) = K_L a\left(C^*_{A,L} - C_{A,L}\right) \tag{IV.3}$$

where K_G and K_L are the global mass transfer coefficients for the gas phase and for the liquid phase, and $C^*_{A,G}$ and $C^*_{A,L}$ are the concentration of A in equilibrium with the liquid phase and with the gas phase. $C^*_{A,L}$ can be obtained through Henry's law (Sander 2015):

$$C^*_{A,L} = H \cdot p_A \tag{IV.4}$$

where H is Henry's law constant for the system at a given temperature and p_A is the partial pressure of A in the gas phase. Since oxygen has limited solubility in water, the resistance to mass transfer is mostly

in the liquid film, and K_L can be approximated to k_L. As such, the oxygen transfer rate (OTR) from the gas phase to the liquid phase can be written as

$$OTR = k_L a\left(C^* - C_L\right) \tag{IV.5}$$

Mass transfer by the modelled turbulence was included as an increase in diffusivity (D_{AB}^t):

$$D_{AB}^{eff} = D_{AB}^m + D_{AB}^t \tag{IV.6}$$

with D_{AB}^{eff} as the effective diffusivity and D_{AB}^m as the molecular diffusivity. The turbulent diffusivity was explicitly computed as (Tominaga and Stathopoulos 2007)

$$D_{AB}^t = \frac{v^t}{Sc^t} \tag{IV.7}$$

with v^t as the turbulent kinematic viscosity and Sc^t as the turbulent Schmidt number (which was considered to be 0.7).

For the simulation, a large eddy simulation (LES) model was used. LES solves the turbulence at large scales, while small scales (of dimensions lower than the smallest cells) are approximated through a turbulence model. LES results in a 3D, time-dependant solution, less computationally expensive than direct numerical simulation. LES relies on spatial filtering of the Navier-Stokes equations, with spatial filtering of a function $f(x_i,t)$ defined as (Revstedt et al. 1998)

$$\overline{f(x_i,t)} = \int_{-\infty}^{+\infty} G\left(x_i - x_i'\right) f\left(x_i',t\right) dx_i' \tag{IV.8}$$

with x as the distance, t as the time and G as a filter function. With this spatial filtering, the Navier-Stokes equations become

$$\frac{\partial \bar{u}_i}{\partial x_i} = 0 \tag{IV.9}$$

for the conservation of mass and

$$\frac{\partial \bar{u}_i}{\partial t} + \bar{u}_j \frac{\partial \bar{u}_i}{\partial x_j} = -\frac{1}{\rho}\frac{\partial \bar{p}}{\partial x_i} + v\frac{\partial}{\partial x_j}\frac{\partial \bar{u}_i}{\partial x_j} - \frac{\partial \tau_{ij}}{\partial x_j} + \bar{F}_i \tag{IV.10}$$

for the conservation of momentum. In these equations, u is the velocity, ρ is the density, p is the pressure and F is a source term. τ_{ij}, the sub-grid scale stress tensor, is computed as

$$\tau_{ij} = \overline{u_i u_j} - \bar{u}_i \bar{u}_j \tag{IV.11}$$

The turbulent scales below the cut-off length (Δ) were modelled using a wall-adapting local eddy-viscosity (WALE) model (Ducros et al. 1998), where the kinematic viscosity is computed as

$$v^t = (C_w \Delta)^2 \frac{\left(S_{ij}^d S_{ij}^d\right)^{\frac{3}{2}}}{\left(\bar{S}_{ij}\bar{S}_{ij}\right)^{\frac{5}{2}} + \left(S_{ij}^d S_{ij}^d\right)^{\frac{5}{4}}} \tag{IV.12}$$

where C_w is a constant (0.325) and where

$$S_{ij}^d = \frac{1}{2}\left(\bar{g}_{ij}^2 + \bar{g}_{ij}^2\right) - \frac{1}{3}\delta_{ij}\bar{g}_{kk}^2 \tag{IV.13}$$

$$\bar{g}_{ij} = \frac{\partial \bar{u}_i}{\partial x_j} \tag{IV.14}$$

$$\bar{g}_{ij}^2 = \bar{g}_{ik}\bar{g}_{kj} \tag{IV.15}$$

$$\bar{S}_{ij} = \frac{1}{2}\left(\frac{\partial \bar{u}_i}{\partial x_j} + \frac{\partial \bar{u}_j}{\partial x_i}\right) \tag{IV.16}$$

with S_{ij}^d as an operator based on the square of $\bar{g}_{ij}$, the gradient velocity tensor; δ_{ij} as the Kronecker delta function and $\bar{S}_{ij}$ as the strain rate tensor of the resolved scales.

The time step was chosen to keep the Courant-Friedrich-Lewy number below 1. Post-processing was performed using ParaView 5.6.3 (Kitware, USA).

To validate the model, the bioreactor was filled with deoxygenated water and the dissolved oxygen concentration was measured with an oxygen sensor. The k_La was estimated with the relation (Scargiali et al. 2010)

$$p_{O_2}(t) = p_{O_2}^{sat}\,(1 - e^{-k_La \cdot t}) \tag{IV.17}$$

with p_{O_2} as the partial oxygen pressure and $p_{O_2}^{sat}$ as the partial oxygen pressure at saturation.

IV.2.2. Sulfite oxidation method

For an initial comparison of the oxygen mass transfer in different agitated vessels, the sulfite oxidation method was used. In the presence of a catalyser (e.g., Cu^{2+} ions), sulfite ions in solution are oxidised to sulfate according to the reaction (Ruchti et al. 1985)

$$SO_3^{2-} + \frac{1}{2}O_2 \longrightarrow SO_4^{2-} \tag{IV.18}$$

This reaction is fast, ensuring the C_L is near-zero, and its velocity is controlled by the OTR from the gas phase to the liquid phase. Under these conditions, and considering Equations IV.5 and IV.18, the OTR becomes

$$OTR = k_La \cdot C^* = -\frac{1}{2}\frac{d[SO_3^{2-}]}{dt} \tag{IV.19}$$

allowing for k_La estimation from the variation in sulfite concentration. This sulfite concentration can be queried by addition to an iodine solution, as sulfite reacts with iodine according to the reaction (Szekeres 1974)

$$SO_3^{2-} + I_2 + H_2O \longrightarrow SO_4^{2-} + 2H^+ + 2I^- \tag{IV.20}$$

The excess iodine is titrated with thiosulfate, through the following reaction:

$$2S_2O_3^{2-} + I_2 \longrightarrow S_4O_6^{2-} + 2I^- \tag{IV.21}$$

The vessels were filled with distilled water (80 mL for the PBS MINI 0.1 and the spinner flasks and 300 mL for the PBS MINI 0.5), and 50 mM of sodium sulfite (Sigma-Aldrich, USA) and 1 mM of copper sulfate (PanReac AppliChem, Spain) were added. Following solubilisation, and at regular intervals (~ 1 h for the first 6 h, after 24 h and, for the PBS MINI 0.5, after 48 h), 1.0 samples were

collected from the bioreactors and immediately added to a mixture of 1.0 mL of iodine/iodide solution (0.1 M; Sigma), 2 mL of 2 N HCl (Thermo Fisher Scientific, USA) and 18.5 mL of distilled water. The excess iodine was titrated with 0.03 M thiosulfate (Honeywell, USA), until the solution, initially brown, was clear.

IV.2.3. Maximum cell density estimation

The rate at which oxygen is consumed by the cells, or the oxygen uptake rate (OUR) is defined as (Doran 1995)

$$OUR = q_{O_2} \cdot X \tag{IV.22}$$

where q_{O_2} is the specific oxygen consumption rate and X is the cell density. The culture becomes limited by oxygen when the rate at which it is consumed by the cells is greater than the rate of its transfer from the gas phase to the medium (OUR > OTR). In these conditions, where all of the oxygen transferred to the medium is immediately consumed by the cells, the dissolved oxygen concentration can be considered to be zero. As such, combining the expressions for the OTR (Equation IV.5) and for the OUR (Equation IV.22), and setting C_L to zero, the maximum cell density before oxygen limitations, X_{max}, becomes:

$$X_{max} = \frac{k_L a \cdot C^*}{q_{O_2}} \tag{IV.23}$$

IV.3. Results

IV.3.1. Initial analysis of oxygen mass transfer in agitated systems

Prior to developing the CFD model, an initial study of the oxygen mass transfer on different agitated systems (PBS MINI 0.1 and 0.5, and 100 mL spinner flasks) was performed through the sulfite oxidation method (Figure IV.1). Amongst the four different systems tested, the $k_L a$ was found to be highest for the baffled spinner flask, followed by the non-baffled spinner flask, the PBS MINI 0.1 and the PBS MINI 0.5. When comparing the k_L, the PBS MINI 0.1 and 0.5 were found to be more efficient than both spinner flask systems.

IV.3.2. Velocity profiles of the VWBR

Envisaging a more thorough understanding of the oxygen mass transfer in the VWBRs, a CFD simulation was performed. Initial studies were performed at the operational conditions used in Chapters II and III – the PBS MINI 0.1 MAG vessels working at 30 rpm. Post-processing analysis was performed after reaching a pseudo-steady state.

Figure IV.2 depicts the modelled velocity field heatmaps in a vertical cross section of the 100 mL VWBR. This velocity analysis indicates both the zones with lower agitation velocity (dark blue), as well as those under higher mixing (red). Expectedly, a higher local velocity (up to 7.0×10^{-2} m·s^{-1}) is

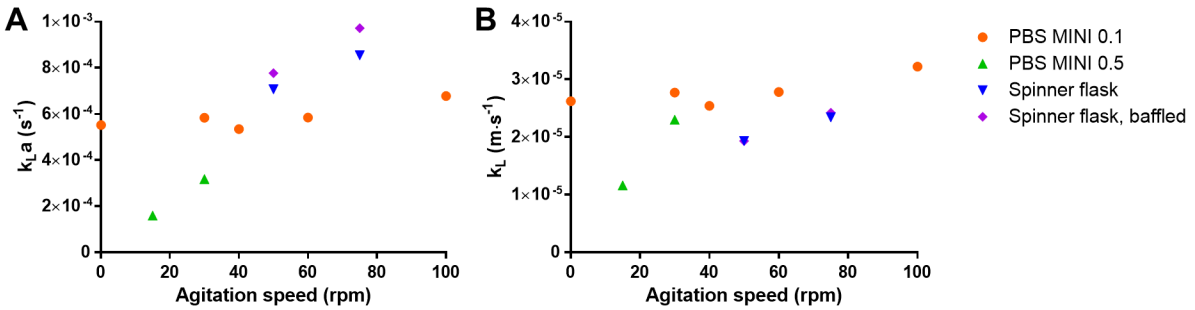

Figure IV.1 – Variation of the average **A** volumetric oxygen mass transfer coefficient (k_La) and **B** oxygen mass transfer coefficient (k_L) with the agitation speed obtained through the sulfite oxidation method for the PBS MINI 0.1, PBS MINI 0.5, and non-baffled and baffled 100 mL spinner flasks.

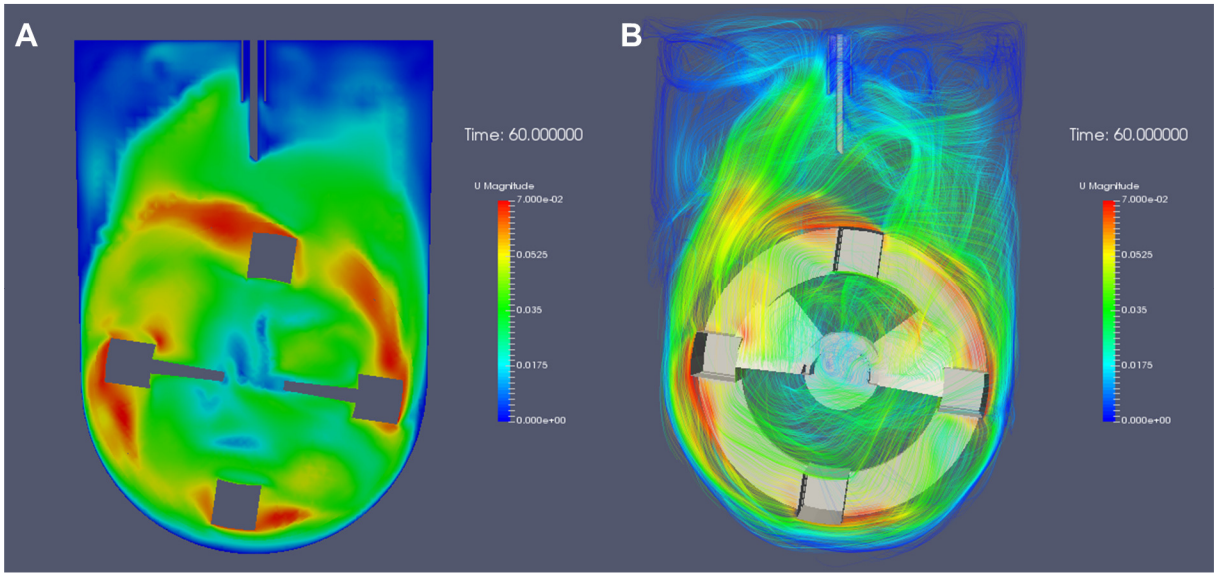

Figure IV.2 – Heatmaps of the velocity field in a vertical cross section the PBS MINI 0.1 MAG vessel **A** without and **B** with tracers.

observed around the outer wheel, as an aftermath of the impeller movement. At the top of the vessel, the velocity is considerably lower, especially in the topmost corners. As such, these areas might be considered dead zones, which can potentially be overcome by not filling the vessel completely. Throughout the remainder of the vessel, the velocity is mostly stable (green areas, with a velocity of about 3.5×10^{-2} $m \cdot s^{-1}$), due to the efficient mixing provided by the large impeller and its unique combination of radial and axial agitation. In fact, as observed in Figure IV.2B, the liquid is pushed by the vertical wheel towards the top-centre of the vessel, ensuring a substantial mixing even in this area.

IV.3.3. Oxygen mass transfer in the VWBR

Following the simulation of the velocity field in the VWBR, the average k_La was estimated for various rotation speeds and compared to experimental data, obtained via oxygen measurement with a sensor (Figure IV.3). The k_La was found to linearly increase with the agitation speed, and the CFD model was able to accurately predict the k_La for a range of agitation speeds from 10 rpm to 40 rpm, with a considerable deviation (~ 19%), among the values tested, only for an agitation of 20 rpm.

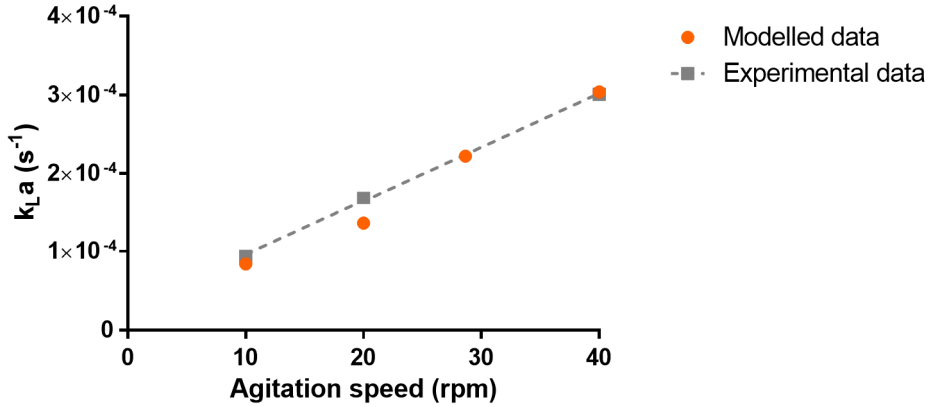

Figure IV.3 – Variation of the average volumetric oxygen mass transfer coefficient (k_La) with the agitation speed and estimations obtained through the CFD model.

The k_La in the PBS MINI 0.1 calculated in this study allows to estimate the maximum density of cells that the system is expected to support before cell growth is limited by oxygen availability (Table IV.1). This estimation was performed using the modelled k_La at 30 rpm, considering 1) bioreactor aeration through the headspace only, with atmospheric air and 2) the medium properties are identical to water. The maximum cell concentration was computed (Equation IV.23) for different specific oxygen consumption rates described in the literature, and was estimated to be among 4.5×10^5 cells·mL^{-1} to 5.0×10^7 cells·mL^{-1}.

Table IV.1 – Estimation of the maximum cell density which can be obtained in the PBS MINI 0.1 bioreactor before oxygen limitations, and parameters used for this calculation.

Parameter	Value	Reference
k_La (s^{-1})	2.2×10^{-4}	This work
H for water/oxygen at 37 °C (mol·m^{-3}·Pa^{-1})	1.1×10^{-5}	Sander (2015)
C^* (mol·m^{-3})	2.3×10^{-1}	Equation IV.4
q_{O_2} (mol·cell^{-1}·s^{-1})	1.0×10^{-18}–1.1×10^{-16}	Varum et al. (2011), Zhang et al. (2012), Turner et al. (2014)
OTR/OUR_{max} (mol·m^{-3}·s^{-1})	5.1×10^{-6}	Equation IV.5
X_{max} (cells·mL^{-1})	4.5×10^5–5.0×10^7	Equation IV.23

IV.4. Discussion

While hiPSCs hold substantial promise for the treatment of various diseases, including CVDs, their potential can only be harnessed if platforms for their reliable expansion at clinical scale are used. While the 100 mL VWBRs have already shown promise for hiPSC expansion (Chapter II) and cardiac

differentiation (Chapter III), the bioproduction of the high numbers of cells required for biomedical use require scale-up to at least 500 mL or 3 L bioreactors. A thorough characterisation of the bioreactor systems at various scales using CFD will allow for the application of evidence-based criteria for this scale-up process.

This work aimed at characterising the VWBRs in terms of oxygen mass transfer. Following the creation and refinement of the mesh, the velocity field inside the bioreactor was simulated (Figure IV.2). The velocity profiles obtained were found to be in concordance with a previous report of hydrodynamic modelling of the PBS MINI 0.1 (Borys et al. 2021). These results showing efficient mixing in 100 mL bioreactor vessel, with higher local velocity trailing the movement of the vertical wheel, as well as minor dead zones in the upper corners of the vessel. The presence of these dead zones could be mitigated or avoided by using lower volumes. In fact, our previous experiments of hiPSC culture in these bioreactors (Chapters II and III) were performed in a 60 mL volume, just enough to fully cover the vertical wheel. However, understanding exactly how this affects the bioreactor hydrodynamics (namely, if there are still any dead zones or if the lower volume leads to more areas with higher local velocity) will require modelling under these conditions. Nevertheless, the combination of radial and axial agitation results in a lemniscate velocity profile (Figure IV.2B), resulting in a better homogeneity in comparison to the purely or mostly axial profile from traditional STBRs. In fact, the velocity profiles of spinner flasks and STBRs present a notorious difference between the local velocity next to the impeller and the bulk of the bioreactor, even when multiple impellers are applied and agitating at high speed (Taghavi et al. 2011, Azargoshasb et al. 2016, Borys et al. 2019). This increased homogeneity is beneficial for routine culture, and especially important for differentiation approaches, where both local molecule/factor concentrations are crucial, as well as a low dispersion of aggregate sizes (Bauwens et al. 2008, Chen et al. 2015).

With an estimation of the hydrodynamic profile in the 100 mL VWBR, the k_La was then estimated by CFD and compared to experimental data. The CFD simulations resulted in a close fit to the experimental data, with only a significant deviation for the 20 rpm stirring speed. The k_La at 30 rpm was estimated at 2.2×10^{-4} s^{-1}. Equivalent volume bioreactors are reported with k_La around 0.1 s^{-1}, however, unlike the PBS MINI vessels, those bioreactors are sparged and measurements were performed at substantially higher stirring (Gill et al. 2008).

The sulfite oxidation method relies on the oxidation of sodium sulfite to sodium sulfate under the presence of a catalyst (such as Cu^{2+}) to compute the k_La of a system (Cooper et al. 1944). While this is a simple protocol, the values of k_La obtained through this method may be overestimated, as such, other, more precise approaches, such as the dynamic method, are preferred (Van't Riet 1979). In fact, a k_La of 5.8×10^{-4} s^{-1} was obtained through the sulfite method for the PBS MINI 0.1 at 30 rpm, a 164% overestimation of this value. Nevertheless, given the lack of information in the literature ascertaining the k_La of non-sparged agitated systems, the sulfite method was applied for an initial analysis of the oxygen mass transfer in the PBS MINI 0.1 (80 mL working volume) and 0.5 (300 mL working volume), as well as baffled and non-baffled 100 mL spinner flasks (80 mL working volume). Under these circumstances, the PBS MINI 0.1 was found to have comparable, albeit lower, k_La to both baffled and non-baffled spinner flasks. Comparison of the k_L reveals an opposite scenario—the highest values for the PBS MINI VWBRs. As such, while the agitation of the PBS MINI 0.1 appears to improve the oxygen mass transfer,

the specific surface area is smaller, leading to an impaired volumetric oxygen transfer. With the increase in scale, from the PBS MINI 0.1 to the PBS MINI 0.5, the specific area, and consequently the k_La, was found to decrease. It is expected that the increased towards higher scales might reduce the k_La even further, as such, the VWBRs starting from the 3 L vessel are sparged.

The value of k_La estimated through CFD was used for an approximation on the maximum cell density the culture could sustain before oxygen limitations. This occurs at the point where the oxygen consumed by the cells (measured through the OUR) is greater than the oxygen transfer from the gaseous phase to the liquid (OTR). Depending on the value used for the specific oxygen consumption rate, the maximum cell concentration was estimated at 4.5×10^5–5.0×10^7 cells·mL^{-1}. hiPSC expansion as aggregates typically results in cell densities of 10^5–10^6 cells·mL^{-1} (Table II.2), as such, oxygen starvation in the PBS MINI 0.1 is a concern. Furthermore, it may help explain our limitations in expanding hiPSCs to over 2.5×10^6 cells·mL^{-1} (Figure II.4). Nevertheless, the q_{O2} values described in the literature for hPSCs are very distinct (with a difference of two orders of magnitude). The rate of oxygen consumption in various mammalian cell types was found to vary mostly between 10^{-18}–10^{-15} mol·cell^{-1}·s^{-1} and to correlate positively with cell size and protein content (Wagner et al. 2011). In fact, q_{O2} values above 10^{-16} mol·cell^{-1}·s^{-1} were generally observed only for highly specialised cells such as cardiomyocytes (Sridharan et al. 2008) and hepatocytes (Foy et al. 1994). As such, hPSCs are expected to have lower oxygen consumption rates, not only due to their small size and complexity, but also their reliance on glycolysis (Vander Heiden et al. 2009, Varum et al. 2011). Using an intermediate value (about 2.5×10^{-17} mol·cell^{-1}·s^{-1} as reported by Zhang et al. (2012)) would result in a calculated maximum cell density of 2.0×10^6 cells·mL^{-1}. A more robust estimation of X_{max} would benefit from q_{O2} measurements for our cells in our expansion conditions. Furthermore, the estimated maximum cell concentration was based on a series of assumptions, including no k_La variation with temperature and water properties for the medium, which may not reflect a real culture scenario. The main advantage of having established a CFD model to describe the bioreactor in terms of oxygen mass transfer is its usability for the characterisation under culture conditions. At a later stage, the cells can also be considered in the model, to provide more realistic results in terms of oxygen transfer in the bioreactor.

The final objective of this work will be the characterisation of oxygen mass transfer in VWBRs at various scales. This characterisation will constitute a powerful tool to guide the scale-up of VWBR culture and, in particular, to predict the bioreactor aeration strategy, The model was already implemented at the 100 mL scale, and allowed to obtain a more intricate knowledge of this bioreactor, laying the ground for studies at the 500 mL scale and beyond.

IV.5. Conclusions

Most studies on hiPSC culture in bioreactors already reported are limited to laboratory scales. Considering the high costs of hiPSC culture media, scale-up to production volumes would ideally be performed with thorough information on the associated differences in the hydrodynamic behaviour of the vessel. While empirical scale-up equations exist for traditional bioreactors, due to the recency of VWBRs, they are not yet sufficiently studied in this regard. This work aimed at developing a CFD model which could characterise the VWBR in terms of oxygen mass transfer, specifically the k_La, at various

scales. After establishment and optimisation of the model, for the PBS MINI 0.1, the k_La was found to be in agreement with experimental data, and estimated at 2.2×10^{-4} s^{-1} for a 30 rpm agitation speed. This successful implementation of the model at the 100 mL scale will ease the model implementation at higher scales, allowing for a more detailed knowledge of the differences in oxygen mass transfer with the scale-up and, prospectively, for the development of correlations which may allow for a scale-up of the culture with minimal trial-and-error and, consequently, with minimal losses of time and reagents for optimisation.

IV.6. References

Azargoshasb, H., S. M. Mousavi, O. Jamialahmadi, S. A. Shojaosadati and S. B. Mousavi (2016). Experiments and a three-phase computational fluid dynamics (CFD) simulation coupled with population balance equations of a stirred tank bioreactor for high cell density cultivation. *The Canadian Journal of Chemical Engineering* **94**(1): 20-32.

Bauwens, C. L., R. Peerani, S. Niebruegge, K. A. Woodhouse, E. Kumacheva, M. Husain and P. W. Zandstra (2008). Control of human embryonic stem cell colony and aggregate size heterogeneity influences differentiation trajectories. *Stem Cells* **26**(9): 2300-2310.

Borys, B. S., T. Dang, T. So, L. Rohani, T. Revay, T. Walsh, M. Thompson, B. Argiropoulos, D. E. Rancourt, S. Jung, Y. Hashimura, B. Lee and M. S. Kallos (2021). Overcoming bioprocess bottlenecks in the large-scale expansion of high-quality hiPSC aggregates in vertical-wheel stirred suspension bioreactors. *Stem Cell Res Ther* **12**(1): 55.

Borys, B. S., A. Le, E. L. Roberts, T. Dang, L. Rohani, C. Y. Hsu, A. A. Wyma, D. E. Rancourt, I. D. Gates and M. S. Kallos (2019). Using computational fluid dynamics (CFD) modeling to understand murine embryonic stem cell aggregate size and pluripotency distributions in stirred suspension bioreactors. *J Biotechnol* **304**: 16-27.

Borys, B. S., T. So, J. Colter, T. Dang, E. L. Roberts, T. Revay, L. Larijani, R. Krawetz, I. Lewis, B. Argiropoulos, D. E. Rancourt, S. Jung, Y. Hashimura, B. Lee and M. S. Kallos (2020). Optimized serial expansion of human induced pluripotent stem cells using low-density inoculation to generate clinically relevant quantities in vertical-wheel bioreactors. *Stem Cells Transl Med* **9**(9): 1036-1052.

Chen, V. C., J. Ye, P. Shukla, G. Hua, D. Chen, Z. Lin, J. C. Liu, J. Chai, J. Gold, J. Wu, D. Hsu and L. A. Couture (2015). Development of a scalable suspension culture for cardiac differentiation from human pluripotent stem cells. *Stem Cell Res* **15**(2): 365-375.

Cooper, C. M., G. A. Fernstrom and S. A. Miller (1944). Performance of Agitated Gas-Liquid Contactors. *Ind Eng Chem* **36**: 504.

Croughan, M. S., D. Giroux, D. Fang and B. Lee (2016). Novel Single-Use Bioreactors for Scale-Up of Anchorage-Dependent Cell Manufacturing for Cell Therapies *Stem Cell Manufacturing*. C. L. d. Silva, L. G. Chase and M. M. Diogo. Cambridge, Elsevier**:** 105-139.

de Almeida Fuzeta, M., N. Bernardes, F. D. Oliveira, A. C. Costa, A. Fernandes-Platzgummer, J. P. Farinha, C. A. V. Rodrigues, S. Jung, R. J. Tseng, W. Milligan, B. Lee, M. Castanho, D. Gaspar, J. M. S. Cabral and C. L. da Silva (2020). Scalable Production of Human Mesenchymal Stromal Cell-

Derived Extracellular Vesicles Under Serum-/Xeno-Free Conditions in a Microcarrier-Based Bioreactor Culture System. *Front Cell Dev Biol* **8**: 553444.

de Sousa Pinto, D., C. Bandeiras, M. de Almeida Fuzeta, C. A. V. Rodrigues, S. Jung, Y. Hashimura, R. J. Tseng, W. Milligan, B. Lee, F. C. Ferreira, C. Lobato da Silva and J. M. S. Cabral (2019). Scalable Manufacturing of Human Mesenchymal Stromal Cells in the Vertical-Wheel Bioreactor System: An Experimental and Economic Approach. *Biotechnol J* **14**(8): e1800716.

Doran, P. M. (1995). Mass transfer. *Bioprocess Engineering Priniciples*.

Ducros, F., F. Nicoud and T. Poinsot (1998). Wall-adapting local eddy-viscosity models for simulations in complex geometries. *Numerical Methods for Fluid Dynamics VI*: 293-299.

Earls, J. K., S. Jin and K. Ye (2013). Mechanobiology of human pluripotent stem cells. *Tissue Eng Part B Rev* **19**(5): 420-430.

Foy, B. D., A. Rotem, M. Toner, R. G. Tompkins and M. L. Yarmush (1994). A device to measure the oxygen uptake rate of attached cells: importance in bioartificial organ design. *Cell Transplant* **3**(6): 515-527.

Gill, N. K., M. Appleton, F. Baganz and G. J. Lye (2008). Design and characterisation of a miniature stirred bioreactor system for parallel microbial fermentations. *Biochemical Engineering Journal* **39**(1): 164-176.

Halloin, C., K. Schwanke, W. Lobel, A. Franke, M. Szepes, S. Biswanath, S. Wunderlich, S. Merkert, N. Weber, F. Osten, J. de la Roche, F. Polten, K. Christoph Wollert, T. Kraft, M. Fischer, U. Martin, I. Gruh, H. Kempf and R. Zweigerdt (2019). Continuous WNT Control Enables Advanced hPSC Cardiac Processing and Prognostic Surface Marker Identification in Chemically Defined Suspension Culture. *Stem Cell Reports* **13**(2): 366-379.

Kropp, C., H. Kempf, C. Halloin, D. Robles-Diaz, A. Franke, T. Scheper, K. Kinast, T. Knorpp, T. O. Joos, A. Haverich, U. Martin, R. Zweigerdt and R. Olmer (2016). Impact of Feeding Strategies on the Scalable Expansion of Human Pluripotent Stem Cells in Single-Use Stirred Tank Bioreactors. *Stem Cells Transl Med* **5**(10): 1289-1301.

Kwok, C. K., Y. Ueda, A. Kadari, K. Gunther, S. Ergun, A. Heron, A. C. Schnitzler, M. Rook and F. Edenhofer (2018). Scalable stirred suspension culture for the generation of billions of human induced pluripotent stem cells using single-use bioreactors. *J Tissue Eng Regen Med* **12**(2): e1076-e1087.

Lembong, J., R. Kirian, J. D. Takacs, T. R. Olsen, L. T. Lock, J. A. Rowley and T. Ahsan (2020). Bioreactor Parameters for Microcarrier-Based Human MSC Expansion under Xeno-Free Conditions in a Vertical-Wheel System. *Bioengineering (Basel)* **7**(3): 73.

Revstedt, J., L. Fuchs and C. Trägårdh (1998). Large eddy simulations of the turbulent flow in a stirred reactor. *Chemical Engineering Science* **53**(24): 4041-4053.

Rodrigues, C. A. V., T. P. Silva, D. E. S. Nogueira, T. G. Fernandes, Y. Hashimura, R. Wesselschmidt, M. M. Diogo, B. Lee and J. M. S. Cabral (2018). Scalable culture of human induced pluripotent cells on microcarriers under xeno-free conditions using single-use vertical-wheel (TM) bioreactors. *Journal of Chemical Technology and Biotechnology* **93**(12): 3597-3606.

Ruchti, G., I. Dunn, J. Bourne and U. Von Stockar (1985). Practical guidelines for the determination of oxygen transfer coefficients (KLa) with the sulfite oxidation method. *The Chemical Engineering Journal* **30**(1): 29-38.

Sander, R. (2015). Compilation of Henry's law constants (version 4.0) for water as solvent. *Atmos. Chem. Phys.* **15**(8): 4399-4981.

Sayed, N., C. Liu and J. C. Wu (2016). Translation of Human-Induced Pluripotent Stem Cells: From Clinical Trial in a Dish to Precision Medicine. *J Am Coll Cardiol* **67**(18): 2161-2176.

Scargiali, F., A. Busciglio, F. Grisafi and A. Brucato (2010). Simplified dynamic pressure method for kLa measurement in aerated bioreactors. *Biochemical Engineering Journal* **49**(2): 165-172.

Shi, Y., H. Inoue, J. C. Wu and S. Yamanaka (2017). Induced pluripotent stem cell technology: a decade of progress. *Nat Rev Drug Discov* **16**(2): 115-130.

Sousa, M. F., M. M. Silva, D. Giroux, Y. Hashimura, R. Wesselschmidt, B. Lee, A. Roldao, M. J. Carrondo, P. M. Alves and M. Serra (2015). Production of oncolytic adenovirus and human mesenchymal stem cells in a single-use, Vertical-Wheel bioreactor system: Impact of bioreactor design on performance of microcarrier-based cell culture processes. *Biotechnol Prog* **31**(6): 1600-1612.

Sridharan, V., J. Guichard, C. Y. Li, R. Muise-Helmericks, C. C. Beeson and G. L. Wright (2008). O(2)-sensing signal cascade: clamping of O(2) respiration, reduced ATP utilization, and inducible fumarate respiration. *Am J Physiol Cell Physiol* **295**(1): C29-37.

Stolberg, S. and K. E. McCloskey (2009). Can shear stress direct stem cell fate? *Biotechnol Prog* **25**(1): 10-19.

Szekeres, L. (1974). Analytical chemistry of the sulphur acids. *Talanta* **21**(1): 1-44.

Taghavi, M., R. Zadghaffari, J. Moghaddas and Y. Moghaddas (2011). Experimental and CFD investigation of power consumption in a dual Rushton turbine stirred tank. *Chemical Engineering Research and Design* **89**(3): 280-290.

Tominaga, Y. and T. Stathopoulos (2007). Turbulent Schmidt numbers for CFD analysis with various types of flowfield. *Atmospheric Environment* **41**(37): 8091-8099.

Turner, J., L. E. Quek, D. Titmarsh, J. O. Kromer, L. P. Kao, L. Nielsen, E. Wolvetang and J. Cooper-White (2014). Metabolic profiling and flux analysis of MEL-2 human embryonic stem cells during exponential growth at physiological and atmospheric oxygen concentrations. *PLoS One* **9**(11): e112757.

Van't Riet, K. (1979). Review of measuring methods and results in nonviscous gas-liquid mass transfer in stirred vessels. *Industrial & Engineering Chemistry Process Design and Development* **18**(3): 357-364.

Vander Heiden, M. G., L. C. Cantley and C. B. Thompson (2009). Understanding the Warburg effect: the metabolic requirements of cell proliferation. *Science* **324**(5930): 1029-1033.

Varum, S., A. S. Rodrigues, M. B. Moura, O. Momcilovic, C. A. Easley IV, J. Ramalho-Santos, B. Van Houten and G. Schatten (2011). Energy metabolism in human pluripotent stem cells and their differentiated counterparts. *PLoS One* **6**(6): e20914.

Wagner, B. A., S. Venkataraman and G. R. Buettner (2011). The rate of oxygen utilization by cells. *Free Radic Biol Med* **51**(3): 700-712.

Yuan, X., A. C. Tsai, I. Farrance, J. Rowley and T. Ma (2018). Aggregation of Culture Expanded Human Mesenchymal Stem Cells in Microcarrier-based Bioreactor. *Biochem Eng J* **131**: 39-46.

Zhang, J., E. Nuebel, D. R. Wisidagama, K. Setoguchi, J. S. Hong, C. M. Van Horn, S. S. Imam, L. Vergnes, C. S. Malone, C. M. Koehler and M. A. Teitell (2012). Measuring energy metabolism in cultured cells, including human pluripotent stem cells and differentiated cells. *Nat Protoc* **7**(6): 1068-1085.

Zweigerdt, R. (2009). Large scale production of stem cells and their derivatives. *Adv Biochem Eng Biotechnol* **114**: 201-235.

CHAPTER V.

CONCLUSIONS AND FUTURE TRENDS

For many years, CVDs have been the group of diseases which claimed the most lives in the world. According to the World Health Organization (WHO), ischaemic heart disease, in particular, has been responsible 16% of all deaths in 2019 (https://www.who.int/news-room/fact-sheets/detail/the-top-10-causes-of-death, accessed on the 25th of May 2021). Naturally, given the increasing incidence of these diseases, new answers for them must be developed.

This thesis aimed at developing an integrated protocol for expansion and cardiac differentiation of hiPSCs in 100 mL VWBRs, as well characterising the oxygen mass transfer in these bioreactors, envisaging a scale-up of these protocol to larger scales. Aiming towards this objective, the work was divided into three smaller parts: expansion (Chapter II), cardiac differentiation (Chapter III) and bioreactor characterisation (Chapter IV).

Considering future implications of this work, namely in terms of prospective clinical applications, an aggregate culture system was envisioned. In fact, culturing the cells as aggregates forgoes the use of external matrices, which reduces downstream steps (in comparison to culture on microcarriers or encapsulated in a biomaterial where the cells may have to be separated from the matrix) and facilitates the GMP compliance of the process, due both to the lack of an external matrix and to the process step reduction. Another step towards GMP compliance is the use of VWBRs—being single-use, closed systems, contamination of the culture is limited.

In order to develop an expansion process in the VWBRs, different strategies were attempted, namely, a fed-batch feeding strategy and supplementation with DS. Aggregate culture of hiPSCs in VWBRs was successful, and supplementation of the media with DS led to a two-fold increase in cell number, to a maximum of $(2.3 \pm 0.2) \times 10^6$ cells·mL^{-1}, which is especially advantageous for Regenerative Medicine or for pharmacological applications as an organ may contain 10^9 cells (Zweigerdt 2009). Applying a perfusion feeding strategy could possibly result in even higher cell densities (Kropp et al. 2016), especially if combined with *in silico* modelling to predict an optimal set of conditions for cell culture (Manstein et al. 2021). While the 100 mL VWBR vessels are not naturally compatible with perfusion, this feeding strategy is possible in vessels starting from 3 L (which, volume-wise, would also be more appropriate for biomanufacturing of the cells for clinical settings).

An integrated protocol for hiPSC expansion and cardiac differentiation was then developed. The expansion conditions first established on Chapter II had to be revised to achieve an aggregate diameter of about 300 µm in 3 days (Branco et al. 2019). For this purpose, the inoculation density was doubled (to 5.0×10^5 cells·mL^{-1}), the medium was supplemented with Pluronic F-68 (due to its shear-protecting effect (Tharmalingam et al. 2008)), and DS was not added (due to possible aggregate size reduction). Day 3 aggregates had an average diameter of 298 ± 25 µm and were differentiated with the $GiWi_{cont}$ protocol. Cardiomyocyte percentages after differentiation varied substantially between replicates, from 0% to 73.3% and about 80% of the initial cells were lost throughout differentiation. Furthermore, while some extent of cardiac commitment was observed through qRT-PCR, the presence of non-cardiac mesendoderm was also suggested. These results indicate optimisation still is required in order to ensure the robustness of the protocol, for instance, in terms of ideal aggregate size and small molecule concentration (which may be different from static conditions), as well as the expansion phase, which may benefit from a change to a perfusion or cyclic perfusion feeding (Kempf et al. 2014). Nevertheless,

the results also indicate this integrated protocol is, in fact, viable, at least with the tested cell line. After obtaining a more optimal set of conditions, the resulting cardiomyocytes may benefit from a purification and maturation protocol, for instance, by culture in glucose-depleted, fatty acid–rich medium (Horikoshi et al. 2019).

Both the expansion and differentiation protocols were performed using media with xenogeneic components. The generation of cells for *in vivo* applications will require either a removal of the animal components or, preferably, culture in completely xeno-free media. The formulation of some of these media is completely disclosed, allowing for their production in-house. In fact, some protocols successfully use E8 produced in-house for hPSC expansion (Burridge et al. 2015, Halloin et al. 2019). Cardiac differentiation in the xeno-free medium CDM3 was already achieved, both in 2D (Burridge et al. 2014) and in bioreactors (Halloin et al. 2019). Combining these two media for integrated expansion and cardiac differentiation of hiPSCs would not only provide a xeno-free protocol for cardiomyocyte generation, it would also greatly reduce the costs of the culture—a point which still limits stem cell–based applications at a clinical scale. The extent of cost reduction would naturally depend on the performance differences between the xeno-free and xenogeneic media.

Naturally, when increasing the scale of the bioreactor, the culture environment also changes, necessitating an adaptation of some of the parameters, most notably, the agitation and the aeration. The CFD model developed in Chapter IV aimed at characterising the oxygen mass transfer environment in the PBS MINI 0.1. The average k_La of the system could be estimated through CFD, and was comparable to experimental data. The establishment of this model and its adaptation towards higher scales, will allow to study how the culture microenvironment changes throughout the scale-up process, and to predict which adaptations have to be performed in order to obtain equivalent culture conditions. Obtaining an initial set of conditions *in silico* will allow for substantial time and resource savings when scaling up the integrated expansion and cardiac differentiation protocol, in comparison to an empirical trial-and-error approach.

Although this thesis represents a work-in-progress, it was the first report of cardiac differentiation of hiPSCs in VWBRs and represented an important step towards achieving a protocol for cardiomyocyte production under GMP-compatible conditions. As a robust protocol is developed, more information will be gathered about the process, specifically, in how the culture conditions affect the final cardiomyocyte yield. Understanding these relations will be crucial towards implementing a QbD approach. By moving the quality control to the process itself and not just the final product, QbD will be determining in generating a more robust bioprocess and ultimately saving time and costs (Lipsitz et al. 2016). Another important tool for this purpose is machine learning, which was already shown to predict failed batches at day 5 of differentiation with over 80% accuracy and precision (Williams et al. 2020).

As the field advances, more exciting developments in cardiovascular research may allude to novel protocols which can better replicate the *in vivo* cardiogenesis in a short time. Reducing the protocol duration is crucial when targeting precision medicine applications—the time between patient cell isolation and administration of the final cell product must be as short as possible to minimise the risk of death. The development of efficient cardiac differentiation systems, which may ideally forgo, or at least limit the need for purification and maturation, will definitely mark major breakthroughs towards tackling

the ever-rising prevalence of CVDs in the world. These more efficient systems may result from a combination of methods described in section I.2. With the advent of reports of successful hiPSC cardiac differentiation in bioreactors (Halloin et al. 2019, Laco et al. 2020), and following promising *in vivo* data with hESC-derived CPCs (Menasché et al. 2018), clinical trials with hiPSC-derived cardiomyocytes are expected to follow in the near future.

There still is a long path until a widespread use of hiPSC-based cell products in medicinal practices. Nevertheless, especially when considering the recency (14 years) of hiPSC technology, a significant portion of that path has already been treaded. As more is known about the complexity of the human body, and as it is being translated to *in vitro* culture, Regenerative Medicine is closer than ever to being more than just a promise, and Prometheus's regenerating liver more than just a myth.

V.1. References

Branco, M. A., J. P. Cotovio, C. A. V. Rodrigues, S. H. Vaz, T. G. Fernandes, L. M. Moreira, J. M. S. Cabral and M. M. Diogo (2019). Transcriptomic analysis of 3D Cardiac Differentiation of Human Induced Pluripotent Stem Cells Reveals Faster Cardiomyocyte Maturation Compared to 2D Culture. *Sci Rep* **9**(1): 9229.

Burridge, P. W., A. Holmstrom and J. C. Wu (2015). Chemically Defined Culture and Cardiomyocyte Differentiation of Human Pluripotent Stem Cells. *Curr Protoc Hum Genet* **87**: 21 23 21-21 23 15.

Burridge, P. W., E. Matsa, P. Shukla, Z. C. Lin, J. M. Churko, A. D. Ebert, F. Lan, S. Diecke, B. Huber, N. M. Mordwinkin, J. R. Plews, O. J. Abilez, B. Cui, J. D. Gold and J. C. Wu (2014). Chemically defined generation of human cardiomyocytes. *Nat Methods* **11**(8): 855-860.

Halloin, C., K. Schwanke, W. Lobel, A. Franke, M. Szepes, S. Biswanath, S. Wunderlich, S. Merkert, N. Weber, F. Osten, J. de la Roche, F. Polten, K. Christoph Wollert, T. Kraft, M. Fischer, U. Martin, I. Gruh, H. Kempf and R. Zweigerdt (2019). Continuous WNT Control Enables Advanced hPSC Cardiac Processing and Prognostic Surface Marker Identification in Chemically Defined Suspension Culture. *Stem Cell Reports* **13**(2): 366-379.

Horikoshi, Y., Y. Yan, M. Terashvili, C. Wells, H. Horikoshi, S. Fujita, Z. J. Bosnjak and X. Bai (2019). Fatty Acid-Treated Induced Pluripotent Stem Cell-Derived Human Cardiomyocytes Exhibit Adult Cardiomyocyte-Like Energy Metabolism Phenotypes. *Cells* **8**(9): 1095.

Kempf, H., R. Olmer, C. Kropp, M. Ruckert, M. Jara-Avaca, D. Robles-Diaz, A. Franke, D. A. Elliott, D. Wojciechowski, M. Fischer, A. Roa Lara, G. Kensah, I. Gruh, A. Haverich, U. Martin and R. Zweigerdt (2014). Controlling expansion and cardiomyogenic differentiation of human pluripotent stem cells in scalable suspension culture. *Stem Cell Reports* **3**(6): 1132-1146.

Kropp, C., H. Kempf, C. Halloin, D. Robles-Diaz, A. Franke, T. Scheper, K. Kinast, T. Knorpp, T. O. Joos, A. Haverich, U. Martin, R. Zweigerdt and R. Olmer (2016). Impact of Feeding Strategies on the Scalable Expansion of Human Pluripotent Stem Cells in Single-Use Stirred Tank Bioreactors. *Stem Cells Transl Med* **5**(10): 1289-1301.

Laco, F., A. T. Lam, T. L. Woo, G. Tong, V. Ho, P. L. Soong, E. Grishina, K. H. Lin, S. Reuveny and S. K. Oh (2020). Selection of human induced pluripotent stem cells lines optimization of

cardiomyocytes differentiation in an integrated suspension microcarrier bioreactor. *Stem Cell Res Ther* **11**(1): 118.

Lipsitz, Y. Y., N. E. Timmins and P. W. Zandstra (2016). Quality cell therapy manufacturing by design. *Nat Biotechnol* **34**(4): 393-400.

Manstein, F., K. Ullmann, C. Kropp, C. Halloin, W. Triebert, A. Franke, C. M. Farr, A. Sahabian, A. Haase, Y. Breitkreuz, M. Peitz, O. Brustle, S. Kalies, U. Martin, R. Olmer and R. Zweigerdt (2021). High density bioprocessing of human pluripotent stem cells by metabolic control and in silico modeling. *Stem Cells Transl Med* **10**(7): 1063-1080.

Menasché, P., V. Vanneaux, A. Hagege, A. Bel, B. Cholley, A. Parouchev, I. Cacciapuoti, R. Al-Daccak, N. Benhamouda, H. Blons, O. Agbulut, L. Tosca, J. H. Trouvin, J. R. Fabreguettes, V. Bellamy, D. Charron, E. Tartour, G. Tachdjian, M. Desnos and J. Larghero (2018). Transplantation of Human Embryonic Stem Cell-Derived Cardiovascular Progenitors for Severe Ischemic Left Ventricular Dysfunction. *J Am Coll Cardiol* **71**(4): 429-438.

Tharmalingam, T., H. Ghebeh, T. Wuerz and M. Butler (2008). Pluronic enhances the robustness and reduces the cell attachment of mammalian cells. *Mol Biotechnol* **39**(2): 167-177.

Williams, B., W. Lobel, F. Finklea, C. Halloin, K. Ritzenhoff, F. Manstein, S. Mohammadi, M. Hashemi, R. Zweigerdt, E. Lipke and S. Cremaschi (2020). Prediction of Human Induced Pluripotent Stem Cell Cardiac Differentiation Outcome by Multifactorial Process Modeling. *Front Bioeng Biotechnol* **8**: 851.

Zweigerdt, R. (2009). Large scale production of stem cells and their derivatives. *Adv Biochem Eng Biotechnol* **114**: 201-235.